UNIVERSITÄT
BAYREUTH

Towards a 'chassis' for magnetosome biosynthesis: large-scale genome engineering in the magnetic bacterium *Magnetospirillum gryphiswaldense*

Dissertation

zur Erlangung des akademischen Grades einer Doktorin

der Naturwissenschaften (Dr. rer. nat.)

in der Bayreuther Graduiertenschule für Mathematik und Naturwissenschaften (BayNAT)

der Universität Bayreuth

vorgelegt von

Theresa Zwiener

aus München

Bayreuth, 2022

Die vorliegende Arbeit wurde in der Zeit von April 2016 bis Juli 2022 in Bayreuth am Lehrstuhl Mikrobiologie unter Betreuung von Herrn Professor Dr. Dirk Schüler angefertigt.

Vollständiger Abdruck der von der Bayreuther Graduiertenschule für Mathematik und Naturwissenschaften (BayNAT) der Universität Bayreuth genehmigten Dissertation zur Erlangung des akademischen Grades einer Doktorin der Naturwissenschaften (Dr. rer. nat.).

Dissertation eingereicht am: 26.07.2022

Zulassung durch das Leitungsgremium: 15.09.2022

Wissenschaftliches Kolloquium: 17.02.2023

Amtierender Direktor: Prof. Dr. Hans Keppler

Prüfungsausschuss:

Prof. Dr. Dirk Schüler   (Gutachter)

Prof. Dr. Matthias Noll   (Gutachter)

Prof. Dr. Andreas Möglich   (Vorsitz)

Prof. Dr. Stefan Heidmann

INDEX

LIST OF PUBLICATIONS

Publications comprised in this thesis

Manuscript 1

Genome-wide identification of essential and auxiliary gene sets for magnetosome biosynthesis in *Magnetospirillum gryphiswaldense*

Silva K.T., M. Schüler, F. Mickoleit, **<u>T. Zwiener</u>**, F.D. Müller, R.P. Awal, A. Weig, A. Brachmann, R. Uebe, and D. Schüler.

Manuscript 2

Identification and elimination of genomic regions irrelevant for magnetosome biosynthesis by large-scale deletion in *Magnetospirillum gryphiswaldense*

<u>Zwiener T.</u>, F. Mickoleit, M. Dziuba, C. Rückert, T. Busche, J. Kalinowski, D. Faivre, R. Uebe, and D. Schüler

Manuscript 3

Towards a 'chassis' for bacterial magnetosome biosynthesis: genome streamlining of *Magnetospirillum gryphiswaldense* by multiple deletions

<u>Zwiener T.</u>, M. Dziuba, F. Mickoleit, C. Rückert, T. Busche, J. Kalinowski, R. Uebe, and D. Schüler

Additional co-authored publications which originated from this thesis

Manuscript 4

Single-step transfer of biosynthetic operons endows a non-magnetotactic *Magnetospirillum* strain from wetland with magnetosome biosynthesis

Dziuba M.V., **T. Zwiener**, R. Uebe, and D. Schüler.

Environmental Microbiology (2020) 22(4):1603–1618

Manuscript 5

A gradient-forming MipZ protein mediating the control of cell division in the magnetotactic bacterium *Magnetospirillum gryphiswaldense*

Toro-Nahuelpan M., L. Corrales-Guerrero, **T. Zwiener**, M. Osorio-Valeriano, F.D. Müller J.M. Plitzko, M. Bramkamp, M. Thanbichler and D. Schüler.

Molecular Microbiology (2019) 112(5):1423–1439

Contributions to publications

Manuscript 1:

KTS and DS designed the study. KTS, <u>TZ</u>, FM, AB, RPA and FDM performed experiments. KTS, MS, <u>TZ</u>, RU, AW and FDM categorized gene essentiality and analysed the data. <u>TZ</u>, FM, FD and RPA created 'clean' deletion mutants and generated TEM micrographs. KTS, MS, and DS wrote the paper with contributions from all authors.

Manuscript 2:

<u>TZ</u> and DS conceptualized the study. <u>TZ</u> performed the genetic manipulation and the characterization of the strains. FM and RU analysed putative auxiliary determinants for magnetosome biosynthesis. MD designed and generated plasmid pTpsMAG1. DF performed TEM, (HR)TEM, and XEDS for EDP analysis. CR, TB, and JK carried out resequencing of strains. <u>TZ</u> and DS wrote the manuscript. All authors read and approved the final manuscript.

Manuscript 3:

<u>TZ</u> and DS conceived the study and designed the experiments. <u>TZ</u> carried out the genetic manipulation and the characterization of the strains. <u>TZ</u>, DS, FM and RU designed genetic stability assays. MD designed and generated plasmid pMDJM3. CR, TB, and JK performed resequencing of strains. <u>TZ</u> and DS wrote the manuscript.

ABBREVIATIONS

Cbb3	Terminal oxidase
ccmI/CcmI (CycH)	Tetratricopeptide repeat (TPR)-containing gene/protein
C_{mag}	A proxy for the average magnetic orientation of bacterial cells in liquid media based on light-scattering
Cre	Causes recombination
DNA	Deoxyribonucleic acid
dsbB/DsbB	Gene/protein of disulfide bond pathway
feo/Feo	Ferrous iron transporter (gene or protein)
Fnr	Fumarate and nitrate reduction regulator protein
Fur	Ferric uptake regulator
galK/GalK	Galactokinase (gene or protein)
Gm	Gentamycin
gusA	β-Glucoronidase (gene)
IS	Insertion sequence
Km	Kanamycin
lox	Locus of X-over
loxP	Locus of X-over P1
MAI	Genomic magnetosome island
mam/Mam	Magnetosome membrane (gene or protein)
MCS	Multiple cloning site
MICP	Microbially induced calcite precipitation
MMC	Mitomycin C
*mms/*Mms	Magnetosome particle-membrane specific (gene or protein)
MTB	Magnetotactic bacteria
Nap	Nitrate reductase, periplasmic
Nif	Nitrogen fixation (gene cluster)
Nir	Nitrite reductase
Nor	Nitric oxide reductase
nt	nucleotide
OP3	Obsidian pool 3
pks	Polyketide synthase (gene cluster)

recA/RecA	Recombination protein A (gene or protein)
ROI	Region of interest
sacB	Levansucrase (gene)
TEM	Transmission electron microscopy
Tet	Tetracycline
ure	Urease operon or genes
urt	ABC-type (ATP-binding) transporter operon or genes for urea transport
WT	Wild type

SUMMARY

Magnetotactic bacteria biosynthesize specific organelles, so-called magnetosomes, which are membrane-enclosed magnetic iron minerals that enable the cells to align along geomagnetic field lines. The magnetic bacterium *Magnetospirillum gryphiswaldense* has emerged as model organism for the analysis of magnetosome biosynthesis and bioproduction. In *M. gryphiswaldense*, the genomic magnetosome island (MAI) encodes all genetic determinants required for this intricate biosynthesis process, but harbours also numerous mobile genetic elements, repeats and genetic 'junk'. The boundaries of the MAI and the role of its intervening and adjacent regions regarding their relevance for magnetosome biosynthesis and growth under lab conditions are still unclear. Because of the inherent genetic instability of the magnetosome biosynthesis gene clusters, the elimination of intervening and adjacent gene content and the substitution of the native MAI by a compact magnetosome expression cassette is highly desirable. In addition, recent observations suggested the involvement of further auxiliary determinants for magnetosome biosynthesis encoded outside the MAI, which however, have not yet been identified. Furthermore, the future use of *M. gryphiswaldense* will require techniques for large-scale genome editing.

In this thesis, first, new putative auxiliary determinants outside the MAI supporting the complex magnetosome formation process were verified by targeted deletion. Second, an allelic replacement method based on homologous recombination was validated and optimized for large-scale genome mutagenesis up to at least ~100 kb. Thereby, new boundaries of the MAI were defined, and a large region with no function in magnetosome biosynthesis spanning ~73 kb could be eliminated and replaced by a compact and contiguous ~38 kb cassette comprising solely the essential biosynthetic gene clusters, but devoid of irrelevant or problematic gene content. This technique was further used to identify and eliminate problematic gene content including putative prophages, active mobile genetic elements, and irrelevant gene clusters outside the MAI.

Ultimately, combinatory deletions including large regions, active mobile genetic elements, and phage-related genes were combined in a nearly 5.5% genome-reduced strain, thereby providing the first proof-of-principle for large-scale engineering of magnetotactic bacteria.

Altogether, the results of this thesis will be useful for future genome manipulations to generate prospective chassis strains for improved magnetosome engineering and enhanced stable high-yield magnetosome production in *M. gryphiswaldense*.

ZUSAMMENFASSUNG

Magnetotaktische Bakterien besitzen die Fähigkeit spezielle Organellen, sogenannte Magnetosomen, zu synthetisieren. Das Magnetbakterium *Magnetospirillum gryphiswaldense* stellt dabei einen Modellorganismus für die Analyse der Magnetosomen-Biosynthese und -Bioproduktion dar. Die für die Kontrolle der Magnetosomen-Biosynthese relevanten Gene sind in *M. gryphiswaldense* in einer genomischen Magnetosomeninsel (MAI) lokalisiert. Letztere kodiert ebenfalls eine Vielzahl mobiler genetischer Elemente, *repeats*, sowie '*genetic junk*'. Die Grenzen der MAI als auch die Funktionen der Regionen zwischen den Magnetosomen-Operons sowie angrenzender Regionen sind hinsichtlich ihrer Relevanz für die Magnetosomen-Biosynthese und das zelluläre Wachstum unter Laborbedingungen noch weitestgehend unerforscht. Aufgrund der genetischen Instabilität der Magnetosomen-*Cluster* wäre die Deletion der Regionen zwischen den Operons als auch der Austausch der nativen MAI durch eine kompakte Kassette, welche alle Magnetosomen-Gene enthält, von großem Interesse und für zukünftige genetische Manipulationen in *M. gryphiswaldense* und anderen Magnetbakterien von großer Bedeutung. Neueste Forschungsergebnisse sprechen außerdem dafür, dass am komplexen Ablauf der Magnetosomen-Biosynthese weitere unterstützende Faktoren außerhalb der MAI beteiligt sein könnten. Zudem erfordert die zukünftige genetische Manipulation in *M. gryphiswaldense* und anderen Magnetbakterien passende Methoden für ausgedehntere genetische Manipulationen.

In der vorliegenden Arbeit wurden neue Kandidaten-Gene außerhalb der MAI, welche an der Magnetosomen-Biosynthese beteiligt sind, durch gezielte Deletion verifiziert. Des Weiteren konnte eine Technik basierend auf homologer Rekombination für die großflächige genetische Manipulation von bis zu ~100 kb validiert werden. Dabei konnten neue Grenzbereiche der MAI für mögliche Deletionen definiert und eine Region irrelevant für die Funktion in der Magnetosomen-Biosynthese mit einem Ausmaß von ~73 kb durch eine kompakte Kassette, die alle Magnetosomen-Gene enthält, ersetzt werden. Dieselbe Methode wurde schließlich dazu verwendet, um weiteren problematischen Geninhalt wie potentielle Prophagen und aktive mobile genetische Elemente außerhalb der MAI zu identifizieren und eliminieren.

Letztlich konnte durch kombinatorische Genomreduktion ausgedehnter Regionen, vermeintlicher Prophagen und aktiver mobiler genetische Elemente ein bis zu 5,5% genom-reduzierter Stamm konstruiert, sowie die Machbarkeit (*proof-of-principle*) zur genetischen Optimierung magnetotaktischer Bakterien erbracht werden.

Insgesamt bilden die Ergebnisse der vorliegenden Arbeit die Grundlage für die zukünftige Konstruktion eines angehenden *chassis*, um die genetische Manipulation der Magnetosomen zu verbessern sowie stabile und hohe Magnetosomen-Erträge aus *M. gryphiswaldense* zu erzeugen.

CHAPTER I: General introduction

1.1 Magnetotactic bacteria

Magnetotactic bacteria (MTB) were first described in 1963 by Salvatore Bellini, a medical doctor at the University of Pavia in Italy. During microscopy analysis he noticed that a group of bacteria was unexpectedly swimming in one distinct direction [1, 2]. However, the mechanism of their magnetic perception remained largely hidden and unexplored until the American microbiologist Richard Blakemore independently rediscovered MTB in 1975 [3]. The unique feature to navigate along the Earth's geomagnetic field lines is referred to as 'magnetotaxis' [4]. In combination with aerotaxis it represents an efficient tool for these bacteria to support their microaerophilic or anaerobic lifestyle to find growth-favouring zones in marine or freshwater sediments [5–8]. MTB species are distributed in a wide range of Gram-negative bacterial lineages including the Alphaproteobacteria, Gammaproteobacteria, Deltaproteobacteria, Nitrospirae classes, the candidate phyla Latescibacteria as well as candidate division OP3 [9–15]. These bacteria are ubiquitously present in aquatic sediments and exhibit a high morphological, metabolical and physiological heterogeneity like magnetotactic cocci, rods, vibrios, ovoid cells, spirilla, or multicellular species [9, 16–22].

All MTB share the exceptional property to synthesize magnetic nanoparticles, so-called magnetosomes, which serve as magnetic sensors and are generally arranged in single or multiple intracellular chains, often along the motility axis [23–25]. The particles are membrane-enclosed nanocrystals of monocrystalline magnetite (Fe_3O_4) or greigite (Fe_3S_4) [3, 9, 26–32]. Thereby, the number, size, and shape vary considerably between phylogenetic groups [16, 33, 34].

Because of their fastidious lifestyle and yet unknown cultivation requirements, only few MTB members can be cultured in the laboratory. Thus, research progress has also been dependent on the development of cultivation strategies as well as genetic manipulation. Until now, the best-studied representatives of MTB regarding physiology and magnetosome biosynthesis are *Magnetospirillum gryphiswaldense* MSR-1 and *M. magneticum* AMB-1 [32, 35]. Because of its tractability and relatively straightforward cultivation the freshwater alphaproteobacterium *M. gryphiswaldense* [36–38] has emerged as the most extensively studied MTB based on literature, enabling the analysis of particle biosynthesis and the study of magnetosome

bioproduction. *M. gryphiswaldense* also represents the model organism investigated in this thesis.

1.2 The alphaproteobacterium *Magnetospirillum gryphiswaldense*

In 1990, the Gram-negative alphaproteobacterium *M. gryphiswaldense* was isolated from the sediment of the eutrophic river Ryck near Greifswald, Germany [29, 31, 36]. Based on its chemoorganoheterotrophic lifestyle using different organic acids as electron donors, and oxygen or nitrate as terminal electron acceptors, *M. gryphiswaldense* grows microaerophilic, anaerobic, or autotrophic [29–31, 39]. Cells of *M. gryphiswaldense* have a helical morphology and are bipolar monotrichously flagellated (Fig. 1). Their length varies between 2 to 4 µm and a width of 0.4 to 0.8 µm [38, 40–42]. Under optimal anaerobic growth conditions, a single cell produces up to 100 cuboctahedral magnetosomes of about 40 nm in diameter, which consist of a magnetite core (Fe_3O_4) enveloped by a proteinaceous phospholipid membrane. The particles within the cells are assembled in a single or two linear chains [40–45]. Magnetosome formation has recently become a model for the highly ordered biosynthesis of prokaryotic organelles.

The recent development of diverse genetic manipulation techniques and ease of cultivation in the laboratory made *M. gryphiswaldense* a model organism for studying magnetosome biomineralization, cell biology, as well as organelle formation. Since the majority of MTB cannot be cultivated or genetically manipulated but contain magnetic nanoparticles with potentially interesting properties with regard to shape, size and magnetic properties, *M. gryphiswaldense* might serve as a promising host for the homologous and heterologous expression of bacterial magnetosome clusters in the future.
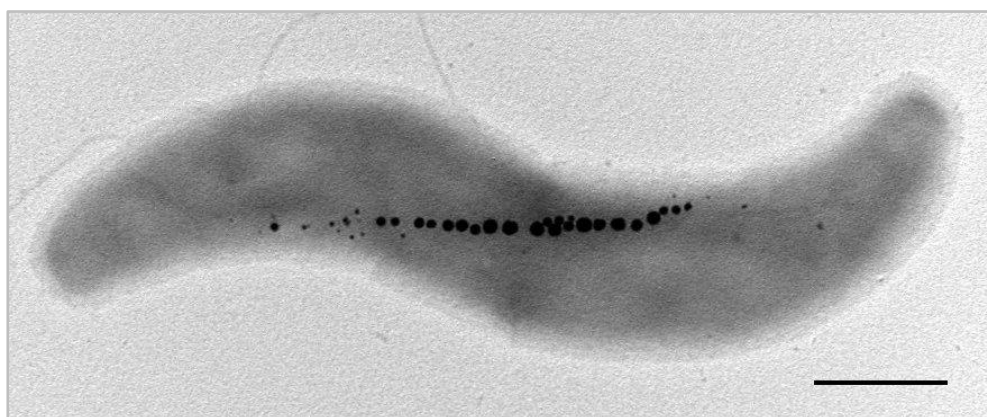

Figure 1. Transmission electron micrograph (TEM) of a representative wild type (WT) cell of *M. gryphiswaldense*. The latter biomineralizes up to 100 magnetosomes per cell, which are chain-like arranged at midcell and visible as electron dense particles. The image was taken from Zwiener et al. (2021) [46]. Scale bar: 500 nm.

1.3 Magnetosomes as promising 'tools' for future *real-world* applications?

Besides their biological function as geomagnetic field sensors in MTB, bacterial magnetosomes exhibit extraordinary properties, such as high crystallinity, a strong magnetization as well as precise morphologies and uniform sizes [24, 47], which can hardly be achieved by chemical synthesis. Moreover, magnetosomes are colloidal stable in a variety of buffers and solvents due to their natural proteinaceous phospholipid membrane that prevents aggregation of the magnetite cores. In contrast, chemically synthesis routes still require further coating or ligand exchange reactions to be dispersible, as well as purification steps and post-treatments as by-products or residual surfactants are assumed to be detrimental to the applicability and biocompatibility of the particles.

The proteinaceous magnetosome membrane provides sites for covalent attachment of foreign moieties and thus, enables the functionalization of the particle surface in a controllable and highly selective manner [47–49]. These features make purified magnetosomes a promising tool with potential for biotechnological and biomedical applications (Fig. 2). For example, foreign functional moieties and polypeptides such as fluorophores, enzymes, or antibodies, as well as organic shells can be genetically fused to magnetosome membrane anchors *in vivo* [50–56]. Furthermore, it has been demonstrated that *M. gryphiswaldense* and magnetosome biosynthesis can be used as platform to study the molecular mechanism of human diseases [57–59], and in food science [60]. Additionally, the modification of the particle surface by genetic engineering allowed the utilization of isolated magnetosomes as multimodal reporters for magnetic imaging [60, 61], as nanocarriers for magnetic drug targeting [62–65], or for magnetic hyperthermia applications [66–68]. Although great efforts are made not only to optimize magnetosome biosynthesis [69–71], but also to improve their purification [72, 73], particle production is still expensive, yields are low, and the isolation procedure is time-consuming.
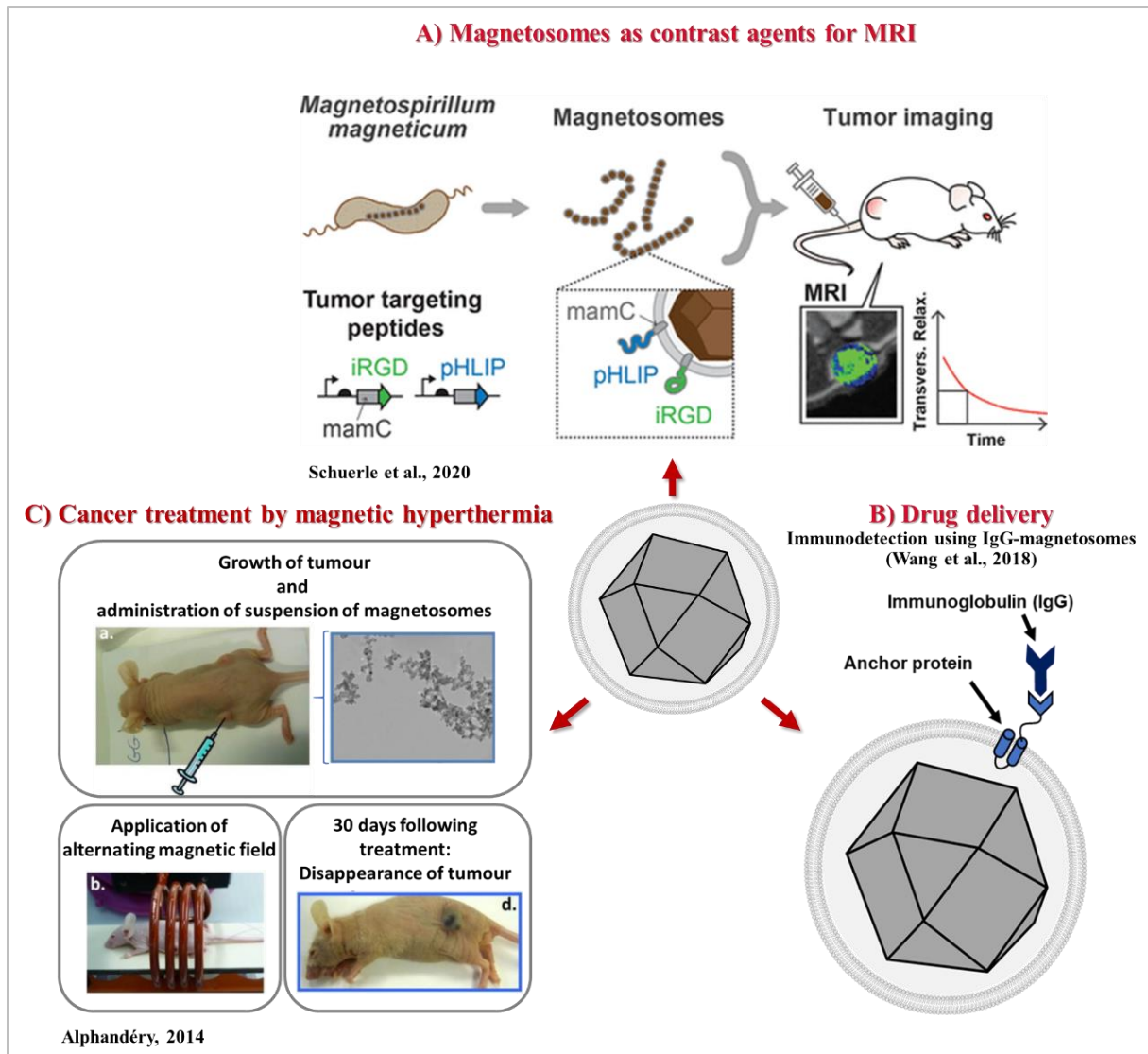
Figure 2. Examples of potential, highly attractive biotechnological and biomedical applications of magnetosomes from *M. gryphiswaldense*. Images were taken from different references as indicated. For instance, genetically engineered magnetosomes were used as *in vivo* contrast agents for MRI **(A)** [66], anti-tumour effects of therapeutics on a carcinoma cell line were demonstrated by using bacterial magnetic particle-based gene delivery systems **(B)** [58], or treatment of breast tumours of mice by magnetic hyperthermia based on injected magnetosomes **(C)** [69].

1.4 Genetics of magnetosome formation in *M. gryphiswaldense*

1.4.1 The genomic magnetosome island

During the last decades magnetosome biosynthesis has shown to be strictly controlled by genes arranged in a specific genomic <u>m</u>agnetosome <u>i</u>sland, the MAI. The complex biogenesis process comprises four different steps [32, 45, 74]: First, vesicles are formed by invagination of the cytoplasmic membrane. Second, specific magnetosome proteins are sorted to the magnetosome membrane. Third, iron is transported into the membrane vesicles followed by the nucleation of magnetite, maturation, and crystal growth. Fourth, the magnetosome chain is assembled and positioned for segregation during cell division (Fig. 3A, i–iv).

In *M. gryphiswaldense* a set of about 30 proteins was identified to be functional in magnetosome biosynthesis. The corresponding *mam* (<u>m</u>agnetosome <u>m</u>embrane), *mms* (<u>m</u>agnetic particle-<u>m</u>embrane <u>s</u>pecific) and *feo* genes are clustered within the ~100 kb genomic MAI [32, 75–77]. Besides, the intervening and adjacent regions (Fig. 3B; R2, R4, R6 and R8) also harbour hypothetical genes or genes with known functions (Fig. 3B, black), numerous mobile genetic elements (Fig. 3B, blue), repeats and genetic 'junk' (e.g., several incomplete and pseudogenes as well as non-coding genetic content). Commonly, genomic islands in pathogenic and environmental microorganisms are known to contribute to rapid evolution, diversification, and adaption by horizontal gene transfers [78, 79]. Thereby, the host may receive virulence factors or metabolic pathways [79–81]. To date, three evolutionary hypotheses have been reported for the magnetosome island: the first describes a single common ancestor of all MTB [82, 83]. The second states that the magnetic features evolved independently several times [84]. The third hypothesis assumes that multiple occasions of horizontal gene transfer happened including the possibility of a single ancestor [77, 85, 86].

In the MAI of *M. gryphiswaldense*, the magnetosome biosynthesis genes are clustered into five polycistronic operons, *mamAB*$_{op}$, *mamGFDC*$_{op}$, *mamXY*$_{op}$, *mms6*$_{op}$ and *feoAB1*$_{op}$, which control all specific steps of magnetosome biosynthesis (Fig. 3B; R1, R3, R5 and R7) [32, 75–77]. The large (16.4 kb) *mamAB*$_{op}$ comprises 17 genes (*mamH, -I, -E, -J, -K, -L, -M, -N, -O, -P, -A, -Q, -R, -B, -S, -T*, and *-U*) encoding e.g., transporters, magnetosome membrane proteins, proteases, cytochrome *c*-type proteins, as well as iron oxidases. Furthermore, genes encoded by the *mamAB*$_{op}$ are involved in magnetosome chain formation [87–89].

In the genomes of other MTB, a couple of magnetosome genes are conserved among all MTB so far examined. For example, genetic determinants required for magnetosome formation are

located within the *mamAB_{op}*, and the genes *mamABEIKLMOPQ* are conserved in all magnetite-producing MTB, while *mamABEIKMOPQ* are also conserved in greigite-producing MTB [23]. Differences in the gene sequences are assumed to result in the synthesis of differentially shaped magnetic nanoparticles like elongated or bullet-shaped magnetosomes. The underlying molecular mechanisms of the highly controlled magnetosome biosynthesis still needs further analysis to elucidate the complex biomineralization process. However, most MTB cannot be cultivated or genetically manipulated. Genetic transfer of the magnetosome biosynthesis pathway to non-magnetic bacterium by genomic insertion of major magnetosome operons has only succeeded twice, namely in *Rhodospirillum rubrum* and *Magnetospirillum* sp. 15-1 [90, 91], but failed for many other, also closely related microorganisms suggesting further, yet unidentified determinants being necessary for magnetosome biosynthesis. Therefore, *M. gryphiswaldense* represents a highly interesting host for homologous and heterologous expression of bacterial magnetosome gene clusters in the future, and will help to study genetic and morphological diversity of magnetosomes (also from uncultivated MTB) and their synthesis.

Although magnetosome biosynthesis is not understood in every detail, it is known that only *mamE, -L, -M, -O, -Q*, and *-B* are essential for rudimentary magnetite formation in the absence of residual MAI genes as deletion of the respective genes led to non-magnetic phenotypes in *M. gryphiswaldense* [74]. Other genes of the *mamAB_{op}* as well as those from *mamGFDC_{op}*, *mamXY_{op}*, *mms6_{op}* and *feoAB1_{op}* encode accessory functions for magnetosome formation. Deletion mutants of the smaller *mamGFDC_{op}* (~2 kb, encodes *mamG, -F, -D*, and *-C*), *mms6_{op}* (~3.4 kb, encodes *mms36, mms48, mmxF*, and *mms6*), *feoAB1_{op}* (~2.4 kb, encodes *feoA1*, and *-B1*) or *mamXY_{op}* (~5 kb, encodes *ftsZm, mamZ, -X*, and *-Y*) show severe defects in morphology, size and organization of magnetite crystals, but still form small irregular crystallites [87, 92, 93, R. Uebe unpublished]. The MamGFDC proteins seem to be involved in the regulation of magnetite crystal size, while three of those proteins were shown to be sufficient for WT-like magnetosome formation [52, 92]. The *mms6_{op}* with its four encoded proteins seems to control crystal size, morphology, and particle number [87]. Proteins encoded by the *mamXY_{op}* are assumed to regulate magnetite crystallization, the correct positioning of the magnetosome chain and seem to be functional in redox balance [89, 93, 94].

Interestingly, genetic overexpression of biosynthesis-related gene clusters by duplication of *mamAB_{op}*, *mamGFDC_{op}*, *mamXY_{op}* and *mms6_{op}* in the WT background of *M. gryphiswaldense* resulted in a particle overproducer strains, biomineralizing up to 170 magnetosomes per cell

partially with an enlarged size (Fig. 3C–E) [95]. Thereby, stepwise amplification of the $mms6_{op}$ resulted in the formation of increasingly larger crystals (increase of ~35%), while the duplication of the major magnetosome operons $mamAB_{op}$, $mamGFDC_{op}$, $mamXY_{op}$ and $mms6_{op}$ yielded an overproducing strain in which magnetosome numbers were 2.2-fold increased [95].

As mentioned above, in *M. gryphiswaldense*, the five key operons are separated by stretches containing numerous hypothetical genes, mobile genetic elements, non-essential genes, repeats and genetic 'junk' [87, 77]. In the past, spontaneous rearrangements and deletions within the MAI could be observed during subcultivation of *M. gryphiswaldense*, resulting in weakly or even non-magnetic phenotypes [77, 86, 96]. The presence of numerous transposable elements of intervening MAI regions is assumed to cause genetic instability of the MAI to some extent and might be responsible for these spontaneous mutants.
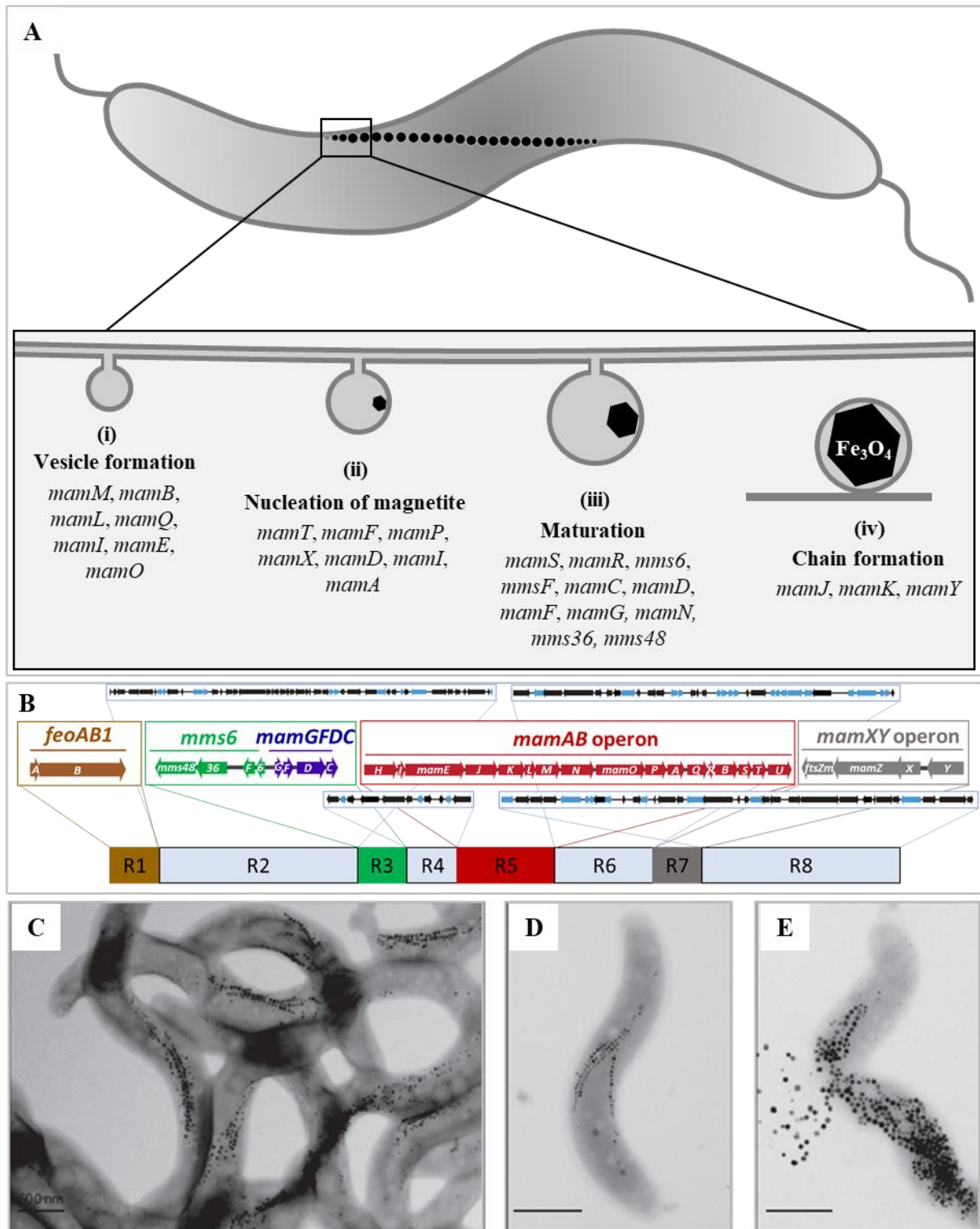
Figure 3. Model of the stepwise process of magnetosome biosynthesis and genomic organization of the magnetosome island (MAI) in *M. gryphiswaldense*. A) The mechanism of magnetosome formation starts with the formation of vesicles that originate from the inner cytoplasmic membrane (i), passes over to the nucleation of magnetite (ii) and crystal maturation (iii), and ends with the arrangement of magnetosomes in a chain-like manner (iv). The schematic illustration is adapted from Schüler et al. (2020) [37]. **B)** The magnetosome biosynthesis genes are organized in five key operons as indicated, i.e. the operons *feoAB1* (brown), *mms6* (green), *mamGFDC* (violet), *mamAB* (red) and *mamXY* (grey). Interspacing regions R2, R4, R6 and R8 encode hypothetical genes, genes with

known functions (black) or mobile genetic elements (blue). **C–E)** TEM micrographs of a magnetosome overexpression strain, taken from Lohße et al. (2016) [95]. Scale bars: 500 nm.

However, the relevance of intervening and adjacent MAI regions for magnetosome biosynthesis is not known and questions regarding conspicuously liable problematic gene content for cell growth, genetic stability, as well as their essential functions are still open. Additionally, the boundaries of the MAI and the role of distal and MAI-adjacent regions remain unclear. For future genetic analysis and manipulation of magnetosome biosynthesis, it would therefore be highly desirable to answer these questions and to investigate the feasibility of substituting the endogenous MAI by a compact magnetosome expression cassette devoid of genetic 'junk'.

Besides this distinct genomic region of magnetosome genes, several auxiliary determinants have been identified [32], which exhibit both direct or indirect functions in magnetosome biosynthesis, as well as functions in general metabolic and regulatory cellular pathways. Therefore, the following sections focus first on the molecular organization of the magnetosome island and afterwards on auxiliary determinants involved in magnetosome biosynthesis outside this genomic island.

1.4.2   Auxiliary determinants outside the MAI influencing magnetosome formation

Apart from specific and essential functions encoded within the MAI, further auxiliary and generic genetic determinants for magnetosome biosynthesis are localized somewhere else in the core genome of *M. gryphiswaldense*. For example, the ferric uptake regulator Fur is involved in global iron homeostasis, which also affects magnetite biomineralization [97]. Since a *fur* deletion mutant produces fewer and slightly smaller but still functional magnetite crystals compared to the wild type (WT), Fur plays an indirect role in magnetosomal iron uptake [97]. Moreover, proteins involved in redox balance like periplasmic nitrate and nitrite reductases (Nap and NirS), fumarate and nitrate reduction regulator protein (Fnr) as well as the terminal oxidase Cbb3 involved in aerobic respiration and may affect the synthesis of mixed-valence iron oxide magnetite [Fe(II)Fe(III)$_2$O$_4$], were demonstrated to be linked to magnetite biomineralization [94, 98, 99]. However, none of these auxiliary determinants play an essential role in magnetosome biomineralization and since heterologous expression of magnetosome biosynthesis has only been successful in *R. rubrum* [90] and *Magnetospirillum* sp. 15-1 [91], further auxiliary determinants outside the MAI were hypothesized to be involved in magnetosome biosynthesis.

At the beginning of this work, new putative auxiliary determinants for magnetosome biosynthesis were identified by a systematic genome-wide transposon mutagenesis approach and magnetosome membrane proteomics [100]. However, potential polar effects on the expression of downstream genes, effects of the Tn5-insertion to certain domains of the gene products, occurrence of transcriptional readthrough and partially reduced functionality of hit genes by insertion into terminal regions of the gene could influence the magnetosome phenotype of mutants and thus, need to be excluded. For this reason, the role/function of candidate genes located outside the MAI with putative roles in magnetosome biosynthesis needs to be assessed by targeted deletion mutagenesis, thereby generating 'clean' (unmarked) deletion mutants.

1.5 Genetic analysis and manipulation of *M. gryphiswaldense*

The discovery and characterization of magnetosome genes and clusters described in the previous paragraphs were the result of genetic analysis using the methods described in the following.

After isolation and the establishment of first cultivation approaches of *M. gryphiswaldense* in 1990, the basis for magnetosome biosynthesis research was laid by Schultheiss and Schüler (2003) [101] through the development of genetic manipulation techniques in *M. gryphiswaldense* by conjugation. At the same time, using proteomics and reverse genetics, first magnetosome biosynthesis genes were identified [75, 76]. Genetic manipulation was further developed by introducing deletion mutagenesis by RecA-mediated homologous recombination using SacB for counterselection, which confers sensitivity to sucrose, as well as a Cre-*lox* based method [101–103]. However, the SacB-based counterselection method was proven not to be reliable, likely because of rapid spontaneous gene inactivation upon selective pressure, leading to numerous false-positive clones [92]. Therefore, this method was extended by a GalK-based counterselection system for markerless gene deletion and chromosomal tagging (explained in more detail below) [104]. Furthermore, new vectors for chromosomal integration for high-level constitutive or inducible magnetosome expression of fusion proteins were constructed [105]. Using a Tn5-based transposition system, expression cassettes could be inserted into the genome at random positions. Although it cannot be excluded that the

transcriptional activity of the insertion sites might affect gene expression, so far only minor effects were observed.

Despite great efforts for the development of targeted genomic manipulation techniques in the last years, the genetic 'toolbox' for MTB is still limited. Additionally, the application of such manipulation techniques for large-scale deletions and genome streamlining is so far a new territory in the field of MTB.

For gene deletions in *M. gryphiswaldense*, two techniques have been developed: the first recombination method, which is based on the Cre-*loxP* system of the P1 phage, is a simple two-component system used for the excision of larger fragments up to ~53 kb [87, 92, 103]. This technique utilizes two different suicide vectors containing *lox* sequences (*lox71* and *lox66*) and amplified upstream and downstream regions (Fig. 4A/B). Vectors need to be integrated next to the genomic target by homologous recombination in two independent steps (Fig. 4C/D). Afterwards, addition of the Cre recombinase encoded on plasmid pLYJ87 [106], which belongs to the integrase family of site-specific recombinases, catalyses the reciprocal site-specific recombination of DNA at *loxP* sites, resulting in the excision of the target region from which the deletant has to be subsequently cured (Fig. 4E) [103].

The Cre-*lox* based method has several disadvantages as it is time-consuming and laborious since it needs the construction and insertion of two different vectors and an additional helper plasmid. In addition, *loxP* nucleotides remain in the genomic target region as so-called 'scars'.
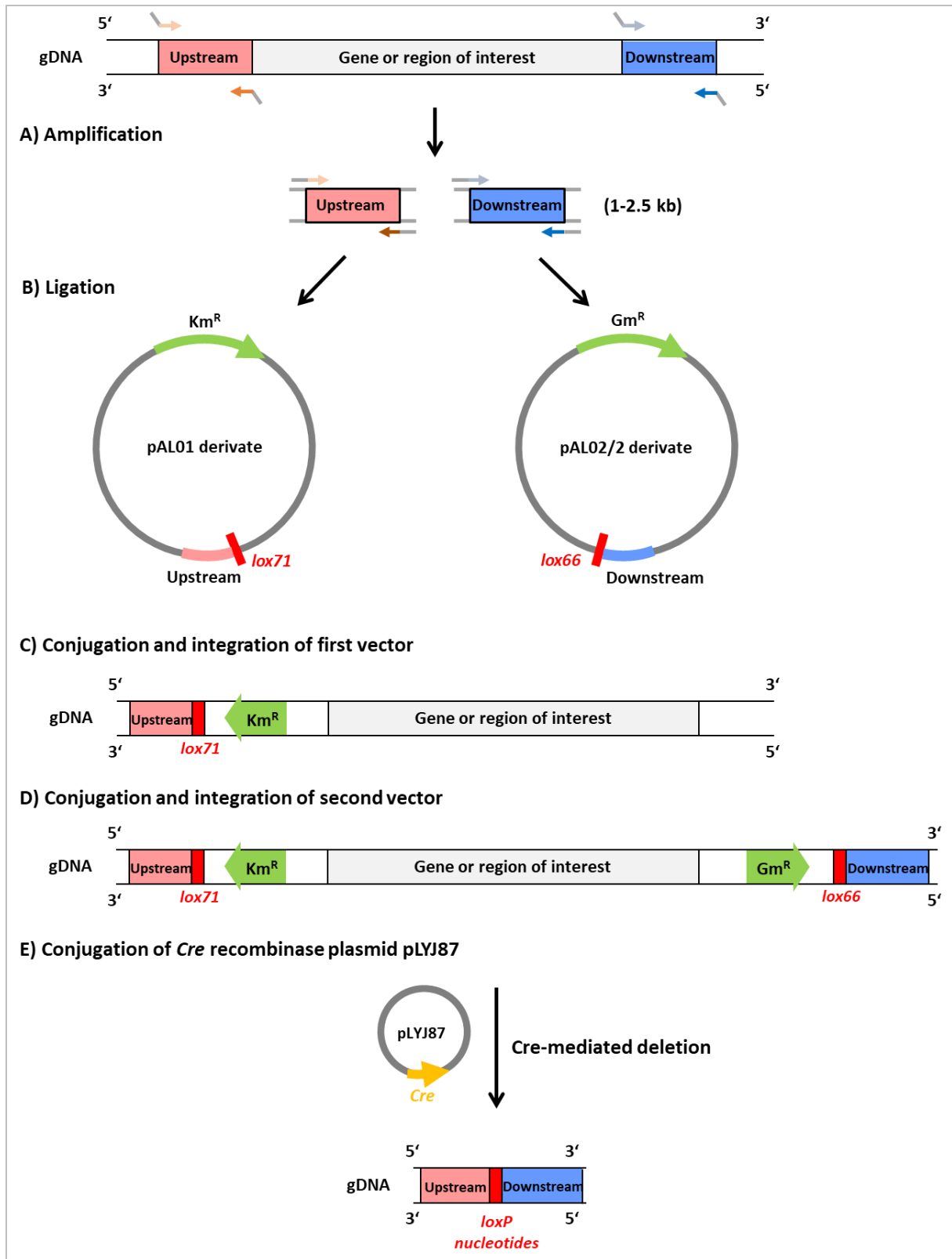
Figure 4. Scheme of the Cre-*lox* based genomic manipulation method (modified after Lohße et al. (2011) [87]). A–B) The up- and downstream region of the deletion target are amplified and ligated into the suicide vectors. **C)** Integration of the first suicide vector containing the *lox71* sequence and a kanamycin resistance cassette (Km^R) as marker. **D)** Next, the second suicide vector containing the *lox66* site and a gentamycin resistance cassette (Gm^R) have to be inserted next to the genomic target by homologous recombination. **E)** Afterwards, conjugation with the

Cre recombinase plasmid pLYJ87 results in Cre-mediated deletion of the target. Only *loxP* nucleotides remain in the genome and the cell has to be cured from the *Cre* recombinase vector.

The second technique for chromosomal deletions is based on allelic replacement by two consecutive homologous recombinations mediated by RecA and counterselected by lethal galactokinase GalK, and is so far only used for smaller deletions (<20 kb) [104]. After construction of one single suicide vector (Fig. 5A–C), the latter is integrated up- or downstream of the gene or region of interest by the first homologous recombination event (Fig. 5D). The second homologous recombination is carried out after induction of a promotor for the expression of the galactokinase gene (*galK*). The respective enzyme catalyses the phosphorylation of galactose, and since *M. gryphiswaldense* is unable to metabolize galactose-phosphate, it accumulates to toxic levels inside the cell. Hence, only cells that excised the plasmid by a second RecA-mediated homologous recombination can survive, thereby either reconstituting to the WT or resulting in the desired deletion mutant (Fig. 5E).

Figure 5. Schematic illustration of pORFM-GalK-based markerless *in-frame* gene deletion (modified after F. Müller, unpublished). Deletion is performed by two homologous recombination events mediated by RecA and counterselected using the suicide gene *galK* that encodes a galactokinase with lethal activity [104].

A) Amplification of the up- and downstream regions of the gene or region of interest (ROI). **B)** Fusion of the up- and downstream regions of ROI through overlap PCR. **C)** Ligation of the PCR product into the multiple cloning site (MCS) of the pORFM-GalK vector. **D)*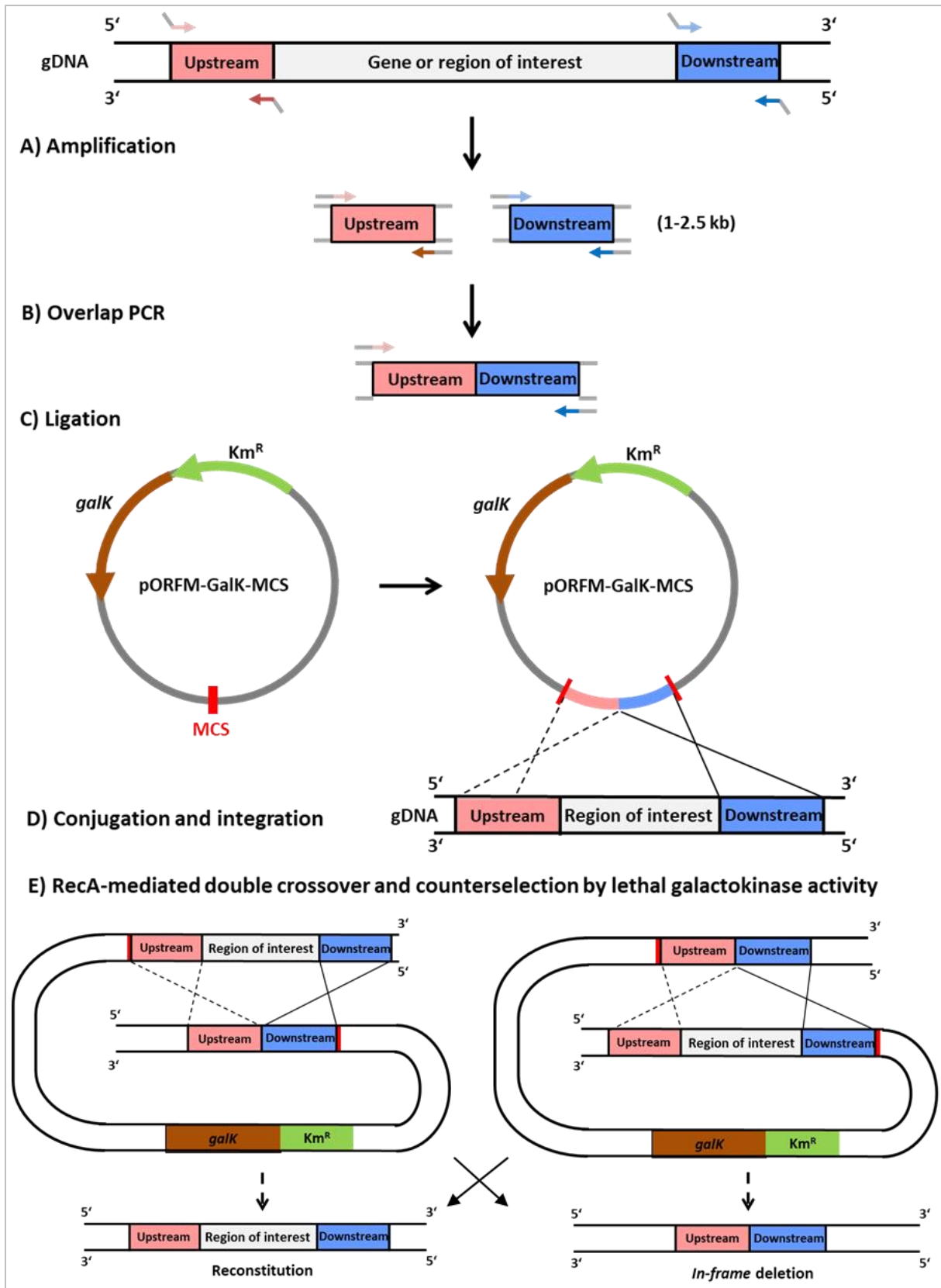* Conjugation into different *M. gryphiswaldense* strains and integration of the plasmid into the genome through homologous recombination. **E)** A second recombination event causes a positive *in-frame* ROI deletion enforced by GalK, or the reconstitution to the WT.

The allelic replacement method requires only one vector and takes advantage of the counterselection of the vector excision by double-crossover, resulting in scarless deletions. However, this method has so far been employed only for the deletion of smaller fragments (<20 kb), but not tested for the excision of larger regions and multiple deletions. It would therefore be highly desirable to evaluate both gene deletion methods with respect to their practicability, efficiency and performance in large-scale mutagenesis and engineering of *M. gryphiswaldense*.

1.6 Genome reduction and engineering of prokaryotic genomes

Since its isolation, the analysis of *M. gryphiswaldense* in the lab and large-scale magnetosome bioproduction is limited due to several adverse features. For example, reproducible cultivation at larger scale has proven difficult because of the rather fastidious and sometimes fluctuating growth. Another unwanted feature is the inherent genetic instability, in particular of the magnetic phenotype and foreign genes, such as chromogenic reporters (e.g. *gusA*) or genetic markers for antibiotic or counterselection (e.g. *galK*). For example, spontaneous rearrangements and deletions within the MAI could be observed during subcultivation of *M. gryphiswaldense*, resulting in weakly or non-magnetic mutants [77, 86, 96]. In addition, unbalanced multicopy expression of the large *mamAB* operon from replicative plasmid is known to be unstable in *M. gryphiswaldense* [95]. For future genetic manipulation and (over)expression of magnetosome or foreign genes, the improvement of genetic stability would be highly beneficial.

In other bacteria, such problems are addressed and often alleviated by large-scale deletions and genome reduction. In most cases, the objective is the improvement of bacterial properties to turn cells into microbial factories. The favourable characteristics displayed by chassis hosts are e.g., genetic stability, robustness against environmental stress, to retain and/or enhance biological fitness (e.g., cell growth), improved protein production, enhanced expression of endogenous and heterologous pathways, and to reduce the content of non-essential genomic

regions [107–115]. Numerous examples of different bacteria with improved features or reduced genomes can be found in the literature (*Escherichia coli*, *Pseudomonas putida*, *Corynebacterium glutamicum*, *Shewanella oneidensis*, *Acinetobacter baylyi*, *Streptomyces avermitilis*, and *Vibrio natriegens*) [109–115]. Thereby, various genes or gene sets, such as prophages, active mobile genetic elements or irrelevant gene clusters were eliminated, resulting in chassis strains with improved properties. For example, deletion of prophage genes in *S. oneidensis* doubled growth yield [116], improved growth and transformation efficiency in *C. glutamicum* [117], enhanced genotypic stability in *P. putida* [113, 114, 118], and increased robustness toward stress in *V. natriegens* [115]. Increased transformability and reduced mutation rates were reached by deleting active mobile genetic elements in *A. baylyi* [119]. Deletion by large-scale genome reduction including non-essential genes and mobile genetic elements resulted in several favourable properties, such as high electroporation efficiency and accurate propagation of recombinant genes in *E. coli* [111]. Efficient production of foreign metabolites was achieved by systematic deletion of non-essential genes in *S. avermitilis* [107]. However, in other examples, deletion of such genes was accompanied by negative effects on cell fitness as described for the elimination of cryptic prophage genes in *E. coli* [109], or during genome minimization in *Bacillus subtilis* [110].

In nature, bacteria adapt to changing conditions by undergoing mutations, i.e. parts of the genome are rearranged. This reorganization of the genome is often driven by active mobile genetic elements. *M. gryphiswaldense* possesses numerous putative mobile genetic elements. During routine genetic manipulation, inactivation of introduced foreign genes by mobile genetic elements could be observed. However, their activity and contribution to the observed instability has not been experimentally tested. Therefore, their systematic analysis (e.g. their location in the genome) would be of high interest, as well as the localization or activity of putative prophage genes and an undefined set of candidates for irrelevant gene clusters. Comparable genome reduction approaches as described above have been impeded due to the unavailability of efficient methods in magnetotactic bacteria. However, it would be of high interest to generate a genome-reduced *M. gryphiswaldense* strain by combinatory deletions including large irrelevant clusters, active mobile genetic elements, and phage-related genes, thereby representing the first proof-of-principle for large-scale engineering of magnetotactic bacteria.

1.7 Scope of this work

This thesis contributed to the SYNTOMAGX project that aims to establish a synthetic biology approach for the magnetization of foreign organisms. Beside the transfer of MAI genes to foreign non-magnetic bacteria, it also aims to set the stage for the future expression of the entire magnetosome biosynthesis pathway from uncultivated MTB producing different magnetosome types in *M. gryphiswaldense* as a host. Thus, the study of genetic and morphologic diversity in *M. gryphiswaldense* will reveal new insights into bacterial magnetosomes biosynthesis. In the research field of magnetotactic bacteria, *M. gryphiswaldense* has emerged as the main model organism for magnetosome biosynthesis and bioproduction. Consequently, it might be used as a future high-yield production host of homologous or heterologous nanocrystals for various biotechnological and biomedical applications.

Previously, it has been assumed that additional, non-magnetosome genes are involved in the biomineralization process [100] and recent evidence argues for the involvement of further auxiliary determinants for magnetosome biosynthesis encoded outside the MAI [120]. In the beginning of this work, putative candidate genes involved in magnetosome biosynthesis outside the MAI have been identified by a systematic genome-wide transposon mutagenesis approach [120]. Therefore, the first aim of my thesis was to identify and evaluate further auxiliary determinants outside the MAI (Fig. 6). By generating 'clean' (i.e., unmarked) deletion mutants the putative role of several candidate genes potentially involved in magnetosome biosynthesis should be verified [120, 121].

Since genetic transfer of MAI genes to non-magnetic, partially closely related microorganisms and other MTB difficult to manipulate failed so far, the second part of this thesis was motivated by the overarching goal to genetically optimize *M. gryphiswaldense*, thereby generating an universal expression host for analysis of foreign and native magnetosome genes and gene clusters. Hence, the second and major aim of this thesis was to engineer *M. gryphiswaldense* for (i) facilitated genetic manipulation, and (ii) to test, whether growth and (iii) genetic stability could be enhanced for more robust and stable growth as well as improved magnetosome biosynthesis in the future (Fig. 6).

To this end, first, two different techniques, a Cre-*lox*-based method, and an allelic replacement method, should be evaluated with respect to their usability and efficiency for large-scale deletions. Second, the boundaries of the MAI and the role of its intervening and adjacent MAI regions had to be interrogated regarding their relevance for magnetosome biosynthesis and cell growth under lab conditions. Third, the native magnetosome island containing putatively irrelevant or problematic gene content should be functionally substituted by a compact cassette

comprising all essential gene clusters for magnetosome biosynthesis. Fourth, it should be investigated whether the deletion of comparable genomic regions/genes or gene clusters, which have been eliminated in other bacterial chassis strains [111, 116], have similar positive effects in *M. gryphiswaldense*.

In summary, in this work a strategy for large-scale genome editing and genetic engineering was established, thereby generating a library of deletion mutants for the future construction of improved 'chassis' strains.
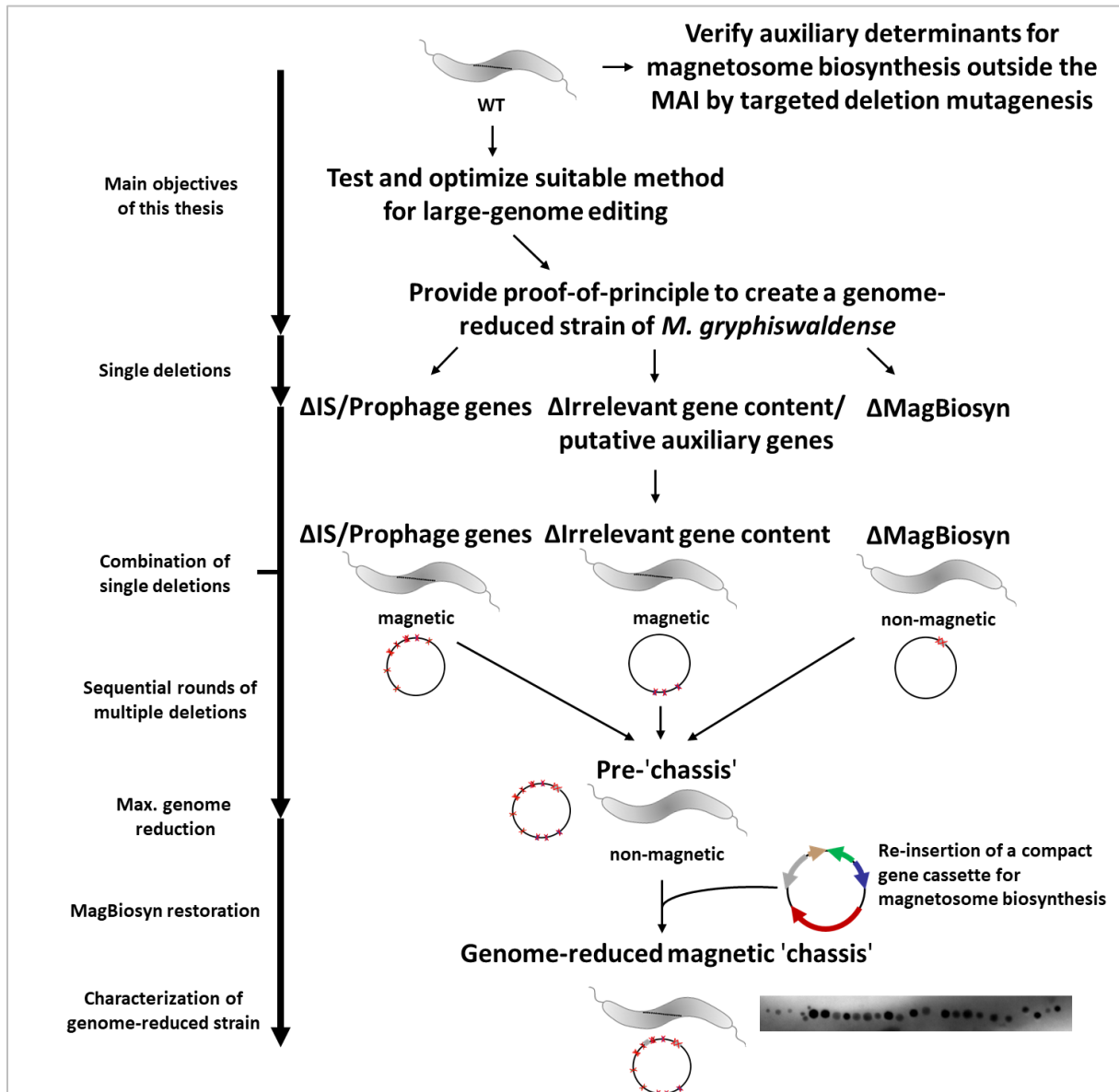
Figure 6. Schematic outline showing the main objectives and general procedures of this thesis. Two methods were evaluated to define a suitable method for large-scale genome editing. Using the favourable method, proof-of-principle is provided for genome streamlining of *M. gryphiswaldense*, thereby generating a genome-reduced strain ('chassis') for further genetic engineering. Additionally, putative auxiliary determinants for magnetosome biosynthesis outside the MAI were analysed. The figure is adapted from Zwiener et al., (2020) [46].

CHAPTER II: Summary of manuscripts and discussion

The overarching aspect of all chapters of this doctoral thesis is the optimization of *M. gryphiswaldense* for the analysis of the native or foreign magnetosome biosynthesis and for future engineering approaches, as well as the improvement of magnetosome biosynthesis in *M. gryphiswaldense*. Three research articles (Chapter IV, V and VI) originate from this thesis as final result. The following sections discuss the key findings of each research article in a general context describing how the obtained results solve questions regarding auxiliary determinants for magnetosome biosynthesis, and how a future *M. gryphiswaldense* chassis strain could be constructed.

Manuscript 1: Genome-wide identification of essential and auxiliary gene sets for magnetosome biosynthesis in *Magnetospirillum gryphiswaldense*

Recently, several studies suggested that auxiliary factors outside the well-characterized MAI gene clusters might be involved in magnetosome biosynthesis. For example, since heterologous reconstruction of magnetosome biosynthesis has only been achieved in *R. rubrum* and *Magnetospirillum* sp. 15-1 [90, 91], further subsidiary determinants outside the MAI might play an important role in magnetosome biosynthesis. So far, auxiliary determinants have mainly been identified by reverse genetics and candidate approaches. In Chapter IV, the first comprehensive transposon mutagenesis study in MTB is delineated. Thereby, about 200 insertants with mild to severe impairment in magnetosome biosynthesis were identified, half of them located outside the MAI. This abundance of putative candidate genes involved in magnetosome biosynthesis required its categorization by genome analysis, which resulted in a priori classification of gene essentiality for the deletion of the most promising genes or gene clusters. Interestingly, consistent with their predicted roles, identified genes are part of general cellular pathways and not MTB-specific. Accessory genes with functions in metabolic pathways like cellular redox balance or iron homeostasis (*nap*, *nirS*, *nirN*, *norC*, *norB*, *fnr*, *cbb3* or *fur*) have recently been documented [94, 97–99, 106, 122, 123]. In the current study, known accessory genes are not only confirmed, but also further putative genes involved in magnetosome biosynthesis revealed, supporting the hypothesis that magnetosome biosynthesis dependents on a specific metabolic profile [124]. Although a conspicuously high number of

false positive clones could be observed, the present data still suggested an indirect or more subtle function of such hit genes in magnetosome biosynthesis.

Transposon mutagenesis has a couple of important limitations. For example, magnetosome phenotypes of mutants might be influenced by potential polar effects on the expression of downstream genes, effects of the Tn5-insertion to only certain domains of the gene products, occurrence of transcriptional readthrough and partially reduced functionality of hit genes by insertion into the terminal region, resulting in false-positive phenotypes. Therefore, verification of Tn5-mutants by 'clean' deletions is needed.

Finally, further auxiliary determinants in unexpected cellular processes like sulfate assimilation, oxidative protein folding, and cytochrome *c* maturation were identified.

My contribution to this research article was to classify mutants hit outside the MAI and to assess the role of the most promising candidates in magnetosome biosynthesis. For verification, targeted deletion of the respective genes was performed. Thereby, *ccmI* (*cycH*) or *dsbB* were eliminated and analysed. CcmI is a tetratricopeptide repeat (TPR)-containing protein, part of the CcmFHI module involved in stereospecific ligation of heme *b* to thiol-reduced apo-cyt *c* and acts as an apo-cyt *c* chaperone. The unmarked *ccmI* deletion mutant was deficient in magnetosome formation, but particle synthesis was not completely abolished. DsbB belongs to the disulfide bond (DSB) pathway of periplasmic oxidative protein folding. A null mutant of *dsbB* (Δ*dsbB*) clearly showed a smaller number of magnetosomes, whereas the size of the particles was not significantly reduced.

Both deletions (Δ*ccmI* and Δ*dsbB*) could verify the observations made during transposon mutagenesis. These included reduced magnetic responses and white colony appearances compared to the WT (brown colonies), thereby confirming phenotypes of both Tn5-mutants.

Beside the above-mentioned identification of new auxiliary determinants for magnetosome biosynthesis (i.e., *ccmI* or *dsbB*), there might be one distinct additional determinant outside the MAI, the putative *urea* operon in *M. gryphiswaldense*. This operon is addressed and discussed in the following sub-chapter, as it had become suspicious in Tn5-mutagenesis several times.

In summary, the documented results successfully cope with the challenge to identify auxiliary determinants. Although 'clean' deletion mutants revealed no severe impairment in magnetosome biosynthesis, the experimental data provided will highly contribute to a better

understanding of the complex process of magnetosome biosynthesis and its involved determinants.

The *M. gryphiswaldense urea* operon is potentially involved in magnetosome biosynthesis

In Silva et al. (2020), a putative urea uptake system became unexpectedly suspicious during Tn5-mutagenesis. Two independent insertants showed reduced magnetic responses, accompanied by white/brown or white colony appearances compared to the WT (brown colonies). For one mutant an insertion into the gene *urtB*, known to be functional in urea uptake was found, while the other insertion occurred inside *urtE* (Fig. 7A, blue arrows). The hit in *urtB* gene showed white colony appearances and the respective cells produced both WT and flake-like magnetosome particles as indicated by TEM. On the contrary, the hit in the *urtE* gene resulted in white and brown colony appearances with WT-like cell phenotypes (Fig. 7B). However, the respective electron micrographs of these Tn5-mutants were only analysed in a qualitative and not in a quantitative manner. Both genes are known to be part of the urea transporter operon in other bacteria and were previously unsuspected to be involved in magnetosome biosynthesis. Prompted by these results their role in magnetosome biosynthesis was further analysed. For example, phenotypes of Tn5-mutants were verified by targeted deletion of the respective genes. In the following, unpublished data are summarized, thereby providing the first potential urea uptake system and its role in magnetosome biosynthesis in *M. gryphiswaldense*.

First, the analysis of the adjacent regions of the genes *urtB* and *urtE* revealed that both genes are part of a ~5.5 kb cluster with five *urt* genes (*urtABCDE*) encoding a putative urea transporter (MSR1_02170–02210). Downstream of this cluster, the putative urease cluster (~5 kb) is located encoding seven *ure* genes (*ureABCDEFG*; MSR1_02100–02160) (Fig. 7A) completing a potential *urea* operon.
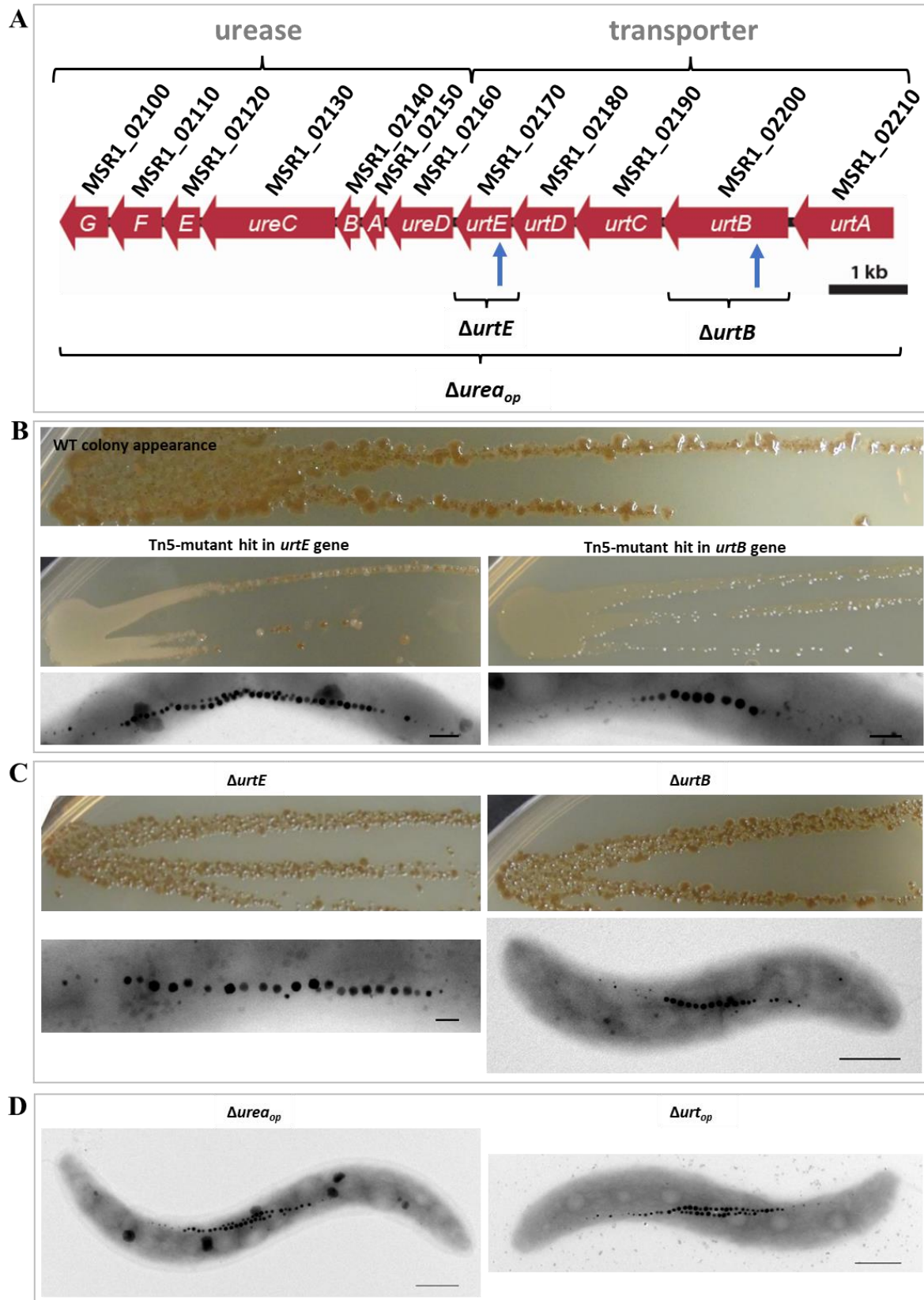
Figure 7. Molecular organization and analysis of the putative *urea* operon in *M. gryphiswaldense*. A) The putative ABC-type transporter is encoded by genes *urtABCDE* (MSR1_02170–02210), while genes *ureABCDEFG* (MSR1_02100–02160) code for the putative urease. During transposon mutagenesis, *urtB* and *urtE* were hit (blue arrows). In addition, the extent of deletion mutants Δ*urtB*, Δ*urtE* and Δ*urea*_op_ are indicated. **B)** Colony appearances

on agar plates containing increased iron concentrations (500 µM versus 50 µM) and medium volume (140 ml versus 100 ml) of WT, Tn5-mutants *urtB* and *urtE*, and TEM micrographs of the respective mutants. Scale bars: 100 nm. **C)** Δ*urtB* and Δ*urtE* mutants exhibit a WT-like colony appearance (regarding colour), and TEM micrographs revealed WT-like magnetosome formation. Scale bars: Δ*urtB*, 500 nm; Δ*urtE*, 100 nm. **D)** TEM micrographs of mutants Δ*urea$_{op}$* (urea operon) and Δ*urt$_{op}$* (urea transporter) indicating WT-like magnetosome formation. Scale bars: 500 nm.

In nature, a diversity of organisms excretes urea into the environment, making it available as nitrogen source for bacteria. Urea is a small and uncharged molecule that can pass the bacterial membrane, but is often taken up by energy-dependent transport systems [125]. An ABC-type (ATP-binding cassette) transporter, encoded by the *urt* operon, is part of the urea uptake system and catalyses the ATP-driven, energy-dependent transport of urea from the environment into the cell [125–127]. The expression of this *urt* operon could be regulated, for instance, in response to nitrogen limitation in *C. glutamicum* and *Cyanobacteria* [126–130]. After import into the cell, urea (CH_4N_2O) as a nitrogenous compound is hydrolysed in the cell to two ammonia (NH_3) and one carbonic acid (H_2CO_3) molecule via the formation of carbamic acid (H_3CNO_2) by the cytoplasmic enzyme urease (urea amidohydrolase) (Fig. 8) [131, 132].
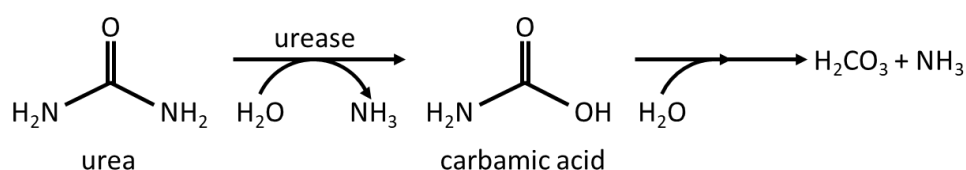
Figure 8. Urea decomposition pathway. Urea (CH_4N_2O) is hydrolysed in two ammonia (NH_3) and one carbonic acid molecule (H_2CO_3) via the formation of carbamic acid (H_3CNO_2) by the cytoplasmic enzyme urease. Modified from Sigurdarson et al. (2018) [131].

This key enzyme of the global nitrogen cycle was the first enzyme to be crystallized [133]. It represents a multi-subunit complex composed of three subunits named α, β and γ, which are mostly organized in heterotrimers [134, 135]. Bacterial urease operons (*ure*) encode regulatory, structural, and accessory genes that vary in its genetic organization [132, 136]. Urease-producing bacteria are called ureolytic. They can be found in nearly all ecosystems and include anaerobic, micro-aerophilic, and aerobic microorganisms [137]. One of the most intensively studied ureolytic bacterium is *Sporosarcina pasteurii*, which synthesizes the subunits UreA, UreB and UreC of the urease main structure. The latter are functional in amino acid transport and metabolism, while UreD, UreE and UreF represent essential urease accessory proteins assigned to post-translational modification, protein turnover and chaperons [137]. While *S. pasteurii* produces urease constitutively, other organisms like *C. glutamicum* strictly regulate

the expression of urease genes in response to environmental or intracellular stimuli, such as substrate availability, growth phase, nitrogen status, or pH [131, 138, 139]. For example, as for the expression of the *urt* operon, transcription of the *ure* gene cluster could be controlled in response to nitrogen starvation in *C. glutamicum* [125]. Furthermore, it has also been reported that urease expression can be iron-repressed by the transcriptional regulator Fur in response to iron restriction in *Helicobacter hepaticus* [139].

In *M. gryphiswaldense*, verification of Tn5-mutants by 'clean' deletions of genes hit by Tn5-mutagenesis was needed. Therefore, unmarked deletion mutants of *urtB*, *urtE* and the whole *urea*$_{op}$ ($\Delta urtB$, $\Delta urtE$ and $\Delta urea_{op}$; Fig 7A) were generated. However, in contrast to Tn5-mutants, null mutants indicated no reduced magnetic response or differences in colony appearances compared to the WT (Fig. 7C), and TEM micrographs of $\Delta urtB$, $\Delta urtE$ and $\Delta urea_{op}$ deletion mutants showed WT-like magnetosome formation (Fig. 7D).

Next, it was investigated whether the WT strain and the $\Delta urea_{op}$ deletion mutant were able to grow on urea instead of sodium nitrate as nitrogen source under different urea concentrations and aerobic conditions. For that purpose, sodium nitrate was replaced by 0–1 mM urea, (Fig. 9A). As result, the WT showed urea-dependent growth, which increased with increasing urea concentrations up to about 0.5 mM (Fig. 9A). These findings resembled results found in other bacteria like the microbially induced calcite precipitation (MICP) mineralized in *S. pasteurii* that showed enhanced cell growth on urea containing medium [137]. The same conditions were used to analyse mutant strains. As expected, the *M. gryphiswaldense* mutant $\Delta urea_{op}$ was unable to utilize urea in the medium and compared to the WT grew to lower cell densities under different urea concentrations (Fig. 9A).

To further analyse the influence of urea-dependent growth with regard to magnetosome biosynthesis, WT cells were grown at different urea concentrations and analysed by TEM. Interestingly, micrographs revealed various magnetosome phenotypes e.g., WT-like or smaller magnetosomes, and flake-like particles in contrast to cells grown with NO_3^- or NH_4^+ (Fig. 9B). Hence, urea degradation might interfere with magnetite biomineralization and the energy-consuming process of magnetosome biosynthesis. Furthermore, the variation in environmental parameters like a pH shift during urea degradation might influence magnetosome formation (pH effects on cell growth have been described before) [131, 140].
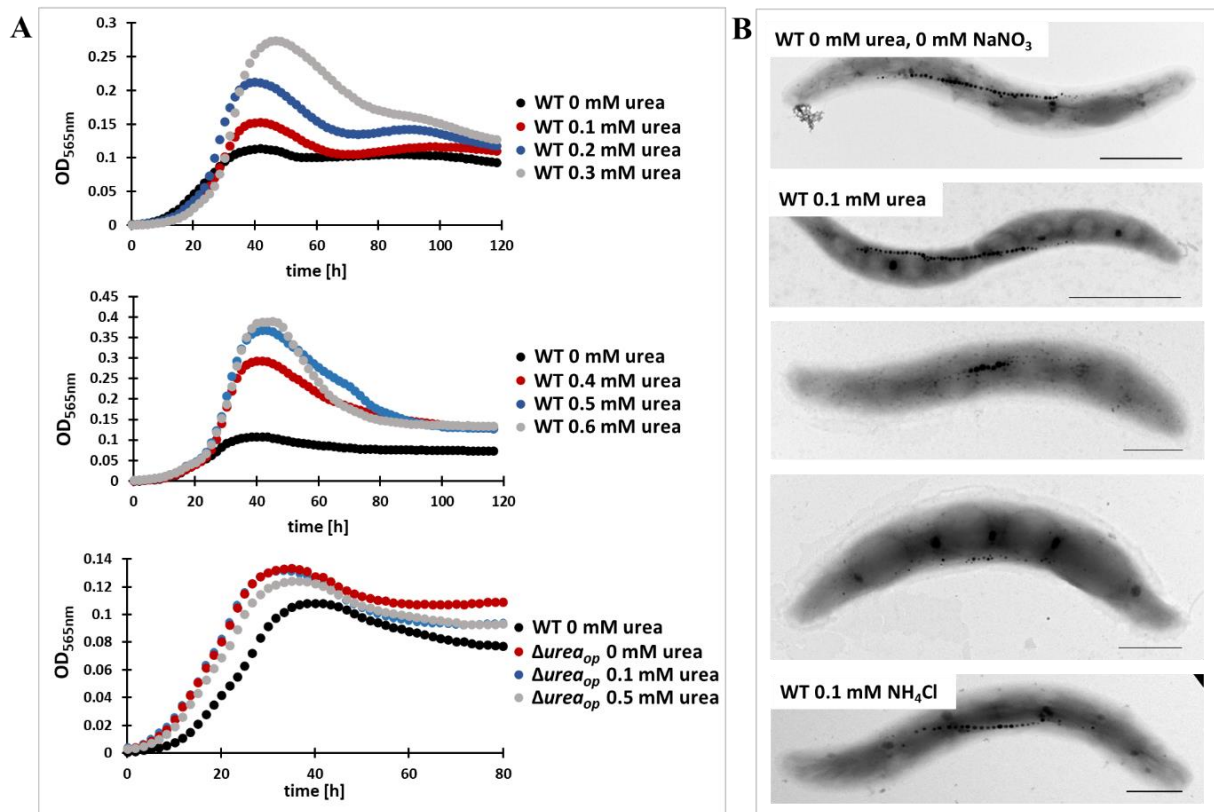
Figure 9. Phenotypic characterization of *M. gryphiswaldense* WT and the Δ*urea$_{op}$* mutant strain grown under different nitrogen sources. A) Growth profiles of the WT and Δ*urea$_{op}$*, cultures grown at different urea concentrations and 1 g peptone. Growth experiments were performed at 28°C under aerobic conditions. Each strain was analysed in triplicates (the curves show the calculated average; standard deviations <5%). **B)** Electron micrographs of the WT grown without urea and sodium nitrate indicated WT-like magnetosome formation. TEM micrographs of WT cells grown at different urea concentrations and aerobic conditions showed various magnetosome phenotypes, exemplary shown on 0.1 mM urea. WT cells grown in ammonium medium (NH$_4$Cl) exhibited WT-like magnetosome phenotypes. Scale bars: 500 nm.

Although no phenotype regarding magnetosome formation (e.g. number or shape) was observed upon deletion, a second site mutation in Tn5-mutants is rather unlikely since in the respective mutants two independent genes were hit during transposon mutagenesis. Selection of a suppressor mutation might be a possible explanation. Thus, the inactivation of the urease operon might be harmful to cells, which consequently show growth deficiencies. However, a second mutation in another gene might alleviate or revert the phenotypic effect of the already existing mutation. In contrast to this hypothesis, no link between urea degradation and magnetosome formation could be found so far.

Overall, the obtained data make it difficult to draw any conclusions how the *urea* operon of *M. gryphiswaldense* is involved in magnetosome formation. Since two independent genes in the *urea* operon were hit, a role in magnetosome biosynthesis could neither be confirmed nor

excluded so far. Future follow-up experiments, such as investigations regarding the influence of the pH during urea-dependent growth on magnetosome biosynthesis, are therefore required.

Manuscript 2: Identification and elimination of genomic regions irrelevant for magnetosome biosynthesis by large-scale deletion in *Magnetospirillum gryphiswaldense*

Chapter V demonstrates that the RecA-based method using GalK-counterselection is suitable for the efficient large-scale mutagenesis in *M. gryphiswaldense* by analysing 24 deletions covering about 167 kb of non-redundant genome content. By deletion and replacement of the MAI and adjacent regions, it could be shown that a contiguous stretch of ~100 kb can be deleted by allelic replacement. Thereby, 13 successful and four non-deletable targets enabled the identification of new boundaries of the MAI as well as further regions irrelevant for magnetosome biosynthesis and cellular growth. It was also shown that the MAI can be substituted by a compact magnetosome expression cassette comprising solely all essential biosynthetic gene clusters, but devoid of irrelevant or problematic gene content. Overall, 24 deletion mutants showed that the homologous recombination with *galK* as selection marker provides the most efficient and powerful tool for genome manipulation in *M. gryphiswaldense* at the current state of knowledge, and cope with the aim of this thesis to improve genetic manipulation.

Previously, two different techniques, a Cre-*lox*-based and an allelic replacement method based on homologous recombination were developed for deletion mutagenesis in *M. gryphiswaldense* [87, 103, 104]. The Cre-*lox*-based method enabled deletions up to ~53 kb, while the RecA-based method using GalK-counterselection could be used for the excisions of up to 20 kb [87, 103]. Further genetic techniques for large-scale genome engineering of magnetic bacteria are still limited. Thus, both methods were compared regarding their suitability for the deletion of large genomic fragments inside and outside the MAI of *M. gryphiswaldense*. Excluding time for cloning, the Cre-*lox* based method proved to be more time-consuming as the three consecutive cycles of laborious conjugation, plate growth, clonal selection, screening, and PCR-verification needed up to six weeks, whereas excisions by double-crossovers were typically obtained in only about three weeks. In addition, using Cre-*lox* based method, *loxP* nucleotides remain in the genomic target region as so-called 'scars', while the allelic replacement method resulted in scarless deletions. Therefore, the RecA-based technique using GalK-counterselection was identified as most efficient for large-scale mutagenesis in *M. gryphiswaldense*.

Interestingly, occasionally false positive clones were frequently obtained during the deletion process, in particular for difficult or essential targets. These clones did not lose their kanamycin resistance and hence, were still harbouring the suicide vector. This phenomenon was accompanied by inactivation of GalK and its lethal activity due to spontaneous IS insertions into its respective gene allowing illegitimate recombination. However, this observation was not surprising since such findings have also been made for the *sacB* gene of entrapment vectors during mutagenesis of *B. subtilis* and others [141], and assisted to later identify the majority of active mobile genetic elements in *M. gryphiswaldense* (*ISMgr2* and *tn-tandems*). Using *galK* as selection marker decreased the number of false positive clones observed for *sacB* counterselection in *M. gryphiswaldense* [142, 104].

Since the MAI is known for the genomic instability of its biosynthetic gene clusters, all key magnetosome biosynthesis genes and a large region with no function in magnetosome biosynthesis spanning ~73 kb could be eliminated and replaced by a compact and contiguous ~38 kb cassette comprising solely the essential biosynthetic gene clusters, but devoid of irrelevant or problematic gene content. During these sequential deletions, strain ΔM13 featured the largest deletion, i.e. a contiguous stretch of ~100 kb was deleted, thereby defining new boundaries of the MAI.

Next, the role of candidate genes with putative roles during magnetosome biosynthesis located outside the MAI was assessed. One group of these candidates was recently retrieved by genome-wide transposon mutagenesis, in which a colony appearance deviant from the dark-brown color of the WT served as a proxy for impaired magnetosome biomineralization [120]. Another category was comprised of candidate genes, whose gene products were found to be genuinely associated with magnetosome particles purified from disrupted *M. gryphiswaldense* cells [100]. Most interesting targets for mutagenesis were further selected based on their conservation in other *Magnetospirilla* and/or a conspicuous genomic neighborhood.

Ten null mutants were generated for 23 genes which became suspicious because (i) they are conserved in other MTB, (ii) have a genetic context with putative function in magnetosome biosynthesis, (iii) the genes located in the neighborhood of Tn-hits or genes were found by proteomics respectively and/or (iv) Tn-hits or products were found to be associated with the magnetosome membrane by proteomics. Identified genes had predicted functions related to the TonB-system, cell wall biosynthesis as well as hypothetical functions and putative transmembrane proteins of respective genes with unknown functions. Some mutants (Δ*msr1_20490*, Δ*msr1_30910–30940*, and Δ*msr1_30840*) displayed a slightly reduced C*mag*

(<1) compared to WT-levels with values of 1–2. However, TEM analysis revealed the formation of magnetosomes that were apparently indistinguishable from the WT with respect to number, size, shape, and alignment in the mutants Δ*msr1_17870–17940*, Δ*msr1_20490*, Δ*msr1_24180*, Δ*msr1_30910–30940*, Δ*msr1_33570* and Δ*msr1_33770*. The observed reduced C$_{mag}$ value is likely due to subtle differences in cell shape and/or cell surface, rather than direct effects on magnetosome biosynthesis. Putative candidates identified by proteomics might be indeed involved in magnetosome biosynthesis, but their function might be only required in conditions not tested in this study or can be substituted by other magnetosome proteins. Hence, contrary to the hypothesis, none of candidates play an obvious or strong role in magnetosome biosynthesis under the conditions tested.

Manuscript 3: Towards a 'chassis' for bacterial magnetosome biosynthesis: genome streamlining of *Magnetospirillum gryphiswaldense* by multiple deletions

For a certain number of bacteria, moderate genome reduction has been shown to streamline metabolic pathways, to enhance the expression of recombinant proteins, the physiological performance, and/or cell growth [112–119, 143]. In the research field of magnetotactic bacteria, *M. gryphiswaldense* has emerged as the main model organism for magnetosome biosynthesis and magnetosome bioproduction. The latter would benefit from a genome-streamlined *M. gryphiswaldense* host that enables stable high-yield magnetosome production.

In Chapter VI, the first approach for genome streamlining of *M. gryphiswaldense* by combination of multiple scarless deletions of non-overlapping ~227,600 bp is described, resulting in a strain with a nearly 5.5% reduced genome content.

First, seven putative prophage regions were identified and a partial set of prophages as well as putative capsid genes, integrases, excisionases and a recombinase gene (*hin2*) were deleted separately. Growth of all deletants was largely indistinguishable from the WT. Using mitomycin C (MMC) that triggers the cellular SOS response and is known to induce prophages to enter the lytic cycle, only the *hin2* mutant proved to be less sensitive compared to WT and could be re-grown after MMC-treatment. These results differ from examples of prophage gene deletion in other bacteria, which doubled growth yield [116] or improved growth and transformation efficiency in *C. glutamicum* [117]. However, these results are similar to the observed increased robustness toward stress in *V. natriegens* [115]. Growth under non-stress conditions indicated mostly neutral effects in *M. gryphiswaldense*, which is accompanied by negative effects on cell fitness as described for the elimination of cryptic prophage genes in *E. coli* [109].

Second, during routine genetic manipulation, two types of active mobile genetic elements each with two variants (*ISMgr2* and *tn-tandems*) were identified in an 'IS-trap'-screen by using *gusA* or *galK* as reporters in *M. gryphiswaldense*. The first type is a bipartite insertion element referred to as *ISMgr2* (*ISMgr2-1*, *ISMgr2-2* and *ISMgr2-3*) with 99.8% protein identity. Two additional homologs of *tnpB*, termed *ISMgr2-tnpB-hyp-1* and *ISMgr2-tnpB-hyp-2,* with lower protein identity (20.8%) were identified. The second type of active mobile elements is represented by a transposon tandem (*tn-tandem*) present in the genome of *M. gryphiswaldense*

in 19 identical (100% nt) copies. In addition, one of the transposons, *tn2* alone is found in two more identical single copies. Single deletion mutants of *ISMgr2-1*, *ISMgr2-2*, *ISMgr2-3*, *ISMgr2-tnpB-hyp-1* and *ISMgr2-tnpB-hyp-2* displayed WT-like growth and magnetosome biosynthesis under lab growth and stress conditions.

Third, further large genomic regions irrelevant for cell growth under lab conditions and magnetosome biosynthesis, such as a putative *pks* (polyketide synthase) and *nif* (likely linked to nitrogen fixation) cluster were identified and deleted.

Previously tested favourable or neutral deletions were combined in sixteen subsequent rounds of deletion. The final strains ΔTZ-16 (lacking ~3.49% of the WT genome) and ΔTZ-17 (lacking ~5.48%) were devoid of selected large irrelevant gene clusters, mobile genetic elements, as well as phage-related and native MAI genes, which were substituted by a compact cassette comprising all key magnetosome biosynthetic genes. Both strains indicated WT-like growth and magnetosome production. However, when challenged with MMC, growth performance proved to be less sensitive compared to the WT and both strains were re-grown after MMC-treatment due to the loss of *hin2*.

In the genome of *M. gryphiswaldense* about 140 predicted mobile genetic elements, of which 38 reside within the MAI, were identified so far. Interestingly, the MAI harbours one copy of *ISMgr2* and four copies of *tn-tandems*, which were found to be the most active mobile genetic elements in *M. gryphiswaldense*. The stability of the MAI in the final strains was tested by evaluating the stability of the reporter gene *gusA* and the magnetic phenotype, and furthermore compared to the WT. In fact, the genetic stability of the magnetic phenotype seemed to be more robust compared to the WT. This result resembles observations made in *A. baylyi*, in which reduced mutation rates by deleting active mobile genetic elements were described [119].

However, by genome sequencing in the final strain an additional copy of the active IS element *ISMgr2* was located on a new genomic position in *M. gryphiswaldense* indicating recent activity, i.e. transposition to a new location, during manipulation. This is a known phenomenon of active mobile genetic elements that is also found e.g., in genome-reduced *E. coli* [111], making the deletion of all active mobile genetic elements in *M. gryphiswaldense* even more difficult.

In conclusion, this study represents the first proof-of-principle for the genomic streamlining of magnetotactic bacteria, providing a library of genome-reduced strains which might be used to

generate further strains in different combinations to turn *M. gryphiswaldense* into a chassis for stable and high-yield production of magnetic nanoparticles in the future.

CHAPTER III: Final Conclusion and Future Perspectives

The aims of this thesis were (i) to identify further auxiliary determinants for magnetosome biosynthesis outside the MAI, (ii) to establish an efficient method for large-scale engineering and (iii) to provide and investigate a proof-of-principle approach for genome streamlining of *M. gryphiswaldense*. Further putative auxiliary genes for magnetosome biosynthesis were identified. Although many of them were falsified, the results still suggest that the basis for magnetosome biosynthesis is prepared by a more general metabolic network rather than by specific single genes. An interesting candidate for future research might be the *urea* operon, which despite of ambiguous results has to be analysed in more detail.

In addition, in this thesis the RecA-based method using the GalK-counterselection system was found to be the most efficient method for *M. gryphiswaldense*. However, it still has limitations; for example, the allelic replacement technique is time-consuming and the deletion of all multiple copies of identified active mobile genetic elements as well as the *tn-tandems* is currently not within a realistic range due to the numerous abundances and extensive sequence similarity between individual copies and their persistent tendency to spread during genetic manipulation. Therefore, development of more advanced gene editing technologies, like CRISPR/Cas9-based methods [144] or Multiplex Automated Genomic Engineering (MAGE) [144–152], might overcome the mentioned limitations for further studies on MTB as already shown for other microorganisms like *Streptococcus pneumoniae* and *E. coli* [144]. For example, such a method might be used in future approaches to delete multiple genes of active mobile genetic elements like *tn-tandems*, thereby improving the genetic stability of the *M. gryphiswaldense* genome.

Furthermore, ongoing IS activity was found in the course of genetic manipulation as an unexpected copy of the active IS element *ISMgr2* was inserted into a new genomic location by transposition. However, genetic stability assays of the final strains also indicated that its combinatory deletion enhances genetic stability. In addition, deletion of further genetic 'junk' and the substitution of native magnetosome clusters by a compact cassette might contribute to an enhanced genetic stability.

In this thesis, I also documented the first proof-of-principle to construct a genome-reduced magnetotactic strain as microbial cell factory. Most deletions (putative prophage genes, large irrelevant gene clusters, MAI interspacing regions) were found to be neutral with respect to

magnetosome biosynthesis and cell growth. Deletion of the recombinase gene *hin2* showed an effect by a slightly improved resilience to mitomycin C (MMC)-induced stress.

Genetic transfer of MAI genes to non-magnetic bacteria has only succeeded in two instances, for *R. rubrum* and *Magnetospirillum* sp. 15-1, but failed for many other (closely) related microorganisms [90, 91]. Since the genetic manipulation techniques for magnetotactic bacteria are still limited, it is of high interest to use *M. gryphiswaldense* as a host for homologous and heterologous magnetosome gene expression and high-yield production of magnetic nanoparticles. In future approaches of engineering genome-reduced strains, it should be focussed on the improvement of the genetic stability to turn *M. gryphiswaldense* into a stable, high-yield magnetosome production strain. Therefore, identified active transposable elements (*ISMgr2*) should be eliminated. Deletion of *tn-tandems* with high abundances and extensive sequence similarity between multiple copies might also enhance genetic stability of the genome in *M. gryphiswaldense*. To this end, genetic manipulation techniques should be improved as already described. Furthermore, the ~100 kb region (ΔM13) of MAI genes and its interspacing and adjacent regions as well as the *feoAB1*$_{op}$ should be deleted and replaced by a compact cassette that contains all magnetosome genes, thereby avoiding unnecessary genetic instability of the MAI. In addition, it would be interesting to analyse whether the compact MAI cassette is more stable at locations more distant from known active mobile genetic elements. Variations in the mutation rates with greater instability at locations that are closer to active genetic elements were e.g. measured in an *A. baylyi* mutant [119].

Deletion of prophage genes or irrelevant gene clusters seems to be less important for a future engineered strain, since the neutral or positive effects might not be relevant for reaching high cell densities or for high-yield magnetosome production in a bioreactor under controlled anaerobic conditions. However, it might be interesting to analyse the effects of deleting further prophage genes still residing in the genome of the respective final strains like the putative prophage genes of P6.

In preliminary experiments performed in the final part of this thesis, conjugation experiments of a *hsdR* null mutant were performed. HsdR is part of a DNA restriction modification system in *M. gryphiswaldense*. Preliminary results derived from conjugation experiments suggested improved conjugation efficiencies upon *hsdR* deletion compared to the WT. It might therefore be promising to introduce this deletion as Martínez-García et al. (2014) described a strain that tolerated acquired and replicated exogenous DNA by the complete deletion of the *hsdRMS* genes in *P. putida* [113].

Aside from deleting active mobile genetic elements, a higher genetic stability of the *M. gryphiswaldense* genome was achieved by the additional deletion of *recA*, as it has been shown recently [96]. However, *recA* deletion resulted in decelerated cell growth, which might be overcome by introducing an inducible *recA*-system followed by the targeted deletion of the endogenous *recA* in *M. gryphiswaldense*, thereby allowing a strictly controlled *recA* expression as it has been shown in *B. subtilis* [152].

For high-yield magnetosome production, magnetosome biosynthesis genes might be overexpressed by the insertion of two or three compact magnetosome biosynthesis cassettes, comparable to approaches reported by Lohße et al. (2016) [95]. The introduction of optimized, stronger or inducible promotors might even enhance expression levels.

Interestingly, large-scale genome reduction did not enhance cell growth of *M. gryphiswaldense*. It is unknown whether the selected genes were inappropriate or the wrong candidates to reach a detectable result. Alternatively, the number of identified factors or their proportion of the genome might not have been sufficient. The magnetotactic bacterium *M. gryphiswaldense* could be genome-reduced by ~5.5%. In other bacteria much larger parts (up to 15% of the genome) had to be eliminated for favourable effects [111, 112]. However, the risk of detrimental effects on robust cell growth simultaneously increases caused by the deletion of genes with essential functions. Generating a genome-reduced strain without unfavourable effects on cell growth is not trivial and has been shown e.g., for *E. coli* [111, 153] and *C. glutamicum* [112]. Further studies describe deletions of irrelevant gene clusters, transposable elements and phage-related genes resulting in enhanced cell growth [113, 119, 143]. The genome-streamlined *M. gryphiswaldense* described in this thesis successfully copes with the challenge to retain WT-like growth despite its tremendous genome reduction. The aim to engineer *M. gryphiswaldense* for improved, more robust, and stable growth will be subject of future studies. However, obtained final strains did not show compromised cell growth as it was observed for other genome-reduced strains [109, 110, 112, 119] and hence, no essential genes or genes with additive effects were eliminated during combinatory deletions.

Overall, the findings of this thesis will further contribute to domestication and large-scale engineering of *M. gryphiswaldense* and other magnetotactic bacteria. Future expansion of this work is in progress and might result in improved chassis strains and may turn *M. gryphiswaldense* into a versatile platform and microbial cell factory for synthetic biology and magnetosome production.

REFERENCES

1. Bellini S. Further studies on "magnetosensitive bacteria". Chinese J of Oceanol and Limnol 2009a. 27:6–12.

2. Bellini S. On a unique behavior of freshwater bacteria. Chinese J of Oceanol and Limnol 2009b. 27:3–5.

3. Blakemore R. Magnetotactic bacteria. Science 1975. 190:377–379.

4. Frankel RB. Magnetic guidance of organisms. Annu Rev Biophys Bioeng 1984. 13:85–103.

5. Bazylinski DA. Controlled biomineralization of magnetic minerals by magnetotactic bacteria. Abstracts of Papers of the American Chemical Society 1995. 209(APR):92–GEOC.

6. Bazylinski DA, Moskowitz BM. Microbial biomineralization of magnetic iron minerals: microbiology, Magnetism; and environmental significance. In: Banfield J.F., Nealson K.H. (eds) Geomicrobiology: interactions between microbes and minerals (Rev Mineral Vol 35). Mineralogical Society of America, Washington, DC 1997:181–223.

7. Frankel RB, Bazylinski DA, Johnson MS, Taylor BL. Magneto-Aerotaxis in marine coccoid bacteria. Biophy J 1997. 73(2):994–1000.

8. Simmons SL, Sievert SM, Frankel RB, Bazylinski DA, Edwards KJ. Spatiotemporal distribution of marine magnetotactic bacteria in a seasonally stratified coastal salt pond. Appl Environ Microbiol 2004. 70:6230–6239.

9. Lefèvre CT, Bazylinski DA. Ecology, diversity, and evolution of magnetotactic bacteria. Microbiol Mol Biol Rev 2013. 77(3):497–526.

10. Kolinko S, Richter M, Glöckner F-O, Brachmann A, Schüler D. Single-cell genomics reveals potential for magnetite and greigite biomineralization in an uncultivated multicellular magnetotactic prokaryote. Environ Microbiol Rep 2014. 6:524–531.

11. Kolinko S, Richter M, Glöckner F-O, Brachmann A, Schüler D. Single-cell genomics of uncultivated deep-branching magnetotactic bacteria reveals a conserved set of magnetosome genes. Environ Microbiol 2015. 18:21–37.

12. Kolinko S, Wanner G, Katzmann E, Kiemer F, Fuchs BM, Schüler D. Clone libraries and single cell genome amplification reveal extended diversity of uncultivated magnetotactic bacteria from marine and freshwater environments. Environ Microbiol 2013. 15:1290–1301.

13. Kolinko S, Jogler C, Katzmann E, Wanner G, Peplies J, Schüler D. Single-cell analysis reveals a novel uncultivated magnetotactic bacterium within the candidate division OP3. Environ Microbiol 2012. 14:1709–1721.

14. Lin W, Li J, Pan Y. Newly isolated but uncultivated magnetotactic bacterium of the phylum Nitrospirae from Beijing, China. Appl Environ Microbiol 2012. 78:668–675.

15. Lin W, Pan Y. A putative greigite-type magnetosome gene cluster from the candidate phylum Latescibacteria. Environ Microbiol Rep 2015. 7:237–242.

16. Lin W, Pan Y, Bazylinski DA. Diversity and ecology of and biomineralization by magnetotactic bacteria. Environ Microbiol Rep 2017. 9:345–356.

17. Schüler D, Frankel R. Bacterial magnetosomes: microbiology, biomineralization and biotechnological applications. Appl Microbiol Biotechnol 1999. 52:464–473.

18. Jogler C, Kube M, Schübbe S, Ullrich S, Teeling H, Bazylinski DA, Reinhardt R, Schüler D. Comparative analysis of magnetosome gene clusters in magnetotactic bacteria provides further evidence for horizontal gene transfer. Environ Microbiol 2009.11:1267–77.

19. Delong EF, Frankel RB, Bazylinski DA. Multiple evolutionary origins of magnetotaxis in bacteria. Science 1993. 259:803–6.

20. Flies CB, Peplies J, Schüler D. Combined approach for characterization of uncultivated magnetotactic bacteria from various aquatic environments. Appl Environ Microbiol 2005. 71:2723–31.

21. Rodgers FG, Blakemore RP, Blakemore NA, Frankel RB, Bazylinski DA, Maratea D, Rodgers C. Intercellular structure in a many-celled magnetotactic prokaryote. Arch Microbiol 1990. 154:18–22.

22. Pósfai M, Lefevre CT, Trubitsyn D, Bazylinski DA, Frankel RB. Phylogenetic significance of composition and crystal morphology of magnetosome minerals. Front Microbiol 2013. 4:344.

23. Bazylinski DA, Frankel RB. Magnetosome formation in prokaryotes. Nat Rev Microbiol 2004. 2:217–230.

24. Faivre D, Schüler D. Magnetotactic bacteria and magnetosomes. Chem Rev 2008. 108:4875–4898.

25. Müller F, Schüler D, Pfeiffer D. A compass to boost navigation – Cell biology of bacterial magnetotaxis. J Bacteriol 2020. 202(21):e00398-20.

26. Farina M, Esquivel D, Lins de Barros H. Magnetic iron-sulphur crystals from a magnetotactic microorganism. Nature 1990. 343:256–258.

27. Mann S, Sparks NHC, Frankel R, Bazlinski DA, Jannasch HW. Biomineralization of ferrimagnetic greigite (Fe_3S_4) and iron pyrite (FeS_2) in a magnetotactic bacterium. Nature 1990. 343:258–261.

28. Frankel RB, Blakemore RP, Wolfe RS. Magnetite in freshwater magnetotactic bacteria. Science 1979. 203:1355–1356.

29. Schüler D. Versuche zur Isolierung und Charakterisierung magnetotaktischer Bakterien. Diplomarbeit, Ernst-Moritz-Arndt Universität Greifswald. 1990.

30. Schüler D. *Doctoral thesis*: Isolierung und Charakterisierung magnetischer Bakterien - Untersuchungen zur Magnetitbiomineralisation in *Magnetospirillum gryphiswaldense*. Technische Universität, München. 1994.

31. Schüler D, Köhler M. The isolation of a new magnetic spirillum. Zentralblatt Mikrobiologie 1992. 147:150–151.

32. Uebe R, Schüler D. Magnetosome biogenesis in magnetotactic bacteria. Nat Rev Microbiol 2016. 14:621–637.

33. Jogler C, Wanner G, Kolinko S, Niebler M, Amann R, Petersen N, Kube M, Reinhardt R, Schüler D. Conservation of proteobacterial magnetosome genes and structures in an uncultivated member of the deep-branching *Nitrospira* phylum. Proc Natl Acad Sci USA (2011). 108:1134–1139.

34. Lefèvre CT, Bennet M, Landau L, Vach P, Pignol D, Bazylinski DA, Frankel RB, Klumpp S, Faivre D. Diversity of magneto-aerotactic behaviors and oxygen sensing mechanisms in cultured magnetotactic bacteria. Biophys J 2014. 107(2):527–538.

35. Komeili, A. Molecular mechanisms of compartmentalization and biomineralization in magnetotactic bacteria. FEMS Microbiol Rev 2012. 36:232–255.

36. Schleifer KH, Schüler D, Spring S, Weizenegger M, Amann R, Ludwig W, Köhler M. The genus Magnetospirillum gen. nov. description of *Magnetospirillum gryphiswaldense* sp. nov. and transfer of *Aquaspirillum magnetotacticum* to *Magnetospirillum magnetotacticum* comb. nov. Syst Appl Microbiol 1991. 14:379–85.

37. Schüler D, Monteil CL, Lefèvre CT. Microbe of the Month: *Magnetospirillum gryphiswaldense*. Trends in Microbiol 2020. S0966-842X(20)30163-3.

38. Schüler D. Molecular analysis of a subcellular compartment: The magnetosome membrane in *Magnetospirillum gryphiswaldense*. Arch Microbiol 2004. 181:1–7.

39. Geelhoed JS, Kleerebezem RDY, Sorokin Stams AJ, and van Loosdrecht MC. Reduced inorganic sulfur oxidation supports autotrophic and mixotrophic growth of Magnetospirillum strain J10 and *Magnetospirillum gryphiswaldense*. Environ Microbiol 2010. 12:1031–1040.

40. Scheffel A, Gruska M, Faivre D, Linaroudis A, Graumann PL, Plitzko J, Schüler D. An acidic protein aligns magnetosomes along a filamentous structure in magnetotactic bacteria. Nature 2006. 440:110–114.

41. Scheffel A, Schüler D. The acidic repetitive domain of the *Magnetospirillum gryphiswaldense* MamJ protein displays hypervariability but is not required for magnetosome chain assembly. J Bacteriol 2007. 189:6437–6446.

42. Katzmann E, Scheffel A, Gruska M, Plitzko JM, Schüler D. Loss of the actin-like protein MamK has pleiotropic effects on magnetosome formation and chain assembly in *Magnetospirillum gryphiswaldense*. Mol Microbiol 2010. **77**:208–224.

43. Katzmann E, Müller FD, Lang C, Messerer M, Winklhofer M, Plitzko JM, Schüler D. Magnetosome chains are recruited to cellular division sites and split by asymmetric septation. Mol Microbiol 2011. 82(6):1316–1329.

44. Toro-Nahuelpan M, Giacomelli G, Raschdorf O, Borg S, Plitzko JM, Bramkamp, M, Schüler D, Müller F-D. MamY is a membrane-bound protein that aligns magnetosomes and the motility axis of helical magnetotactic bacteria. Nature Microbiol 2019. 4(11):1978–1989.

45. Müller F, Schüler D, Pfeiffer D. A compass to boost navigation: cell biology of bacterial magnetotaxis. J Bacteriol 2020. 202(21):e00398-20.

46. Zwiener T, Dziuba M, Mickoleit F, Rückert C, Busche T, Kalinowski J, Uebe R, Schüler D. Towards a 'chassis' for bacterial magnetosome biosynthesis: genome streamlining of *Magnetospirillum gryphiswaldense* by multiple deletions. Microb Cell Fact 2021. 20(1):35.

47. Mickoleit F, Schüler D. Generation of nanomagnetic biocomposites by genetic engineering of bacterial magnetosomes. Bioinspired Biomim Nanobiomater 2019. 8 (1):86–98.

48. Ceyhan B, Alhorn P, Lang C, Schüler D, Niemeyer CM. Semisynthetic biogenic magnetosome nanoparticles for the detection of proteins and nucleic acids. Small 2006. 2(11):1251–1255.

49. Vargas G, Cypriano J, Correa T, Leão P, Bazylinski DA, Abreu F. Applications of magnetotactic bacteria, magnetosomes and magnetosome crystals in biotechnology and nanotechnology: mini-review. Molecules 2018. 23(10):2438.

50. Rosenfeldt S, Mickoleit F, Jörke C, Clement JH, Markert S, Jérôme V, Schwarzinger S, Freitag R, Schüler D, Uebe R, Schenk AS. Towards standardized purification of bacterial magnetic nanoparticles for future in vivo applications. Acta Biomat 2021. 120:293–303.

51. Mickoleit F, Schüler D. Generation of multifunctional magnetic nanoparticles with amplified catalytic activities by genetic expression of enzyme arrays on bacterial magnetosomes. Adv Biosyst 2018. 2:1700109.

52. Mickoleit F, Lanzloth C, Schüler D. A versatile toolkit for controllable and highly selective multifunctionalization of bacterial magnetic nanoparticles. Small 2020. 16(16):e1906922.

53. Pollithy A, Romer T, Lang C, Müller FD, Helma J, Leonhardt H, Rothbauer U, Schüler D. Magnetosome expression of functional camelid antibody fragments (nanobodies) in *Magnetospirillum gryphiswaldense*. Appl Environ Microbiol 2011. 77(17):6165–71.

54. Borg S, Rothenstein D, Bill J, Schüler D. Generation of multi-shell magnetic hybrid nanoparticles by encapsulation of genetically engineered and fluorescent bacterial magnetosomes with ZnO and SiO2. Small 2015. 11(33):4209–17.

55. Mickoleit F, Schüler D. Generation of nanomagnetic biocomposites by genetic engineering of bacterial magnetosomes. Bioinspired Biomim Nanobiomater 2018. 8(1):86–98.

56. Mickoleit F, Borkner CB, Toro-Nahuelpan M, Herold HM, Maier DS, Plitzko JM, Scheibel T, Schüler D. *In vivo* coating of bacterial magnetic nanoparticles by magnetosome expression of spider silk-inspired peptides. Biomacromolecules 2018. 19(3):962–72.

57. Mickoleit F, Jérôme V, Freitag R, Schüler D. Bacterial magnetosomes as novel platform for the presentation of immunostimulatory, membrane bound ligands in cellular biotechnology. Adv Biosyst 2020. 4(3):e1900231.

58. Zeytuni N, Uebe R, Maes M, Davidov G, Baram M, Raschdorf O, Friedler A, Miller Y, Schüler D, Zarivach R. Bacterial magnetosome biomineralization a novel platform to study molecular mechanisms of human CDF-related Type-II diabetes. PLoS ONE 2014. 9(5):e97154.

59. Wang X, Wang J-G, Geng Y-Y, Wang J-J, Zhang X-M, Yang S-S, Jiang W, Liu W-Q. An enhanced anti-tumor effect of apoptin cecropin B on human hepatoma cells by using bacterial magnetic particle gene delivery system. Biochem Biophys Res Commun 2018. 496(2):719–725.

60. Li A, Zhang H, Zhang X, Wang Q, Tian J, Li Y, Li J. Rapid separation and immunoassay for low levels of *Salmonella* in food using magnetosome-antibody complex and real-time fluorescence quantitative PCR. J Sep Sci 2010. 33:3437–3443.

61. Heinke D, Kraupner A, Eberbeck D, Schmidt D, Radon P, Uebe R, Schüler D, Briel A. MPS and MRI efficacy of magnetosomes from wild-type and mutant bacterial strains. IJMPI 2017. 3(2):1706004.

62. Kraupner A, Eberbeck D, Heinke D, Uebe R, Schüler D, Biel A. Bacterial magnetosomes – nature's powerful contribution to MPI tracer research. Nanoscale 2017. 9(18):5788–93.

63. Lang C, Schüler D. Biogenic nanoparticles: production, characterization, and application of bacterial magnetosomes. J Phys Condens Matter 2006. 18:2815–28.

64. Lisy MR, Hartung A, Lang C, Schüler D, Richter W, Reichenbach JR, Kaiser WA, Hilger I. Fluorescent bacterial magnetic nanoparticles as bimodal contrast agents. Invest Radiol 2007. 42(4):235–41.

65. Schwarz S, Fernandes F, Sanroman L, Hodenius M, Lang C, Himmelreich U, Fama G, Schmitz-Rode T, Schüler D, Hoehn M, Zenke M, Hieronymus T. Synthetic and biogenic magnetite nanoparticles for tracking of stem cells and dendritic cells. J Mag Mag Mat 2009. 321(10):1533–1538.

66. Schuerle S, Furubayashi M, Soleimany AP, Gwisai T, Huang W, Voigt C, Bhatia SN Genetic encoding of targeted contrast agents for *in vivo* tumor imaging. ACS Synth Biol 2020. 9(2):392–401.

67. Hergt R, Dutz S, Röder M. Effects of size distribution on hysteresis losses of magnetic nanoparticles for hyperthermia. J Phys Condens Matter 2008. 20:385214.

68. Alphandéry E, Guyot F, Chebbi I. Preparation of chains of magnetosomes, isolated from *Magnetospirillum magneticum* strain AMB-1 magnetotactic bacteria, yielding efficient treatment of tumors using magnetic hyperthermia. Int J Pharm. 2012;434(1–2):444–52.and dendritic cells. J Magn Magn Mater 2009. 321(10):1533–8.

69. Alphandéry E. Perspectives of breast cancer thermotherapies. J Cancer 2014. 5(6):472–479.

70. Heyen U, Schüler D. Growth and magnetosome formation by microaerophilic *Magnetospirillum* strains in an oxygen-controlled fermentor. Appl Microbiol Biotechnol 2003. 61:536–544.

71. Riese C, Uebe R, Rosenfeldt S, Schenk AS, Jérôme V, Freitag R, Schüler D. An automated oxystat fermentation regime for microoxic cultivation and magnetosome production in *Magnetospirillum gryphiswaldense*. Microb Cell Fact 2020. 19:206.

72. Fernández-Castané A, Li H, Thomas ORT, Overton TW. Development of a simple intensified fermentation strategy for growth of *Magnetospirillum gryphiswaldense* MSR-1: physiological responses to changing environmental conditions. N Biotechnol 2018. 46:22–30.

73. Xu J-K, Zhang F-F, Sun J-J, Sheng J, Wang F, Sun M. Bio and nanomaterials based on Fe_3O_4. Molecules 2014. 19:21506–21528.

74. Lohße A, Borg S, Raschdorf O, Kolinko I, Tompa E, Posfai M, Faivre D, Baumgartner J, Schüler D. Genetic dissection of the *mamAB* and *mms6* operons reveals a gene set essential for magnetosome biogenesis in *Magnetospirillum gryphiswaldense*. J Bacteriol 2014. 196:2658–69.

75. Grünberg K, Wawer C, Tebo B. M, Schüler, D. A large gene cluster encoding several magnetosome proteins is conserved in different species of magnetotactic bacteria. Appl Environ Microbiol 2001. 67:573–582.

76. Grünberg K, Müller, EC, Otto A, Reszka R, Linder D, Kube M, Reinhardt R, Schüler D. Biochemical and proteomic analysis of the magnetosome membrane in *Magnetospirillum gryphiswaldense*. Appl Environ Microbiol 2004. 70:1040–50.

77. Ullrich S, Kube M, Schübbe M, Reinhardt R, Schüler D. A hypervariable 130-kilobase genomic region of *Magnetospirillum gryphiswaldense* comprises a magnetosome island which undergoes frequent rearrangements during stationary growth. J Bacteriol 2005. 187:7176–7184.

78. Dobrindt, Hochhut B, Hentschel U, Hacker J. Genomic islands in pathogenic and environmental microorganisms. Nat Rev Microbiol, 2004. 2(5):414–24.

79. Desvaux M, Dalmasso G, Beyrouthy R, Barnich N, Delmas J, Bonnet R. Pathogenicity factors of genomic island in intestinal and extraintestinal *Escherichia coli*. Fron Microbiol 2020. 11:2065.

80. Juhas M, van der Meer JR, Gaillard M, Harding RM, Hood DW, Crook DW. Genomic islands: tools of bacterial horizontal gene transfer and evolution. FEMS Microbiol Rev 2009. 33(2):376–93.

81. Penn K, Jenkins C, Nett M, Udwary DW, Gontang EA, McGlinchey RP, Foster B, Lapidus A, Podell S, Allen EE, Moore BS, Jensen PR. Genomic islands link secondary

metabolism to functional adaptation in marine Actinobacteria. ISME J 2009. 3(10):1193–203.

82. Abreu F, Cantão ME, Nicolás MF, Barcellos FG, Morillo V, Almeida LGP, do Nascimento FF, Lefèvre CT, Bazylinski DA, de Vasconcelos ATR, Lins U. Common ancestry of iron oxide- and iron-sulfidebased biomineralization in magnetotactic bacteria. ISME J 2011. 5:1634–1640

83. Jogler C, Lin W, Meyerdierks A, Kube M, Katzmann E, Flies C, Pan Y, Amann R, Reinhardt R, Schüler D. Toward cloning of the magnetotactic metagenome: identification of magnetosome island gene clusters in uncultivated magnetotactic bacteria from different aquatic sediments. Appl Environ Microbiol 2009. 75:3972–3979.

84. DeLong EF, Frankel RB, Bazylinski DA. Multiple evolutionary origins of magnetotaxis in bacteria. Science 1993. 259:803– 806.

85. Jogler C, Kube M, Schübbe S, Ullrich S, Teeling H, Bazylinski DA, Reinhardt R, Schüler D. Comparative analysis of magnetosome gene clusters in magnetotactic bacteria provides further evidence for horizontal gene transfer. Environ Microbiol 2009. 15:1267–1277.

86. Schübbe S, Kube M, Scheffel A, Wawer C, Heyen U, Meyerdierks A, Madkour MH, Mayer F, Reinhardt R, Schüler D. Characterization of a spontaneous nonmagnetic mutant of *Magnetospirillum gryphiswaldense* reveals a large deletion comprising a putative magnetosome island. J Bacteriol 2003. 185:5779–90.

87. Lohße A, Ullrich S, Katzmann E, Borg S, Wanner G, Richter M, Voigt B, Schweder T, Schüler D. Functional analysis of the magnetosome island in *Magnetospirillum gryphiswaldense*: the *mamAB* operon is sufficient for magnetite biomineralization. PLoS One 2011. 6:e25561.

88. Uebe R, Junge K, Henn V, Poxleitner G, Katzmann E, Plitzko JM, Zarivach R, Kasama T, Wanner G, Pósfai M, Böttger L, Matzanke B, Schüler D. The cation diffusion facilitator proteins MamB and MamM of *Magnetospirillum gryphiswaldense* have distinct and complex functions, and are involved in magnetite biomineralization and magnetosome membrane assembly. Mol Microbiol 2011. 82(4):818–35.

89. Toro-Nahuelpan M, Giacomelli G, Raschdorf O, Borg S, Plitzko JM, Bramkamp M, Schüler D, Müller FD. MamY is a membrane-bound protein that aligns magnetosomes and the motility axis of helical magnetotactic bacteria. Nature Microbiol 2019. 4(11):1978–89.

90. Kolinko I, Lohße A, Borg S, Raschdorf O, Jogler C, Tu Q, Pósfai M, Tompa E, Plitzko JM, Brachmann A, Wanner G, Müller R, Zhang Y, Schüler D. Biosynthesis of magnetic nanostructures in a foreign organism by transfer of bacterial magnetosome gene clusters. Nat Nanotechnol 2014. 9:193–197.

91. Dziuba MV, Zwiener T, Uebe R, Schüler D. Single-step transfer of biosynthetic operons endows a non-magnetotactic *Magnetospirillum* strain from wetland with magnetosome biosynthesis. Environ Microbiol 2020. 22(4):1603–18.

92. Scheffel A, Gardes A, Grünberg K, Wanner G, Schüler D. The major magnetosome proteins MamGFDC are not essential for magnetite biomineralization in *Magnetospirillum gryphiswaldense* but regulate the size of magnetosome crystals. J Bacteriol 2008. 190: 377–86.

93. Raschdorf O, Müller FD, Pósfai M, Plitzko JM, Schüler D. The magnetosome proteins MamX, MamZ and MamH are involved in redox control of magnetite biomineralization in *Magnetospirillum gryphiswaldense*. Mol Microbiol 2013. 89(5):872–86.

94. Müller FD, Raschdorf O, Nudelman H, Messerer M, Katzmann E, Plitzko JM, Zarivach R, Schüler D. The FtsZ-like protein FtsZm of *Magnetospirillum gryphiswaldense* likely interacts with its generic homolog and is required for biomineralization under nitrate deprivation. J Bacteriol 2014. 196:650–659.

95. Lohße A, Kolinko I, Raschdorf O, Uebe R, Borg S, Brachmann A, Plitzko JM, Müller R, Zhang Y, Schüler D. Overproduction of magnetosomes by genomic amplification of biosynthesis-related gene clusters in a magnetotactic bacterium. Appl Environ Microbiol 2016. 82(10):3032–41.

96. Kolinko I, Jogler C, Katzmann E, Schüler D. Frequent mutations within the genomic magnetosome island of *Magnetospirillum gryphiswaldense* are mediated by RecA. J Bacteriol 2011. 193:5328–34.

97. Uebe R, Voigt B, Schweder T, Albrecht D, Katzmann E, Lang C, Böttger L, Matzanke B, Schüler D. Deletion of a fur-like gene affects iron homeostasis and magnetosome formation in *Magnetospirillum gryphiswaldense*. J Bacteriol 2010. 192(16):4192–5204.

98. Li Y, Katzmann E, Borg S, Schüler D. The periplasmic nitrate reductase Nap is required for anaerobic growth and involved in redox control of magnetite biomineralization in *Magnetospirillum gryphiswaldense*. J Bacteriol 2012. 194:4847– 4856.

99. Li Y, Raschdorf O, Silva K.T. Schüler D The terminal oxidase cbb_3 functions in redox control of magnetite biomineralization in *Magnetospirillum gryphiswaldense*. J Bacteriol 2014. 196(14):2552–2562.

100. Raschdorf O, Bonn F, Zeytuni N, Zarivach R, Becher D, Schüler D. A quantitative assessment of the membrane-integral sub-proteome of a bacterial magnetic organelle. J Proteomics 2018. 172:89–99.

101. Schultheiss D, Schüler D. Development of a genetic system for *Magnetospirillum gryphiswaldense*. Arch Microbiol 2003. 179:89–94.

102. Sternberg N, Hamilton D. Bacteriophage P1 site-specific recombination. I. Recombination between *loxP* sites. J Mol Biol 1981. 150:467–486.

103. Ullrich S, Schüler D. Cre-*lox*-based method for generation of large deletions within the genomic magnetosome island of *Magnetospirillum gryphiswaldense*. Appl Environ Microbiol 2010. 76:2439–44.

104. Raschdorf O, Plitzko JM, Schüler D, Müller FD. A tailored *galK* counterselection system for efficient markerless gene deletion and chromosomal tagging in *Magnetospirillum gryphiswaldense*. Appl Environ Microbiol 2014. 80(14):4323–30.

105. Borg S, Hofmann J, Pollithy A, Schüler D. New vectors for chromosomal integration enable high-level constitutive or inducible magnetosome expression of fusion proteins in *Magnetospirillum gryphiswaldense*. Appl Environ Microbiol 2014. 80(8):2309–16.

106. Li Y, Bali S, Borg S, Katzmann E, Ferguson SJ, Schüler D. Cytochrome *cd*1 nitrite reductase NirS is involved in anaerobic magnetite biomineralization in *Magnetospirillum gryphiswaldense* and requires NirN for proper *d*1 heme assembly. J Bacteriol 2013. 195:4297– 4309.

107. Komatsu M, Uchiyama T, Ōmura S, Cane DE, Ikeda H. Genome-minimized *Streptomyces* host for the heterologous expression of secondary metabolism. Proc Natl Acad Sci USA 2010. 107:2646–2651.

108. Ikeda H, Kazuo SY, Omura S. Genome mining of the *Streptomyces avermitilis* genome and development of genome-minimized hosts for heterologous expression of biosynthetic gene clusters. J Ind Microbiol Biotechnol 2014. 41:233–250.

109. Wang X, Kim Y, Ma Q, Hong SH, Pokusaeva K, Sturino JM, Wood TK. Cryptic prophages help bacteria cope with adverse environments. Nature Commun 2010. 1:147.

110. Reuß DR, Commichau FM, Gundlach J, Zhu B, Stülke J. The blueprint of a minimal cell: *MiniBacillus*. Microbiol Mol Biol 2016. 80(4):955–87.

111. Pósfai G, Plunkett 3rd G, Fehér T, Frisch D, Keil GM, Umenhoffer K, Kolisnychenko V, Stahl B, Sharma SS, de Arruda M, Burland V, Harcum SW, Blattner FR. Emerging properties of reduced-genome *Escherichia coli*. Science 2006. 312(5776):1044–46.

112. Baumgart M, Unthan S, Kloß R, Radek A, Polen T, Tenhaef N, Müller MF, Küberl A, Siebert D, Brühl N, Marin K, Hans S, Krämer R, Bott M, Kalinowski J, Wiechert W, Seibold G, Frunzke J, Rückert C, Wendisch V, Noack S. *Corynebacterium glutamicum* chassis C1*: building and testing a novel platform host for synthetic biology and industrial biotechnology. ACS Synth Biol 2017. 7(1):132–44.

113. Martínez-García E, Nikel PI, Aparicio T, de Lorenzo V. *Pseudomonas* 2.0: genetic upgrading of *P. putida* KT2440 as an enhanced host for heterologous gene expression. Microb Cell Fact 2014. 13:159.

114. Lieder S, Nikel PI, de Lorenzo V, Takors R. Genome reduction boosts heterologous gene expression in *Pseudomonas putida*. Microb Cell Fact 2015. 14:23.

115. Pfeifer E, Michniewski S, Gätgens C, Münch E, Müller F, Polen T, Millard A, Blombach B, Frunzke J. Generation of a prophage-free variant of the fast-growing bacterium *Vibrio natriegens*. Appl Environ Microbiol 2019. 85(17):e00853–19.

116. Gödeke J, Paul K, Lassak J, Thormann KM. Phage-induced lysis enhances biofilm formation in *Shewanella oneidensis* MR-1. ISME J 2011. 5(4):613–26.

117. Baumgart M, Unthan S, Rückert C, Sivalingam J, Grünberger A, Kalinowski J, Bott M, Noack S, Frunzke J. Construction of a prophage-free variant of *Corynebacterium glutamicum* ATCC 13032 for use as a platform strain for basic research and industrial biotechnology. Appl Environ Microbiol 2013. 79(19):6006–15.

118. Martínez-García E, Jatsenko T, Kivisaar M, de Lorenzo V. Freeing *Pseudomonas putida* KT2440 of its proviral load strengthens endurance to environmental stresses. Environ Microbiol 2015. 17(1):76–90.

119. Suárez GA, Renda BA, Dasgupta A, Barrick JE. Reduced mutation rate and increased transformability of transposon-free *Acinetobacter baylyi* ADP1-ISx. Appl Environ Microbiol. 2017;83(17):e01025-e1117.

120. Silva KT, Schüler M, Mickoleit F, Zwiener T, Müller FD, Awal RP, Weig A, Brachmann A, Uebe R, Schüler D. Genome-wide identification of essential and auxiliary gene sets for magnetosome biosynthesis in *Magnetospirillum gryphiswaldense*. mSystems 2020. 5(6):e00565–20.

121. Zwiener T, Mickoleit F, Dziuba M, Rückert C, Busche T, Kalinowski J,Faivre D, Uebe R, Schüler D. Identification and elimination of irrelevant genomic content for magnetosome biosynthesis by large-scale deletion in *Magnetospirillum gryphiswaldense*. BMC Microbiol 2021. 21:65.

122. Zhang C, Meng X, Li N, Wang W, Sun Y, Jiang W, Guan G, Li Y. Two bifunctional enzymes with ferric reduction ability play complementary roles during magnetosome synthesis in *Magnetospirillum gryphiswaldense* MSR-1. J Bacteriol 2013. 195:876–885.

123. Wen T, Guo F, Zhang Y, Tian J, Li Y, Li J, Jiang W. A novel role for Crp in controlling magnetosome biosynthesis in *Magnetospirillum gryphiswaldense* MSR-1. Sci Rep 2016. 6:21156.

124. Ji B, Zhang S-D, Zhang W-J, Rouy Z, Alberto F, Santini C-L, Mangenot S, Gagnot S, Philippe N, Pradel N, Zhang L, Tempel S, Li Y, Medigue C, Henrissat B, Coutinho PM, Barbe V, Talla E, Wu L-F. The chimeric nature of the genomes of marine magnetotactic coccoid-ovoid bacteria defines a novel group of *Proteobacteria*. Environ Microbiol 2017. 19:1103–1119.

125. Beckers G, Bendt A K, Krämer R, Burkovski A. Molecular identification of the urea uptake system and transcriptional analysis of urea transport- and urease-encoding genes in *Corynebacterium glutamicum*. J Bacteriol 2004. 186(22):7645–7652.

126. Su Z, Olman V, Mao F, Xu Y. Comparative genomics analysis of NtcA regulons in cyanobacteria: regulation of nitrogen assimilation and its coupling to photosynthesis. Nucleic Acids Res 2005. 33:5156–5171.

127. Solomon CM, Collier JL, Berg GM, Glibert PM. Role of urea in microbial metabolism in aquatic systems: a biochemical and molecular review. Aquatic Microbial Ecology 2010. 59:67–88.

128. Silberbach M, Burkovski A. Application of global analysis techniques to *Corynebacterium glutamicum*: new insights into nitrogen regulation. J Biotechnol 2006. 126:101–110.

129. Valladares A, Montesinos ML, Herrero A, Flores E. An ABC-type, high-affinity urea permease identified in cyanobacteria. Mol Microbiol 2002. 43:703–715.

130. Tolonen AC, Aach J, Lindell D, Johnson ZI, Rector T, Stehen R, Church GM, Chrisholm SW. Global gene expression of *Prochlorococcus* ecotypes in response to changes in nitrogen availability. Mol Syst Biol 2006. 2:53.

131. Sigurdarson JJ, Svane S, Karring H. The molecular processes of urea hydrolysis in relation to ammonia emissions from agriculture. Rev Environ Sci Biotechnol 2018. 17:241–258.

132. Mobley HL, Island MD, Hausinger RP. Molecular biology of microbial ureases. Microbiol Reviews 1995. 59(3):451–480.

133. Sumner JB. Isolation and crystallization of the enzyme urease. J Biol Chem 1926. 1926(69):435–41.

134. Jabri E, Carr MB, Hausinger RP, Karplus PA. The crystal structure of urease from *Klebsiella aerogenes*. Science 1995. 268:998–1004.

135. Ha NC, Oh ST, Sung JY, Cha KA, Lee MH, Oh BH. Supramolecular assembly and acid resistance of *Helicobacter pylori* urease. Nat Struct Biol 2001. 8:505–509.

136. Liu Q, Chen Y, Yuan M, Du G, Chen J, Kang Z. A *Bacillus paralicheniformis* iron-containing urease reduces urea concentrations in rice wine. Appl Environ Microbiol 2017. 83(17):e01258-17.

137. Ma L, Pang A-P, Luo Y, Lu X, Lin F. Beneficial factors for biomineralization by ureolytic bacterium *Sporosarcina pasteurii*. Microb Cell Fact 2020. 19:12.

138. Nolden L, Beckers G, Möckel B, Pfefferle W, Nampoothiri KM, Krämer R, Burkovski A. Urease of *Corynebacterium glutamicum*: organization of corresponding genes and investigation of activity. FEMS Microbiol Lett 2000. 189:305–310.

139. Belzer C, van Schendel BAM, Kuipers EJ, Kusters JG, van Vliet AHM. Iron-responsive repression of urease expression in *Helicobacter hepaticus* is mediated by transcriptional regulator Fur. Infect Immun 2007. 75(2):745–752.

140. Moisescu C, Ardelean II, Benning LG. The effect and role of environmental conditions on magnetosome synthesis. Front Microbiol 2014. 5:49.

141. Solyga A, Bartosik D. Entrapment vectors – How to capture a functional transposable element. Pol J Microbiol 2004. 53(3):139–144.

142. Schultheiss D, Kube M, Schüler D. Inactivation of the flagellin gene flaA in *Magnetospirillum gryphiswaldense* results in nonmagnetotactic mutants lacking flagellar filaments. Appl Environ Microbiol 2004. 70:3624–31.

143. Choi JW, Yim SS, Kim MJ, Jeong KJ. Enhanced production of recombinant proteins with *Corynebacterium glutamicum* by deletion of insertion sequences (IS elements). Microb Cell Fact 2015. 14:207.

144. Jiang W, Bikard D, Cox D, Zhang F, Marraffini LA. RNA-guided editing of bacterial genomes using CRISPR-Cas systems. Nature Biotech 2013. 31:233–239.

145. Rogers JK, Church GM: Multiplexed engineering in biology. Trends Biotechnol 2016. 34:198–206.

146. Wang HH, Isaacs FJ, Carr PA, Sun ZZ, Xu G, Forest CR, Church GM: Programming cells by multiplex genome engineering and accelerated evolution. Nature 2009. 460:894–898.

147. Nyerges A, Csorgo B, Nagy I, Balint B, Bihari P, Lazar V, Apjok G, Umenhoffer K, Bogos B, Posfai G, Pál C. A highly precise and portable genome engineering method allows comparison of mutational effects across bacterial species. Proc Natl Acad Sci USA 2016. 113:2502–2507.

148. Nyerges A, Csörgő B, Nagy I, Latinovics D, Szamecz B, Pósfai G, Pal C. Conditional DNA repair mutants enable highly precise genome engineering. Nucl Acids Res 2014. 42:e62.

149. Jensen SI, Lennen RM, Herrgard MJ, Nielsen AT. Seven gene deletions in seven days: fast generation of *Escherichia coli* strains tolerant to acetate and osmotic stress. Sci Rep 2015. 5:17874.

150. Isaacs FJ, Carr PA, Wang HH, Lajoie MJ, Sterling B, Kraal L, Tolonen AC, Gianoulis TA, Goodman DB, Reppas NB. Precise manipulation of chromosomes *in vivo* enables genome-wide codon replacement. Science 2011. 333:348–353.

151. Lajoie MJ, Rovner AJ, Goodman DB, Aerni HR, Haimovich AD, Kuznetsov G, Mercer JA, Wang HH, Carr PA, Mosberg JA, Rohland N, Schultz PG, Jacobson JM, Rinehart J, Church GM, Isaacs FJ. Genomically recoded organisms expand biological functions. Science 2013. 342:357–360.

152. Ma NJ, Moonan DW, Isaacs FJ. Precise manipulation of bacterial chromosomes by conjugative assembly genome engineering. Nat Protocol 2014. 9:2285–2300.

153. Yu BJ, Sung BH, Koob MD, Lee CH, Lee JH, Lee WS, Kim MS, Kim SC. Minimization of the *Escherichia coli* genome using a Tn5-targeted *Cre/loxP* excision system. Nat Biotechnol 2002. 20(10):1018–23.

CHAPTER IV:

Genome-Wide Identification of Essential and Auxiliary Gene Sets for Magnetosome Biosynthesis in *Magnetospirillum gryphiswaldense*

Karen T. Silva,[a] Margarete Schüler,[a] Frank Mickoleit,[a] Theresa Zwiener,[a] Frank D. Müller,[a] Ram Prasad Awal,[a] Alfons Weig,[b] Andreas Brachmann,[c] René Uebe,[a] Dirk Schüler[a]

[a]Department of Microbiology, University of Bayreuth, Bayreuth, Germany

[b]KeyLab Genome Analysis and Bioinformatics, University of Bayreuth, Bayreuth, Germany

[c]Genetics Section, Bio Center, Ludwig-Maximilians-Universität München, Munich, Germany

Karen T. Silva and Margarete Schüler contributed equally to this work. Author order was determined on the basis of seniority.

154.

Genome-Wide Identification of Essential and Auxiliary Gene Sets for Magnetosome Biosynthesis in *Magnetospirillum gryphiswaldense*

Karen T. Silva,[a] Margarete Schüler,[a] Frank Mickoleit,[a] Theresa Zwiener,[a] [ID]Frank D. Müller,[a] Ram Prasad Awal,[a] Alfons Weig,[b] Andreas Brachmann,[c] [ID]René Uebe,[a] [ID]Dirk Schüler[a]

[a]Department of Microbiology, University of Bayreuth, Bayreuth, Germany
[b]KeyLab Genome Analysis and Bioinformatics, University of Bayreuth, Bayreuth, Germany
[c]Genetics Section, Bio Center, Ludwig-Maximilians-Universität München, Munich, Germany

Karen T. Silva and Margarete Schüler contributed equally to this work. Author order was determined on the basis of seniority.

ABSTRACT Magnetotactic bacteria (MTB) stand out by their ability to manufacture membrane-enclosed magnetic organelles, so-called magnetosomes. Previously, it has been assumed that a genomic region of approximately 100 kbp, the magnetosome island (MAI), harbors all genetic determinants required for this intricate biosynthesis process. Recent evidence, however, argues for the involvement of additional auxiliary genes that have not been identified yet. In the present study, we set out to delineate the full gene complement required for magnetosome production in the alphaproteobacterium *Magnetospirillum gryphiswaldense* using a systematic genome-wide transposon mutagenesis approach. By an optimized procedure, a Tn*5* insertion library of 80,000 clones was generated and screened, yielding close to 200 insertants with mild to severe impairment of magnetosome biosynthesis. Approximately 50% of all Tn*5* insertion sites mapped within the MAI, mostly leading to a nonmagnetic phenotype. In contrast, in the majority of weakly magnetic Tn*5* insertion mutants, genes outside the MAI were affected, which typically caused lower numbers of magnetite crystals with partly aberrant morphology, occasionally combined with deviant intracellular localization. While some of the Tn*5*-struck genes outside the MAI belong to pathways that have been linked to magnetosome formation before (e.g., aerobic and anaerobic respiration), the majority of affected genes are involved in so far unsuspected cellular processes, such as sulfate assimilation, oxidative protein folding, and cytochrome *c* maturation, or are altogether of unknown function. We also found that signal transduction and redox functions are enriched in the set of Tn*5* hits outside the MAI, suggesting that such processes are particularly important in support of magnetosome biosynthesis.

IMPORTANCE *Magnetospirillum gryphiswaldense* is one of the few tractable model magnetotactic bacteria (MTB) for studying magnetosome biomineralization. So far, knowledge on the genetic determinants of this complex process has been mainly gathered using reverse genetics and candidate approaches. In contrast, nontargeted forward genetics studies are lacking, since application of such techniques in MTB has been complicated for a number of technical reasons. Here, we report on the first comprehensive transposon mutagenesis study in MTB, aiming at systematic identification of auxiliary genes necessary to support magnetosome formation in addition to key genes harbored in the magnetosome island (MAI). Our work considerably extends the candidate set of novel subsidiary determinants and shows that the full gene complement underlying magnetosome biosynthesis is larger than assumed. In particular, we were able to define certain cellular pathways as specifically important for magnetosome formation that have not been implicated in this process so far.

Magnetotactic bacteria (MTB) are able to navigate in the geomagnetic field by virtue of unique intracellular organelles, so-called magnetosomes. These magnetic field sensors are membrane enclosed crystals of a magnetic iron mineral, magnetite (Fe_3O_4) or greigite (Fe_3S_4), which are aligned in one or more intracellular chains by specific cytoskeletal structures. From this ordered crystal arrangement, a magnetic moment results which orients the bacterial cell along geomagnetic field lines (1–4). Impressive progress has been made during the last 2 decades in unraveling the genetic circuitry behind magnetosome formation, mostly through the study of two model organisms, the *Alphaproteobacteria Magnetospirillum gryphiswaldense* MSR-1 (5, 6) and *Magnetospirillum magnetotacticum* AMB-1 (7). This revealed that the biosynthesis of magnetosomes (magbiosyn) in bacterial cells is an intricate stepwise process which comprises the (i) invagination of the cytoplasmic membrane to form the magnetosome membrane (MM), either as vesicle-like permanent invagination or as detached vesicle, (ii) sorting of magnetosome proteins to the MM, either prior to, concomitantly with, or after invagination, (iii) iron transport into the vesicle and mineralization as magnetic crystal, and (iv) magnetosome chain assembly and cellular positioning for segregation during cell division (8–11). The multitude of intertwined actions underlying these stages is orchestrated and tightly controlled by more than 30 genes located in a dedicated genomic region called magnetosome island (MAI) (12, 13). It harbors all so far known specific magbiosyn determinants, which are organized in five characterized gene clusters/operons (*feoAB1*, *mms6*, *mamGFDC*, *mamXY*, and *mamAB*) (10) that were first identified by a reverse genetics approach based on a combination of proteomics and comparative genomics (14). These key gene clusters of the MAI are separated by stretches harboring genes of yet unknown but irrelevant function for magnetosome biosynthesis (15, 16). For *M. gryphiswaldense*, it has been shown that the largest of these potential transcription units, the *mamAB* operon, contains the set of essential magnetosome genes sufficient to bring about at least rudimentary magnetosome biomineralization (15). Comparison of (meta)genomes from cultured and uncultured MTB species revealed lineage-specific variations in MAI architecture; however, a small set of core genes (*mamABEIKMOPQ*), largely congruous with the content of the *mamAB* cluster, is conserved across the broad MTB diversity (17–20). For *Rhodospirillum rubrum* (21) and a hitherto nonmagnetic *Magnetospirillum* sp. (22), it could be demonstrated that it is possible to convey the capability for magbiosyn by transfer of the five biosynthetic gene clusters identified in the MAI of *M. gryphiswaldense* and related MTB. This, among other hints, lends support to the hypothesis that the magbiosyn trait may have been propagated by horizontal gene transfer (19, 20). However, repeated attempts to achieve magnetization of other foreign organisms by transplantation have failed so far (M. V. Dziuba and D. Schüler, unpublished data). This strongly suggests that there must be additional, auxiliary determinants in the genome that allow proper use of the MAI genes in the first place. In fact, several earlier studies on *M. gryphiswaldense* have identified functions encoded outside the MAI that are important for magnetosome formation, for instance, genes involved in redox control during aerobic (23) and anaerobic (i.e., denitrifying) respiration (24, 25), as well as in iron reduction (26) and iron homeostasis (27). In addition, a global regulator of carbon metabolism has been assigned a new role in control of magbiosyn in *M. gryphiswaldense* (28). Yet, how magnetosome formation is integrated into the network of cellular pathways of MTB remains poorly resolved. It is likely that further auxiliary functions are required for this process, possibly regarding membrane biosynthesis capacities and modalities or maturation of proteins and specific cofactors as well as activity modulation of proteins by chaperonins. For a complete understanding of the complex process of magnetosome biosynthesis, it is fundamental to identify all the auxiliary genes that define a genetic background supportive for the expression of the magbiosyn trait. In this context, it is

also an important question whether further essential magbiosyn genes outside the MAI can be retrieved.

In MTB, the profound gain in knowledge on biosynthetic determinants and their function in magnetosome formation has been mainly accomplished through reverse genetics and candidate approaches. In contrast, only few studies based on unbiased genome-wide forward methods have been undertaken. One of such well-established and unbiased techniques for identification of a comprehensive set of genes involved in a certain phenotype/pathway is transposon (Tn) mutagenesis. In this forward genetic method, transposons are used to randomly interrupt genes genome wide, and a suitable screening procedure is deployed to select mutant phenotypes indicating impairment of the pathway under study. Generally, the application of such mutagenesis approaches in MTB has been complicated by a number of specific challenges. Thus, most MTB are recalcitrant to grow and be manipulated, genetic tools for high-throughput approaches are limited, there are only inefficient screening methods for the assessment of subtle magnetosome mutant phenotypes, and there is an inherent genetic instability of the magnetic phenotype that leads to spontaneous loss of (parts of) the MAI, with a particularly high frequency under stress conditions (12, 29). A number of transposon mutagenesis studies have been published for the alphaproteo-bacterium *Magnetospirillum magneticum* AMB-1 in the past, using Tn*5* (30, 31) or a hyperactive mariner transposon (32, 33). In these studies, a rather limited number of mutants has been screened, ranging from several hundred (32) to a few thousand clones (30, 31, 33), aimed at the identification of mutants entirely devoid of magneto-somes but not considering identification of subtler magnetosome phenotypes. Suspi-ciously, despite that, some of the studies failed to retrieve essential key genes (30, 31), which were later detected as part of the MAI by reverse genetics. Komeili and coworkers analyzed two unique nonmagnetic mutants for which insertion mapped to magnetosome genes (32). A study by Nash reported that approximately 90% of the nonmagnetic mutants identified were due to spontaneous mutations, and the majority of truly non- or partially magnetic mutants showed an insertion in the MAI. In five cases, genes outside the MAI were affected, two of them encoding redox proteins and one a transcriptional regulator (33). In a more recent nonexhaustive analysis using UV/chemical mutagenesis to identify genes involved in magbiosyn in the emerging MTB model organism *Desulfovibrio magneticus* RS-1, six mutant alleles located in magnetot-actic gene clusters were identified along with four outside these regions, among them two genes encoding ion transporters (34).

In *M. gryphiswaldense*, another important model for studying magbiosyn, systematic transposon mutagenesis to identify genes involved in magbiosyn has not been con-ducted so far. This was the aim of the present genome-wide Tn*5* insertion mutagenesis study. We favored conventional Tn mutagenesis over transposon insertion sequencing (Tn-seq) (35), since the magnetic phenotype conferred by the complex magnetosome organelle is only poorly linked to fitness under lab growth conditions. Thus, we needed a more direct proxy than growth fitness for the screening of insertion mutants. The main technical challenges were the achievement of a suitable transposition efficiency and the development of a sensitive screening approach practical for large numbers of clones. After solving these problems, we generated and screened a library of 80,000 transposon insertion mutants. From that, we retrieved 195 stable weakly magnetic or nonmagnetic alleles. The majority of the nonmagnetic mutants had hits within the MAI, whereas most of the weakly magnetic mutants were struck in genes outside the MAI. Among those were several genes already previously linked to magbiosyn, but the majority represented novel potential determinants for magbiosyn. In total, we identified 85 genes outside the MAI for which transposon insertion resulted in a distinguishable but moderate decrease of the ability of mutant cells to biominer-alize regular magnetite crystals. These genes may, therefore, encode auxiliary functions for magbiosyn.

RESULTS AND DISCUSSION

It was expected that inactivation of auxiliary genes would evoke a rather weak impairment of the magnetotactic trait. Therefore, our experimental approaches faced the challenge of discerning subtle mutant phenotypes during the screening process. Two steps had to be optimized. The transposition efficiency had to be maximized to generate a sufficiently large number of transposon clones. Then, a method suitable for the discrimination of subtle differences in the magnetic phenotype (gradually from weakly magnetic to nonmagnetic) and practical for the screening of thousands of clones had to be devised.

Development of a reliable screening procedure for the mass identification of mutants impaired in magnetosome biosynthesis. First, we sought to effectively identify—against the background of cells with wild-type magnetic (WTmag) properties—rare mutants suffering to different degrees from defects in magnetite biomineralization, i.e., cells with diminished magnetic (Wmag) phenotypes, producing fewer, smaller, or aberrantly shaped magnetosomes as well as cells with an entirely nonmagnetic (Nmag) phenotype . Microscopic characterization and the determination of c_{mag} (i.e., a proxy for the average magnetic orientation of bacterial cells in liquid medium based on light-scattering [36]) are not practical for screening large numbers of samples. We also found that methods employed in earlier forward genetics studies on MTB, such as magnetic depletion by passage through magnetized columns (34) or visible accumulation of cell pellets in 96-well plates exposed to magnets (32, 33), did not provide the sensitivity to discern subtle differences in magnetic phenotypes. Similarly impractical was the use of a range of other phenotypic proxies (data not shown), such as reduced cellular iron content and magnetic distortion of colony shape (37). In contrast, a known characteristic of *M. gryphiswaldense* that can be easily assessed by visual inspection is the color of magnetic versus nonmagnetic colonies on solid media, with magnetic cells having a darker brown colony appearance due to the black color of intracellularly accumulated magnetite and nonmagnetic cells forming whitish colonies (12, 13, 29, 38, 39). Typically, colonies on these solid media are small, cells form only few magnetosomes, and the use of nontranslucent media such as activated charcoal agar (38, 39) makes it difficult to resolve subtle differences in colony color. However, by testing a range of medium compositions and incubation regimes, we found a substantial increase in colony size (up to 4 to 5 mm, typically 2.5 mm) on large plates (15 cm) with increased medium volume (140 ml versus 100 ml, yielding a thicker agar layer) and increased iron concentration (500 μM versus 50 μM). Prolonged micro- or anoxic incubation (>14 days, optimally 20 days) at lower temperature (<28°C) was found to maximize the expression of the magnetic phenotype, intensifying the colony color due to increased magnetite biomineralization to a dark brown that could be easily recognized on translucent medium (Fig. 1 and 2). Generally, colony size and color were significantly enhanced by low seeding density (ca. 100 colonies per 15-cm plate, i.e., ca. 1 to 2 colonies/cm²).

To validate our screening method, we plated single colonies of mutant strains, ΔmamAB, ΔmamXY, Δmms6, and Δ(mms6-mamGFDC-XY) operon mutants, with well-described impairments in magnetosome biomineralization (15). They cover phenotypes ranging from WTmag to Wmag with gradually reduced magnetosome sizes and numbers and Nmag. Even weak mutant phenotypes could be easily distinguished by different colony colors (Fig. 2) and were recovered with >90% efficiency when mixed with wild-type cultures in spiking experiments (see Fig. S2 in the supplemental material).

Construction of a highly active transposon delivery vector. In earlier MTB transposon mutagenesis experiments, frequencies of transposition with Tn*5* varied from 1.9×10^{-4} (40) to 2.7×10^{-7} (30) in AMB-1, whereas for *M. gryphiswaldense*, insertion frequencies of 10^{-4} to 10^{-5} per recipient have been reported (pSUP1021) (38). However, we found insertion frequencies from different Tn*5* vectors tested under high-throughput conditions to be very low (<10^{-8}), fluctuating, and poorly reproduc-

a. Tn5-insertion mutagenesis: optimized vector and medium
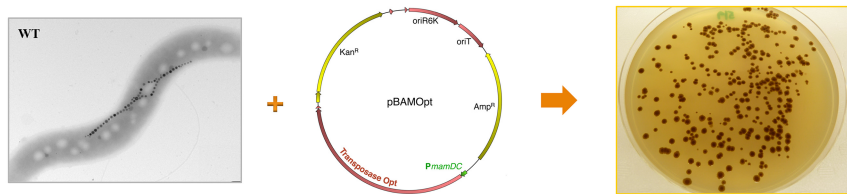
Tn5-insertion library
80.000 insertion-mutant clones

b. Visual screen for N/Wmag phenotype (colony color)
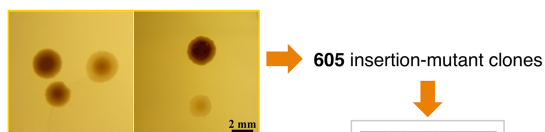
605 insertion-mutant clones
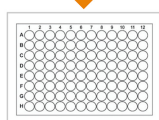
c. Initial analysis to sort out severely growth-impaired clones (22%)

d. Insertion site mapping (Arbitrary PCR, Hybrid Capture)

474 *bona fide* N/Wmag clones
insertions inMAI:168, exMAI:306

e. Detailed analysis for subset of clones: growth and c_{mag}, TEM

278 characterized clones
insertions inMAI:120, exMAI:158
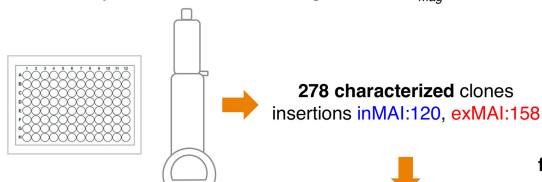
f. Sorting out WTmag clones (30%, >75% exMAI insertions)

195 confirmed N/Wmag clones, insertions inMAI:100, exMAI:95
(**85 putative auxiliary genes** for magnetosome biosynthesis)
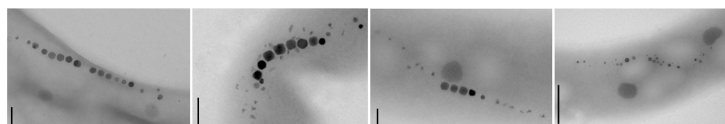
FIG 1 Generation and screening of a genome-wide Tn5 insertion library of *M. gryphiswaldense*. The experimental approach, workflow, and yield of insertion mutants are shown. Details on steps a to f are given in the text.

ible. We therefore engineered a broad-range Tn5-based transposon vector (pBAM1) (41, 42). To enhance expression of the Tn5 transposase, the respective pBAM1 gene (55% G+C content) was replaced by a synthetic allele that was codon optimized for expression in *M. gryphiswaldense* (62.8% G+C content) and placed under the control of the strong native *mamDC45* promoter (42) in the vector pBAMOpt (Fig. 1a). In pilot matings, this optimized plasmid yielded a reproducibly increased transposition frequency of approximately 2×10^{-5}, and Tn5 insertions in 70 randomly selected clones were found to be distributed fairly randomly across the entire genome (data not shown).

Generation and screening of a genome-wide Tn5 insertion library. For construction of a genome-wide *M. gryphiswaldense* Tn5 insertion library (for the experimental work flow, see Fig. 1), we performed seven independent mating experiments for conjugational transfer of the optimized pBAMOpt vector in order to maximize the number of independent Tn5 insertants. To also allow growth of mutants potentially affected in aerobic or anaerobic respiration, mating reactions were split and incubated under either anoxic or microoxic conditions for 2 to 3 weeks. Overall, this resulted in a
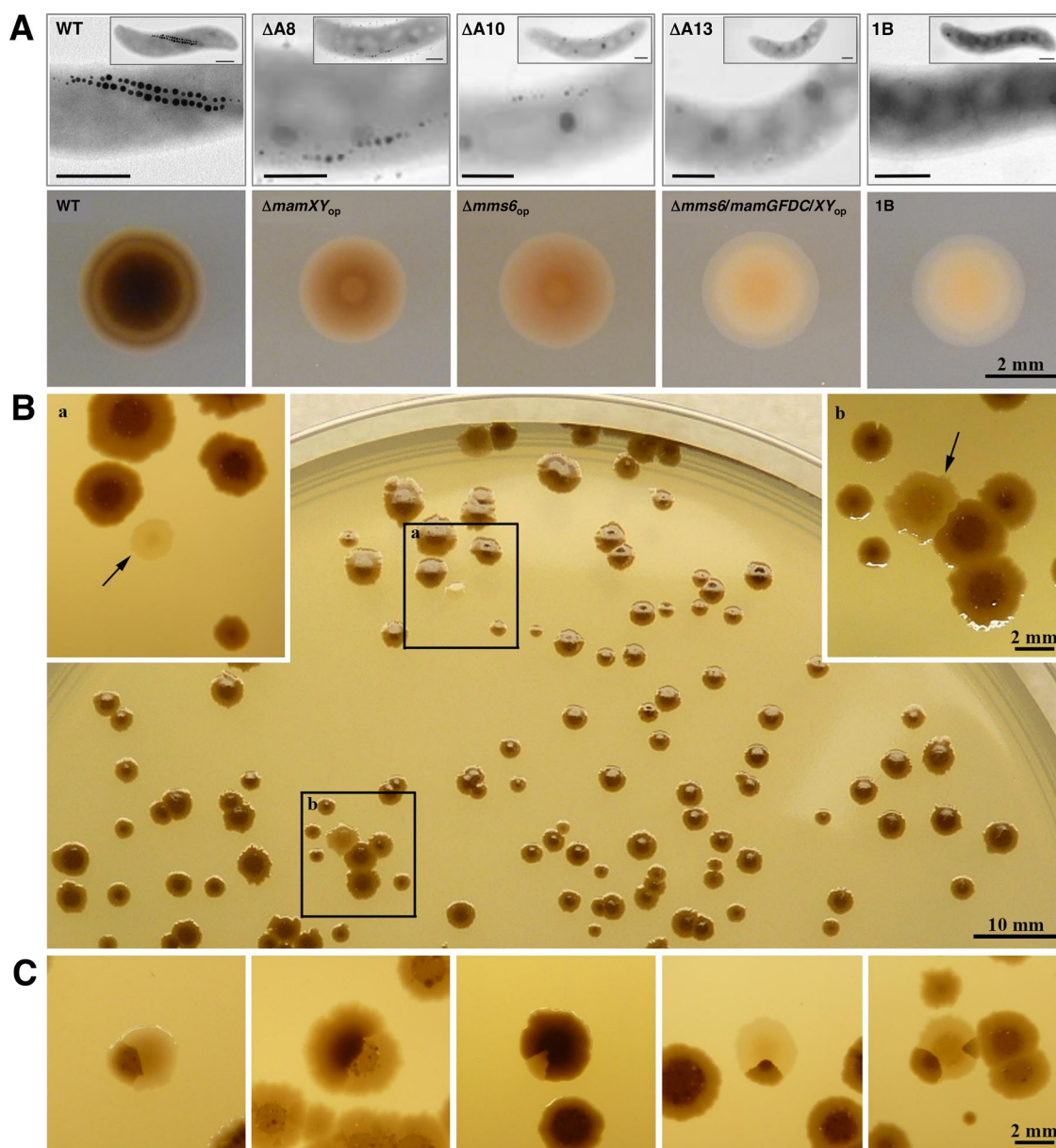
FIG 2 Resolution of the Wmag/Nmag screening procedure demonstrated by examples of different colony appearance. (A) Transmission electron microscopic (TEM) phenotype of magnetosome mutants generated previously and their correlated individual colony appearance. From left: cells of *M. gryphiswaldense* wild type, cells of *M. gryphiswaldense* deletion mutants ΔA8, ΔA10, and ΔA13 (15), and cells of a spontaneous MAI deletion mutant (MSR-1B) (13). Scale bars (top), 400 nm. Mid-cell magnifications are shown together with small insets of the respective whole-cell image. Wild-type colonies are dark brown, Δ*mamXY*op and Δ*mms6*op colonies show intermediate color, and the 1B and Δ*mms6*-Δ*GFDC*-Δ*XY*op colonies are cream colored and translucent. op = operon. (B) Agar plate with colonies of *M. gryphiswaldense* transposon clones grown on ICFM medium for 14 days at 28°C under anoxic conditions. Large dark brown colonies are interspersed with colonies of lighter brown to cream color. The insets show dark magnetic colonies and a whitish colony of an Nmag clone (arrow) (a) or a light brown colony of a Wmag clone (arrow) (b). (C) Aberrant colony phenotypes that were occasionally observed, including twinned, split, or sectored colonies composed of magnetic and non/weakly magnetic cells. This interesting phenomenon might be caused by a fluctuation of phenotypes (transient loss or gain of magnetic phenotype due to regulatory effects).

Tn*5* insertant library of approximately 80,000 kanamycin (Km)-resistant *M. gryphiswaldense* clones (Fig. 1a). The phenotypic screening procedure for Wmag and Nmag clones (Fig. 1b to f) consisted of several steps. The initial screen by visual inspection yielded 605 colonies of conspicuous color, representing putative magbiosyn mutants (Fig. 1b). Among them, initial growth analysis in 96-well plates revealed approximately 22% severely growth-impaired clones. These were sorted out, assuming that their apparent

magnetic deficiency could be a secondary effect of reduced viability (Fig. 1c). The residual 474 clones were considered bona fide magnetosome mutants (Fig. 1d). Anecdotally, we observed that some clones with a clear N/Wmag phenotype on plates reverted to WTmag upon passaging in liquid culture. This prompted us to conduct a more detailed analysis for a representative fraction (278 clones) of the 474 bona fide mutants (Fig. 1e), for which the initial screen was followed by two passages in liquid culture under microoxic conditions, in order to systematically reassess growth and magnetic response (c_{mag}) of the clones and to identify potential false-positive clones (i.e., those for which the N/Wmag phenotype was not stable). During all subcultivations, we carefully sought to avoid prolonged stationary growth and storage as well as oxidative stress, since these conditions were previously suspected to induce spontaneous loss of the magnetosome phenotype caused by endogenous transpositions as well as chromosomal deletions and rearrangements within the MAI (12, 13, 29). We found wild-type-like growth in 65% of the 278 analyzed N/Wmag mutants, while approximately one-third (35%) of the clones exhibited moderate growth deficiencies. Clones that displayed a c_{mag} lower than 80% of the wild type after two passages in liquid medium were considered Wmag, and clones with a c_{mag} of 0 were considered Nmag. A wild-type-like c_{mag} ($\geq$80% of wild type [+++]) was shown by 30% (Fig. 1f), a nonmagnetic phenotype ($-$) by 31%, and a weak magnetic response (between 40% and 80% of wild type [++] or <40% of wild type [+]) by 39% of the clones. The corresponding mutant cells displayed a variety of phenotypes, with magnetosomes being entirely absent (Nmag), reduced in size and/or number, and/or of misshapen appearance (Table 1).

(i) Clones with unstable, ambiguous, or false-positive phenotypes. While, for more than two-thirds of the analyzed 278 clones, the bona fide Nmag/Wmag phenotype was confirmed, for almost one-third of them, the magnetosome phenotype proved to be unstable or absent. Although we did not evaluate all 474 bona fide N/Wmag clones by these rather laborious tests, we assume that the observed trend is likely to hold also for the residual set of 196 mutants.

In the 83 "revertant" clones, insertions mapped to genes within the MAI (inMAI) in 24% of the cases (20/83) and to genes outside the MAI (exMAI) in 76% of the cases (63/83). The observed phenomenon of phenotype reversion might be due to one or more of the following reasons. First, a small proportion of Km-resistant colonies might have descended from more than a single cell, giving rise to mixed phenotypes in one apparent colony (Fig. 2C). Second, (some of) these clones may represent "false positives" of our screen for N/Wmag mutants. The rather weak magbiosyn impairment expected from mutations in exMAI genes likely resulted in more subtle deviations from wild-type colony appearance, increasing the probability of misjudging the true magnetosome phenotype. This explanation would be in accordance with the observed doubled frequency of "reversals" in the set of clones where Tn5 insertion maps to genes outside the MAI (63/158 exMAI clones [40%]) compared to 20/120 (17%) inMAI clones. For example, during several independent rounds of transposon mutagenesis and screening, we retrieved a sometimes conspicuously high number of hits to genes encoding potential functions in cell wall biosynthesis/modification (see Fig. S3). However, null mutants of the respective genes/operons (deletion ranges shown in Fig. S3) displayed a wild-type-like rather than a N/Wmag phenotype in c_{mag} and transmission electron microscope (TEM) analysis (T. Zwiener, F. Mickoleit, M. Dziuba, C. Rückert, T. Busche J. Kalinowski, D. Faivre, R. Uebe, and D. Schüler, under review). Thus, they likely represent false positives that were erroneously selected during the initial screen as N/Wmag mutants due to a potential change in colony appearance caused by an altered cell surface.

Third, the observed "reversal" to wild-type magnetic properties could also be indicative of an underlying regulatory phenomenon resulting in heterogeneity within supposedly clonal cells of a colony or population. Thus, it is possible that a subset of cells reversibly reduces or shuts down magnetosome biosynthesis either stochastically

TABLE 1 Ultrastructural analysis of magnetosomes in magnetosome mutants: particle shapes[a] and chain-types

Schematic illustration of phenotype observed by TEM	Description of electron dense particles	Example locus-tag (gene name), annotation, TEM
	regular magnetosomes, long chain localized at midcell	Wildtype
	short chain at midcell, scattered flakes	MGMSRv2_**0199** (*livM*-like) permease of high-affinity branched chain amino acid transporter
	short, delocalized chain, scattered flakes	MGMSRv2_**0450** (*fixG*) ferredoxin associated with *cbb₃*-type terminal oxidase
	short chain at midcell, regular magnetosomes	MGMSRv2_**1555** (*etfA*) electron transfer protein
	short chain at midcell, regular and defect magnetosomes, scattered flakes	MGMSRv2_**0532** gene encoding conserved protein of unknown function (DUF155)
	short chain at midcell, regular and defect magnetosomes	MGMSRv2_**3192** (*ccmI*) protein involved in c-type cytochrome maturation
	short chain at midcell with regular magnetosomes, flakes at the chain ends	MGMSRv2_**0511** (*dsbB*) membrane protein involved in periplasmic disulfide bond formation
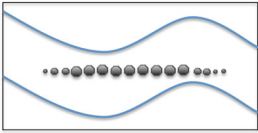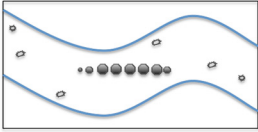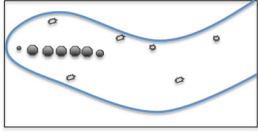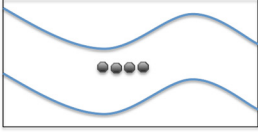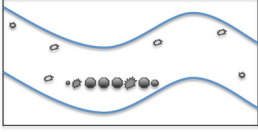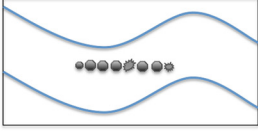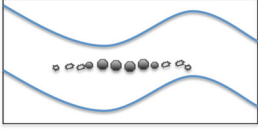
[a]Dark-colored hexagons: regularly shaped and sized, WT-like magnetosomes; dark-colored spiny shapes: irregular magnetosomes; smaller light-colored shapes: thin irregularly shaped, sometimes needle-like particles (flakes) or other aberrantly shaped structures. Selected Wmag clones with Tn5 insertions outside MAI (exMAI) in genes of different functional categories (electron transport, cytochrome *c* maturation, structural disulfide bond formation, amino acid transport) were analyzed by TEM analysis. Here, we summarize the range of typical aberrations with respect to magnetic crystal size and/or number that we found in cells with a Wmag phenotype compared to the that for the wild type. In most cases, cells show shorter magnetosome chains with wild-type crystal morphologies interspersed by more or less defect crystal shapes and/or scattered flakes (80). Also, nearly regular chains with two distinct crystal types were observed. Magnetosome chains in the mutant cells typically retained their centered location but occasionally were also found delocalized at one of the poles. Apart from deviations in magnetosome structure and positioning, we observed general morphological peculiarities, such as aberrant cell shapes and sizes, or larger polyphosphate granules among Tn5 insertion mutants, but these are not described or quantified here.

or in response to unknown stimuli, in which case, they would display a N/Wmag phenotype in the screen. The observation of color-sectored "split" colonies consisting of magnetic and nonmagnetic cells (Fig. 2C) seems to be consistent with this assumption. A similar observation of "false-positive" Nmag mutants in *D. magneticus* RS-1 was

interpreted as being due to either a proportion of Nmag cells naturally occurring in RS-1 cultures or to lagging expression of the magnetic phenotype in cells after iron starvation (34). This phenomenon of unstable magnetic characteristics may, therefore, be a more common but not yet appreciated feature in MTB.

Another conspicuous observation of the present study is the recovery of a small fraction of mutants (10 of 95 confirmed magnetic mutants in exMAI genes [11%]) (Fig. 1) that were permanently devoid of magbiosyn due to Tn*5* insertion in genes outside the MAI. Their nonmagnetic behavior seemed to be caused neither by severe metabolic impairment, as only minor growth defects were observed, nor by second site mutations in the MAI. The latter was verified for two randomly selected mutants by whole-genome analysis, which confirmed single Tn*5* insertions in two different genes (putative transport protein MGMSRv2_2042 and a beta-ketoacyl synthase domain protein MGMSRv2_1257) (see Table S2) apart from minor sequence alterations (single nucleotide polymorphisms [SNPs]) in several accessory genes of the MAI and some genes outside the MAI. The nonmagnetic phenotype of the 10 exMAI clones seemed to suggest an auxiliary, possibly even essential, role of the affected genes in magbiosyn. However, this appears unlikely, since the Nmag phenotype could not be confirmed in the corresponding unmarked deletion mutants that we constructed (in one case, for MGMSRv2_3634 encoding malic enzyme, the construction of a null mutant turned out to be impossible). Instead, five of the null mutants showed wild-type magnetic properties, and four exhibited an only slightly decreased c_{mag} value. Also, all but one of the deletion mutants (MGMSRv2_2042 encoding the putative transporter) were severely growth impaired. Thus, most probably, the observed nonmagnetic behavior of the Tn*5* insertion mutants was due to polar effects on the expression of downstream genes. Nevertheless, with respect to regulation-dependent instable magnetic phenotypes, it is interesting to note that one of the 10 Nmag/exMAI genes encodes a diguanylate cyclase (MGMSRv2_3633), and another three of these exMAI genes (MGMSRv2_1015, MGMSRv2_2042, and MGMSRv2_3634) are located in putative transcription units with genes encoding diguanylate cyclases. Given the importance of the second messenger c-di-GMP in bacterial signal transduction networks (43), the observed Nmag phenotype may also hint at hierarchical regulation processes acting on magbiosyn on/offset upon unknown stimuli (potentially only present under screening conditions). Future research is needed to show the role of these candidate auxiliary genes in magbiosyn.

(ii) Tn*5* insertions in genes of the magnetosome island. Figure 3 shows the distribution of mapped Tn*5* insertion positions across the *M. gryphiswaldense* genome.

In 168 (35%) of the 474 bona fide N/Wmag mutants, Tn*5* insertion mapped to genes within the MAI (inMAI). Notably, the average number of identified Tn*5* hits per gene locus within the 100 kbp of the MAI was nearly three times higher than the average number for the genome (see Fig. S4). Of the 168 inMAI mutants, 120 (71%) were characterized phenotypically in addition to colony color, revealing a stable N/Wmag phenotype for 100 of them (83% of 120 characterized; 77 Nmag, 23 Wmag). This represents approximately 50% of all 195 stable N/Wmag clones and essentially all unambiguous Nmag clones (77/87 [89%]; see above for exceptional cases of putative Nmag clones outside the MAI). In contrast, only 21% (23/108) of all retrieved stable Wmag mutants mapped to the MAI. Since the key determinants for magbiosyn identified to date all reside in the MAI, this result was expected. Nearly all (99%) of the stable nonmagnetic inMAI mutants were hit at different positions within the *mamAB* operon (Fig. S4). Notably, we also retrieved N/Wmag hits in the *mamJ* and *mamK* genes, which do not play a key role in magbiosyn itself but rather in magnetosome chain formation, although it has been shown that deletion of *mamK* results in pleiotropic effects, among them, a significant reduction of magnetosome numbers per cell (44). Also, Tn*5* insertion in *mamJ* or *mamK* may have a polar effect on downstream gene expression of essential magbiosyn genes in the *mamAB* operon.

Some of the MAI genes represented Nmag as well as Wmag mutant alleles (*mamB*, *mamI*, *mamO*, *mamK*, and *mamN* [number of Nmag ≫ number of Wmag]; *mamA*
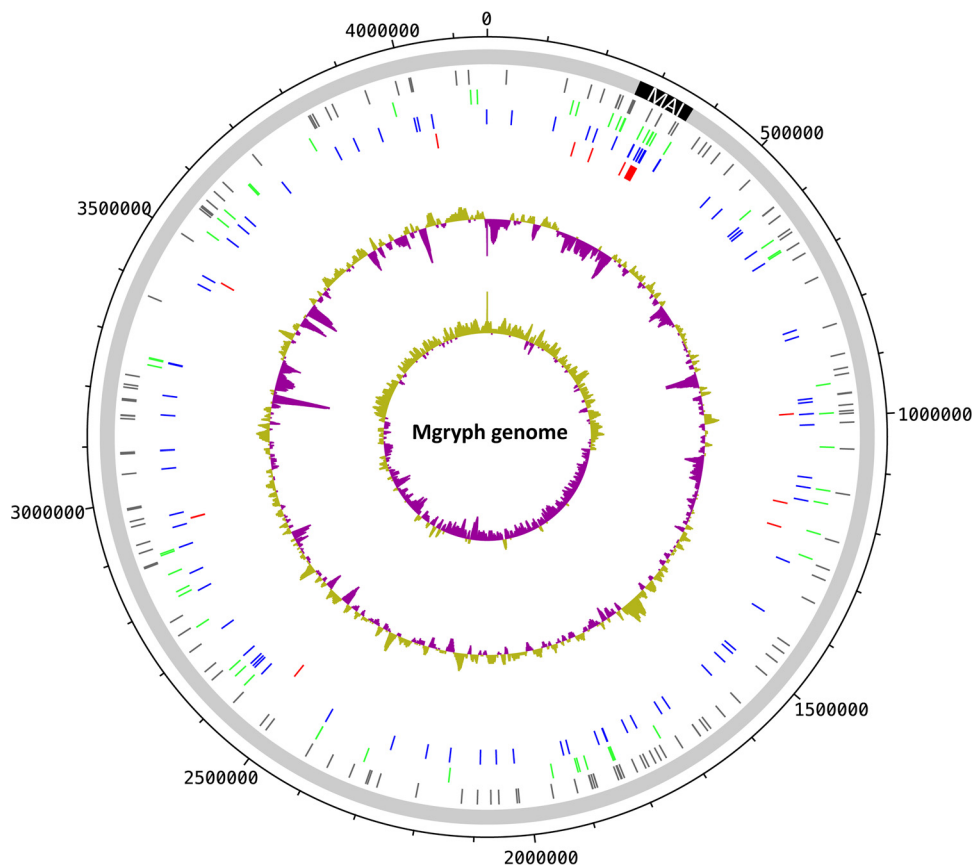
FIG 3 Distribution of Nmag/Wmag Tn*5* insertion sites across the genome of *M. gryphiswaldense* (Mgryph). Ticks (in circles from outside to inside): gray, insertion sites of clones that have been characterized by colony color only; green, insertion sites in WTmag clones; blue, insertion sites in Wmag clones; red, insertion sites in Nmag clones; %(G+C), with values greater than the average GC content in purple and lower than the average in green; GC skew, with values greater than 0 in purple and values less than 0 in green.

[number of Nmag > number of Wmag]; *mamP* [number of Nmag < number of Wmag]). Several MAI genes showed only Wmag mutant phenotypes (*mms6*, *mms36*, *mmsF*, *mamH*, *mamR*, *mamZ*, *mamX*, *feoA1*, and *feoB1*). Neither Wmag nor Nmag mutants were identified in *mamU*, *mamY*, *ftsZ*-like, or, notably, any of the genes of the *mamGFDC* operon. This is consistent with known weak phenotypes of targeted gene deletions (15, 16, 45, 46).

Tn*5* insertion in essential genes of the *mamAB*$_{op}$ of the MAI led to a Wmag instead of a nonmagnetic phenotype in 14% of clones or had no effect on magnetic properties at all (WTmag) in 12% of the clones. This observation may be surprising at first glance. However, it is possible that Tn*5* insertion in these cases affects only certain domains of the gene products, leading to the expression of truncated but at least partially functional proteins. Alternatively, transcriptional readthrough may occur, giving rise to the same effect. Also, in putative transcriptional units, expression of genes downstream of those affected by Tn*5* insertion may still be possible if transcription commences from internal, so far unknown promoters.

(iii) Tn*5* insertions in genes outside the MAI. For 306 (65%) of the 474 bona fide N/Wmag clones, Tn*5* insertions mapped to genes outside the magnetosome island (exMAI). Of these, 158 (52%) were characterized in more detail, yielding 95 Tn*5* insertants (60%) with a confirmed N/Wmag phenotype. These 95 hits correspond to a set of 85 exMAI genes which comprise a pool of putative auxiliary functions for magnetosome biosynthesis (Fig. 1f) (the small fraction of 11% nonmagnetic mutants affected in genes outside the MAI was described above). The majority of the stable

magnetosome mutants with Tn*5* insertion in exMAI genes displayed a Wmag phenotype (85/95 [89%]). exMAI Wmag mutants also represent the dominant fraction of the total of recovered stable Wmag mutants (85/108 [79%]). Since a high frequency of spontaneous deletions in the MAI has been reported for *M. gryphiswaldense* (12, 13), we verified the integrity of the essential *mamAB* operon by PCR amplification for all phenotypically characterized mutants where Tn*5* insertion in an exMAI gene was mapped by arbitrary PCR (ARB-PCR) (selected subset of 72/158 exMAI mutants) (data not shown).

(iv) Wmag mutants affected in genes outside the MAI. Several functional categories of genes were frequently found in the overall pool of exMAI Tn*5* insertants (verified N/Wmag and WTmag, respectively) (Table S2A) (residual bona fide N/Wmag) (Table S2B). These comprise genes involved in (i) redox reactions (e.g., electron transport, cytochrome *c* maturation, and nitrite and nitric oxide reduction), (ii) sulfur metabolism (e.g., cysteine biosynthesis and disulfide bond formation), (iii) signal reception/transduction and chemotaxis/motility, (iv) membrane transport, (v) nitrogen metabolism, (vi) regulation of gene expression, and (vii) fatty acid/lipid metabolism. Strikingly, a number of pathways received multiple hits of Tn*5* insertion, which are explained in detail below. In addition, we recovered some genes of central and carbon metabolism as well as numerous genes encoding conserved proteins of unknown function, among them, some transmembrane proteins, exported proteins, and tetratricopeptide repeat (TPR) containing proteins potentially mediating protein-protein interactions.

To assess whether certain classes of gene functions are characteristic for the set of exMAI Tn*5* hits identified here, we compared the gene product annotations of exMAI Tn*5* hits to those of the whole *M. gryphiswaldense* proteome in a gene ontology (GO) term enrichment analysis (Fisher's exact test [FET]) (see Fig. S1). The test set contained all 75 exMAI Tn*5* insertants with a stable Wmag phenotype, whereas the reference set consisted of the remaining protein-coding sequences of the genome (3,717 genes, 123 MAI genes not included). The FET analysis revealed 57 GO terms significantly overrepresented (P value < 0.05) in the set of Tn5 hits, which correspond to 36 genes (see Table S3). It is noteworthy that among the overrepresented GO terms, "oxidation-reduction process" and "protein histidine kinase activity" are linked to a conspicuously high number of genes within the test set of magnetosome impaired Tn*5* hits (13 and 6 of 36 genes, respectively), indicating that redox reactions and signal transduction events may be of particular importance in support of magbiosyn.

Recently, a number of studies suggested that proteins encoded outside the MAI are potential auxiliary players in magnetosome formation, among them, specific redox-active enzymes. Some of them, such as nitric oxide reductase Nor (24), cytochrome cd_1 nitrite reductase Nir (25), and oxidases such as terminal oxidase Cbb3 (an oxygen sensor [23]), were also part of the potential auxiliary gene set delineated in our present transposon mutagenesis study (Nor, Fig. 4D; Table S2A and B) (Nir and Cbb3, Table S2A and B). This corroborates their potential supportive function in magnetosome formation. In contrast, other genes encoding redox enzymes implicated in the process earlier, for instance, two types of ferric reductase (26), the periplasmic nitrate reductase Nap (24), or regulators such as the ferric uptake regulator (*Mg*Fur, MGMSRv2_3137) (27) and the oxygen sensor *Mg*Fnr, (MGMSRv2_2946, gene *aadR*) (47), have not been retrieved as magnetically deficient Tn*5* insertion clones in our analyses, possibly due to our less-than-fully saturated screen (86% as determined according to the Poisson distribution from the number of Tn*5* hits per gene locus). Interestingly, a different type of regulator, the global carbon metabolism regulator Crp, has recently also been implicated in magbiosyn. Deletion of MGR_1896 [MSR1(L)_26600], encoding a member of the Crp family, has been found to impair magbiosyn, leading to strongly decreased iron content of the cells and misshapen magnetosome crystals (28). Here, we identified a gene encoding a further member of the Crp/Fnr family as a bona fide Wmag Tn*5* insertion (MGMSRv2_1404), which has also been found among the differentially
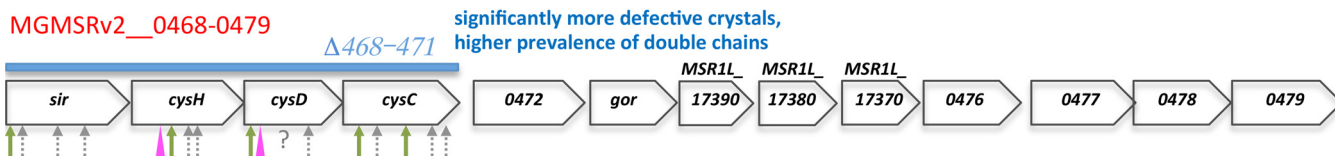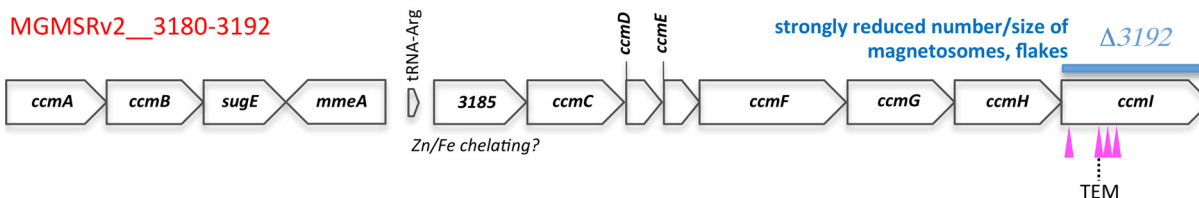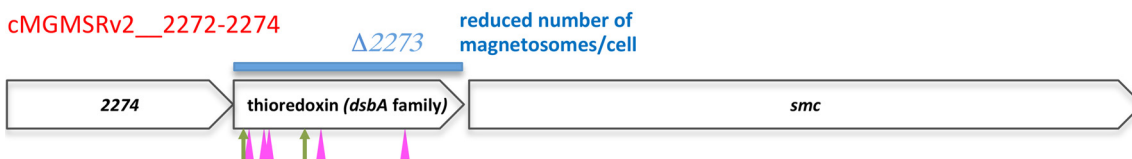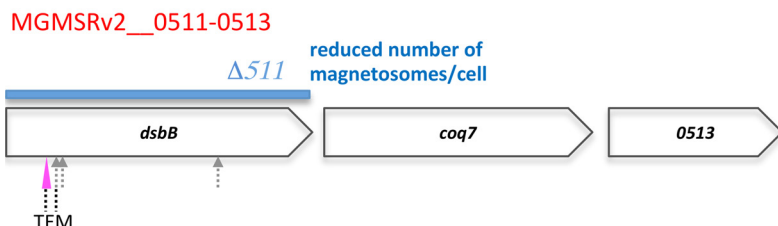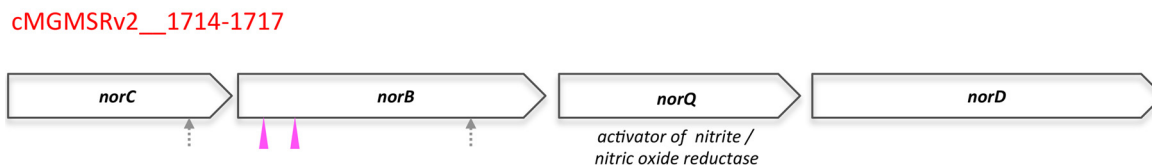
FIG 4 Molecular organization of gene clusters which received more than two Tn5 insertions and are correlated with magnetosome mutant phenotypes. (A to D) Gene clusters are delineated by locus tag ranges (in red above each cluster, corresponding to the MSR-1 v2 genome, MGMSRv2__[number]; "c" means encoded on complementary strand). Open reading frames are labeled either with gene name or with corresponding locus tags of the MSR-1 v2 genome (number only) or the R3/S1 genome (MSR1L_[number]). Tn5 insertion sites are indicated by arrows (green, WTmag; gray, not magnetically characterized; pink, clones at same hit position present as WTmag or Wmag; ?, unknown insertion position) and arrowheads (pink, Wmag). Deletion ranges in deletion mutants are indicated by blue bars above the respective cluster. Availability of TEM images for transposon clones is indicated as well as the respective magnetic phenotype of the constructed null mutants.

expressed genes in a recent transcriptomics study (upregulated under low-oxygen conditions [48]). These findings suggest a link between global carbon metabolism and the energy-consuming process of magbiosyn in the MTB cell. Further notable instances, where the present results are in accordance with earlier suggestions of an auxiliary role in magbiosyn, belong to the class of membrane transporters. Thus, we recovered a N/Wmag Tn5 insertion in a gene encoding a TauE-like transport protein (MGMSRv2_1267) that belongs to the same family as a protein from *D. magneticus* RS-1,

whose encoding gene has been found to yield Nmag cells upon mutation (34). Another potential transport protein, recently identified as a novel candidate for a true magnetosome membrane protein in a proteome analysis by (49), was also part of the N/Wmag gene set identified in our screen (MGMSRv2_3281). This protein belongs to a Bax1 inhibitor family (PF01027; http://pfam.xfam.org/), and a bacterial member of this family has been shown to function as pH-sensitive calcium leak across membranes (50).

(v) Gene clusters/pathways with multiple Tn5 hits. In the course of seven independent rounds of transposon mutagenesis and screening, we observed a conspicuous accumulation of Tn5 insertion events in exMAI genes of specific cellular pathways. In Fig. 4A to D, these genes are depicted in their genomic context (potential operons). Notably, N/Wmag and (revertant) WTmag alleles were often found closely adjacent in the same gene. Particularly frequent Tn5 insertions were found in genes involved in sulfate assimilation, oxidative protein folding, nitric oxide reduction (denitrification pathway), and cytochrome *c* maturation. In the following, we will focus on these pathways.

(vi) Sulfate assimilation. We retrieved 17 mutants where Tn5 insertion mapped in close proximity to one of four adjacent genes of a putative transcription unit involved in sulfate assimilation (Fig. 4A). The accumulation of Tn5 hits in these four genes is conspicuous, even though it turned out that only two of seven clones that we characterized showed a stable Wmag phenotype. These clones were affected in *cysD* (MGMSRv2_0470) and *cysH* (MGMSRv2_0469) encoding ATP sulfurylase and phosphoadenosine phosphosulfate (PAPS) reductase, respectively. We constructed a markerless deletion mutant of the four-gene operon MGMSRv2_0496 to -0470 (Fig. 4A), which exhibited impaired growth especially under oxic conditions but synthesized magnetosome crystals in approximately normal size and number per cell. However, a decisive difference to wild-type cells was the higher prevalence of cells with double magnetosome chains of reduced length and an almost three times increased fraction of imperfect particles, mostly twinned crystals, in null mutant cells. The generation of reduced sulfur during sulfate assimilation affects cysteine biosynthesis and the formation of crucial electron transfer moieties such as iron-sulfur clusters and, hence, has an impact on electron flow and redox state maintenance. Since these processes are known to play an important role in the formation of magnetosomes (23–25, 51–53), their impairment can be expected to have a negative effect on magbiosyn. Interestingly, the expression of sulfate assimilation genes harbored in the above-described Tn5 insertion hot spot has been found to be upregulated in a differential expression study upon shift to high-iron conditions in *M. gryphiswaldense* (54).

(vii) Cytochrome *c*-type biogenesis pathway. We recovered four different Tn5 insertions in a cluster of cytochrome *c* (cyt *c*) maturation genes (Fig. 4B). Notably, they exclusively map to the *ccmI* (*cycH*) gene (MGMSRv2_3192). The cyt *c* biogenesis protein CcmI (CycH) is a tetratricopeptide repeat (TPR)-containing protein thought to act as an apo-cyt *c* chaperone. It is part of the CcmFHI module involved in stereospecific ligation of heme *b* to thiol-reduced apo-cyt *c*. In the cyt *c* maturation system of the alphaproteobacterium *Rhodobacter capsulatus*, CcmI consists of two segments, the N-terminal membrane-spanning CcmI-1 and the C-terminal periplasmic CcmI-2, which are supposed to have different functions (55, 56): CcmI-2 mediates the electron transfer from the cytoplasm to the thiol-oxidized periplasmic apo-cyt *c*, whereas CcmI-1 is responsible for stereospecific ligation of heme *b* to the thiol-reduced apo-cyt *c*. *M. gryphiswaldense* CcmI exhibits a bipartite architecture similar to the homologous *R. capsulatus* protein. All four Tn5 insertions observed in our study mapped to the N-terminal CcmI-1-segment of the *M. gryphiswaldense* protein (see Fig. S5) and yielded a Wmag phenotype in the respective insertion mutants. Two of the four insertion mutants of *ccmI*, strains 11 (20/9) and 26 (5/9), were analyzed in more detail. They synthesized a reduced number of particles with smaller diameter (on average seven particles per cell with a diameter of 21 nm), leading to decreased magnetic response compared to that of wild-type cells (c_{mag} values of 0.96). In TEM images of mutant cells, short magneto-

some chains were found, with mature magnetosomes frequently interspersed by misshapen crystals (Table 1). We constructed an unmarked *ccmI* deletion mutant, which was found to be even more deficient in magnetosome formation, although magbiosyn was not completely abolished (see Table S4). It is likely that the observed ultrastructural deviations in the mutant strains are due to an impairment of cyt *c* maturation caused by reduced CcmI activity, since the MAI harbors four *c*-type cytochromes which, by their putative redox capabilities, may have an important role in the process of magnetosome formation (so-called magnetochromes MamP/E/T/X [57, 58]). Given the presence of additional 32 genes encoding *c*-type cytochromes in the *M. gryphiswaldense* genome, a lower capacity for cyt *c* maturation will likely also inhibit other enzyme systems, for instance, the activity of anaerobic/aerobic respiration enzymes.

(viii) Disulfide bond formation pathway. We recovered 11 Tn5 mutants with insertions in two genes encoding proteins of the disulfide bond (DSB) pathway of periplasmic oxidative protein folding (Fig. 4C), one encoding a DsbA-like protein (MGMSRv2_2273, affected in 7 of the 11 cases) and one encoding DsbB (MGMSRv2_0511, affected in 4 of the 11 cases). c_{mag} characterization of the seven *dsbA* alleles showed a stable Wmag phenotype for six of them and also for the one *dsbB* allele tested. As revealed by TEM analysis, cells of the Wmag *dsbB* insertion displayed mid-cell-positioned magnetosome chains with mature crystals but flakes at the chain ends (Table 1). Upon unmarked deletion of the *dsbB* gene, cells of the null mutant ($\Delta dsbB$) clearly showed a smaller number of magnetosomes, whereas the size of magnetosomes was not significantly reduced (Table S4). The deletion mutant of the *dsbA*-like gene exhibited very short magnetosome chains, occasionally flakes at the chain ends, or few disconnected crystals or flakes (Table S4).

Together, our results suggest that proper folding of periplasmic proteins by disulfide bond formation is a prerequisite for efficient magnetosome biosynthesis. Indeed, several magnetosome membrane proteins possess more than one cysteine residue and might be substrates of this oxidative folding pathway. In proteins that are exported from the cytoplasm to the cell envelope (periplasm, outer membrane, and extracellular environment), disulfide bond formation is part of a maturation process which contributes to their structural stabilization and, thus, ensures their functionality (59). In *Escherichia coli* and other bacteria, several periplasmic disulfide bond-forming proteins (thiol-disulfide oxidoreductases which are members of the thioredoxin superfamily and contain pairs of cysteine residues) are involved in DSB. Periplasmic DsbA introduces disulfide bonds in its protein substrate as it is translocated across the cytoplasmic membrane and becomes reoxidized by the cytoplasmic membrane protein DsbB that in turn passes the electrons to the terminal electron acceptor via a quinone. Periplasmic DsbC and DsbG are protein disulfide isomerases that can correct wrongly positioned disulfide bonds in proteins with more than two cysteine residues. DsbC and DsbG are reduced by the cytoplasmic membrane protein DsbD which, in turn, is provided with electrons from the cytoplasmic thioredoxin system (60). In *M. gryphiswaldense*, DSB seems to comprise homologs of DsbA (MGMSrv2_2273) and DsbB (MGMSrv2_0511) as well as a putative fusion protein of DsbC and DsbD (MGMSrv2_4064). A homolog for DsbG known to protect single cysteine residues in periplasmic proteins from oxidation (61) has not been detected in *M. gryphiswaldense*. DsbA and DsbB are encoded in separate transcription units (Fig. 4C), suggesting that there are many different substrates for the DSB pathway in *M. gryphiswaldense* rather than only few specific ones in which case a *dsbAB* operon would have been expected (60).

Whereas in *E. coli* several DSB protein substrates have been identified (among them, the outer membrane protein OmpA, periplasmic alkaline phosphatase PhoA, the flagellar protein FlgI, the lipopolysaccharide [LPS] assembly protein LptD, the cell division protein FtsN, several lipoproteins, metal transporters, and amino acid/peptide transporters [59]), there are so far no experimentally verified DSB substrates in *M. gryphiswaldense*. However, several membrane proteins of the MAI may be substrates of this pathway, as they possess two or more (up to eight) cysteine residues. Considering the

current magnetosome vesicle formation model (9, 10), MAI membrane proteins exhibiting domains oriented toward the luminal side of the magnetosome vesicle may have been exposed to the periplasm prior to vesicle formation. Where these protein domains contain cysteine residues, they should have been protected from oxidation by the formation of disulfide bonds. MAI membrane proteins that contain more than two cysteines in predicted luminal domains (62) are MamE/F/G/H/N/P/S/T/X/Z (large luminal domains, MamE/P/S/T/X/Z; even number of cysteine residues, MamF/N). If some of these proteins are indeed DSB substrates, impairment of this pathway will have a negative effect on the structural stability and, hence, the abundance of these proteins, which could account for the observed Wmag phenotype of the respective Tn5 insertion mutants. Furthermore, since several periplasmic thiol-redox reactions of the cytochrome *c* maturation system (involving, for instance, CcmH, CcmG, and apo-cyt *c*) depend on the functionality of DSB (63), and given the special importance of cyt *c* for proper function of the magnetochromes MamP/E/T/X, impairment of DSB can be expected to have a fundamentally disturbing effect on the process of magnetosome formation.

Conclusions. In recent years, it has become more and more apparent that the genetic and structural complexity of magbiosyn is larger than originally assumed. It gradually emerges that, apart from the approximately 30 core genes initially thought to orchestrate the magnetic phenotype, there must be many more. We previously observed that transfer of the magbiosyn capability by transplantation of the MAI is possible for certain organisms such as *Rhodospirillum rubrum* (21) and the nonmagnetotactic *Magnetospirillum* sp. strain 15-1 (22), but it failed for many others tested, including *E. coli* (M. V. Dziuba and D. Schüler, unpublished data). This leads to the pivotal question of what the supportive functions required for magbiosyn are in addition to known genes of the MAI. Solving this question would enhance our understanding of microbial biomineralization but also bears great relevance for the fields of synthetic biology and biotechnology (64); for instance, it would considerably facilitate approaches for magnetization of other (micro)organisms.

In the present study, we identified 195 *M. gryphiswaldense* clones compromised in magbiosyn by using a systematic transposon mutagenesis approach. In approximately 50% of the cases, the affected genes were found to be located within the MAI, among them, essentially all of those where transposon insertion yields a stable nonmagnetic phenotype. This underscores the widely proven essentiality of the MAI for the process of magbiosyn and validates our experimental approach. In the other 50% of the N/Wmag genes, encoded outside the MAI, we recovered several that have recently been linked to magnetosome formation as putative supporting determinants, such as nitrate reduction and denitrification (24), thus corroborating the findings of earlier studies and verifying our identification strategy. In contrast to observations reported by earlier studies (12, 13, 33), in none of the tested exMAI Tn5 insertion clones were spontaneous MAI deletions the reason for the observed magbiosyn impairment. That we failed, on the other hand, to retrieve some of the known auxiliary candidates such as iron reductases or the Fur regulator may be due to the fact that our screen is, as expected, not exhaustive (86% probability that all relevant loci have been detected). Another reason may be that the screening approach is still too insensitive for very subtle mutant phenotypes. Nevertheless, our systematic study presents the so far most comprehensive set of auxiliary gene candidates for magbiosyn. In particular, it newly defines certain cellular pathways as specifically important for magbiosyn that are conserved in MTB but have not been implicated in this process so far, such as periplasmic disulfide bond formation, cytochrome *c* maturation, and sulfate assimilation.

In theory, recent high-throughput specifications of Tn mutagenesis (e.g., Tn-seq [35, 65]) may, by their unbiased high-throughput design, have the potential to yield a more rigorous assessment. Approaches such as Tn-seq have proven to be extremely powerful in delineating complete numbers of alleles involved in several bacterial pathways, e.g.,

the production of antibiotics (66), sporulation (67), or methylotrophy (68). However, a great advantage of our conventional approach of genome-wide transposon insertion mutagenesis in the search for genes supporting magbiosyn is that it allows direct targeting of growth/fitness-unrelated functions, which cannot be easily selected against in Tn-seq approaches. Also, with our conventional approach, a correlation between pheno- and genotype at the level of clones is possible.

Apart from the result of a manageable pool of putative auxiliary determinants as the basis for further experimental work, there are two main insights from our study. First, and notably, outside the MAI, we could not detect further MTB-specific gene clusters involved in magbiosyn. Rather, the process of magbiosyn seems to be particularly dependent on the function of a number of general cellular pathways; apparently, it is vulnerable if these pathways are impaired. Their genes (i) ensure the proper folding of proteins that directly take part in the process of magbiosyn, (ii) provide the cell with sufficient amounts of redox mediators by affecting their maturation, such as in the case of cyt *c*, or by enabling their biosynthesis through furnishing important amino acids such as cysteine in the case of iron sulfur clusters, (iii) act in/modify cellular nitrogen metabolism, (iv) balance cellular energy metabolism, (v) take part in cell wall biosynthesis/modification (with reservations, since the genes of this category may pop up as false positives in the visual screen because of changes in colony appearance caused by an altered cell surface), and (vi) are responsible for signaling and regulatory cues in the context of magbiosyn. Except for the magbiosyn-specific signaling modules, all of the pathways mentioned above may result in decreased cellular fitness when disturbed. However, insertion mutants affected in these genes were found to grow rather well yet were more or less severely affected in magbiosyn as judged by the structural defects of magnetosomes and chains. Thus, the pathways we identified seem to affect magbiosyn particularly strongly.

Second, our results suggest that regulation of magnetosome formation may be interlaced with cellular state by cues from cellular (energy) metabolism. Transcriptional regulators of specific MAI genes may serve as auxiliary genes, since ill-balanced expression levels might be sufficient to disturb the process of magbiosyn and cause an aberrant magnetic phenotype. An extreme case may be exemplified by nonmagnetic Tn*5* insertions affected in metabolic genes, such as those encoding malic enzyme and others (see above). One could imagine that certain pathways, when impaired, challenge cellular fitness in a specific way, requiring larger efforts of the cell to cope with the corresponding stress situation, thereby leading to a cutdown of cellular resources for magbiosyn as a beneficial but nonvital process and, thus, resulting in a mutant magnetic phenotype. If so, one could expect that magbiosyn as a costly process is not turned on at all to save all resources for stress management. The consequence would be a nonmagnetic phenotype. Future experimental work is necessary to evaluate the hypotheses inferred from the results of the present study. In this context, it would be interesting to also address the question about a (master) regulator(s) for magbiosyn (other than oxygen) that may act as a "switch" integrating different types of cellular information with magbiosyn to regulate on/offset of this costly process depending on the cellular state.

Finally, we close these considerations with a different interpretation of our data. Although specific auxiliary genes for magbiosyn may exist—and several of the genes retrieved in this study might turn out as such—it is also possible that the ground for magbiosyn is prepared by a more general metabolic network rather than by specific single genes. Our observation of basic conserved cellular pathways as particularly relevant for magnetosome formation and the broad spectrum of functions in the delineated set of candidate auxiliary genes support this notion. It would also be in line with the hypothesis of an earlier study proposing that the potential of an organism to synthesize magnetosomes is dependent on a specific metabolic profile (69).

MATERIALS AND METHODS

Bacterial strains, plasmids, and growth conditions. *Escherichia coli* strain WM3064 was grown in LB medium with 300 μM diaminopimelic acid (DAP) (70). Routinely, bacterial strains were cultivated on solid media with 1.5% (wt/vol) agar. For strains carrying recombinant plasmids, media were supplemented with 25 μg/ml kanamycin (Km) for *E. coli* WM3064 and 5 μg/ml Km and 30 μg/ml ampicillin (Amp) for *M. gryphiswaldense*. Bacterial strains and plasmids used in this study are described in Table S1A in the supplemental material.

Cultivation of *Magnetospirillum gryphiswaldense* MSR-1. (i) Plate cultivation of *M. gryphiswaldense* cells for phenotypic screening. In summary, maximum expression of the magnetic phenotype was achieved using the following optimized conditions, which were then consistently applied throughout all subsequent experiments: 140 ml of improved colony formation medium (ICFM), i.e., flask standard medium (FSM [51]) supplied with an increased amount of iron (500 μM), in large-size (150 mm) Petri dishes at low seeding density of a maximum of 100 Km-resistant Tn-insertant colonies per plate (1 to 2 colonies per cm²) with an increased incubation time (>14 days) at 28°C under microoxic (2% O_2 in the headspace) or fully anoxic (100% N_2 in the headspace) conditions.

(ii) Liquid cultivation. *M. gryphiswaldense* was grown microaerobically in FSM at 30°C with moderate agitation (120 rpm). To record growth curves, microaerobically grown precultures of all strains were inoculated at an optical density at 565 nm (OD_{565}) of 0.025 into 3 ml FSM with 8 mM sodium nitrate (oxic, microoxic, and anoxic growth) or 4 mM ammonium chloride instead of sodium nitrate (oxic growth only) in six-well plates with duplicates per strain. Cultures were then incubated for 48 h at room temperature under oxic, microoxic, and anoxic conditions. For oxic conditions, the plates were placed under ambient oxygen concentration, while for microoxic conditions, plates were incubated in metal jars with 2% O_2 in 98% N_2. Anaerobic conditions were achieved by incubation in a 100% N_2 atmosphere in glass jars. OD_{565} was then measured at regular time intervals with an Infinite M200 Pro plate reader (Tecan, Switzerland), shaking the plates for 40 s before each measurement. To avoid disturbance of anoxic conditions, OD_{565} was only measured at 0 and 48 h for anaerobic cultures. At the end of the experiment, aliquots of cultures were taken to analyze cellular magnetic response (c_{mag}) with an Ultrospec 2100 pro (Biosciences, Amersham) photometer as described previously (36) and to prepare transmission electron microscope (TEM) samples.

Oxygen band formation and gas production were analyzed in oxygen gradient tubes containing FSM with 0.3% agar inoculated with cell cultures from microoxic Hungate tubes. Oxygen gradient tubes were incubated for 48 h at 27°C under atmospheric conditions.

DNA protocols. DNA isolation, digestion, ligation, and transformation were essentially according to standard methods (70). PCR products and vector inserts were sequenced using BigDye Terminator version 3.1 chemistry (Applied Biosystems, Darmstadt, Germany) on an ABI 3700 capillary sequencer.

Construction of the transposition vector pBAMOpt. To increase transposition frequencies in *M. gryphiswaldense*, the transposase-encoding *tnpA* gene residing in the engineered mini-Tn5 transposon vector pBAM1 (41) was replaced by a synthetic codon-optimized allele under the control of a strong native promoter (P$_{mamDC45}$) (42), resulting in the plasmid pBAMOpt (Fig. 1). The synthetic transposase gene with the native promoter P$_{mamDC45}$ was designed and synthesized by GeneArt (Thermo Fisher Scientific) and provided in a standard vector that was transformed into *E. coli* DH5α. The strain was grown, and the plasmid was extracted and digested with Swa/PmeI. The DNA band of the correct size was then purified and cloned into a linearized pBAM1 devoid of its transposase gene. pBAMOpt with the optimized transposase and native strong promoter was checked for correct sequence.

Construction of a Tn5 insertion library. The pBAMOpt plasmid was used to create random Tn5 insertion mutants in *M. gryphiswaldense*. It was mass conjugated from *E. coli* WM3064 to *M. gryphiswaldense* wild-type cells as previously described (38), using 10^9 *M. gryphiswaldense* cells and a donor/recipient ratio of 1:1. The resulting cell pool was then plated on large selection plates (Km, 5 μg/ml) as described above in "Plate cultivation of *M. gryphiswaldense* cells for phenotypic screening."

Screening for *M. gryphiswaldense* Tn5 insertion mutants. After at least 14 days at 28°C, *M. gryphiswaldense* conjugation colonies able to grow on FSM-Km, indicating a Tn5 insertion in the genome, were screened for Wmag and Nmag mutants by colony color. This screening was purely visual: only colonies with a color strikingly different from the dark brown color of the wild type (e.g., cream to whitish) were picked, regrown in 96-well plates, and then cultivated in Hungate tubes. At this stage, the c_{mag} value of the mutant culture was measured, and a sample for inspection by TEM was prepared.

Testing for spontaneous deletions in MAI. To account for the expected high rate of spontaneous MAI rearrangements in *M. gryphiswaldense* (12, 29), all clones found by ARB-PCR (see below) to carry a Tn5 insertion in genes outside the MAI were checked for deletions in the *mamAB* operon. Mutants were initially screened for the presence of each gene within the 16-kb region of the *mamAB* operon. PCR was used to amplify 1- to 3-kb sections of the *mam* gene cluster to determine their presence, absence, or change in length. Primers for this screening PCR are listed in Table S1B.

Identification of Tn5 interrupted genes by mapping of Tn insertion sites. Mutants with apparently intact MAI were selected, and transposon insertion sites were identified by arbitrary PCR (ARB-PCR) (41, 71) or by Cartesian pooling (72) in combination with hybrid capture (73). Transposon/genome junctions were sequenced and compared against the genomic DNA sequence of *M. gryphiswaldense* (GenBank accession CP027527 [locus tag MSR1L] [74]; the locus tag MGMSRv2 refers to an older genome sequence [75] with GenBank accession HG794546.1) using the BLAST algorithm to pinpoint Tn5-interrupted genes. All basic bioinformatic operations for genome navigation, insertion site mapping, and gene function prediction were performed in Geneious v9 (Biomatters, Ltd., Auckland, New Zealand). For

graphic visualization of Tn5 insertion site distribution across the *M. gryphiswaldense* genome, DNAplotter (76) was used together with the Artemis platform (77).

Phenotypic characterization of Tn5 mutants. Growth of Tn5 insertants was assessed by measuring optical density (OD) at 565 nm. Cultures with no severe growth defect were further screened for magnetic phenotype by determination of c_{mag} (36). For a set of mutants, cells were also assessed by optical microscopy for their swimming behavior, cell shape, and alignment in response to an externally applied magnetic field. Magnetosome morphology was analyzed with respect to size, shape, and numbers per cell by TEM analysis. For this, concentrated cells were adsorbed onto carbon-coated copper grids (Science Services, Munich, Germany) and imaged at 80 kV without negative staining in a TECNAI F20 microscope (FEI, Eindhoven, Netherlands). Ultrastructural analysis of mutants provided information on modifications in magnetosome biosynthesis as well as magnetosome organization.

Construction of vectors for markerless deletion mutagenesis. Markerless in-frame deletion mutants were constructed using a RecA-mediated homologous recombination system as described previously (78). For the generation of the deletion plasmid, homologous regions of around 900 to 1,000 bp up- and downstream of the gene of interest were amplified with Phusion DNA polymerase (Thermo Scientific), fused by an overlapping PCR, and ligated to "blunt ends" of an EcoRV-digested pORFM-GalK vector. The deletion plasmid was transferred to *M. gryphiswaldense* by conjugation, using *E. coli* WM3064 as a donor strain. Selection for insertion mutants was conducted by incubation on solid Km-medium. After *galK*-based counterselection, correct deletion was verified by PCR and sequencing.

(i) Gene ontology term enrichment analysis. Protein-coding regions of the *M. gryphiswaldense* genome were annotated with the Blast2GO annotation workflow (79) using NCBI's RefSeq protein databases in combination with EBI's InterProScan service as described in the Blast2GO manual. An enrichment analysis of GO terms (Fisher's exact test [FET]) was performed for the gene set of Tn5 hits outside MAI leading to a stable Wmag phenotype (test list, 75 genes) against the annotated GO terms of the *M. gryphiswaldense* protein coding regions (reference list, 3,717 protein coding regions with 123 MAI genes excluded; GenBank accession CP027527) to test whether certain functions are overrepresented in the set of Tn5-interrupted genes compared to that in the genomic background (see cartoon in Fig. S1).

SUPPLEMENTAL MATERIAL

Supplemental material is available online only.

FIG S1, PDF file, 0.4 MB.
FIG S2, PDF file, 0.1 MB.
FIG S3, PDF file, 0.2 MB.
FIG S4, PDF file, 1.7 MB.
FIG S5, PDF file, 1.1 MB.
TABLE S1, PDF file, 0.1 MB.
TABLE S2, PDF file, 0.2 MB.
TABLE S3, PDF file, 0.03 MB.
TABLE S4, PDF file, 0.6 MB.

REFERENCES

1. Frankel RB. 1984. Magnetic guidance of organisms. Annu Rev Biophys Bioeng 13:85–103. https://doi.org/10.1146/annurev.bb.13.060184.000505.
2. Schüler D, Frankel RB. 1999. Bacterial magnetosomes: microbiology, biomineralization and biotechnological applications. Appl Microbiol Biotechnol 52:464–473. https://doi.org/10.1007/s002530051547.
3. Faivre D, Schüler D. 2008. Magnetotactic bacteria and magnetosomes. Chem Rev 108:4875–4898. https://doi.org/10.1021/cr078258w.
4. Popp F, Armitage JP, Schüler D. 2014. Polarity of bacterial magnetotaxis is controlled by aerotaxis through a common sensory pathway. Nat Commun 5:5398. https://doi.org/10.1038/ncomms6398.
5. Schleifer K-H, Schüler D, Spring S, Weizenegger M, Amann R, Ludwig W, Köhler M. 1991. The genus *Magnetospirillum* gen. nov. Description of *Mag-*

netospirillum gryphiswaldense sp. nov. and transfer of *Aquaspirillum magnetotacticum* to *Magnetospirillum magnetotacticum* comb. nov. Syst Appl Microbiol 14:379–385. https://doi.org/10.1016/S0723-2020(11)80313-9.
6. Schüler D, Köhler M. 1992. The isolation of a new magnetic spirillum. Zentralbl Mikrobiol 147:150–151. https://doi.org/10.1016/S0232-4393(11)80377-X.
7. Matsunaga T, Sakaguchi T, Tadakoro F. 1991. Magnetite formation by a magnetic bacterium capable of growing aerobically. Appl Microbiol Biotechnol 35:651–655. https://doi.org/10.1007/BF00169632.
8. Lohße A, Borg S, Raschdorf O, Kolinko I, Tompa E, Pósfai M, Faivre D, Baumgartner J, Schüler D. 2014. Genetic dissection of the *mamAB* and *mms6* operons reveals a gene set essential for magnetosome biogenesis

in *Magnetospirillum gryphiswaldense*. J Bacteriol 196:2658–2669. https://doi.org/10.1128/JB.01716-14.

9. Raschdorf O, Forstner Y, Kolinko I, Uebe R, Plitzko JM, Schüler D. 2016. Genetic and ultrastructural analysis reveals the key players and initial steps of bacterial magnetosome membrane biogenesis. PLoS Genet 12:e1006101. https://doi.org/10.1371/journal.pgen.1006101.

10. Uebe R, Schüler D. 2016. Magnetosome biogenesis in magnetotactic bacteria. Nat Rev Microbiol 14:621–637. https://doi.org/10.1038/nrmicro.2016.99.

11. McCausland HC, Komeili A. 2020. Magnetic genes: studying the genetics of biomineralization in magnetotactic bacteria. PLoS Genet 16:e1008499. https://doi.org/10.1371/journal.pgen.1008499.

12. Ullrich S, Kube M, Schübbe S, Reinhardt R, Schüler D. 2005. A hypervariable 130-kilobase genomic region of *Magnetospirillum gryphiswaldense* comprises a magnetosome island which undergoes frequent rearrangements during stationary growth. J Bacteriol 187:7176–7184. https://doi.org/10.1128/JB.187.21.7176-7184.2005.

13. Schübbe S, Kube M, Scheffel A, Wawer C, Heyen U, Meyerdierks A, Madkour MH, Mayer F, Reinhardt R, Schüler D. 2003. Characterization of a spontaneous nonmagnetic mutant of *Magnetospirillum gryphiswaldense* reveals a large deletion comprising a putative magnetosome island. J Bacteriol 185:5779–5790. https://doi.org/10.1128/jb.185.19.5779-5790.2003.

14. Grünberg K, Müller EC, Otto A, Reszka R, Linder D, Kube M, Reinhardt R, Schüler D. 2004. Biochemical and proteomic analysis of the magnetosome membrane in *Magnetospirillum gryphiswaldense*. Appl Environ Microbiol 70:1040–1050. https://doi.org/10.1128/aem.70.2.1040-1050.2004.

15. Lohße A, Ullrich S, Katzmann E, Borg S, Wanner G, Richter M, Voigt B, Schweder T, Schüler D. 2011. Functional analysis of the magnetosome island in *Magnetospirillum gryphiswaldense*: the *mamAB* operon is sufficient for magnetite biomineralization. PLoS One 6:e25561. https://doi.org/10.1371/journal.pone.0025561.

16. Murat D, Quinlan A, Vali H, Komeili A. 2010. Comprehensive genetic dissection of the magnetosome gene island reveals the step-wise assembly of a prokaryotic organelle. Proc Natl Acad Sci U S A 107:5593–5598. https://doi.org/10.1073/pnas.0914439107.

17. Lefèvre CT, Trubitsyn D, Abreu F, Kolinko S, Jogler C, de Almeida LGP, de Vasconcelos ATR, Kube M, Reinhardt R, Lins U, Pignol D, Schüler D, Bazylinski DA, Ginet N. 2013. Comparative genomic analysis of magnetotactic bacteria from the *Deltaproteobacteria* provides new insights into magnetite and greigite magnetosome genes required for magnetotaxis. Environ Microbiol 15:2712–2735. https://doi.org/10.1111/1462-2920.12128.

18. Lin W, Zhang W, Zhao X, Roberts AP, Paterson GA, Bazylinski DA, Pan Y. 2018. Genomic expansion of magnetotactic bacteria reveals an early common origin of magnetotaxis with lineage-specific evolution. ISME J 12:1508–1519. https://doi.org/10.1038/s41396-018-0098-9.

19. Monteil CL, Perrière G, Menguy N, Ginet N, Alonso B, Waisbord N, Cruveiller S, Pignol D, Lefèvre CT. 2018. Genomic study of a novel magnetotactic *Alphaproteobacteria* uncovers the multiple ancestry of magnetotaxis. Environ Microbiol 20:4415–4430. https://doi.org/10.1111/1462-2920.14364.

20. Monteil CL, Lefèvre CT. 2020. Magnetoreception in microorganisms. Trends Microbiol 28:266–275. https://doi.org/10.1016/j.tim.2019.10.012.

21. Kolinko I, Lohße A, Borg S, Raschdorf O, Jogler C, Tu Q, Pósfai M, Tompa E, Plitzko JM, Brachmann A, Wanner G, Müller R, Zhang Y, Schüler D. 2014. Biosynthesis of magnetic nanostructures in a foreign organism by transfer of bacterial magnetosome gene clusters. Nat Nanotechnol 9:193–197. https://doi.org/10.1038/nnano.2014.13.

22. Dziuba MV, Zwiener T, Uebe R, Schüler D. 2020. Single-step transfer of biosynthetic operons endows a non-magnetotactic *Magnetospirillum* strain from wetland with magnetosome biosynthesis. Environ Microbiol 22:1603–1618. https://doi.org/10.1111/1462-2920.14950.

23. Li Y, Raschdorf O, Silva KT, Schüler D. 2014. The terminal oxidase *cbb*₃ functions in redox control of magnetite biomineralization in *Magnetospirillum gryphiswaldense*. J Bacteriol 196:2552–2562. https://doi.org/10.1128/JB.01652-14.

24. Li Y, Katzmann E, Borg S, Schüler D. 2012. The periplasmic nitrate reductase Nap is required for anaerobic growth and involved in redox control of magnetite biomineralization in *Magnetospirillum gryphiswaldense*. J Bacteriol 194:4847–4856. https://doi.org/10.1128/JB.00903-12.

25. Li Y, Bali S, Borg S, Katzmann E, Ferguson SJ, Schüler D. 2013. Cytochrome *cd*₁ nitrite reductase NirS is involved in anaerobic magnetite biomineralization in *Magnetospirillum gryphiswaldense* and requires NirN for proper *d*₁ heme assembly. J Bacteriol 195:4297–4309. https://doi.org/10.1128/JB.00686-13.

26. Zhang C, Meng X, Li N, Wang W, Sun Y, Jiang W, Guan G, Li Y. 2013. Two bifunctional enzymes with ferric reduction ability play complementary roles during magnetosome synthesis in *Magnetospirillum gryphiswaldense* MSR-1. J Bacteriol 195:876–885. https://doi.org/10.1128/JB.01750-12.

27. Uebe R, Voigt B, Schweder T, Albrecht D, Katzmann E, Lang C, Böttger L, Matzanke B, Schüler D. 2010. Deletion of a fur-like gene affects iron homeostasis and magnetosome formation in *Magnetospirillum gryphiswaldense*. J Bacteriol 192:4192–4204. https://doi.org/10.1128/JB.00319-10.

28. Wen T, Guo F, Zhang Y, Tian J, Li Y, Li J, Jiang W. 2016. A novel role for Crp in controlling magnetosome biosynthesis in *Magnetospirillum gryphiswaldense* MSR-1. Sci Rep 6:21156. https://doi.org/10.1038/srep21156.

29. Kolinko I, Jogler C, Katzmann E, Schüler D. 2011. Frequent mutations within the genomic magnetosome island of *Magnetospirillum gryphiswaldense* are mediated by RecA. J Bacteriol 193:5328–5334. https://doi.org/10.1128/JB.05491-11.

30. Wahyudi AT, Takeyama H, Matsunaga T. 2001. Isolation of *Magnetospirillum magneticum* AMB-1 mutants defective in bacterial magnetic particle synthesis by transposon mutagenesis. Appl Biochem Biotechnol 91–93:147–154. https://doi.org/10.1385/ABAB:91-93:1-9:147.

31. Matsunaga T, Okamura Y, Fukuda Y, Wahyudi AT, Murase Y, Takeyama H. 2005. Complete genome sequence of the facultative anaerobic magnetotactic bacterium *Magnetospirillum* sp. strain AMB-1. DNA Res 12:157–166. https://doi.org/10.1093/dnares/dsi002.

32. Komeili A, Vali H, Beveridge TJ, Newman DK. 2004. Magnetosome vesicles are present before magnetite formation, and MamA is required for their activation. Proc Natl Acad Sci U S A 101:3839–3844. https://doi.org/10.1073/pnas.0400391101.

33. Nash CZ. 2008. Mechanisms and evolution of magnetotactic bacteria. PhD thesis. California Institute of Technology, Pasadena, CA.
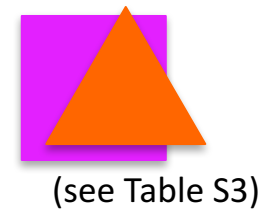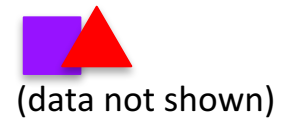
34. Rahn-Lee L, Byrne ME, Zhang M, Le Sage D, Glenn DR, Milbourne T, Walsworth RL, Vali H, Komeili A. 2015. A genetic strategy for probing the functional diversity of magnetosome formation. PLoS Genet 11:e1004811. https://doi.org/10.1371/journal.pgen.1004811.

35. van Opijnen T, Camilli A. 2013. Transposon insertion sequencing: a new tool for systems-level analysis of microorganisms. Nat Rev Microbiol 11:435–442. https://doi.org/10.1038/nrmicro3033.

36. Schüler D, Uhl R, Bäuerlein E. 1995. A simple light-scattering method to assay magnetism in *Magnetospirillum gryphiswaldense*. FEMS Microbiology Lett 132:139–145. https://doi.org/10.1111/j.1574-6968.1995.tb07823.x.

37. Blakemore RP. 1982. Magnetotactic bacteria. Annu Rev Microbiol 36:217–238. https://doi.org/10.1146/annurev.mi.36.100182.001245.

38. Schultheiss D, Schüler D. 2003. Development of a genetic system for *Magnetospirillum gryphiswaldense*. Arch Microbiol 179:89–94. https://doi.org/10.1007/s00203-002-0498-z.

39. Schüler D. 2008. Genetics and cell biology of magnetosome formation in magnetotactic bacteria. FEMS Microbiol Rev 32:654–672. https://doi.org/10.1111/j.1574-6976.2008.00116.x.

40. Matsunaga T, Nakamura C, Burgess JG, Sode K. 1992. Gene-transfer in magnetic bacteria: transposon mutagenesis and cloning of genomic DNA fragments required for magnetosome synthesis. J Bacteriol 174:2748–2753. https://doi.org/10.1128/jb.174.9.2748-2753.1992.

41. Martínez-García E, Calles B, Arévalo-Rodríguez M, de Lorenzo V. 2011. pBAM1: an all-synthetic genetic tool for analysis and construction of complex bacterial phenotypes. BMC Microbiol 11:38. https://doi.org/10.1186/1471-2180-11-38.

42. Borg S, Hofmann J, Pollithy A, Lang C, Schüler D. 2014. New vectors for chromosomal integration enable high-level constitutive or inducible magnetosome expression of fusion proteins in *Magnetospirillum gryphiswaldense*. Appl Environ Microbiol 80:2609–2616. https://doi.org/10.1128/AEM.00192-14.

43. Hengge R. 2009. Principles of c-di-GMP signalling in bacteria. Nat Rev Microbiol 7:263–273. https://doi.org/10.1038/nrmicro2109.

44. Katzmann E, Scheffel A, Gruska M, Plitzko JM, Schüler D. 2010. Loss of the actin-like protein MamK has pleiotropic effects on magnetosome formation and chain assembly in *Magnetospirillum gryphiswaldense*. Mol Microbiol 77:208–224. https://doi.org/10.1111/j.1365-2958.2010.07202.x.

45. Müller FD, Raschdorf O, Nudelman H, Messerer M, Katzmann E, Plitzko JM, Zarivach R, Schüler D. 2014. The FtsZ-like protein FtsZm of *Magnetospirillum gryphiswaldense* likely interacts with its generic homolog and is required for biomineralization under nitrate deprivation. J Bacteriol 196:650–659. https://doi.org/10.1128/JB.00804-13.

46. Scheffel A, Gärdes A, Grünberg K, Wanner G, Schüler D. 2008. The major magnetosome proteins MamGFDC are not essential for magnetite biomineralization in *Magnetospirillum gryphiswaldense* but regulate the

size of magnetosome crystals. J Bacteriol 190:377–386. https://doi.org/10.1128/JB.01371-07.

47. Li Y, Sabaty M, Borg S, Silva KT, Pignol D, Schüler D. 2014. The oxygen sensor MgFnr controls magnetite biomineralization by regulation of denitrification in *Magnetospirillum gryphiswaldense*. BMC Microbiol 14:153. https://doi.org/10.1186/1471-2180-14-153.

48. Wang X, Wang Q, Zhang Y, Wang Y, Zhou Y, Zhang W, Wen T, Li L, Zuo M, Zhang Z, Tian J, Jiang W, Li Y, Wang L, Li J. 2016. Transcriptome analysis reveals physiological characteristics required for magnetosome formation in *Magnetospirillum gryphiswaldense* MSR-1. Environ Microbiol Rep 8:371–381. https://doi.org/10.1111/1758-2229.12395.

49. Raschdorf O, Bonn F, Zeytuni N, Zarivach R, Becher D, Schüler D. 2018. A quantitative assessment of the membrane-integral sub-proteome of a bacterial magnetic organelle. J Proteomics 172:89–99. https://doi.org/10.1016/j.jprot.2017.10.007.

50. Chang Y, Bruni R, Kloss B, Assur Z, Kloppmann E, Rost B, Hendrickson WA, Liu Q. 2014. Structural basis for a pH-sensitive calcium leak across membranes. Science 344:1131–1135. https://doi.org/10.1126/science.1252043.

51. Heyen U, Schüler D. 2003. Growth and magnetosome formation by microaerophilic *Magnetospirillum* strains in an oxygen-controlled fermentor. Appl Microbiol Biotechnol 61:536–544. https://doi.org/10.1007/s00253-002-1219-x.

52. Katzmann E, Eibauer M, Lin W, Pan Y, Plitzko JM, Schüler D. 2013. Analysis of magnetosome chains in magnetotactic bacteria by magnetic measurements and automated image analysis of electron micrographs. Appl Environ Microbiol 79:7755–7762. https://doi.org/10.1128/AEM.02143-13.

53. Moisescu C, Ardelean II, Benning LG. 2014. The effect and role of environmental conditions on magnetosome synthesis. Front Microbiol 5:49. https://doi.org/10.3389/fmicb.2014.00049.

54. Wang Q, Wang X, Zhang W, Li X, Zhou Y, Li D, Wang Y, Tian J, Jiang W, Zhang Z, Peng Y, Wang L, Li Y, Li J. 2017. Physiological characteristics of *Magnetospirillum gryphiswaldense* MSR-1 that control cell growth under high-iron and low-oxygen conditions. Sci Rep 7:2800. https://doi.org/10.1038/s41598-017-03012-4.

55. Sanders C, Turkarslan S, Lee D-W, Daldal F. 2010. Cytochrome *c* biogenesis: the Ccm system. Trends Microbiol 18:266–274. https://doi.org/10.1016/j.tim.2010.03.006.

56. Sanders C, Boulay C, Daldal F. 2007. Membrane-spanning and periplasmic segments of CcmI have distinct functions during cytochrome *c* biogenesis in *Rhodobacter capsulatus*. J Bacteriol 189:789–800. https://doi.org/10.1128/JB.01441-06.

57. Siponen MI, Adryanczyk G, Ginet N, Arnoux P, Pignol D. 2012. Magnetochrome: a *c*-type cytochrome domain specific to magnetotatic bacteria. Biochem Soc Trans 40:1319–1323. https://doi.org/10.1042/BST20120104.

58. Arnoux P, Siponen MI, Lefevre CT, Ginet N, Pignol D. 2014. Structure and evolution of the magnetochrome domains: no longer alone. Front Microbiol 5:117. https://doi.org/10.3389/fmicb.2014.00117.

59. Landeta C, Boyd D, Beckwith J. 2018. Disulfide bond formation in prokaryotes. Nat Microbiol 3:270–280. https://doi.org/10.1038/s41564-017-0106-2.

60. Hatahet F, Boyd D, Beckwith J. 2014. Disulfide bond formation in prokaryotes: history, diversity and design. Biochim Biophys Acta 1844:1402–1414. https://doi.org/10.1016/j.bbapap.2014.02.014.

61. Depuydt M, Leonard SE, Vertommen D, Denoncin K, Morsomme P, Wahni K, Messens J, Carroll KS, Collet JF. 2009. A periplasmic reducing system protects single cysteine residues from oxidation. Science 326:1109–1109. https://doi.org/10.1126/science.1179557.

62. Nudelman H, Zarivach R. 2014. Structure prediction of magnetosome-associated proteins. Front Microbiol 5:9. https://doi.org/10.3389/fmicb.2014.00009.

63. Verissimo AF, Khalfaoui-Hassani B, Hwang J, Steimle S, Selamoglu N, Sanders C, Khatchikian CE, Daldal F. 2017. The thioreduction component CcmG confers efficiency and the heme ligation component CcmH ensures stereo-specificity during cytochrome *c* maturation. J Biol Chem 292:13154–13167. https://doi.org/10.1074/jbc.M117.794586.

64. Vargas G, Cypriano J, Correa T, Leão P, Bazylinski DA, Abreu F. 2018. Applications of magnetotactic bacteria, magnetosomes and magnetosome crystals in biotechnology and nanotechnology: mini-review. Molecules 23:2438. https://doi.org/10.3390/molecules23102438.

65. van Opijnen T, Bodi KL, Camilli A. 2009. Tn-seq: high-throughput parallel sequencing for fitness and genetic interaction studies in microorganisms. Nat Methods 6:767–772. https://doi.org/10.1038/nmeth.1377.

66. Petzke L, Luzhetskyy A. 2009. *In vivo* Tn5-based transposon mutagenesis of *Streptomycetes*. Appl Microbiol Biotechnol 83:979–986. https://doi.org/10.1007/s00253-009-2047-z.

67. Meeske AJ, Rodrigues CDA, Brady J, Lim HC, Bernhardt TG, Rudner DZ. 2016. High-throughput genetic screens identify a large and diverse collection of new sporulation genes in *Bacillus subtilis*. PLoS Biol 14:e1002341. https://doi.org/10.1371/journal.pbio.1002341.

68. Ochsner AM, Christen M, Hemmerle L, Peyraud R, Christen B, Vorholt JA. 2017. Transposon sequencing uncovers an essential regulatory function of phosphoribulokinase for methylotrophy. Curr Biol 27:2579.e6–2588.e6. https://doi.org/10.1016/j.cub.2017.07.025.

69. Ji B, Zhang S-D, Zhang W-J, Rouy Z, Alberto F, Santini C-L, Mangenot S, Gagnot S, Philippe N, Pradel N, Zhang L, Tempel S, Li Y, Médigue C, Henrissat B, Coutinho PM, Barbe V, Talla E, Wu L-F. 2017. The chimeric nature of the genomes of marine magnetotactic coccoid-ovoid bacteria defines a novel group of *Proteobacteria*. Environ Microbiol 19:1103–1119. https://doi.org/10.1111/1462-2920.13637.

70. Sambrook J, Russell DW. 2001. Molecular cloning. CSHL Press, Cold Spring Harbor, NY.

71. Das S, Noe JC, Paik S, Kitten T. 2005. An improved arbitrary primed PCR method for rapid characterization of transposon insertion sites. J Microbiol Methods 63:89–94. https://doi.org/10.1016/j.mimet.2005.02.011.

72. Vandewalle K, Festjens N, Plets E, Vuylsteke M, Saeys Y, Callewaert N. 2015. Characterization of genome-wide ordered sequence-tagged *Mycobacterium* mutant libraries by Cartesian pooling-coordinate sequencing. Nat Commun 6:7106. https://doi.org/10.1038/ncomms8106.

73. Duncavage EJ, Magrini V, Becker N, Armstrong JR, Demeter RT, Wylie T, Abel HJ, Pfeifer JD. 2011. Hybrid capture and next-generation sequencing identify viral integration sites from formalin-fixed, paraffin-embedded tissue. J Mol Diagn 13:325–333. https://doi.org/10.1016/j.jmoldx.2011.01.006.

74. Uebe R, Schüler D, Jogler C, Wiegand S. 2018. Reevaluation of the complete genome sequence of *Magnetospirillum gryphiswaldense* MSR-1 with single-molecule real-time sequencing data. Genome Announc 6:150. https://doi.org/10.1128/genomeA.00309-18.

75. Wang X, Wang Q, Zhang W, Wang Y, Li L, Wen T, Zhang T, Zhang Y, Xu J, Hu J, Li S, Liu L, Liu J, Jiang W, Tian J, Li Y, Schüler D, Wang L, Li J. 2014. Complete genome sequence of *Magnetospirillum gryphiswaldense* MSR-1. Genome Announc 2:e00171-14. https://doi.org/10.1128/genomeA.00171-14.

76. Carver T, Thomson N, Bleasby A, Berriman M, Parkhill J. 2009. DNAPlotter: circular and linear interactive genome visualization. Bioinformatics 25:119–120. https://doi.org/10.1093/bioinformatics/btn578.

77. Carver T, Harris SR, Berriman M, Parkhill J, McQuillan JA. 2012. Artemis: an integrated platform for visualization and analysis of high-throughput sequence-based experimental data. Bioinformatics 28:464–469. https://doi.org/10.1093/bioinformatics/btr703.

78. Raschdorf O, Plitzko JM, Schüler D, Müller FD. 2014. A tailored *galK* counterselection system for efficient markerless gene deletion and chromosomal tagging in *Magnetospirillum gryphiswaldense*. Appl Environ Microbiol 80:4323–4330. https://doi.org/10.1128/AEM.00588-14.

79. Götz S, García-Gómez JM, Terol J, Williams TD, Nagaraj SH, Nueda MJ, Robles M, Talón M, Dopazo J, Conesa A. 2008. High-throughput functional annotation and data mining with the Blast2GO suite. Nucleic Acids Res 36:3420–3435. https://doi.org/10.1093/nar/gkn176.

80. Raschdorf O, Müller FD, Pósfai M, Plitzko JM, Schüler D. 2013. The magnetosome proteins MamX, MamZ and MamH are involved in redox control of magnetite biomineralization in *Magnetospirillum gryphiswaldense*. Mol Microbiol 89:872–886. https://doi.org/10.1111/mmi.12317.
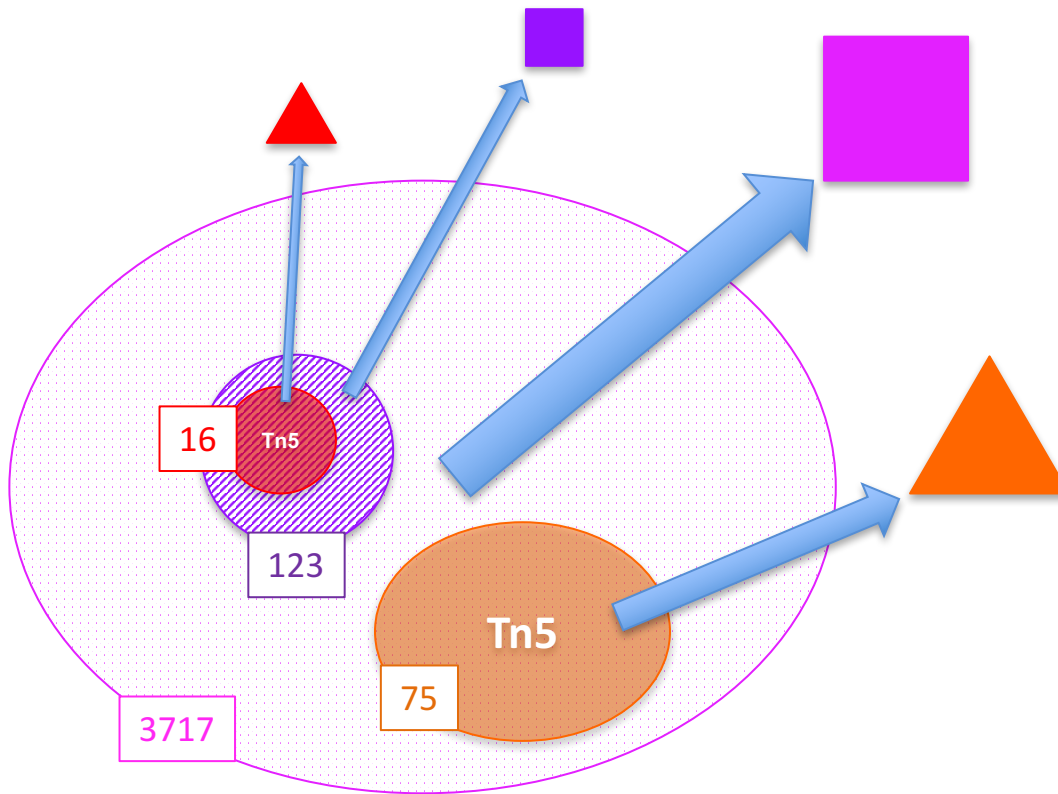
GO term sets

Comparison of GO term sets

(data not shown)

(see Table S3)

16

Tn5

123

3717

Tn5

75

MGMSRv2__3373-3377 (3378)

$\Delta 3373-3376$

slightly reduced Cmag

| 3373 glycosyl transf., fam. 2 | 3374 cupin-domain | 3375 methyltransferase | 3376 epimerase/dehydratase (NAD) | 3377 oxidoreductase family (NAD) | MSR1_30960 methyltransferase FkbM family |
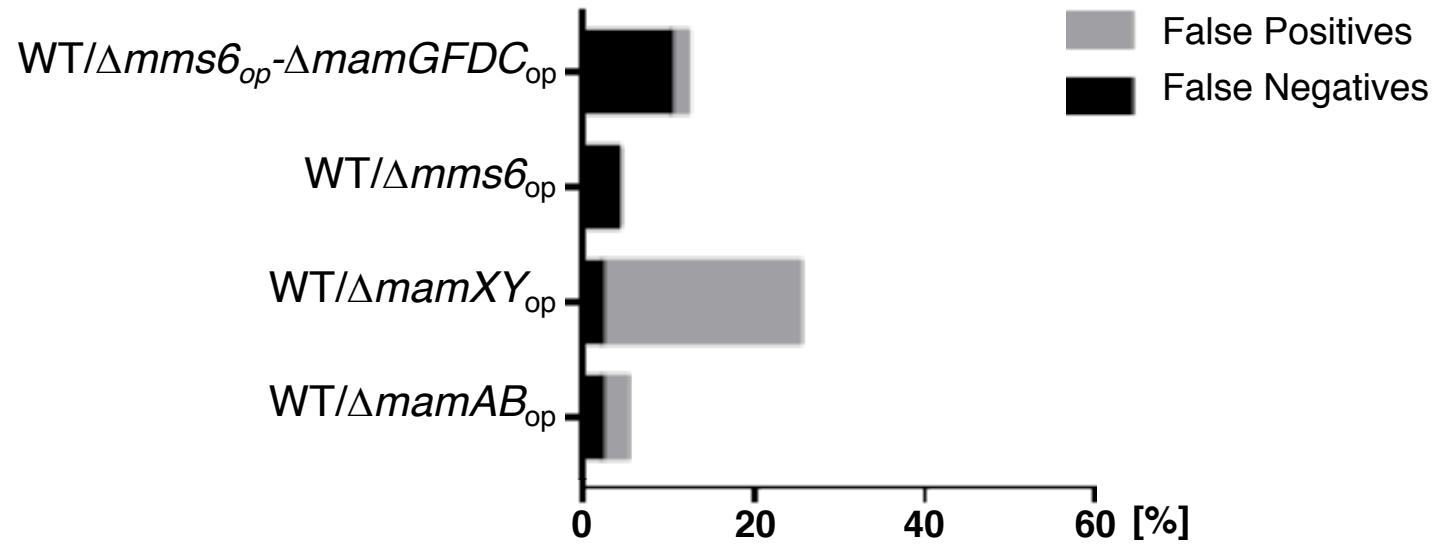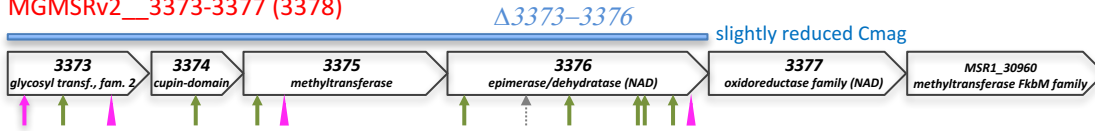
putative cell wall biogenesis/ modification

MGMSRv2__4001-4006

$\Delta 4002$

no magnetosome phenotype

| 4001 binds Fe₄S₄ cluster, radical SAM protein | 4002 Lys-transf. to membr. lipids, 7 TM | pepA(1) Leu-aminopeptidase, Manganese-ion-binding | pepA(2) N-terminally shorter than pepA(1) | holC DNA pol. III, χ subunit (replication) | 4006 |

TEM
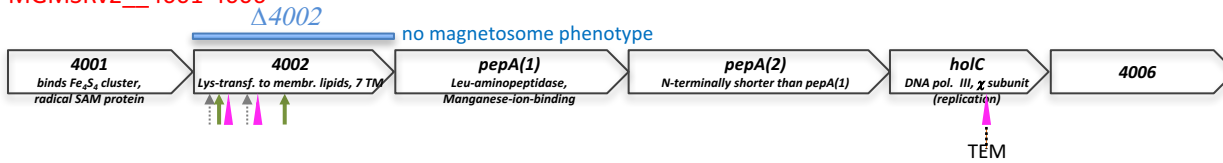
putative cell wall modification

cMGMSRv2__0149-0152

$\Delta 0149$

slightly reduced Cmag
cell shape more spiralized

| 0152 Zn-sensing chemoreceptor? | 0151 | 0150 | 0149 MSR1_20490 FecR protein, concanavalin A-like lectin/glucanase superfamily |

?
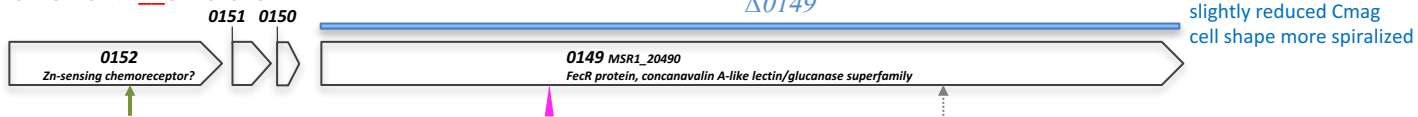
Legend:
- ⇩ 1 unique Tn-hit
- genome average: 1.995 hits/gene locus
- MAI average: 7.38 hits/gene locus
- Nmag fraction of characterized
- Wmag fraction of characterized
- *wt*mag fraction of characterized
- ⇩ 1 unique Tn-hit/kb of gene

hits/gene locus: MAI average

hits/gene locus: genome average
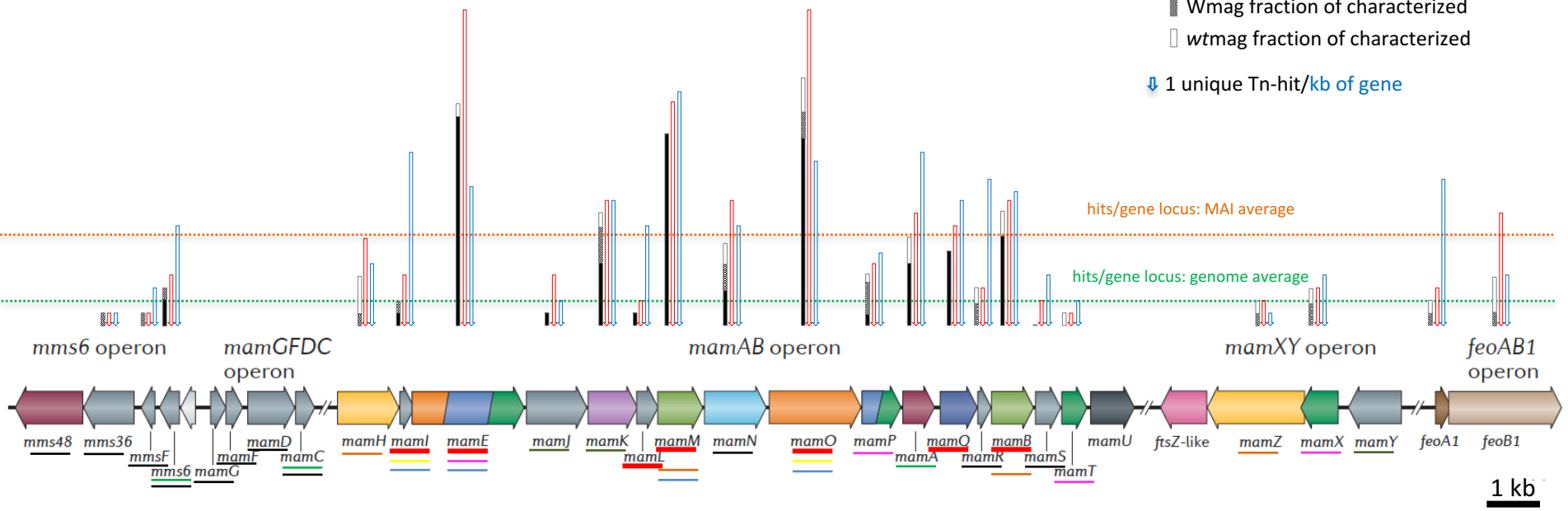
mms6 operon | *mamGFDC* operon | *mamAB* operon | *mamXY* operon | *feoAB1* operon

mms48 *mms36* *mmsF* *mms6* *mamG* *mamF* *mamD* *mamC* | *mamH* *mamI* *mamE* *mamJ* *mamK* *mamL* *mamM* *mamN* *mamO* *mamP* *mamA* *mamQ* *mamR* *mamB* *mamS* *mamT* *mamU* | *ftsZ*-like *mamZ* *mamX* *mamY* | *feoA1* *feoB1*

1 kb

A

Lxxxxxx**L**xxxxxx**L**xxxxxx**L**xxxxxx**L**

TM 1

cytoplasmic

MIW**LIFAGLALATIAILVL**P**LL**RAKTAP**L**SRAEYD**L**TVYRDQ**L**AEIEVE**L**ERGTLSADQA

TM 2

periplasmic

VAARTEIQRRILALGGATKPDAAQ**A**TRSWK**LATVLALVVPLLAFGLYVFLGAP**MLPDQPY

TPR 1   **TPR 2**

AARADKIKEMQDQGEMIRTMVASLTAKLEKNPNDGKGWGMLGRSLRVLGQKDQAINAYRK

TPR 3   **TPR 4**

AIALLPADTGSRMELAGLLLEDIPQGAVLPPEFVGLMREVLAVDPDNMDALYFAGIGALQ

MGDTRRARELWTKVMVQLPEGEDKSEMKKQIDGLQ

C_{mag} 3 > 1 > 2 > 4

B

TM 1   periplasmic   **TM 2**

MVRAMT**SSRFLPLFVLAVSVC**ALATAYVAQYGFGLRP**C**SL**C**LTQRVPFAVAGILALIALL

TM 3   periplasmic

RP**L**SWQR**ALM**ALAGLAFLINAGIAVYHVGVEQKWWDST**C**AASQSGAVNLNDLSALMSKPA

TM 4

EAR**C**DEPAWQWH**GITMAALNIVFSGGLALVVLAAL**PRKGRR

C

sigP

M KVLAW**LC**AALVALSAPAVSAAGKDDSFPIDRVLGKADAPITIIEYASTT**CGHC**ATFHKG

TLPEVKKNWIDTGKA**K**LVYRDFPTGPAGLSIGA**A**SMIAH**C**AGPERYFGVLGLIMEQQDKWL

GSKDPLDALKKTVRLAGLTGEDVDA**C**LQRQDLFQGIQVRAEHGHEQFKIDSTPSFVVNGK

LVVGAKSYEDFNKILMEAGK

C_{mag} 1/5 > 2/3 > 4/6/7

Table S1 A. Bacterial strains and plasmids used in this study.

Bacterial strains / plasmids	Relevant characteristics	Reference
Strains		
M. gryphiswaldense		
WT		D. Schüler and M. Köhler, Zentralblatt Mikrobiol 147, 1992
E. coli		
DH5α	F⁻ *sup*E44 Δ*lac*U169 (Φ80 *lac*ZDM15) *hsd*R17 *recA*1 *end*A1 *gyr*A96 *thi*-1 *rel*A1	Invitrogen
WM3064	donor strain for conjugation, *dap* auxotroph (*thr*B1004 *pro thi rps*L *hsd*S *lac*ZΔM15 RP4-1360 Δ(*ara*BAD)567 Δ*dap*A1341::[erm pir])	W. Metcalf (unpublished)
Plasmids		
pBAM1 (original)		E. Martínez-García *et al.*, BMC Microbiol 11, 2011
GeneArt® plasmid	synthetic transposase (P$_{mamDC45}$)	This study
pBAMOpt	synthetic transposase (P$_{mamDC}$)	This study

Table S1 B. Primers used in this study.

Name	Sequence (5'-3')
IB056	ATGGAACCTGGCAGATCAGAAGT
IB057	TCAAAGAACAATCCAGAACTCTTGG
IB058	ATGAGGAAGAGCGGTTGCGC
IB059	TCATCCTGCGAGAACGGCGA
IB060	ATGATTGAAATTGGCGAGACCA
IB061	CTCAATGAGACCTTCTACATCGACTG
IB062	ATGGCAGTAAGCGATGCGG
IB063	TCACTGCACGGTCATCCACA
IB064	ATGGGTACGCCAGGGGG
IB065	TTATTTCGGAACCAGTATGGAAAGC
IB140	ATGGAACCTGGCAGATCAGA
IB141	CCACATCACCATTGAACATG
ARB6	GGCACGCGTCGACTAGTACNNNNNNNNNNACGCC
ARB2	GGCACGCGTCGACTAGTAC
Me-O-extF	CGGTTTACAAGCATAACTAGTGCGGC
Me-O-intF	AGAGGATCCCCGGGTACCGAGCTCG
Me-I-extR	CTCGTTTCACGCTGAATATGGCTC
Me-I-intR	CAGTTTTATTGTTCATGATGATATA

Table S2.A. Tn5 insertion clones selected as Nmag/Wmag during visual screening of the mutagenesis library, and characterized in detail.

exMAI	Locus-tag MSR1(L), GenBank acc. CP027526, CP027527 (R. Uebe *et al*, Genome Announc 6, 2018)	Insertion position MSR1(L)	Locus-tag MGMSRv2, GenBank acc. HG794546 (X. Wang *et al.*, Genome Announc 2, 2014)	Insertion Position in MGMSRv2	inMAI = n, exMAI = y	(putative) functional category	Annotation	Growth	Magnetic response	Growth2	Magnetic response2	Comments
exMAI non-magnetic	MSR1L_12470	1.235.408	MGMSRv2_1015	1.061.482	n	peptide hydrolysis	conserved protein of unknown function, peptidase S1 family	0,086	0	++	-	
	MSR1L_11940	1.182.493	MGMSRv2_1068	1.114.215	n	nitrogen metabolism	putative glutamate synthase [NADPH] small chain	0,07	0	++	-	
	MSR1L_10000	989.365	MGMSRv2_1257	?	n	fatty acid biosynthesis	fatty acid biosynthesis gene (beta-ketoacyl-synthase, N-terminal domain), part of a large cluster of putative fatty acid biosynthesis genes	0,14	0	+++	-	
	MSR1L_02290	232.226	MGMSRv2_2009	2.115.735	n	signaling, MCP	methyl-accepting chemotaxis receptor/sensory transducer	0,21	0	+++	-	
	MSR1L_01960	191.436	MGMSRv2_2042	2.156.058	n	membrane transport?	uncharacterized membrane protein with 2 EamA domains	0,196	0		-	
	MSR1L_32750	3.463.440	MGMSRv2_3565	3.646.533	n	nucleotide-hydrolysis?	putative HAD-superfamiliy hydrolase (phosphohydrolase)	0,11	0	+++	-	
	MSR1L_27630	2.940.618	MGMSRv2_3633	3.718.703	n	signaling	GGDEF domain-containing protein	0,13	0	+++	-	
	MSR1L_27640	2.941.097	MGMSRv2_3634	3.719.855	n	central metabolism	NAD(P)-dependent malic enzyme	0,077	0	++	-	
	MSR1L_23600	2.526.558	MGMSRv2_4041	4.134.803	n	PHB biosynthesis	poly-beta-hydroxybutyrate polymerase PhbC	0,132	0	++	-	
	MSR1L_38790	4.044.656	MGMSRv2_4153	4.251.079	n	extracytoplasmic solute receptor	putative TRAP-type uncharacterized transporter solute receptor, TAXI family	0,091	0	++	-	
	MSR1L_20490_corr	2.154.630	MGMSRv2_0149	170.891	n	iron sensor?	Laminin G-domain containing FecR-protein, Ca-binding metalloprotease	0,105	0,29	++	+	huge protein (31 kDa); periplasmic iron dicitrate sensor?
	MSR1L_18220	1.921.916	MGMSRv2_0391	419.789	n	signaling, MCP	methyl-accepting chemotaxis receptor	0,11	0,47	++	+	
	MSR1L_06710	669.779	MGMSRv2_0611	659.012	n	nitrogen metabolism	putative asparagine synthetase (glutamine-hydrolyzing)	0,121	0,36	++	+	
	MSR1L_14910	1.507.490	MGMSRv2_1555	1.600.378	n	redox process	electron transfer flavoprotein (alpha subunit)	0,11	0,3	+++	+	
	MSR1L_15190	1.540.079	MGMSRv2_1585	1.636.230	n	membrane transport?	membrane protein (DUF 2339)	0,166	0,4	++	+	large protein with 26 transmembrane domains
	MSR1L_05990	592.468	MGMSRv2_1716	1.813.723	n	anaerobic respiration	nitric oxide reductase (cyt *c*) subunit B (NorB)	0,024	0,3	+	+	
	MSR1L_05990	592.296	MGMSRv2_1716	1.813.903	n	anaerobic respiration	nitric oxide reductase (cyt *c*) subunit B (NorB)	0,14	0,07	+	+	
	MSR1L_05930	586.731	MGMSRv2_1722	1.818.698	n	iron sensor?	Cadherin-like domain containing FecR-proten, Ca-binding metalloprotease	0,072	0,38	++	+	
	MSR1L_20710	2.203.220	MGMSRv2_2075	2.190.040	n	protein-protein interaction	TPR-domain containing protein	0,1	0,58	+++	+	
	MSR1L_22700	?	MGMSRv2_2273	2.403.749	n	periplasmatic oxidative protein folding	thiol:disulfide interchange protein, DsbA-like	0,155	0,1	++	+	
	MSR1L_22700	?	MGMSRv2_2273	2.403.925	n	periplasmatic oxidative protein folding	thiol:disulfide interchange protein, DsbA-like	0,204	0,1	+++	+	

MSR1L_22700	?	MGMSRv2_2273	2.404.129	n	periplasmatic oxidative protein folding	thiol:disulfide interchange protein, DsbA-like	0,076	0,24	++	+	
MSR1L_38410	4.012.732	MGMSRv2_2474	2.585.698	n	DNA repair	DNA mismatch repair protein MutL	0,18	0,78	+++	+	
MSR1L_27560	2.931.775	MGMSRv2_3625	3.709.861	n	flagellar biosynthesis	flagellar biosynthesis protein FlhA	0,22	0,22	+++	+	
MSR1L_25430	2.703.940	MGMSRv2_3871	3.964.826	n	oligopeptide transport?	putative oligopeptide transporter subunit, periplasmic-binding component of ABC superfamily transporter	0,106	0,36	++	+	
MSR1L_00450	50.460	MGMSRv2_0031	?	n	signaling, histidine kinase	two-component sensor histidine kinase	0,16	0,8	+++	++	
MSR1L_01450	139.796	MGMSRv2_0134	127.051	n	?	uncharacterized protein	0,15	1	+++	++	intergenic (upstream of gene)
MSR1L_20000	2.092.038	MGMSRv2_0199	255.584	n	membrane transport	inner-membrane translocator, LivM-like	0,15	0,67	+++	++	
MSR1L_19740	2.059.355	MGMSRv2_0225	268.207	n	?	probable intracellular septation protein A	0,125	0	++	++	gene *ispZ;* absence of protein can cause a cell division defect in an intracellularly replicating bacterium
MSR1L_19360	2.023.169	MGMSRv2_0266	305.286	n	?	Cadherin-like domain containing proten, Ca-binding metalloprotease	0,244	0,86	+++	++	
MSR1L_30250	3.200.894	MGMSRv2_0365	399.091	n	solute transport	ammonium transporter AmtB	0,16	1,25	+++	++	
MSR1L_18150	1.909.781	MGMSRv2_0398	429.605	n	nutrient mobilization	exopolyphosphatase	0,12	1,44	+++	++	
MSR1L_17640	1.847.099	MGMSRv2_0450	492.828	n	redox process	FixG-like cyt *c* oxidase (iron-sulfur cluster -binding protein)	0,21	0,78	+++	++	
MSR1L_17440	1.829.717	MGMSRv2_0469	509.958	n	sulfur metabolism	phosphoadenylyl-sulfate reductase (thioredoxin) CysH	0,081	1,05	++	++	
MSR1L_17430	1.828.697	MGMSRv2_0470	510.978	n	sulfur metabolism	sulfate adenylyltransferase CysD	0,13	0,41	+++	++	
MSR1L_17040	1.784.492	MGMSRv2_0511	556.222	n	periplasmatic oxidative protein folding	putative disulfide bond formation protein DsbB	0,13	0,31	+++	++	
MSR1L_16850	1.763.821	MGMSRv2_0532	577.258	n	?	DU155 domain-containing protein	0,14	0,87	+++	++	
MSR1L_16320	1.705.544	MGMSRv2_0732	767.537	n	signaling, histidine kinase	sensor histidine kinase with N-terminal methylesterase/transferase domains	0,078	0,87	++	++	
MSR1L_16160	1.686.013	MGMSRv2_0749	785.805	n	transcription regulation	lambda repressor-like helix-turn-helix domain protein	0,158	0,72	++	++	
MSR1L_14090	1.409.995	MGMSRv2_0853	897.589	n	glycan biosynthesis	glycogen synthase GlgA	0,16	1,15	+++	++	
MSR1L_13060/MSR1L_13070	1.298.733	MGMSRv2_0953/MGMSRv2_0952	996.588	n	transcription regulation	transcriptional regulator, TetR family	0,13	1,36	+++	++	adjacent to *mipZ* , but divergently transcribed
MSR1L_11790	1.168.928	MGMSRv2_1082	1.129.020	n	stringent response	bifunctional (P)ppGpp synthetase II and guanosine-3',5'-bis pyrophosphate 3'-pyrophosphohydrolase, RelA/SpoT family	0,101	0,74	++	++	
MSR1L_11550	1.142.149	MGMSRv2_1113	1.157.041	n	signaling, histidine kinase	sensor histidine kinase	0,088	0,49	+++	++	
MSR1L_11350	1.121.622	MGMSRv2_1133	1.178.778	n	?	beta-lactamase superfamily protein	0,13	1,37	+++	++	
MSR1L_10260	1.014.414	MGMSRv2_1231	1.277.279	n	signaling, phosphorelay	two component sensor histidine kinase/response regulator hybrid protein with phosphorelay domain	0,11	0,88	+++	++	
MSR1L_10050	991.939	MGMSRv2_1252	1.300.432	n	?	putative AMP-dependent synthetase and ligase	0,13	1,29	+++	++	

exMAI weakly magnetic	MSR1L_09800	968.014	MGMSRv2_1279	1.325.408	n	isopreonoid biosynthesis	geranyltranstransferase IspA	0,091	1	++	++	
	MSR1L_09720	961.143	MGMSRv2_1295	1.338.003	n	redox process	NAD(FAD)-dependent disulfide oxidoreductase	0,11	0,94	+++	++	
	MSR1L_08390	832.930	MGMSRv2_1403	1.444.705	n	anaerobic respiration	nitrite reductase NirS (cyt *cd1*)	0,05	0,84	++	++	
	MSR1L_08250	818.664	MGMSRv2_1417	1.459.651	n	outer membrane structure	OmpA-like domain-containing protein	0,069	0,34	++	++	
	MSR1L_15000	1.516.671	MGMSRv2_1565	1.609.691	n	solute transport?	uncharacterized membrane protein with 1 EamA domain	0,11	1,72	+++	++	
	MSR1L_15530	1.578.098	MGMSRv2_1617	1.669.557	n	redox process	putative short chain acyl-CoA dehydrogenase	0,13	1,11	+++	++	
	MSR1L_05880	580.065	MGMSRv2_1726	1.826.130	n	?	uncharacterized membrane protein	0,1	0,94	+++	++	intergenic region 3684/3683 (upstream of gene)
	MSR1L_05370	529.524	MGMSRv2_1777	1.876.671	n	signaling, histidine kinase	two-component sensor histidine kinase	0,11	0,82	+++	++	
	MSR1L_05070	495.250	MGMSRv2_1810	1.910.567	n	lactate utilization?	LUD-domain containing protein	0,05	0,97	+	++	
	MSR1L_26390	2.794.492	MGMSRv2_1971	2.068.843	n	?	uncharacterized protein	0,1	1,54	+++	++	
	MSR1L_02270	227.319	MGMSRv2_2011	2.120.642	n	ammonium assimilation	glutamate synthase [NADPH] large chain	0,14	0,87	+++	++	
	MSR1L_02170	211.717	MGMSRv2_2021	2.136.272	n	membrane transport, nitrogen metabolism	putative ABC transporter, urea, permease protein UrtE	0,184	0,69	+++	++	
	MSR1L_21340	2.276.260	MGMSRv2_2139	2.263.264	n	cofactor biosynthesis	cobalamin biosynthesis protein, CobW/P47K family protein	0,08	1,06	+++	++	
	MSR1L_22700	2.419.586	MGMSRv2_2273	2.404.131	n	periplasmatic oxidative protein folding	thiol:disulfide interchange protein, DsbA-like	0,075	0,63	++	++	
	MSR1L_22700	2.419.644	MGMSRv2_2273	2.404.182	n	periplasmatic oxidative protein folding	thiol:disulfide interchange protein, DsbA-like	0,055	0,98	++	++	
	MSR1L_06440	640.122	MGMSRv2_2461	2.576.127	n	?	uncharacterized exported protein	0,2	1,41	+++	++	
	MSR1L_38310	4.006.480	MGMSRv2_2484	2.591.828	n	?	uncharacterized protein	0,17	0,43	+++	++	intergenic (upstream of gene); downstream of bacterio-hemerythrin
	MSR1L_37510	3.931.308	MGMSRv2_2540	2.648.340	n	?	bacteriophage capsid protein	0,135	0,8	+++	++	region encoding phage proteins!
	MSR1L_36930	3.876.892	MGMSRv2_2673	2.772.479	n	carbon metabolism	methylmalonyl-CoA mutase	0,09	1,25	++	++	
	MSR1L_36480	3.835.835	MGMSRv2_2712	2.811.816	n	protein degradation	metalloprotease TldD/PmbA (zinc-dependent)	0,12	1,3	+++	++	antibiotic maturation/secretion? CcdA (cyt *c* biogenesis protein) degradation?
	MSR1L_36430	?	MGMSRv2_2717	2.817.087	n	iron sensor?	FecR-protein, Ca-binding metalloprotease	0,148	0,88	+++	++	
	MSR1L_35320	3.707.072	MGMSRv2_2825	2.934.877	n	?	putative SAM-dependent methyltransferase	0,1	0,42	+++	++	
	MSR1L_34190	3.604.410	MGMSRv2_2950	3.045.740	n	redox process, nitrogen metabolism	nitrogen fixation protein FixG	0,155	0,92	++	++	
	MSR1L_33940	3.583.056	MGMSRv2_2976	3.068.552	n	flagellum	flagellar biosynthesis protein FliP	0,142	0,7	+++	++	
	MSR1L_33570	3.547.505	MGMSRv2_3009	3.101.013	n	?	exported protein with 2 DUF1566	0,101	0,79	++	++	
	MSR1L_28800	3.052.140	MGMSRv2_3151	3.229.708	n	fatty acid metabolism	putative acyl-CoA carboxylase biotin-carrying subunit alpha chain AccC	0,2	0,9	+++	++	
	MSR1L_29190	3.089.592	MGMSRv2_3192	3.268.233	n	redox process	cytochrome *c*-type biogenesis protein CcmI (CycH)	0,08	0,96	+++	++	

MSR1L_29190	3.089.617	MGMSRv2_3192	3.268.257	n	**redox process**	cytochrome *c* -type biogenesis protein CcmI (CycH)	0,23	0,96	+++	++	
MSR1L_29190	3.089.338	MGMSRv2_3192	3.268.033	n	**redox process**	cytochrome *c* -type biogenesis protein CcmI (CycH)	0,12	1,16	++	++	
MSR1L_29190	?	MGMSRv2_3192	3.268.294	n	**redox process**	cytochrome *c* -type biogenesis protein CcmI (CycH)	0,173	0,79	+++	++	
MSR1L_29810	3.161.209	MGMSRv2_3255	3.337.096	n	**carbon metabolism**	methylmalonyl-CoA mutase	0,09	0,9	+++	++	
MSR1L_30910	3.266.440	MGMSRv2_3373	3.444.257	n	**cell wall formation**	putative glycosyltransferase, family 2	0,101	0,79	++	++	
MSR1L_30910	?	MGMSRv2_3373	3.444.827	n	**cell wall formation**	putative glycosyltransferase, family 2	0,112	0,7	++	++	
MSR1L_30930	3.267.623	MGMSRv2_3375	3.445.620	n	**?**	exported protein, SAM-dependent methyltransferase	0,13	1	++	++	
MSR1L_30940	?	MGMSRv2_3376	3.447.717	n	**cell wall formation**	putative NAD-dependent epimerase/dehydratase	0,19	0,77	+++	++	
MSR1L_32520	3.437.807	MGMSRv2_3542	3.620.060	n	**cell wall formation**	capsular polysaccharide biosynthesis protein CapD	0,11	0,51	+++	++	
MSR1L_32700	3.457.519	MGMSRv2_3560	3.640.612	n	**methionine biosynthesis, sulfur metabolism**	O-succinylhomoserine sufhydrylase MetZ	0,15	1,07	+++	++	
MSR1L_27180	2.889.518	MGMSRv2_3585	3.666.512	n	**signaling, MCP**	methyl-accepting chemotaxis receptor/sensory transducer	0,24	0,94	+++	++	
MSR1L_27780	2.957.189	MGMSRv2_3648	3.735.057	n	**signaling, phosphorelay**	Hpt domain-containing protein	0,11	0,95	+++	++	
MSR1L_26700	2.832.812	MGMSRv2_3736	3.826.289	n	**anaerobic cofactor biosynthesis**	putative sirohydrochlorin cobaltochelatase CbiX	0,113	1,11	+++	++	
MSR1L_24710	2.633.560	MGMSRv2_3942	4.034.134	n	**redox process, fatty acid metabolism**	3-hydroxyacyl-CoA dehydrogenase	0,19	0,94	+++	++	
MSR1L_24490/MSR1L_24500	2.611.886	MGMSRv2_3967/3966	4.056.678	n	**?**	putative cytokinin riboside 5'-monophosphate phosphoribohydrolase (LOG family protein) / beta-lactamase superfamily protein	0,13	1,12	+++	++	may affect 2 genes: hit in intergenic region (upstream of 2 divergently transcribed genes)
MSR1L_24400	2.605.496	MGMSRv2_3976	4.063.068	n	**?**	putative arsenite methyltransferase	0,11	1,12	+++	++	
MSR1L_24330	2.600.607	MGMSRv2_3985	4.069.370	n	**?**	uncharacterized exported protein	0,135	0,91	++	++	
MSR1L_24180	?	MGMSRv2_4002	4.089.224	n	**membrane lipid modification?**	conserved membrane protein of unknown function, phosphatidylglycerol lysyltransferase?	0,122	0,93	++	++	
MSR1L_24180	2.581.355	MGMSRv2_4002	4.089.325	n	**membrane lipid modification?**	conserved membrane protein of unknown function, phosphatidylglycerol lysyltransferase	0,077	0,6	++	++	
MSR1L_24150	?	MGMSRv2_4005	4.093.116	n	**DNA replication**	DNA polymerase III subunit chi	0,15	0,53	+++	++	
MSR1L_38770	4.042.345	MGMSRv2_4151	4.247.156	n	**signaling**	conserved protien of unknown function-diguanylate cyclase (GGDEF and EAL domains)	0,086	0,7	++	++	
MSR1L_39790	4.154.613	MGMSRv2_4260	4.364.696	n	**?**	conserved protein of unknown function (TPR repeat)	0,15	1,04	+++	++	
MSR1L_20470	2.151.586	MGMSRv2_0152	175.870	n	**signaling, MCP**	methyl-accepting chemotaxis receptor, zinc-binding	0,119	1,18	++	+++	
MSR1L_18630	1.950.998	MGMSRv2_0352	388.660	n	**?**	SIR2_2 domain-containing protein	0,122	1,28	+++	+++	

MSR1L_18100	1.902.386	MGMSRv2_0404	437.853	n	signaling, MCP	methyl-accepting chemotaxis receptor with hemerythrin-like metal-binding domain	0,22	1,39	+++	+++	
MSR1L_18080	1.898.487	MGMSRv2_0406	439.802	n	fatty acid biosynthesis	acetyl-CoA carboxylase, biotin carboxylase subunit	0,152	1,11	++	+++	
MSR1L_17950	1.883.271	MGMSRv2_0419	456.515	n	transcription regulation	putative transcriptional regulator, MarR-type	0,243	1,36	+++	+++	
MSR1L_17450	1.831.777	MGMSRv2_0468	508.119	n	sulfur metabolism	putative sulfite reductase	0,15	1,57	+++	+++	
MSR1L_17440	1.829.666	MGMSRv2_0469	509.963	n	sulfate assimilation	phosphoadenylyl-sulfate reductase (thioredoxin) CysH	0,1	1,73	+++	+++	
MSR1L_17430	1.828.762	MGMSRv2_0470	510.913	n	sulfate assimilation	sulfate adenylyltransferase CysD	0,11	1,72	+++	+++	
MSR1L_17420	1.827.992	MGMSRv2_0471	511.608	n	sulfate assimilation	adenylylsulfate kinase CysC	0,18	1,23	+++	+++	
MSR1L_17420	1.828.192	MGMSRv2_0471	512.275	n	sulfate assimilation	adenylylsulfate kinase CysC	0,107	1,28	+++	+++	
MSR1L_16570	1.732.497	MGMSRv2_0560	609.876	n	transport	phosphate transport system permease protein PstA	0,071	0	++	+++	
MSR1L_06670	664.301	MGMSRv2_0607	653.093	n	exo/lipopolysaccharide biosynthesis	putative succinoglycan biosynthesis transport protein ExoP	0,146	1,11	+++	+++	intergenic region only in GenBank acc. CP027526, CP027527 (upstream of gene)
MSR1L_06690	667.630	MGMSRv2_0609	655.028	n	exo/lipopolysaccharide biosynthesis	membrane protein, putative O-antigen polymerase	0,1	1,01	+++	+++	
MSR1L_12860	1.276.617	MGMSRv2_0973	1.018.940	n	lipid binding/transfer	coenzyme Q-binding protein COQ10, START domain-containing protein	0,135	1,46	++	+++	
MSR1L_12410	1.226.809	MGMSRv2_1021	1.069.130	n	?	cyclic nucleotide-binding domain-containing protein	0,203	1,32	+++	+++	
MSR1L_11790	1.167.339	MGMSRv2_1082	1.129.502	n	stringent response	bifunctional (P)ppGpp synthetase II and guanosine-3',5'-bis pyrophosphate 3'-pyrophosphohydrolase, RelA/SpoT family	0,17	1,62	+++	+++	
MSR1L_11470	1.142.149	MGMSRv2_1121	1.168.412	n	?	uncharacterized protein	0,24	1,47	+++	+++	
MSR1L_10730	?	MGMSRv2_1186	1.232.186	n	type I protein secretion	type 1 export protein	0,163	1,23	++	+++	
MSR1L_10730	1.059.011	MGMSRv2_1186	1.232.549	n	type I protein secretion	type 1 export protein	0,104	1,19	++	+++	
MSR1L_10070	993.224	MGMSRv2_1250	1.298.595	n	cell wall formation	lipid A biosynthesis acyltransferase	0,164	1,45	++	+++	
MSR1L_09470/09480	937.138	MGMSRv2_1319/1320	1.362.228	n	redox process, respiratory chain	NADH-quinone oxidoreductase subunit I (NuoI)	0,14	1,15	+++	+++	intergenic region 1319/1320 (upstream of gene 1319, *nuoI*)
MSR1L_05750	569.512	MGMSRv2_1739	1.837.060	n	transport	ABC-transporter, ATP binding component	0,141	1,26	++	+++	
MSR1L_06450	640.814	MGMSRv2_1956	2.051.507	n	?	uncharacterized protein with transmembrane domain	0,142	1,06	+++	+++	
MSR1L_26450	2.801.770	MGMSRv2_1977	2.076.121	n	transport	putative heme/hemopexin transporter protein HxuB	0,1	1,77	+++	+++	
MSR1L_02420	246.061	MGMSRv2_1996	2.101.926	n	?	alpha/beta hydrolase family protein	0,14	1,28	+++	+++	
MSR1L_01820	177.578	MGMSRv2_2056	2.170.297	n	signaling, histidine kinase	sensor histidine kinase with N-terminal sodium/solute symporter domain	0,137	1,39	++	+++	
MSR1L_01720	166.193	MGMSRv2_2066	2.180.906	n	metal-binding	putative zinc- or iron-chelating domain containing protein	0,123	1,19	++	+++	
MSR1L_21760	2.318.242	MGMSRv2_2179	2.304.151	n	?	conserved protein of unknown function (TPR repeat and ferritin-like domain)	0,14	0,96	+++	+++	
MSR1L_22700	2.419.427	MGMSRv2_2273	2.403.972	n	periplasmatic oxidative protein folding	thiol:disulfide interchange protein, DsbA-like	0,168	1,09	+++	+++	

MSR1L_22700	2.419.656	MGMSRv2_2273	2.404.184	n	**periplasmatic oxidative protein folding**	thiol:disulfide interchange protein, DsbA-like	0,249	1,34	+++	+++	
MSR1L_38000	3.973.131	MGMSRv2_2515	2.624.981	n	**nitrogen metabolism**	nitrogen-fixation sustaining protein CowN	0,118	1,24	++	+++	
MSR1L_36200	3.800.006	MGMSRv2_2734	2.842.742	n	**oxygen defence?**	redoxin/thioredoxin domain-containing exported protein	0,202	1,58	+++	+++	
MSR1L_35190	?	MGMSRv2_2838	2.944.375	n	**signaling, histidine kinase**	two-component sensor histidine kinase	0,2	1,51	+++	+++	
MSR1L_34740	3.657.073	MGMSRv2_2882	2.983.125	n	**translation**	methionyl-tRNA formyltransferase Fmt	0,18	1,21	+++	+++	
MSR1L_34720	3.654.049	MGMSRv2_2884	2.986.036	n	**signaling, MCP**	methyl-accepting chemotaxis receptor	0,227	1,28	+++	+++	
MSR1L_34000	3.587.815	MGMSRv2_2970	3.063.271	n	**redox process, chaperone function**	heat shock protein Hsp33 family protein	0,089	2,09	++	+++	
MSR1L_33770	3.567.287	MGMSRv2_2993	3.084.607	n	**?**	uncharacterized protein with transmembrane domains	0,365	1,35	+++	+++	
MSR1L_33430	3.534.455	MGMSRv2_3048	?	n	**DNA restriction**	type I site-specific restriction-modification system, R subunit	0,15	1,16	+++	+++	
MSR1L_29370	?	MGMSRv2_3209	3.285.975	n	**DNA repair**	DNA mismatch repair protein MutS	0,233	1,44	+++	+++	
MSR1L_30580	?	MGMSRv2_3332	3.406.750	n	**?**	uncharacterized protein	0,163	1,46	++	+++	
MSR1L_30810	3.255.094	MGMSRv2_3362	3.431.344	n	**cofactor biosynthesis**	molybdenum cofactor biosynthesis protein MoaA	0,087	1,16	++	+++	
MSR1L_30910	?	MGMSRv2_3373	3.444.257	n	**cell wall formation**	putative glycosyltransferase, family 2	0,246	1,12	++	+++	
MSR1L_30910	?	MGMSRv2_3373	3.444.658	n	**cell wall formation**	putative glycosyltransferase, family 2	0,09	1,18	++	+++	
MSR1L_30920	3.267.147	MGMSRv2_3374	3.445.257	n	**?**	conserved protein of unknown function	0,146	1,05	++	+++	
MSR1L_30930	3.267.623	MGMSRv2_3375	3.445.480	n	**?**	exported protein, SAM-dependent methyltransferase	0,221	1,16	+++	+++	
MSR1L_30940	?	MGMSRv2_3376	3.446.709	n	**cell wall formation**	putative NAD-dependent epimerase/dehydratase	0,084	1,03	++	+++	
MSR1L_30940	?	MGMSRv2_3376	3.447.280	n	**cell wall formation**	putative NAD-dependent epimerase/dehydratase	0,06	1,31	++	+++	
MSR1L_30940	3.268.871	MGMSRv2_3376	3.447.520	n	**cell wall formation**	putative NAD-dependent epimerase/dehydratase	0,115	1,05	++	+++	
MSR1L_30940	?	MGMSRv2_3376	3.447.526	n	**cell wall formation**	putative NAD-dependent epimerase/dehydratase	0,211	1,21	+++	+++	
MSR1L_30940	?	MGMSRv2_3376	3.447.644	n	**cell wall formation**	putative NAD-dependent epimerase/dehydratase	0,22	1,28	+++	+++	
MSR1L_27160	2.886.228	MGMSRv2_3583	3.663.641	n	**peptide hydrolysis**	putative Xaa-Pro aminopeptidase	0,198	1,35	+++	+++	
MSR1L_27190	2.889.708	MGMSRv2_3586	3.668.956	n	**glutathione metabolism**	5-oxoprolinase OplA	0,128	1,49	++	+++	
MSR1L_26800	2.847.442	MGMSRv2_3727	3.811.056	n	**chemotaxis?**	CheR-like methyltransferase with C-terminal TPR-domain	0,131	1,13	++	+++	
MSR1L_25740	2.733.921	MGMSRv2_3840	3.936.201	n	**cell wall formation**	lipopolysaccharide assembly protein A-domain containing protein	0,15	0	+++	+++	
MSR1L_24680	2.631.081	MGMSRv2_3945	4.036.591	n	**cofactor biosynthesis**	ATP:cob(I)alamin adenosyltransferase	0,209	1,18	+++	+++	
MSR1L_24530	2.614.968	MGMSRv2_3963	4.053.246	n	**?**	conserved inner membrane protein, DUF420	0,185	1,24	+++	+++	
MSR1L_24260	2.590.538	MGMSRv2_3992	4.078.926	n	**signaling, MCP**	methyl-accepting chemotaxis receptor	0,1	1,57	+++	+++	

inMAI	Locus-tag MSR1(L), GenBank acc. CP027526, CP027527 (4)	Insertion position MSR1(L)	Locus-tag MGMSRv2, GenBank acc. HG794546 (5)	Insertion Position in MGMSRv2	inMAI = n, exMAI = y	(putative) functional category	Annotation	Growth	Magnetic response	Growth2	Magnetic response2	comments
	MSR1L_24180	?	MGMSRv2_4002	4.089.167	n	membrane lipid modification?	conserved membrane protein of unknown function, phosphatidylglycerol lysyltransferase	0,118	1,06	++	+++	
	MSR1L_24180	?	MGMSRv2_4002	4.089.537	n	membrane lipid modification?	conserved membrane protein of unknown function, phosphatidylglycerol lysyltransferase	0,179	1,22	+++	+++	
	MSR1L_39470	4.123.757	MGMSRv2_4227	4.332.947	n	carbon metabolism, gluconeogenesis	pyruvate phosphate dikinase PpdK	0,1	1,13	++	+++	
	MSR1L_39620	4.136.506	MGMSRv2_4243	4.346.854	n	signaling, histidine kinase	sensor histidine kinase	0,233	1,21	+++	+++	
	MSR1L_26530	2.811.416	MGMSRv2_5S_rRNA_2	2.085.763	n	ribosome component	5S_rRNA_2	0,14	1,13	+++	+++	
	MSR1L_02570	262.088	MGMSRv2_5S_rRNA_2	?	n	ribosome component	5S_rRNA_2	0,14	1,13	+++	+++	
	MSR1L_03470	335.203	MGMSRv2_2368	2.489.301	y		MamB	0,205	0	+++	-	
	MSR1L_03420	330.858	MGMSRv2_2373	2.493.753	y		MamO	0,103	0,04	++	-	
	MSR1L_03380	327.097	MGMSRv2_2377	2.497.515	y		MamK	0,103	0,04	++	-	
	MSR1L_03360	?	MGMSRv2_2379	2.500.968	y		MamE	0,224	0	+++	-	
	MSR1L_03470	?	MGMSRv2_2368	?	y		MamB	0,176	0	+++	-	
	MSR1L_03470	?	MGMSRv2_2368	?	y		MamB	0,181	0	+++	-	
	MSR1L_03390	327.647	MGMSRv2_2377	?	y		MamL	0,261	0	+++	-	
	MSR1L_03380	326.862	MGMSRv2_2377	2.479.749	y		MamK	0,104	0,03	++	-	
	MSR1L_03470	?	MGMSRv2_2368	2.489.212	y		MamB	0,146	0	++	-	
	MSR1L_03470	?	MGMSRv2_2368	2.489.586	y		MamB	0,125	0	++	-	
	MSR1L_03470	334.986	MGMSRv2_2368	2.489.609	y		MamB	0,162	0	++	-	
	MSR1L_03450	?	MGMSRv2_2370	2.490.149	y		MamQ	0,199	0	+++	-	
	MSR1L_03450	?	MGMSRv2_2370	2.490.387	y		MamQ	0,119	0	++	-	
	MSR1L_03450	?	MGMSRv2_2370	2.490.500	y		MamQ	0,197	0	+++	-	
	MSR1L_03450	?	MGMSRv2_2370	2.490.548	y		MamQ	0,188	0	+++	-	
	MSR1L_03440	?	MGMSRv2_2371	2.491.210	y		MamA	0,217	0	+++	-	
	MSR1L_03430	?	MGMSRv2_2372	2.492.065	y		MamP	0,177	0	+++	-	
	MSR1L_03420	?	MGMSRv2_2373	2.492.720	y		MamO	0,209	0	+++	-	
	MSR1L_03420	?	MGMSRv2_2373	2.492.799	y		MamO	0,233	0	+++	-	
	MSR1L_03420	?	MGMSRv2_2373	2.492.922	y		MamO	0,195	0	+++	-	
	MSR1L_03420	?	MGMSRv2_2373	2.493.134	y		MamO	0,195	0	+++	-	
	MSR1L_03420	330.654	MGMSRv2_2373	2.493.431	y		MamO	0,2	0	+++	-	
	MSR1L_03420	331.008	MGMSRv2_2373	2.493.584	y		MamO	0,203	0	+++	-	
	MSR1L_03420	?	MGMSRv2_2373	2.493.591	y		MamO	0,124	0	++	-	
	MSR1L_03420	330.506	MGMSRv2_2373	2.493.908	y		MamO	0,178	0	+++	-	
	MSR1L_03420	330.542	MGMSRv2_2373	2.494.052	y		MamO	0,176	0	+++	-	
	MSR1L_03410	?	MGMSRv2_2374	2.494.784	y		MamN	0,113	0	++	-	
	MSR1L_03400	328.406	MGMSRv2_2375	2.495.915	y		MamM	0,199	0	+++	-	
	MSR1L_03400	328.399	MGMSRv2_2375	2.495.915	y		MamM	0,143	0	++	-	
	MSR1L_03400	?	MGMSRv2_2375	2.495.960	y		MamM	0,116	0	++	-	
	MSR1L_03400	?	MGMSRv2_2375	2.496.081	y		MamM	0,115	0	++	-	
	MSR1L_03400	328.397	MGMSRv2_2375	2.496.206	y		MamM	0,096	0,03	++	-	
	MSR1L_03400	?	MGMSRv2_2375	2.496.274	y		MamM	0,119	0	++	-	
	MSR1L_03400	?	MGMSRv2_2375	2.496.387	y		MamM	0,065	0	++	-	

inMAI non-magnetic	MSR1L_03400	?	MGMSRv2_2375	2.496.401	y		MamM	0,014	0	+	-
	MSR1L_03400	?	MGMSRv2_2375	2.496.620	y		MamM	0,203	0	+++	-
	MSR1L_03400	?	MGMSRv2_2375	2.496.643	y		MamM	0,198	0	+++	-
	MSR1L_03380	?	MGMSRv2_2378	2.499.214	y		MamJ	0,1	0,02	+++	-
	MSR1L_03360	?	MGMSRv2_2379	2.500.017	y		MamE	0,222	0	+++	-
	MSR1L_03360	324.627	MGMSRv2_2379	2.500.104	y		MamE	0,208	0	+++	-
	MSR1L_03360	?	MGMSRv2_2379	2.500.835	y		MamE	0,227	0	+++	-
	MSR1L_03360	323.338	MGMSRv2_2379	2.501.382	y		MamE	0,185	0	+++	-
	MSR1L_03360	?	MGMSRv2_2379	2.501.635	y		MamE	0,251	0	+++	-
	MSR1L_03360	?	MGMSRv2_2379	2.501.720	y		MamE	0,11	0	++	-
	MSR1L_03350	?	MGMSRv2_2380	2.501.994	y		MamI	0,135	0	++	-
	MSR1L_03180	308.180	MGMSRv2_2396	2.515.601	y		Mms6	0,071	0	++	-
	MSR1L_03470	335.431	MGMSRv2_2368	?	y		MamB	0,12	0	+++	-
	MSR1L_03450	334.362	MGMSRv2_2370	?	y		MamQ	0,15	0	+++	-
	MSR1L_03440	333.456	MGMSRv2_2371	?	y		MamA	0,092	0	++	-
	MSR1L_03440	333.129	MGMSRv2_2371	?	y		MamA	0,13	0	+++	-
	MSR1L_03440	333.251	MGMSRv2_2371	?	y		MamA	0,11	0	+++	-
	MSR1L_03440	333.218	MGMSRv2_2371	?	y		MamA	0,13	0	+++	-
	MSR1L_03420	332.100	MGMSRv2_2373	?	y		MamO	0,198	0	+++	-
	MSR1L_03420	330.506	MGMSRv2_2373	?	y		MamO	0,185	0	+++	-
	MSR1L_03420	330.282	MGMSRv2_2373	?	y		MamO	0,13	0	+++	-
	MSR1L_03420	330.879	MGMSRv2_2373	?	y		MamO	0,19	0	+++	-
	MSR1L_03420	330.927	MGMSRv2_2373	?	y		MamO	0,14	0	+++	-
	MSR1L_03410	329.389	MGMSRv2_2374	?	y		MamN	0,14	0	+++	-
	MSR1L_03410	329.084	MGMSRv2_2374	?	y		MamN	0,13	0	+++	-
	MSR1L_03400	328.494	MGMSRv2_2375	?	y		MamM	0,13	0	+++	-
	MSR1L_03400	328.494	MGMSRv2_2375	?	y		MamM	0,13	0	+++	-
	MSR1L_03400	328.211	MGMSRv2_2375	?	y		MamM	0,16	0	+++	-
	MSR1L_03400	327.960	MGMSRv2_2375	?	y		MamM	0,14	0	+++	-
	MSR1L_03400	328.601	MGMSRv2_2375	?	y		MamM	0,14	0	+++	-
	MSR1L_03400	?	MGMSRv2_2375	?	y		MamM	0,14	0	+++	-
	MSR1L_03380	326.998	MGMSRv2_2377	?	y		MamK	0,16	0	+++	-
	MSR1L_03380	327.270	MGMSRv2_2377	?	y		MamK	0,14	0	+++	-
	MSR1L_03380	326.953	MGMSRv2_2377	?	y		MamK	0,14	0	+++	-
	MSR1L_03360	323.068	MGMSRv2_2379	?	y		MamE	0,176	0	+++	-
	MSR1L_03360	323.475	MGMSRv2_2379	?	y		MamE	0,176	0	+++	-
	MSR1L_03360	323.823	MGMSRv2_2379	?	y		MamE	0,193	0	+++	-
	MSR1L_03360	323.688	MGMSRv2_2379	?	y		MamE	0,188	0	+++	-
	MSR1L_03360	324.735	MGMSRv2_2379	?	y		MamE	0,15	0	+++	-
	MSR1L_03360	322.931	MGMSRv2_2379	?	y		MamE	0,16	0	+++	-
	MSR1L_03360	323.936	MGMSRv2_2379	?	y		MamE	0,13	0	+++	-
	MSR1L_03360	323.088	MGMSRv2_2379	?	y		MamE	0,15	0	+++	-
	MSR1L_03360	324.141	MGMSRv2_2379	?	y		MamE	0,2	0	+++	-
magnetic	MSR1L_03440	333.610	MGMSRv2_2371	?	y		MamA	0,12	0,85	+++	+
	MSR1L_03440	333.610	MGMSRv2_2371	?	y		MamA	0,14	0,89	+++	+
	MSR1L_03380	327.473	MGMSRv2_2377	?	y		MamK	0,103	0,44	+	+
	MSR1L_03860	368.977	MGMSRv2_2323	2.459.845	y		MamZ	0,092	0,1	++	+
	MSR1L_03470	?	MGMSRv2_2368	2.489.408	y		MamB	0,177	0,1	+++	+
	MSR1L_03430	?	MGMSRv2_2372	2.491.610	y	magnetochrome	MamP	0,151	0,07	+++	+
	MSR1L_03420	?	MGMSRv2_2373	2.492.443	y		MamO	0,105	0,23	+++	+
	MSR1L_03410	?	MGMSRv2_2374	2.494.624	y		MamN	0,104	0,11	+++	+
	MSR1L_03410	?	MGMSRv2_2374	2.494.745	y		MamN	0,111	0,06	+++	+
	MSR1L_03380	327.647	MGMSRv2_2377	2.497.478	y		MamK	0,147	0	+++	+

inMAI weakly m	MSR1L_03430	332.899	MGMSRv2_2372	?	y	magnetochrome	MamP	0,15	0,06	+++	+
	MSR1L_03870	369.755	MGMSRv2_2322	2.457.648	y	magnetochrome	MamX	0,131	1,16	++	++
	MSR1L_03380	326.953	MGMSRv2_2377	?	y		MamK	0,14	0,87	+++	++
	MSR1L_03160	307.382	MGMSRv2_2398	?	y		Mms36	0,103	0,72	+++	++
	MSR1L_02670	270.213	MGMSRv2_2312	2.446.983	y		FeoB1	0,156	0,75	++	++
	MSR1L_02660	?	MGMSRv2_2313	2.447.939	y		FeoA1	0,144	0,93	++	++
	MSR1L_03870	?	MGMSRv2_2322	2.457.856	y	magnetochrome	MamX	0,204	0,96	+++	++
	MSR1L_03460	?	MGMSRv2_2369	2.489.871	y		MamR	0,144	0,81	++	++
	MSR1L_03350	?	MGMSRv2_2380	2.502.080	y		MamI	0,107	0,62	+++	++
	MSR1L_03180	308.146	MGMSRv2_2396	2.515.559	y		Mms6	0,133	0,81	+++	++
	MSR1L_03170	307.881	MGMSRv2_2397	2.515.856	y		MmsF	0,132	0,72	++	++
	MSR1L_03470	334.986	MGMSRv2_2368	?	y		MamB	0,15	0,6	+++	++
	MSR1L_03340	321.630	MGMSRv2_2381	?	y		MamH	0,106	0,68	++	++
inMAI WTmagnetic	MSR1L_03460	?	MGMSRv2_2369	2.490.029	y		MamR	0,229	1,1	+++	+++
	MSR1L_03430	?	MGMSRv2_2372	2.491.777	y	magnetochrome	MamP	0,271	1,27	+++	+++
	MSR1L_03340	321.870	MGMSRv2_2381	?	y		MamH	0,11	1,37	+++	+++
	MSR1L_02670	271.399	MGMSRv2_2312	2.446.529	y		FeoB1	0,137	1,01	++	+++
	MSR1L_02660	269.922	MGMSRv2_2313	2.447.981	y		FeoA1	0,153	1,47	++	+++
	MSR1L_03490	336.337	MGMSRv2_2366	2.488.276	y	magnetochrome	MamT	0,249	1,34	+++	+++
	MSR1L_03420	?	MGMSRv2_2373	2.492.921	y		MamO	0,124	1,43	++	+++
	MSR1L_03420	?	MGMSRv2_2373	2.493.652	y		MamO	0,295	1,43	+++	+++
	MSR1L_03410	?	MGMSRv2_2374	2.495.482	y		MamN	0,118	1,35	++	+++
	MSR1L_03380	?	MGMSRv2_2377	2.497.629	y		MamK	0,271	1,27	+++	+++
	MSR1L_03360	?	MGMSRv2_2379	2.501.663	y	magnetochrome	MamE	0,263	1,1	+++	+++
	MSR1L_03340	?	MGMSRv2_2381	2.502.366	y		MamH	0,135	1,03	++	+++
	MSR1L_03340	?	MGMSRv2_2381	2.502.685	y		MamH	0,131	1,13	++	+++
	MSR1L_03180	308.322	MGMSRv2_2396	2.515.809	y		Mms6	0,118	1,41	++	+++
	MSR1L_02670	270.908	MGMSRv2_2312	?	y		FeoB1	0,15	1,16	+++	+++
	MSR1L_02670	271.404	MGMSRv2_2312	?	y		FeoB1	0,249	1,34	+++	+++
	MSR1L_03870	369.042	MGMSRv2_2322	?	y	magnetochrome	MamX	0,16	1,11	+++	+++
	MSR1L_03860	368.933	MGMSRv2_2323	?	y		MamZ	0,1	1,36	+++	+++
	MSR1L_03420	330.630	MGMSRv2_2373	?	y		MamO	0,13	1,48	+++	+++
	MSR1L_03410	329.389	MGMSRv2_2374	?	y		MamN	0,11	1,07	+++	+++

Table S2.B. Tn5 insertion clones selected as Nmag/Wmag during visual screening of the mutagenesis library.

Locus-tag MSR1(L), GenBank acc. CP027526, CP027527 (R. Uebe et al, Genome Announc 6, 2018)	Insertion position MSR1(L)	Locus-tag MGMSRv2, GenBank acc. HG794546 (X. Wang et al., Genome Announc 2, 2014)	Insertion Position in MGMSRv2	inMAI = n, exMAI = y	(putative) functional category	Annotation	Comments
MSR1L_00320	35.238	MGMSRv2_0021	22.170	n	RNA	RmlB-23S RNA methyltransferase	*rlmB*
MSR1L_01530	145.647	MGMSRv2_0142	133.754	n	?	exported protein of unknown function	DUF839; TAT-signal!
MSR1L_20490	?	MGMSRv2_0149	150.840	n	toxin?	conserved protein of unknown function	huge ORF (31 kb)!
MSR1L_20280	2.124.592	MGMSRv2_0173	203.045	n	cell wall?	transglutaminase-like protein	DUF2126
MSR1L_20040	2.095.720	MGMSRv2_0195	?	n	redox	aldehyde dehydrogenase	
MSR1L_19820	2.071.226	MGMSRv2_0217	256.053	n	?	conserved protein of unknown function	TPR-protein? long operon 210-222! SrfC and SrfB (virulence effectors) encoded right upstream
MSR1L_19720	2.056.697	MGMSRv2_0227	270.168	n	purine catabolism	aminotransferase class V, purine catabolism	*pucG*
MSR1L_19360	2.023.570	MGMSRv2_0266	?	n	protein secretion?	adhesive surface protein, hemeagglutinin-like?	
MSR1L_19350	2.019.808	MGMSRv2_0267	?	n	protein secretion?	outer membrane efflux protein	PF02321; 14 proteins in MSR-1
MSR1L_19350	2.019.808	MGMSRv2_0267	?	n	protein secretion?	outer membrane efflux protein	PF02321; 14 proteins in MSR-1
MSR1L_18700	1.957.720	MGMSRv2_0345	?	n	nitrogen	nitrogenase iron protein NifH	binds 4Fe-4S-cluster
MSR1L_18160	1.912.974	MGMSRv2_0397	?	n	storage	polyphosphate kinase	*ppK*
MSR1L_17970	1.885.282	MGMSRv2_0417	?	n	transporter	ABC-transporter, substrate-binding protein	Leu-binding? Leu/Ile/Val-binding?
MSR1L_17970	1.884.455	MGMSRv2_0417	?	n	transporter	ABC-transporter, substrate-binding protein	Leu-binding? Leu/Ile/Val-binding?
MSR1L_17900	1.880.358	MGMSRv2_0424	459.294	n	transporter	ABC-transporter, ATPase component	*hmuV* (hemine transporter?) *fecCD (* ABC transporter ferric iron dicitrate permease and ABC transporter ferric iron hydroxamate periplasmic binding protein encoded upstream)
MSR1L_17870	1.876.175	MGMSRv2_0427	463.722	n	transporter	TonB dependent receptor	
MSR1L_17860	1.875.950	MGMSRv2_0428	464.592	n	regulator	AraC-type DNA - binding domain containing protein	transcriptional regulator
MSR1L_17500	1.835.661	MGMSRv2_0463	?	n	signaling, His-kin/RR	His-kinase-response regulator hybrid	GAF-like + PAS + His-Kin + RR
MSR1L_17450	1.830.615	MGMSRv2_0468	508.148	n	sulfur	sulfite reductase	
MSR1L_17450	?	MGMSRv2_0468	508.665	n	sulfur	sulfite reductase	
MSR1L_17450	?	MGMSRv2_0468	509.262	n	sulfur	sulfite reductase	

	MSR1L_17440	1.829.717	MGMSRv2_0469	510.110	n	sulfur	phosphoadenylyl-sulfate reductase (thioredoxin)	cysH
	MSR1L_17440	?	MGMSRv2_0469	510.114	n	sulfur	phosphoadenylyl-sulfate reductase (thioredoxin)	cysH
	MSR1L_17430	?	MGMSRv2_0470	511.348	n	sulfur	sulfate adenylyltransferase	cysD
	MSR1L_17430	1.829.014	MGMSRv2_0470	?	n	sulfur	sulfate adenylyltransferase	cysD
	MSR1L_17420	?	MGMSRv2_0471	511.952	n	sulfur	adenylylsulphate kinase	cysC
	MSR1L_17420	?	MGMSRv2_0471	513.033	n	sulfur	adenylylsulphate kinase	cysC
	MSR1L_17420	?	MGMSRv2_0471	513.150	n	sulfur	adenylylsulphate kinase	cysC
	MSR1L_17410	1.824.506	MGMSRv2_0472	?	n	signaling, His-kin	His-kinase	PAS, no HAMP, His-Kin
	MSR1L_17180	1.799.009	MGMSRv2_0495	539.233	n	sulfur	cystathionine beta-lyase	
	MSR1L_17040	?	MGMSRv2_0511	556.223	n	sulfur	disulfide bond formation protein DsbB	dsbB
	MSR1L_17040	?	MGMSRv2_0511	556.260	n	sulfur	disulfide bond formation protein DsbB	dsbB
	MSR1L_17040	?	MGMSRv2_0511	556.447	n	sulfur	disulfide bond formation protein DsbB	dsbB
	MSR1L_17010	1.782.185	MGMSRv2_0514	557.729	n	peptidase	peptidase family M48 protein	
	MSR1L_16940	1.776.119	MGMSRv2_0521	?	n	carbohydrate catabolism	glycogen debranching enzyme (family 13 glycoside hydrolase)	glgX
	MSR1L_16830	1.762.256	MGMSRv2_0534	?	n	?	uncharacterized protein	2 TM
	MSR1L_16790	1.751.203	MGMSRv2_0538	?	n	lipid metabolism	biotin carboxylase	accC
	MSR1L_16650	1.740.946	MGMSRv2_0551	601.019	n	phosphatase?	rhodanese-like protein	
	MSR1L_06530	647.482	MGMSRv2_0592	?	n	DNA	integrase	
	MSR1L_06710	670.859	MGMSRv2_0611	?	n	amino acid biosynthesis	asparagine synthetase (glutamine-hydrolyzing)	
	MSR1L_05360	527.032	MGMSRv2_0647	?	n	DNA	transposase	IS4 family
	MSR1L_16340	1.706.551	MGMSRv2_0730	765.000	n	metabolism	succinic semialdehyde dehydrogenase	gabD ; 4-amino-butyrate (GABA) degradation
	MSR1L_06910	692.410	MGMSRv2_0762	?	n	?	DUF1398 protein	
	MSR1L_14490	1.455.448	MGMSRv2_0813	?	n	regulator?	cupin-domain protein	transcription factor?
	MSR1L_14380	1.438.539	MGMSRv2_0824	861.701	n	transporter	outer membrane efflux protein	
	MSR1L_13600	1.349.563	MGMSRv2_0902	?	n	signaling, His-kin	His-kinase	x, no PAS, no HAMP, His-Kin
	MSR1L_13120	1.304.145	MGMSRv2_0947	?	n	transporter	high affinity branched-chain amino acid ABC transporter, permease protein (LivM-like)	9 TM
	MSR1L_12940	1.284.321	MGMSRv2_0965	?	n	chemotaxis	methyl-accepting chemotaxis protein	?
	MSR1L_12460	1.231.707	MGMSRv2_1016	?	n	metabolism	acyl-CoA synthetase	
	MSR1L_11550	1.143.631	MGMSRv2_1113	?	n	signaling, His-kin	His-kinase	Chase, PAS, no HAMP, His-Kin
	MSR1L_10740	1.061.185	MGMSRv2_1185	?	n	protein secretion	type I secretion membrane fusion protein, HlyD family	TIGR01843, 5 proteins in MSR-1

MSR1L_10260	1.012.228	MGMSRv2_1231	?	n	signaling, His-kin/RR	His-kinase-response regulator hybrid (Hpt phosphotransfer)	
MSR1L_10100	995.869	MGMSRv2_1247	?	n	?	membrane protein	10 TM
MSR1L_10040	991.007	MGMSRv2_1253	?	n	?	membrane protein	4 TM
MSR1L_09900	979.965	MGMSRv2_1267	1.312.679	n	transporter	TauE-like transmembrane protein	7 TM
MSR1L_09710	959.268	MGMSRv2_1296	?	n	aromatic amino acid catabolism	glutathione-S-transferase family protein	
MSR1L_09700	958.261	MGMSRv2_1297	1.340.313	n	amino acid catabolism	fumarylacetoacetate (FAA) hydrolase	
MSR1L_09340	923.359	MGMSRv2_1331	1.375.903	n	peptidase	ATP-dependent ClpA-ClpP serine protease, proteolytic subunit ClpP	*Desulfovibrio magneticus* RS-1
MSR1L_09260	912.548	MGMSRv2_1339	?	n	competence, DNA-uptake?	ComEC/Rec2-related protein	transmembrane protein
MSR1L_08990	886.867	MGMSRv2_1366	?	n	chemotaxis	methyl-accepting chemotaxis protein	4HB_MCP_1 (4helix bundle sensory module)
MSR1L_08380	831.371	MGMSRv2_1404	?	n	regulator	cNMP-binding Crp-type DNA-binding protein	
MSR1L_07420	741.545	MGMSRv2_1505	?	n	?	uncharacterized protein	
MSR1L_14690	1.475.592	MGMSRv2_1531	?	n	signaling	GGDEF-domain containing protein	6 TM; 30 proteins in MSR-1; 20 proteins in MSR-1 with additional EAL domain (and in part additional signaling domains)
MSR1L_14890	1.505.532	MGMSRv2_1553	?	n	redox	acyl-CoA dehydrogenase	
MSR1L_15490	1.574.547	MGMSRv2_1613	?	n	Flp pilus-assembly?	vWFA-protein	
MSR1L_15630	?	MGMSRv2_1627	1.688.478	n	PKS	conserved protein of unknown function containing polyketide synthase/Fatty acid synthase domain	huge orf! PKS (like 1629)!
MSR1L_15650	1.611.703	MGMSRv2_1629	?	n	PKS	polyketide synthase	
MSR1L_15810	1.644.793	MGMSRv2_1645	?	n	metabolism	phosphoesterase	
MSR1L_15920	1.651.865	MGMSRv2_1656	?	n	chemotaxis	protein-glutamate methylesterase	me-esterase CheB/me-transferase CheR/PAS domain
MSR1L_16000	1.667.809	MGMSRv2_1666	?	n	signaling	signal transduction response regulator, receiver domain	no output domain
MSR1L_16010	1.668.040	MGMSRv2_1667	?	n	chemotaxis	protein-glutamate methylesterase	me-esterase CheB/me-transferase CheR/His-kin/2xRR/GerE output
MSR1L_06180	611.172	MGMSRv2_1694	1.793.463	n	transporter	TrkA-C domain protein	citrate transporter?
MSR1L_05990	592.221	MGMSRv2_1716	1.813.021	n	nitrogen	nitric oxide reductase, subunit B	*norB*
MSR1L_05980	591.755	MGMSRv2_1717	1.814.067	n	nitrogen	nitric oxide reductase, subunit C	*norC*

MSR1L_04990	486.009	MGMSRv2_1818	1.918.186	n	transporter	TonB-dependent receptor	TonB-copper (like OprC, NosA); also in Ca. Magnetoovum chiemensis, Magnetobacterium bavaricum, Magnetobacterium casensis
MSR1L_04660	454.065	MGMSRv2_1852	?	n	cell wall	dTDP-glucose 4,6-dehydratase	*rfbB*
MSR1L_04500	433.577	MGMSRv2_1868	1.973.360	n	chemotaxis	methyl-accepting chemotaxis protein	?
MSR1L_04410	423.819	MGMSRv2_1877	1.981.612	n	chemotaxis	methyl-accepting chemotaxis protein	?
MSR1L_04280	408.245	MGMSRv2_1890	?	n	carbohydrate catabolism	beta-glucosidase	
MSR1L_26390	?	MGMSRv2_1971	2.068.765	n	?	hypothetical protein	
MSR1L_02470	251.139	MGMSRv2_1991	?	n	signaling, His-kin	His-kinase	PAS, no HAMP, His-Kin
MSR1L_02430	246.222	MGMSRv2_1995	?	n	?	uncharacterized protein	
MSR1L_02420	245.417	MGMSRv2_1996	2.102.495	n	cofactor biosynthesis	carboxylesterase BioH	
MSR1L_02200	215.216	MGMSRv2_2018	2.133.125	n	transporter	ABC transporter, urea, permease protein UrtB	
MSR1L_01960	190.748	MGMSRv2_2042	?	n	transporter	transmembrane protein	2 EamA domains
MSR1L_20760	2.207.517	MGMSRv2_2080	2.196.443	n	chemotaxis	signal transduction response regulator, receiver domain	SpoE II output domain
MSR1L_21200	?	MGMSRv2_2124	2.250.192	n	transporter	arsenical pump-driving ATPase	*arsA* ; operon arsenical resistance
MSR1L_21370	2.280.101	MGMSRv2_2142	?	n	transporter	ABC-transporter, ATPase component	amno acid transport?
MSR1L_21600	2.297.952	MGMSRv2_2163	?	n	transporter	TRAP-transporter, DctM	C4-dicarboxylate transport
MSR1L_21620	2.301.213	MGMSRv2_2165	?	n	transporter	TRAP-transporter (DctM-DctQ fused)	C4-dicarboxylate transport
MSR1L_21840	2.332.970	MGMSRv2_2186	?	n	cell division	DNA translocase FtK	
MSR1L_22290	2.376.603	MGMSRv2_2232	?	n	?	DUF1285 protein	
MSR1L_22710	2.420.191	MGMSRv2_2274	?	n	DNA	replicative helicase	
MSR1L_06450	640.814	MGMSRv2_2462	2.576.698	n	?	protein of unknown function	1 TM (C-terminal)
MSR1L_38450	4.016.350	MGMSRv2_2470	?	n	regulator	RNA polymerase sigma-70 factor RpoE	ECF family
MSR1L_38410	4.013.407	MGMSRv2_2474	?	n	DNA	DNA mismatch repair protein MutL	
MSR1L_38130	3.988.532	MGMSRv2_2501	?	n	cell division	cell division protein FtsQ	
MSR1L_37510	3.931.308	MGMSRv2_2614	?	n	phage	bacteriophage capsid protein	
MSR1L_36810	3.866.987	MGMSRv2_2680	?	n	regulator	RecX family protein	interaction with RecA, modulation of RecA activity
MSR1L_36680	3.853.609	MGMSRv2_2693	?	n	redox	cyt c 551	
MSR1L_36410	3.827.540	MGMSRv2_2719	2.820.417	n	transporter	ABC transporter, transmembrane region	
MSR1L_36380	3.822.575	MGMSRv2_2722	?	n	cofactor biosynthesis	decarboxylase	*ubiD* ; ubiquinone biosynthesis

MSR1L_36360	3.819.429	MGMSRv2_2724	2.829.888	n	chemotaxis	methyl-accepting chemotaxis protein	sCache_2
MSR1L_35190	3.697.147	MGMSRv2_2838	?	n	signaling, His-kin	His-kinase	?
MSR1L_34390	3.623.849	MGMSRv2_2917	3.016.900	n	cell cycle regulation?	histidine phosphotransferase	COG5385, downstream: *cheAWYBR* !
MSR1L_34150	3.600.893	MGMSRv2_2954	?	n	redox	cyt c oxidase cbb3-type, subunit I	*fixN*/*ccoN*; 12 TM
MSR1L_33860	3.580.323	MGMSRv2_2984	3.071.684	n	flagellum	flagellar biosynthetic protein FliR	
MSR1L_33760	3.567.138	MGMSRv2_2994	?	n	flagellum	flagellar hook length control protein FliK	
MSR1L_33740	3.564.464	MGMSRv2_2996	3.087.857	n	flagellum	flagellar hook protein FlgE	
MSR1L_33740	?	MGMSRv2_2996	3.087.850	n	flagellum	flagellar hook protein FlgE	
MSR1L_33720	3.560.367	MGMSRv2_2998	?	n	redox	aldehyde dehydrogenase	
MSR1L_33160	3.504.960	MGMSRv2_3027	3.120.125	n	celll wall	soluble lytic transglycosylase	murein degradation
MSR1L_28770	3.049.447	MGMSRv2_3148	3.227.887	n	redox	cyt c-type protein, NapC/NirT multiheme cyt superfamily	Fur regulator right downstream (reverse 3149); Fur family protein upstream close (reverse 3137); NapC/NirT cytochrome c family
MSR1L_29160	3.086.350	MGMSRv2_3189	?	n	redox	heme lyase CcmF	*ccmF*
MSR1L_29180	3.088.874	MGMSRv2_3191	?	n	redox	cyt c-type biogenesis protein CcmH	*ccmH*
MSR1L_29750	3.149.867	MGMSRv2_3248	?	n	cell wall	surface protein with repetitive structure	unique domain structure with Big_6 and Big_3_3
MSR1L_29770	3.155.623	MGMSRv2_3251	?	n	transporter	RND efflux pump, membrane fusion protein	TiGR01730; 11 proteins in MSR-1
MSR1L_29780	3.156.356	MGMSRv2_3252	?	n	transporter	biotin-lipoyl like domain of membrane fusion protein	
MSR1L_30070	3.183.320	MGMSRv2_3280	3.358.689	n	RNA	RsmD	16S rRNA (guanine(966)-N(2))-methyltransferase, operon encoding RNA modifying proteins
MSR1L_30080	3.183.944	MGMSRv2_3281	?	n	transporter?	Bax 1 inhibitor	7 TM; pH-dependent calcium leak across membrane
MSR1L_30090	3.185.910	MGMSRv2_3282	?	n	transporter	ABC-transporter, substrate-binding protein	branched chain amino acids?
MSR1L_30300	3.207.002	MGMSRv2_3303	3.381.111	n	(close to nitrogen)	conserved protein of unknown function	in same direction right downstream recombinase (3302); a little further *glnK* and *amtB* (3299, 3298)
MSR1L_30380	3.212.388	MGMSRv2_3311	?	n	cell division	Maf-like protein	putative inhibitor of septum formation in euk, bacteria, archaea
MSR1L_30390	?	MGMSRv2_3312	3.388.134	n	regulator, (close to cell division)	pyruvate, phosphate dikinase regulatory protein	in operon right upstream of maf (septum formation protein); heme biosyn genes downstream reverse
MSR1L_30580	3.229.922	MGMSRv2_3331	?	n	signaling, His-kin	His-kinase	Chase, no HAMP, His-Kin

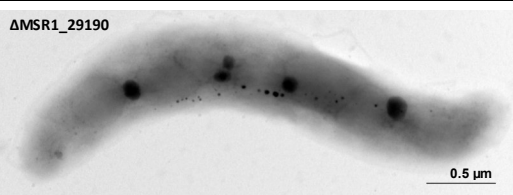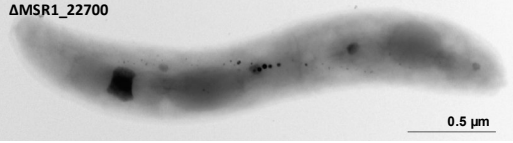|								
MSR1L_30940	?	MGMSRv2_3376	3.447.083	n	cell wall	NAD-dependent epimerase/dehydratase	
MSR1L_31930	3.377.375	MGMSRv2_3485	?	n	cofactor biosynthesis	GTP cyclohydrolase-2	*ribA* ; riboflavin biosynthesis; cofactor of reductases?
MSR1L_27290	2.903.192	MGMSRv2_3596	?	n	peptidase	ATP-dependent ClpA-ClpP serine protease, specificity subunit ClpA	
MSR1L_27410	2.918.802	MGMSRv2_3608	3.695.199	n	tRNA, (close to chemotaxis)	tRNA N(6)-(t(6)A) methylthiotransferase	MtaB (radical SAM)
MSR1L_27740	2.953.002	MGMSRv2_3644	3.731.153	n	signaling, His-kin	His-kinase	
MSR1L_27830	2.962.914	MGMSRv2_3653	3.740.796	n	RNA	ribosome-binding factor A	*rbfA*
MSR1L_28070	2.984.384	MGMSRv2_3680	?	n	transporter	multidrug resistance protein	*norM* ? 11 TM; 2 MatE domains
MSR1L_28090	2.986.821	MGMSR_3682	3.765.579	n	signaling	EAL-domain protein	PF00990; 6 proteins in MSR-1
MSR1L_27100	2.876.769	MGMSRv2_3696	?	n	nitrogen	glutamate synthase [NADPH], small chain	*gltD;* iron -sulfur cluster binding
MSR1L_27050	2.874.384	MGMSRv2_3702	3.785.117	n	oxygen	bacterioferritin - Bfr1	operon of 2 brf genes (deletion: no phenotype (R. Uebe pers. comm.)
MSR1L_26040	2.766.830	MGMSRv2_3810	3.904.094	n	signaling	sensor histidine kinase, x domain + PAS/PAC domain	N-terminal DUF3365
MSR1L_25790	2.738.640	MGMSRv2_3835	?	n	regulator	metal-sensitive transcriptional repressor	Cu, Ni, Co ion binding (Cys, His); transcriptional de-repression when metal bound
MSR1L_25430	2.702.740	MGMSRv2_3871	3.964.834	n	transporter	oligopeptide transporter subunit, periplasmic-binding component of ABC superfamily transporter	*oppA*
MSR1L_24980	2.658.206	MGMSRv2_3916	4.009.636	n	RNA	ATP-dependent RNA helicase SUV3, mitochondrial	
MSR1L_24760	2.638.710	MGMSRv2_3937	?	n	cofactor biosynthesis	aminotransferase	*pabB* ; para-aminobenzoate biosynthesis
MSR1L_24200	2.582.539	MGMSRv2_4000	?	n	metal-binding?	MEMO1 family protein	TIGR00296 + TIGR04335
MSR1L_24180	?	MGMSRv2_4002	4.089.064	n	cell wall	membrane lipid lysyl-group transfer protein	7 TM
MSR1L_24180	?	MGMSRv2_4002	4.089.287	n	cell wall	membrane lipid lysyl-group transfer protein	7 TM
MSR1L_23570	2.518.977	MGMSRv2_4044	4.141.463	n	?	conserved protein of unknown function	
MSR1L_23430/MSR1L_23440	2.506.037	MGMSRv2_4057	?	n	cell wall	surface antigen domain protein	*omp*
MSR1L_23090	?	MGMSRv2_4091	4.188.964	n	signaling, His-kin/RR	signal transduction response regulator, receiver domain + PAS + HisKA + EAL + GGDF	operon 4085-4092! starts with *fliI* , *divk* right downstream of 4091!
MSR1L_39290	4.098.592	MGMSRv2_4209	?	n	TPR	TPR-domain protein	glycosyl transferase family 9
MSR1L_39470	4.121.693	MGMSRv2_4227	4.331.590	n	metabolism	pyruvate, phosphate dikinase	*ppdK*

	Locus-tag MSR1(L), GenBank acc. CP027526, CP027527 (4)	Insertion position MSR1(L)	Locus-tag MGMSRv2, GenBank acc. HG794546 (5)	Insertion Position in MGMSRv2	inMAI = n, exMAI = y	(putative) functional category	Annotation	Comments
	MSR1L_02710	274.133	**MGMSRv2_2308**	2.443.699	y		**vWFA-protein**	
	MSR1L_02670	271.404	MGMSRv2_2312	2.446.524	y	iron	FeoB1	
	MSR1L_02670	271.169	MGMSRv2_2312	2.446.759	y	iron	FeoB1	
	MSR1L_02670	270.945	MGMSRv2_2312	2.447.282	y	iron	FeoB1	
	MSR1L_02670	270.908	MGMSRv2_2312	2.447.396	y	iron	FeoB1	
	MSR1L_02670	270.213	MGMSRv2_2312	2.447.564	y	iron	FeoB1	
	MSR1L_02660	?	MGMSRv2_2313	2.447.834	y	iron	FeoA1	
	MSR1L_03790	362.043	**MGMSRv2_2333**	?	y		**transposase**	
	MSR1L_03720	356.696	**MGMSRv2_2342**	?	y		**uncharacterized protein**	
	MSR1L_03490	?	MGMSRv2_2367	2.488.707	y		MamS	
	MSR1L_03490	?	MGMSRv2_2367	?	y		MamS	
	MSR1L_03470	?	MGMSRv2_2368	2.489.180	y		MamB	
	MSR1L_03450	?	MGMSRv2_2370	2.490.062	y		MamQ	
	MSR1L_03450	?	MGMSRv2_2370	2.490.322	y		MamQ	
	MSR1L_03440	?	MGMSRv2_2371	2.491.288	y		MamA	
	MSR1L_03440	?	MGMSRv2_2371	2.491.553	y		MamA	
inMAI	MSR1L_03430	?	MGMSRv2_2372	2.491.798	y	magnetochrome	MamP	
	MSR1L_03420	?	MGMSRv2_2373	2.492.513	y		MamO	
	MSR1L_03420	?	MGMSRv2_2373	2.492.691	y		MamO	
	MSR1L_03420	?	MGMSRv2_2373	2.492.725	y		MamO	
	MSR1L_03420	?	MGMSRv2_2373	2.493.657	y		MamO	
	MSR1L_03420	?	MGMSRv2_2373	2.493.676	y		MamO	
	MSR1L_03420	?	MGMSRv2_2373	2.494.252	y		MamO	
	MSR1L_03410	?	MGMSRv2_2374	2.494.949	y		MamN	
	MSR1L_03410	?	MGMSRv2_2374	2.495.482	y		MamN	
	MSR1L_03410	?	MGMSRv2_2374	2.495.507	y		MamN	
	MSR1L_03400	?	MGMSRv2_2375	2.495.711	y		MamM	
	MSR1L_03400	?	MGMSRv2_2375	2.496.524	y		MamM	
	MSR1L_03400	?	MGMSRv2_2375	2.496.588	y		MamM	
	MSR1L_03390	327.647	MGMSRv2_2376	2.496.966	y		MamL	
	MSR1L_03380	327.528	MGMSRv2_2377	?	y		MamK	
	MSR1L_03380	?	MGMSRv2_2378	2.498.200	y		MamJ	
	MSR1L_03380	?	MGMSRv2_2378	2.498.495	y		MamJ	
	MSR1L_03380	?	MGMSRv2_2378	2.498.950	y		MamJ	
	MSR1L_03360	?	MGMSRv2_2379	2.500.164	y	magnetochrome	MamE	
	MSR1L_03360	?	MGMSRv2_2379	2.500.909	y	magnetochrome	MamE	
	MSR1L_03360	?	MGMSRv2_2379	2.501.121	y	magnetochrome	MamE	
	MSR1L_03360	?	MGMSRv2_2379	2.501.231	y	magnetochrome	MamE	
	MSR1L_03360	?	MGMSRv2_2379	2.501.283	y	magnetochrome	MamE	
	MSR1L_03360	?	MGMSRv2_2379	2.501.362	y	magnetochrome	MamE	
	MSR1L_03360	?	MGMSRv2_2379	2.501.601	y	magnetochrome	MamE	
	MSR1L_03360	?	MGMSRv2_2379	2.501.700	y	magnetochrome	MamE	

MSR1L_03350	?	MGMSRv2_2380	2.501.812	y		MamI	
MSR1L_03350	?	MGMSRv2_2380	2.501.906	y		MamI	
MSR1L_03340	?	MGMSRv2_2381	2.502.087	y		MamH	
MSR1L_03340	?	MGMSRv2_2381	2.502.815	y		MamH	
MSR1L_03340	?	MGMSRv2_2381	2.503.101	y		MamH	
MSR1L_03180	308.340	MGMSRv2_2396	2.515.320	y		Mms6	

Table S3. exMAI N/Wmag genes associated with overrepresented GO-terms identified by FET-analysis against the genomic background

	MGMSRv2_	MSR1L_	GO-terms	Magnetic phenotype of Tn5 insertion alleles (nc: not-characterized beyond colony color)
1	1252	10050	4-coumarate-CoA ligase activity	Wmag
2	1722	5930	calcium ion binding	Wmag
3	266	19360	calcium ion binding-external encapsulating structure	Wmag+nc
4	1279	9800	dimethylallyltranstransferase activity-geranyltranstransferase activity	Wmag
5	1417	8250	external encapsulating structure	Wmag
6	1082	11790	guanosine tetraphosphate metabolic process-diphosphoric monoester hydrolase activity-GTP diphosphokinase activity-guanosine-3',5'-bis(diphosphate) 3'-diphosphatase activity-purine ribonucleoside bisphosphate metabolic process	Wmag+WTmag
7	398	18150	guanosine-5'-triphosphate,3'-diphosphate diphosphatase activity-exopolyphosphatase activity	Wmag
8	3560	32700	homocysteine biosynthetic process-homocysteine metabolic process	Wmag
9	3966	24500	hydroxyacylglutathione hydrolase activity	Wmag
10	2673	36930	methylmalonyl-CoA mutase activity-tetrapyrrole binding-cobalamin binding	Wmag
11	3255	29810	methylmalonyl-CoA mutase activity-tetrapyrrole binding-cobalamin binding	Wmag
12	2474	38410	mismatch repair-mismatched DNA binding	Wmag+nc
13	450	17640	oxidation-reduction process	Wmag
14	1295	9720	oxidation-reduction process	Wmag
15	1555	14910	oxidation-reduction process	Wmag
16	2011	2270	oxidation-reduction process	Wmag
17	2273	22700	oxidation-reduction process	6Wmag+WTmag
18	2950	34190	oxidation-reduction process	Wmag
19	3942	24710	oxidation-reduction process	Wmag
20	853	14090	oxidation-reduction process-**alpha-1,4-glucan synthase** activity-starch synthase activity-glycogen (starch) synthase activity-UDP-glucosyltransferase activity-glucosyltransferase activity	Wmag
21	1617	15530	oxidation-reduction process-**glutaryl-CoA dehydrogenase** activity	Wmag
22	1403	8390	oxidation-reduction process-oxidoreductase activity, acting on other nitrogenous compounds as donors, cytochrome as acceptor-tetrapyrrole binding-**hydroxylamine reductase** activity-nitrite reductase (NO-forming) activity	Wmag
23	1716	5990	oxidation-reduction process-oxidoreductase activity, acting on other nitrogenous compounds as donors, cytochrome as acceptor-tetrapyrrole binding-**nitric oxide reductase** activity	2 Wmag+nc
24	469	17440	oxidation-reduction process-**phosphoadenylyl-sulfate reductase** (thioredoxin) activity-sulfate assimilation, phosphoadenylyl sulfate reduction by phosphoadenylyl-sulfate reductase (thioredoxin)-oxidoreductase activity, acting on a sulfur group of donors, disulfide as acceptor	Wmag+WTmag+2nc
25	470	17430	oxidation-reduction process-**sulfate adenylyltransferase** activity-sulfate adenylyltransferase (ATP) activity-sulfate reduction	Wmag+WTmag+2nc
26	134	450	protein histidine kinase activity-phosphorelay sensor kinase activity- phosphotransferase activity, nitrogenous group as acceptor-protein kinase activity	Wmag
27	1113	11550	protein histidine kinase activity-phosphorelay sensor kinase activity- phosphotransferase activity, nitrogenous group as acceptor-protein kinase activity	Wmag+nc
28	732	16320	protein histidine kinase activity-phosphorelay sensor kinase activity- phosphotransferase activity, nitrogenous group as acceptor-protein kinase activity	Wmag
29	1231	10260	protein histidine kinase activity-phosphorelay sensor kinase activity- phosphotransferase activity, nitrogenous group as acceptor-protein kinase activity	Wmag+nc
30	1777	5370	protein histidine kinase activity-phosphorelay sensor kinase activity- phosphotransferase activity, nitrogenous group as acceptor-protein kinase activity	Wmag
31	4151	38770	protein histidine kinase activity-phosphorelay sensor kinase activity- phosphotransferase activity, nitrogenous group as acceptor-protein kinase activity	Wmag
32	2976	33940	secretion-secretion by cell-peptide secretion-protein secretion	Wmag
33	3625	27560	secretion-secretion by cell-peptide secretion-protein secretion	Wmag
34	3736	26700	sirohydrochlorin cobaltochelatase activity	Wmag
35	3376	30940	UDP-glucuronate decarboxylase activity	Wmag+5 WTmag+nc
36	2540	37510	virion assembly	Wmag

Table S4. Characteristics of Mgryph deletion mutants* in genes for which Tn5-insertion yielded a magnetosome phenotype

Locus-tag MSR1(L)_	Locus-tag MGMSRv2_	Gene name	Magnetic phenotype (Δ) compared to WT	TEM (Δ)
29190	3192	*ccmI* (*cycH*)	less magnetosomes	
22700	2273	*dsbA*	shorter chains	
17040	511	*dsbB*	smaller and less magnetosomes	
17450-17420	468-471	*sir-cysH-cysD-cysC*	significantly increased number of defective crystals, higher prevalence of cells with double magnetosome chains	
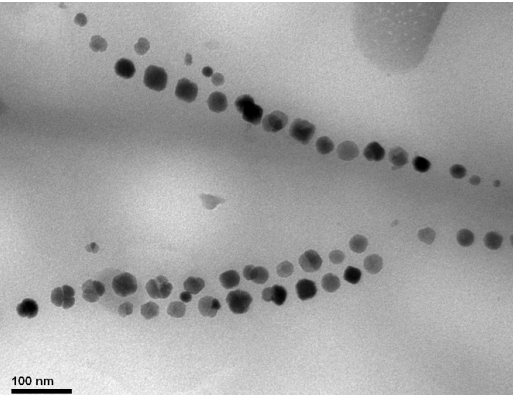
CHAPTER V:

Identification and elimination of genomic regions irrelevant for magnetosome biosynthesis by large-scale deletion in *Magnetospirillum gryphiswaldense*

Theresa Zwiener[1], Frank Mickoleit[1], Marina Dziuba[1,2], Christian Rückert[3], Tobias Busche[3], Jörn Kalinowski[3], Damien Faivre[4,5], René Uebe[1] and Dirk Schüler[1*]

[1]Department of Microbiology, University of Bayreuth, Bayreuth, Germany.

[2]Institute of Bioengineering, Research Center of Biotechnology of the Russian Academy of Sciences, Moscow, Russia.

[3]Center for Biotechnology, University of Bielefeld, Bielefeld, Germany.

[4]Department of Biomaterials, Max Planck Institute of Colloids and Interfaces, Potsdam, Germany.

[5]Aix-Marseille Université, CEA, CNRS, BIAM 13108, Saint Paul lez Durance, France.

BMC Microbiology

Identification and elimination of genomic regions irrelevant for magnetosome biosynthesis by large-scale deletion in *Magnetospirillum gryphiswaldense*

Theresa Zwiener[1], Frank Mickoleit[1], Marina Dziuba[1,2], Christian Rückert[3], Tobias Busche[3], Jörn Kalinowski[3], Damien Faivre[4,5], René Uebe[1] and Dirk Schüler[1*]

Abstract

Background: Magnetosome formation in the alphaproteobacterium *Magnetospirillum gryphiswaldense* is controlled by more than 30 known *mam* and *mms* genes clustered within a large genomic region, the 'magnetosome island' (MAI), which also harbors numerous mobile genetic elements, repeats, and genetic junk. Because of the inherent genetic instability of the MAI caused by neighboring gene content, the elimination of these regions and their substitution by a compact, minimal magnetosome expression cassette would be important for future analysis and engineering. In addition, the role of the MAI boundaries and adjacent regions are still unclear, and recent studies indicated that further auxiliary determinants for magnetosome biosynthesis are encoded outside the MAI. However, techniques for large-scale genome editing of magnetic bacteria are still limited, and the full complement of genes controlling magnetosome formation has remained uncertain.

Results: Here we demonstrate that an allelic replacement method based on homologous recombination can be applied for large-scale genome editing in *M. gryphiswaldense*. By analysis of 24 deletion mutants covering about 167 kb of non-redundant genome content, we identified genes and regions inside and outside the MAI irrelevant for magnetosome biosynthesis. A contiguous stretch of ~ 100 kb, including the scattered *mam* and *mms6* operons, could be functionally substituted by a compact and contiguous ~ 38 kb cassette comprising all essential biosynthetic gene clusters, but devoid of interspersing irrelevant or problematic gene content.

Conclusions: Our results further delineate the genetic complement for magnetosome biosynthesis and will be useful for future large-scale genome editing and genetic engineering of magnetosome biosynthesis.

Keywords: *Magnetospirillum gryphiswaldense*, Magnetosomes, Genome reduction

Background

Besides their function as magnetic sensors and importance as models for prokaryotic organelle biosynthesis, magnetosomes formed by magnetotactic bacteria represent magnetic nanoparticles that are highly attractive for several biotechnological and biomedical applications [1–3]. Because of its tractability and relatively straightforward cultivation, the alphaproteobacterium *Magnetospirillum gryphiswaldense* has emerged as a model for studying the biosynthesis of magnetosomes, as well as their bioproduction and engineering for various applications [4–11]. Magnetosomes isolated from *M. gryphiswaldense* are composed of monocrystalline

* Correspondence: dirk.schueler@uni-bayreuth.de
[1]Department of Microbiology, University of Bayreuth, Bayreuth, Germany
Full list of author information is available at the end of the article

cuboctahedral crystals of magnetite (Fe_3O_4) about 35 nm in size, which are enveloped by a protein-lipid membrane [12]. In the biotechnological and biomedical field, they have been studied, for instance, as nanocarriers for magnetic drug targeting [13–15], multimodal reporters for magnetic imaging [16, 17], and for magnetic hyperthermia applications [18, 19]. In addition, the functionality of magnetosomes can be greatly extended by engineering the magnetite crystals and genetic coupling of magnetosome membrane proteins to foreign functional moieties such as fluorophores, enzymes, antibodies, and organic shells [6, 7, 20–24].

The exquisite properties of magnetosomes, such as high chemical purity and crystallinity, strong magnetization, uniform shapes and sizes [25] are due to the strict control over their biomineralization. This is orchestrated by more than 30 biosynthetic genes, which were mostly found to be clustered in a single chromosomal region, the genomic **ma**gnetosome **i**sland (MAI) [26–29]. The MAI harbors the polycistronic operons *feoAB1op*, *mms6op*, *mamGFDCop*, *mamABop*, and *mamXYop*, which control all specific steps of magnetosome biosynthesis such as the formation of intracellular membrane vesicles, the uptake of iron, magnetite biomineralization, and the assembly of the magnetite crystals into well-ordered chains [3]. The five key operons are separated by stretches containing genes of yet unknown, but irrelevant function for magnetosome biosynthesis [29]. These intervening MAI regions harbor numerous mobile genetic elements, repeats and genetic "junk" (e.g., several incomplete and pseudogenes as well as non-coding genetic content), which are thought to be responsible for genetic instability, i.e., frequent rearrangements, deletions and the spontaneous loss of the magnetic phenotype during subcultivation of *M. gryphiswaldense* [26, 27, 30]. For future genetic analysis and manipulation of magnetosome biosynthesis, it would therefore be highly desirable to eliminate and replace these regions by a compact cassette comprising only the essential biosynthetic gene clusters, but devoid of genetic junk. Mutagenesis by several large, overlapping deletions of up to 61 kb has already demonstrated that a total of 115 kb of the MAI can be eliminated without any detectable effects on growth and magnetosome formation [28, 29]. However, the role of distal and MAI-adjacent regions remains unclear.

Recently, reverse and forward genetic approaches suggested that, besides the well-established *mam/mms/feo* operons within the MAI, there might be further, auxiliary determinants for magnetosome biosynthesis encoded somewhere else in the genome. For example, a genome-wide transposon mutagenesis screen revealed numerous hits outside the MAI [31], however, the putative involvement of several of the afflicted genes still has

to be verified by their clean deletions. In addition, a comprehensive proteomic analysis of the magnetosome membrane revealed several novel genuine constituents [32]. However, their putative roles in magnetosome biosynthesis also still await confirmation by deletion mutagenesis of respective genes.

Large-scale genome analysis and editing in magnetic bacteria would greatly benefit from efficient and reliable techniques for large genetic deletions. For the excision of fragments up to ~ 53 kb a Cre-*lox* based method has been used [28, 29] in *M. gryphiswaldense*. However, this technology has several practical disadvantages, as it requires the cumbersome construction and insertion of two different vectors with *lox* sequences integrating by homologous recombination upstream and downstream of the target region and carrying two different antibiotic resistances. An additional helper plasmid encoding the *Cre* recombinase needs to be conjugated into the host to induce excision of the targeted chromosomal segment, and finally has to be cured from the deletant. In addition, *loxP* nucleotides remain in the genomic target region, causing so-called scars [28]. Alternatively, an allelic replacement method based on homologous recombination has been routinely used for scarless deletions in *M. gryphiswaldense* [33], requiring only one vector, and taking advantage of counterselection of the vector excision by double-crossover using the suicide gene *galK* that encodes a galactokinase with lethal activity [34]. However, this method so far has been employed only for the deletion of smaller fragments (< 20 kb), but not tested for the excision of larger regions.

In this study, we first tested gene deletion methods available for *M. gryphiswaldense* with respect to their practicability and performance in large-scale mutagenesis and engineering. Next, by systematic deletion analysis of the extended MAI as well as adjacent chromosomal regions we interrogated their relevance for magnetosome biosynthesis and growth under lab conditions. Identified irrelevant gene content was substituted by a compact version of all key biosynthetic gene clusters, thereby eliminating much 'junk' and putative detrimental gene content. In addition, further candidate genes outside the MAI that had been putatively implicated in magnetosome biosynthesis by previous reverse and forward genetic approaches were probed by targeted deletions [31, 32].
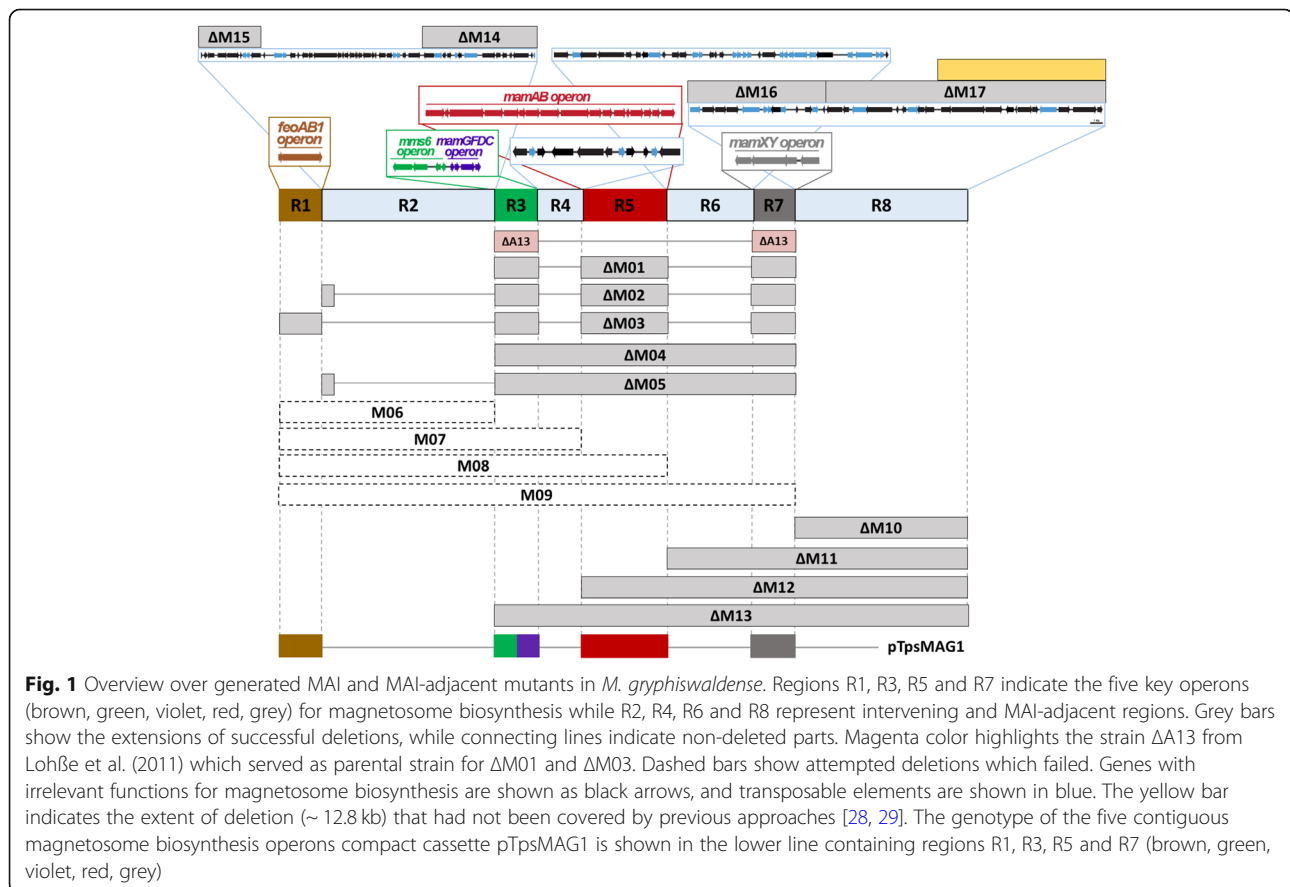
Results
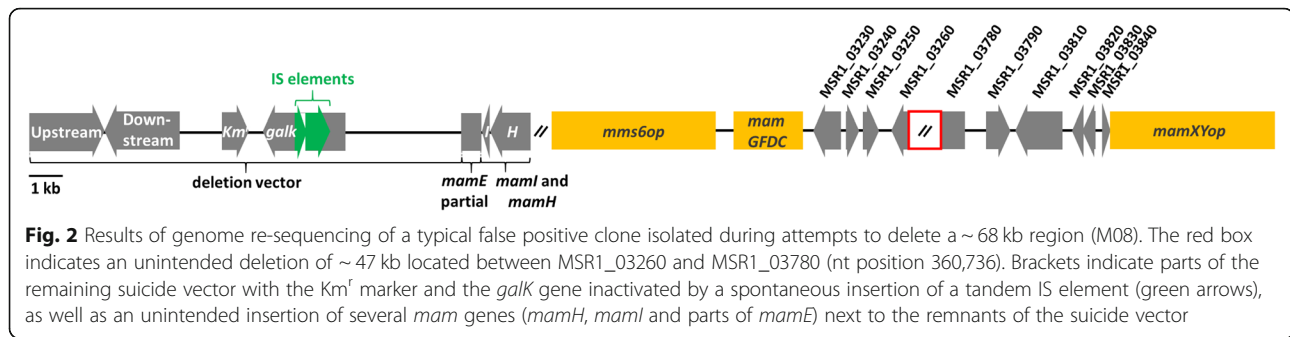
Evaluation of the large-scale deletion method

We first assessed two different techniques with respect to their usability and efficiency to introduce large genomic deletions: A Cre-*lox* based method, which had been used for excision of larger fragments before [28, 29, 35], and an allelic replacement method based on two

consecutive double-crossovers counterselected by lethal GalK [34]. These were tested on two different regions (ΔM01/~ 16 kb, and ΔM04/~ 66 kb) of the MAI (Fig. 1).

By using the Cre-*lox* based method, plenty of clones containing the desired ΔM01 and ΔM04 deletions could be isolated (typically around 20–30 clones with excised target regions per 96 screened clones). Using allelic replacement, between 15–30 clones with the desired double-crossover were typically obtained from 96 screened clones after the final counterselection step. As expected, we found that the use of longer homologous regions of about 1.5–2.5 kb is favorable to yield high numbers of positive clones for larger (>ca. 20 kb) deletions, whereas fragments larger than 2.5 kb were difficult to clone by overlap PCR. Excluding time for cloning, Cre-*lox* based deletions in our hands typically required about 6 weeks because of the need of three consecutive cycles of laborious conjugation, plate growth, clonal selection and screening, which are particularly cumbersome and time-consuming in the rather slow-growing *M. gryphiswaldense*. In contrast, after some streamlining of the workflow, by GalK selection and double-crossovers a clean unmarked deletion mutant was typically obtained and PCR-verified in only about 3 weeks.

During this study, this method later also proved to be highly efficient for deletions of up to about 100 kb. While in most cases proper excisions by double-crossovers could be confirmed by sequencing of PCR products spanning over the excision site, occasionally we identified clones which yielded amplicons of expected size, but did not have lost their insensitivity against kanamycin, indicating the Km[r] marker harbored on the suicide vector to be still residing in the genome. This issue is exemplified by a clone in which we had attempted a ~ 68 kb deletion spanning from *feoAB1op* to *mamABop* (region M08, see below and Fig. 2). Despite their kanamycin insensitivity, all cells had apparently lost the ability to form magnetosomes as expected. However, genome resequencing revealed a large part (~ 44 kb) of the deletion target to be still residing in the chromosome, and a large part (~ 11.4 of ~ 11.7 kb) of the suicide vector was inserted next to it. Conspicuously, the orientation of the homologous downstream region had become inversed, and a ~ 2 kb fragment of *mamABop* (comprising *mamH*, *mamI* and a part of *mamE*) was dislodged from its native position, while the rest of this operon (including several essential magnetosome genes) was absent (Fig. 2), thereby explaining the loss of the

Fig. 1 Overview over generated MAI and MAI-adjacent mutants in *M. gryphiswaldense*. Regions R1, R3, R5 and R7 indicate the five key operons (brown, green, violet, red, grey) for magnetosome biosynthesis while R2, R4, R6 and R8 represent intervening and MAI-adjacent regions. Grey bars show the extensions of successful deletions, while connecting lines indicate non-deleted parts. Magenta color highlights the strain ΔA13 from Lohße et al. (2011) which served as parental strain for ΔM01 and ΔM03. Dashed bars show attempted deletions which failed. Genes with irrelevant functions for magnetosome biosynthesis are shown as black arrows, and transposable elements are shown in blue. The yellow bar indicates the extent of deletion (~ 12.8 kb) that had not been covered by previous approaches [28, 29]. The genotype of the five contiguous magnetosome biosynthesis operons compact cassette pTpsMAG1 is shown in the lower line containing regions R1, R3, R5 and R7 (brown, green, violet, red, grey)

Fig. 2 Results of genome re-sequencing of a typical false positive clone isolated during attempts to delete a ~ 68 kb region (M08). The red box indicates an unintended deletion of ~ 47 kb located between MSR1_03260 and MSR1_03780 (nt position 360,736). Brackets indicate parts of the remaining suicide vector with the Km^r marker and the *galK* gene inactivated by a spontaneous insertion of a tandem IS element (green arrows), as well as an unintended insertion of several *mam* genes (*mamH*, *mamI* and parts of *mamE*) next to the remnants of the suicide vector

magnetic phenotype. Likely, deletion of ~ 47 kb exceeding targeted M08 region had occurred by homologous recombination between two nearly identical ~ 750 bp stretches of two integrase genes residing in R4 and R6, respectively.

Notably, in this clone we also found the suicide gene *galK* (encoding the lethal galactokinase) to be inactivated by insertion of IS elements, thereby prohibiting proper counterselection in the presence of galactose, but favoring the occurrence of spontaneous homologous and non-homologous rearrangements instead. Similarly, during the further course of our mutagenesis approach, false positive clones instead of the intended 'clean' deletions were frequently obtained, in particular for difficult or essential targets. Resequencing of all such suspicious clones revealed that this was always accompanied by *galK* inactivation due to IS insertions (Fig. 2). Nonetheless, considering the benefits of the GalK-based method, it was chosen for all subsequent deletions in this work.

Deletion and replacement of the MAI and adjacent regions

We next generated a library of strains in which we aimed to delete all key magnetosome biosynthesis genes plus as much as possible of the interspacing and flanking gene content from the ~ 100 kb MAI [3]. This region is known to be particularly rich in genetic junk and comprises 39 putative mobile genetic elements [26–29] (Fig. 1, blue arrows). We genetically dissected the MAI and its neighboring region for testing their relevance regarding survival, cell growth and magnetosome biosynthesis. By excluding genes assumed to be relevant or essential for cell growth (e.g. tRNAs and rRNAs), we predicted a region of ~ 134 kb comprising all known key magnetosome clusters and genes potentially irrelevant to the magnetosome formation (Fig. 1), including region R2 that seemed to be successfully deleted in Ullrich et al. (2010), while it appeared to be non-deletable in Lohße et al. (2011). The whole ~ 134 kb region was divided into eight separate regions (R1–8) representing putative deletion targets, which comprised known magnetosome biosynthesis operons (R1, R3, R5, R7), intervening regions

(R2, R4, R6) and a flanking region adjacent to the MAI (R8). Since regions R2 and R8 are spanning large chromosomal areas containing many hypothetical genes with unknown function, they were further divided into smaller parts for deletion. In summary, all regions were covered by 17 partially overlapping deletion targets spanning from ~ 2.5 kb (*feoAB1op*) up to ~ 100 kb (ΔM13) (Fig. 1 and Table S2).

Despite of repeated attempts, we failed to enforce proper deletions of ΔM06–M09 (Fig. 1, dashed bars), which all include the region R2, thereby supporting the assumption by Lohße et al. (2011) of a non-deletable part in this region. By deletions ΔM14 and ΔM15 this non-deletable part was narrowed down to a region of 15.2 kb including *msr1_02770–msr1_03000* (Fig. 1), which in addition to several hypothetical genes encodes a putative toxin-antitoxin system (*msr1_02860–msr1_02870*) that might prevent its simultaneous deletion.

For all other targets, mutants could be readily generated as intended, yielding strains ΔM01–ΔM05 and ΔM10–ΔM17 with defined single deletions ranging from ~ 2.5 kb (*feoAB1op*, deleted in a later step) up to ~ 100 kb (ΔM13) (Fig. 1, grey bars). The ΔA13 mutant from Lohße et al. (2011) (not to be confused with ΔM13, this study), already lacking *mms6op*, *mamGFDCop* and *mamXYop* (Fig. 1), was used as parental strain for the additional deletion of *mamABop* and *feoAB1op* to generate ΔM01 and ΔM03 mutants, respectively. To generate ΔM02, strain ΔA13Δmms5/mmxF lacking *mms6op*, *mamGFDCop*, *mamXYop* and *mms5/mmxF* (R. Uebe, unpublished) was used to delete the *mamABop*. Further deletion of regions R4 and R6 in the ΔM02 background then yielded ΔM05 (Fig. 1). All other deletions were introduced into the WT parent. ΔM01–ΔM05 showed WT-like cell size, shape and morphology, but displayed slightly impaired swimming motility as their parent strains ([29], R. Uebe, unpublished).

As expected, all deletions comprising the known magnetosome clusters were impaired in magnetosome biosynthesis to different degrees. Mutants ΔM01–ΔM05 and ΔM12–ΔM13 lacking the *mamABop* were entirely

devoid of magnetosomes, whereas ΔM11 (deletion of R7 with *mamXYop*, but all other *mam/mms/feo* clusters still present) essentially phenocopied the known intermediate magnetic phenotype typically caused by mutation of the *mamXYop* (Figs. 3 and S1) [36]. This phenotype is characterized by a reduced (40–80% of the WT) C_{mag} (a light-scattering based proxy for the average magnetic orientation of bacterial cells in liquid media [37]), with WT-like magnetite crystals flanked within the magnetosome chain by poorly crystalline flake-like particles. By contrast, elimination of regions outside the *mam/mms/feo* clusters (ΔM10, ΔM14–ΔM17 in R2 and R8) resulted in a WT-like magnetosome phenotype (Fig. S1). These mutants ΔM10 and ΔM14–ΔM17, covering 15 putative mobile genetic elements, phage-related genes and several hypothetical genes, also displayed a WT-like cell growth at 28 °C under aerobic conditions (data not shown).

However, all non-magnetic mutant strains in which deletions covered the *mamABop* (ΔM01–ΔM04) displayed a growth advantage over the WT by reaching higher cell densities (ca. 10–35%) under aerobic conditions or moderate heat stress at 33 °C (Fig. 4). An exception was strain ΔM05, which showed the same mild growth deficiency (lower cell yields) as its parent, probably due to an unidentified spontaneous second site mutation. Growth of non-magnetic ΔM01–ΔM04 and ΔM13 mutants under anaerobic conditions was indistinguishable from the WT. However, in the presence of oxidative stress generated by H_2O_2, ΔM01–ΔM04 grew to higher, and ΔM13 to lower densities than the WT, respectively (Fig. 4). Deleted genes in ΔM13 include a putative aerotaxis-related gene and several hypothetical genes, the loss of which might have caused the decreased sensitivity to oxidative stress.

Next, we tested whether the magnetic phenotypes could be restored by a compact version of all key magnetosome biosynthesis operons. To this end, a transposable cassette comprising *feoAB1op*, *mms6op*, *mamGFDCop*, *mamABop*, and *mamXYop* without intervening gene content was utilized. This cassette was harbored on pTpsMAG1 comprising the MycoMar (*tps*) transposase gene [38]. Reinsertion of the cassette at several random chromosomal locations in ΔM01–ΔM04 and
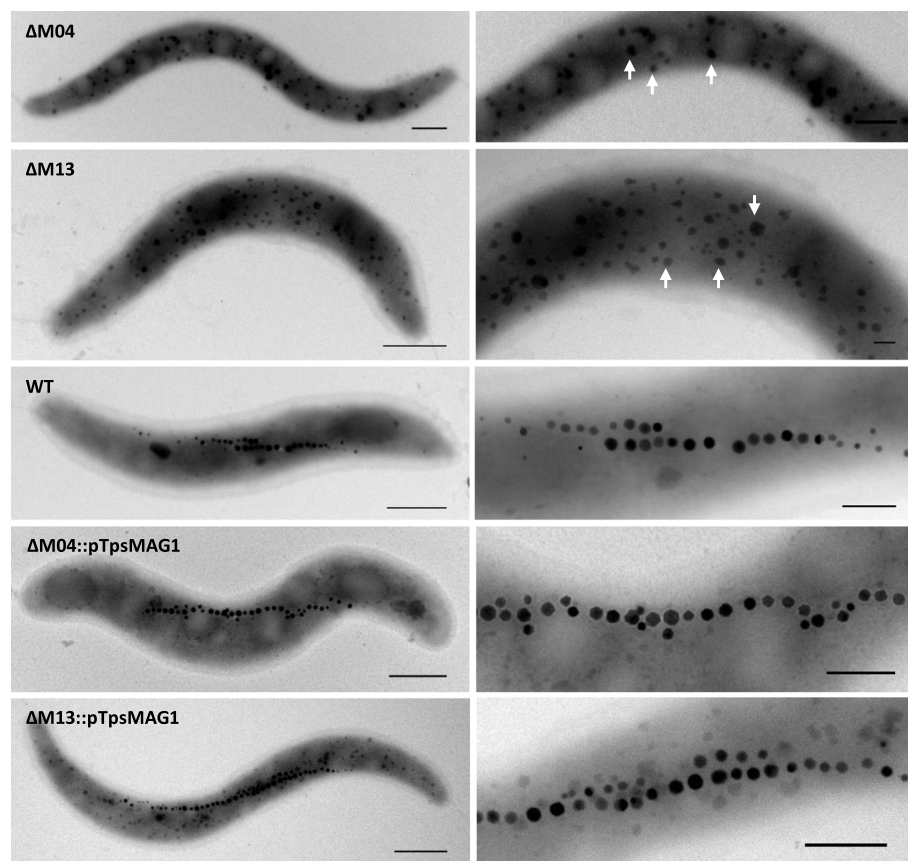
Fig. 3 Phenotypes of non-magnetic mutant strains with largest deletion extents and their respective complemented strains with restored magnetosome biosynthesis. Mutants ΔM04 and ΔM13 are non-magnetic, while complemented mutants show WT-like magnetosome formation. Arrows indicate electron dense particles (EDPs) in mutant strains. Scale bars: left column, 500 nm; right column, 100 nm
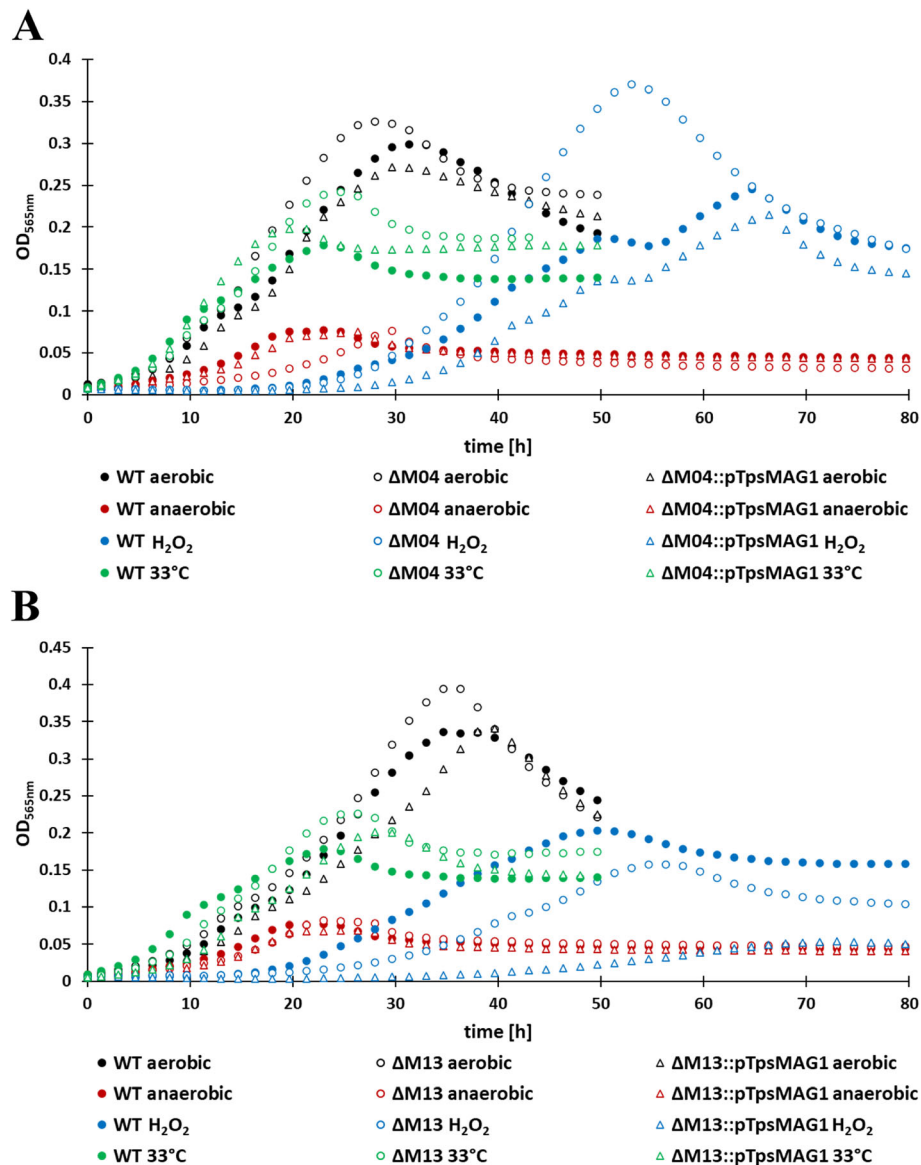
Fig. 4 Growth characteristics of different mutants. Provided are the growth curves of non-magnetic mutant strains with largest deletion extents and their respective complemented strains with restored magnetosome biosynthesis. Growth curves show ΔM04 (**a**), ΔM13 (**b**) and its respective complemented mutants under different growth conditions in comparison to the WT. Growth of the WT is shown in diagrams for both mutants. Each strain was analyzed in technical triplicates, and growth curves represent the average while standard deviation was below 5%

ΔM13 restored magnetosome biosynthesis to WT-levels (Figs. 3 and S1). This again confirmed that deleted genes apart from the *mam*/*mms* gene clusters are dispensable for magnetosome biosynthesis in *M. gryphiswaldense*. The presence of an extra copy of the endogenous *feoAB1op* seems to have no effect on magnetosome biomineralization, but it should be removed in future engineering steps to avoid unintended recombination events. After 're-magnetization', growth rates of ΔM01::pTpsMAG1–ΔM04::pTpsMAG1 and ΔM13::pTpsMAG1 were reduced to WT-levels under aerobic conditions and moderate heat stress. These findings indicate that magnetosome

biosynthesis represents a significant burden that prevents cells from reaching higher cell yields observed in non-magnetic mutants. Under anaerobic conditions, complemented ΔM01::pTpsMAG1–ΔM04::pTpsMAG1 and ΔM13::pTpsMAG1 strains showed WT-like cell yields. Under oxidative stress, complemented ΔM04::pTpsMAG1 revealed slight growth deficiencies (reduction by ~ 12% of WT OD), while the complemented ΔM13::pTpsMAG1 exhibited significantly reduced growth compared to the WT (reduction by ~ 70% of WT-level; Fig. 4).

Of note, in some of the non-magnetic mutants (ΔM01–ΔM05 and ΔM13) (Fig. 3) TEM revealed the presence of

numerous (ca. 90 per cell) irregularly shaped conspicuous electron dense particles ranging 10–125 nm in size (in the following referred to as 'EDP'), scattered over the entire cell. Analysis of strains ΔM03 and ΔM05 by high-resolution electron microscopy revealed that EDPs were amorphous. In addition, energy-dispersive X-ray

spectroscopy (XEDS) showed that the inorganic inclusions were rich in potassium, phosphorus and oxygen, while no significant amounts of iron could be detected (Fig. 5). Variation of culture conditions such as growth in low-iron medium [25] supplemented with 10 μM 2,2′-dipyridyl as non-metabolizable iron chelator, or in medium
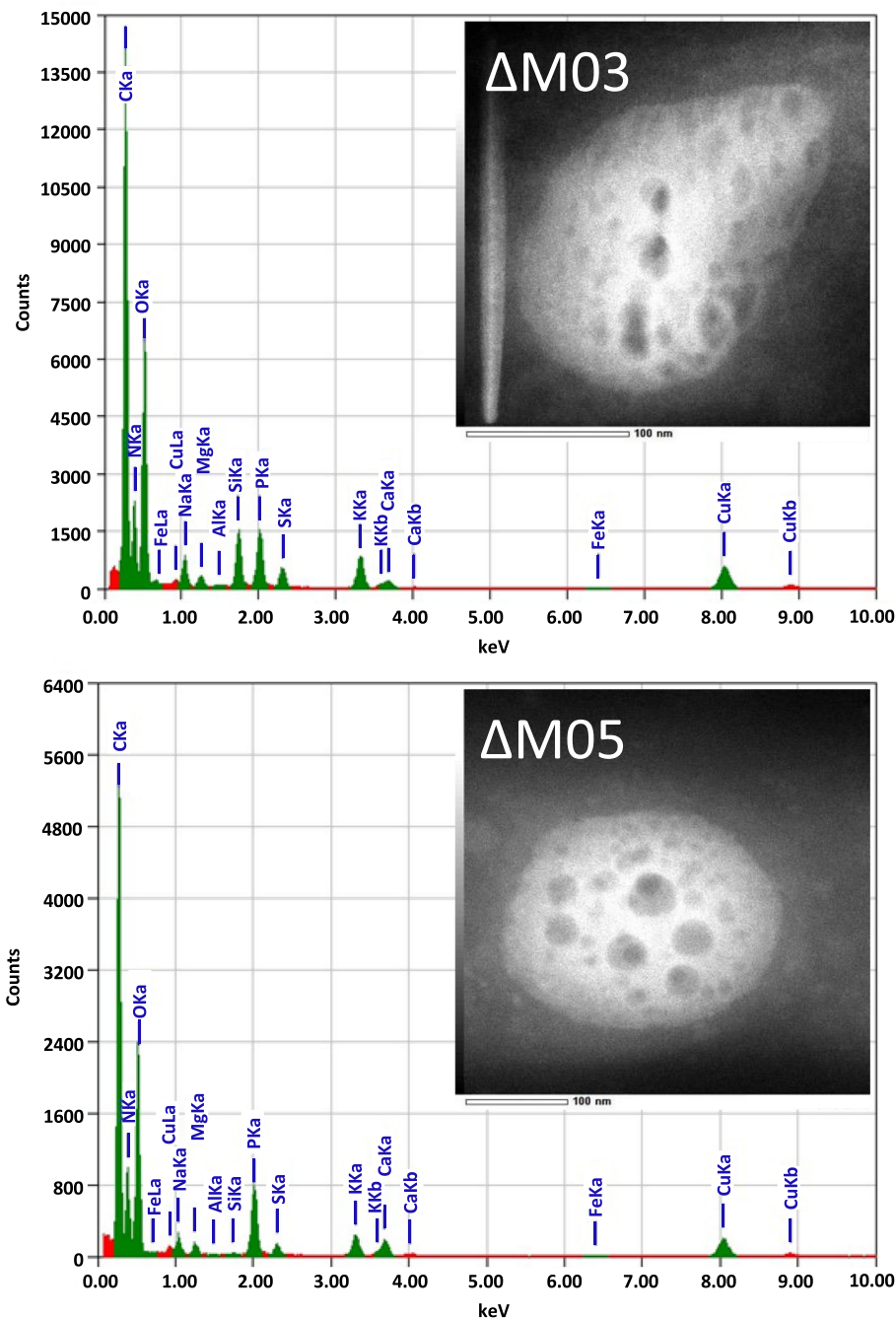
Fig. 5 XEDS spectra and TEM micrographs (insets) of individual EDPs. EDPs were found in deletion strains ΔM01–ΔM05 and ΔM13. Exemplary the mutants ΔM03 and ΔM05 are shown. Spectra indicate that EDPs are rich in potassium, phosphorus and oxygen, while no significant amounts of iron could be detected

oversaturated with 250 μM Fe (III)-citrate did not affect the number, size or appearance of EDPs (data not shown), confirming their independence from iron. Formation of EDPs was neither affected by variation of the phosphate concentration in the medium (0–3 mM), suggesting that low residual phosphate was still saturating for EDP formation. Furthermore, EDPs remained present in cells even after restoration of magnetosome biosynthesis by pTpsMAG1 complementation (Figs. 3 and S1). This indicates that the formation of EDPs is independent of magnetosome biosynthesis, but somehow linked to the deleted genes outside the five key magnetosome biosynthetic clusters. Because of their apparent irrelevance for magnetosome biosynthesis and growth, the identity and formation of EDPs was not explored further in this study.

Overall, the strain with the largest deletion that exhibited WT-like magnetosome biosynthesis upon complementation was ΔM13. In this mutant, a contiguous stretch of ~ 100 kb including all *mam* and *mms6* operons (~ 27 kb) but *feoAB1op*, interspaced or flanked by ~ 73 kb of irrelevant or problematic gene content was deleted and substituted by a contiguous, yet functional version of magnetosome biosynthetic gene clusters (Fig. 1).

Deletion of putative determinants for magnetosome biosynthesis outside the MAI

Next, we assessed the role of candidate genes with putative roles during magnetosome biosynthesis located outside the MAI. One group of these candidates was recently retrieved by genome-wide transposon mutagenesis, in which a colony appearance deviant from the dark-brown color of the WT served as a proxy for impaired magnetosome biomineralization [31]. Another category was comprised of candidate genes, whose gene products were found to be genuinely associated with magnetosome particles purified from disrupted *M. gryphiswaldense* cells [32]. Most interesting targets for mutagenesis were further selected based on their conservation in other magnetospirilla and/or a conspicuous genomic neighborhood. This resulted in the following list of deletion targets (Fig. 6; Table S3):

Candidates identified by Tn5-mutagenesis [31]

– A clone with a reduced C_{mag} was linked to a hit in *msr1_17870*, which is part of a putative operon comprising eleven genes (*msr1_17870–17940*) that is conserved in two other magnetospirilla (Table S3). It has predicted functions related to the TonB-system, which is known to form energized, gated pores that bind and internalize iron chelates in Gram-negative bacteria [39]. Here, we deleted the entire 9.5 kb operon region.

– Several Tn-insertants within a huge (31 kb) monocistronic gene (*msr1_20490*) became suspicious because of their slightly altered colony appearance [31]. The gene encodes a single giant putative surface protein with a predicted mass of 1147 kDa and a repetitive structure, which belongs to the FecR/concanavalin A-like lectin/glucanase superfamily [31]. It is also conserved in several other magnetic and non-magnetic

Fig. 6 Schematic overview over the chromosomal positions of single deletions in this study. The yellow circle shows genes or gene sets targeted for deletion. Grey: MAI; red: M13 deletion; green: putative candidate genes for magnetosome biosynthesis outside the MAI [31, 32]
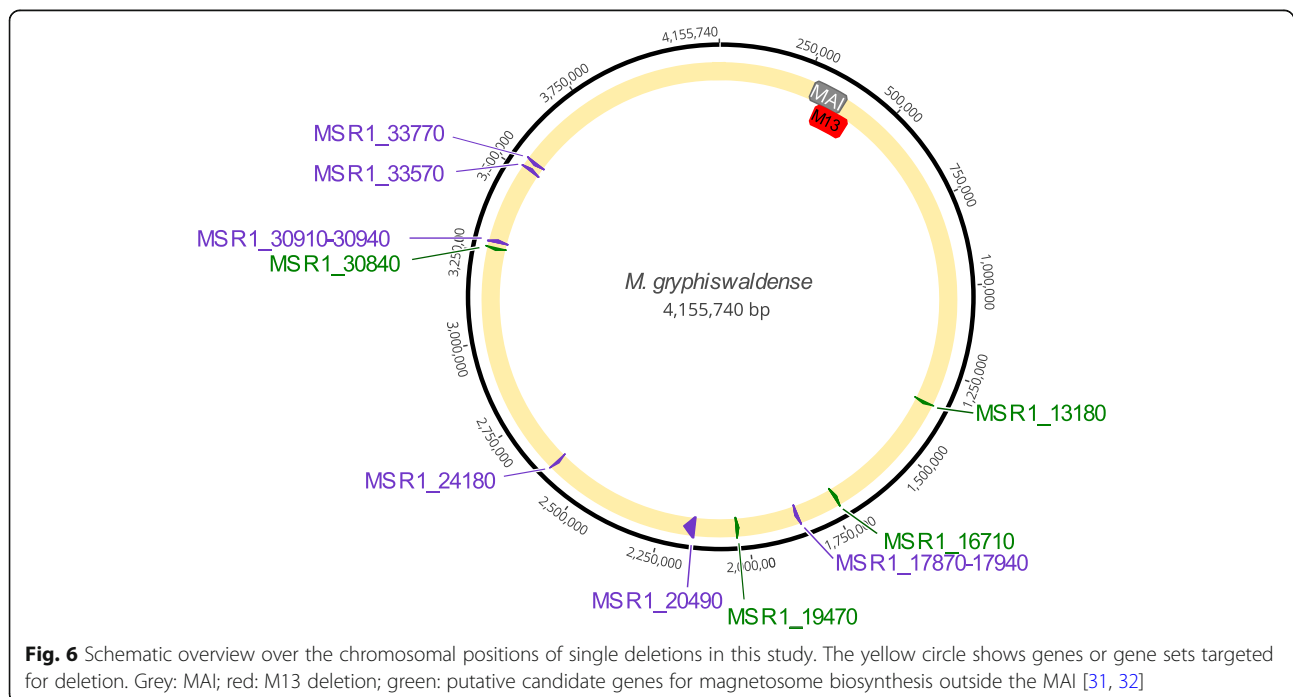
magnetospirilla (Table S3). In our study, we deleted the entire open reading frame of *msr1_20490*.

– Conspicuously, *msr1_24180* was also hit by several independent Tn5-insertions [31] and is conserved in most magnetospirilla (Table S3). It contains a lysyl-phosphatidylglycerol synthase transmembrane region with putative function in cell wall modification [31]. We deleted *msr1_24180* (~ 1 kb) in this study.

– The first four genes (*msr1_30910–30940*) of a six-gene operon were hit several times independently [31] and are conserved in several magnetospirilla (Table S3). The predicted functions (e.g., a glycosyl transferase gene, a dTDP-sugar isomerase, a methyltransferase and epimerase/dehydratase (NAD) gene) may play an important role in cell wall biogenesis or modification reported by Silva et al. (2020). *msr1_30910–30940* (~ 3.5 kb) were deleted in this study.

– *msr1_33570* and *msr1_33770* are hypothetical genes which were also retrieved by the Tn-screen. They are conserved in many magnetospirilla (Table S3). Both genes were deleted (Δ*msr1_33570*, 1.2 kb, Δ*msr1_33770*, 0.3 kb).

Candidates identified by magnetosome membrane proteomics [32]

– MSR1_13180 (10 kDa), MSR1_16710 (9 kDa) and MSR1_19470 (11 kDa) are transmembrane proteins with unknown functions, but orthologs in many magnetospirilla. All three respective genes were deleted individually (0.27 kb, 0.249 kb, 0.33 kb, respectively).

– MSR1_30840 is a transmembrane protein (33 kDa, four TMH) predicted as a putative peptidase, encoded next to potential LPS core biosynthesis genes, which is also conserved in two other magnetospirilla (Table S3). In addition to its detection in the magnetosome membrane [32], *msr1_30840* is within close genomic neighborhood (7.4 kb) to *msr1_30910–30940*, all having received several Tn5-hits [31]. Δ*msr1_30840* was generated in this study (0.951 kb).

Deletion mutants of all targeted genes could be obtained in a straightforward manner. Some of the null mutants (Δ*msr1_20490*, Δ*msr1_30910–30940*, Δ*msr1_30840*) displayed a slightly reduced C_{mag} (< 1), compared to WT-levels of 1–2, and the cell shape of Δ*msr1_20490* seemed to be more spiralized. However, TEM analysis revealed the presence of magnetosomes apparently indistinguishable from the WT with respect to number, size, shape and alignment in all mutants (Fig. S2). Hence, contrary to the previous hypotheses, these genes play no obvious and strong role in magnetosome biosynthesis under the tested conditions.

Discussion

In this study, we tested an approach for large-scale gene deletion in *M. gryphiswaldense* and employed it for the mutational analysis of candidate genes and the elimination of regions irrelevant for magnetosome biosynthesis. We extended the tested range of contiguous MAI deletions by ca. 13 kb compared to Lohße et al. (2011), and show that deletions of up to ~ 100 kb are feasible using allelic replacement based on homologous recombination with reasonable efficiency and time requirement. In total, we generated 24 deletions, ranging from about 0.25–100 kb in size and covering about 167.2 kb. However, we also revealed several pitfalls and potential caveats. When attempting to delete 'recalcitrant' or essential targets, false positive clones may arise, in which the second double-crossover had failed. Instead parts of the vector were retained in the genome through insertion by single homologous or non-homologous recombination, which was often associated with extensive spontaneous rearrangements of the adjacent regions. In all analyzed cases this was caused in the first place by spontaneous inactivation of the suicide gene *galK* by insertion of IS elements, which prohibited counterselection in the presence of galactose. This emphasizes the need of caution by sequence verification of the intended excision site.

Except for ΔM05, *mamABop* deficient non-magnetic deletants showed a growth advantage, which became lost upon 're-magnetization' by complementation. Not surprisingly, magnetosome biosynthesis seems to impose a substantial metabolic burden, resulting in slower growth and lower yields compared to non-magnetic mutants. Neither the deletion of the MAI flanking regions nor any of the candidate genes outside the MAI had a strong and obvious effect on magnetosome biosynthesis, at least under the tested standard conditions. While this finding is unsurprising for the flanking regions, it may hint at an issue for the candidates retrieved in a recent Tn5-mutagenesis study. In these cases, the unaffected magnetosome phenotype of our clean gene deletions indicates that the observed reduced C_{mag} value or the deviant colony appearance of the Tn5-insertants [31] is likely due to subtle differences in cell shape and/or cell surface, rather than to direct effects on magnetosome biosynthesis. This is consistent with the functional prediction of several of these genes in pathways related to cell envelope biosynthesis. However, candidates identified by a previous proteomic study as constituents of the magnetosome membrane are unlikely to simply represent false positives due to contaminations because of the rigorous

magnetosome purification procedure [32]. Instead, these proteins are likely to be indeed native constituents of this compartment, but their function may be only required in conditions not tested in our study or can be substituted by other magnetosome proteins.

Conclusion

Our results further delineate the genetic complement for magnetosome biosynthesis. We engineered a strain, in which a ~ 100 kb region comprising large parts of the MAI and flanking regions was substituted by a compact (~ 38 kb), yet fully functional cassette containing the five key magnetosome biosynthetic operons *mamGFDCop*, *mms6op*, *mamABop*, *mamXYop*, and *feoAB1op*, but devoid of any flanking and intervening regions. The elimination of about 73 kb of genetic junk and 39 putative mobile genetic elements (equivalent to ~ 33% of all known putative mobile genetic elements in the genome of *M. gryphiswaldense*) may contribute to increased genetic stability, as already suggested by a recent study [40].

Methods

Bacterial strains, vectors, and cultivation conditions

Bacterial strains and plasmids used in this study are listed in Table S1. *Escherichia coli* strains were grown as previously described [41]. For the cultivation of *E. coli* WM3064 lysogeny broth (LB) medium was supplemented with 25 μg/ml (final concentration) kanamycin (Km), 15 μg/ml gentamycin (Gm), 12 μg/ml tetracycline (Tet) and 1 mM DL-α,ε-diaminopimelic acid (DAP). Liquid cultures of *M. gryphiswaldense* strains were grown microaerobically in flask standard medium (FSM) [5] at 28 °C under moderate shaking (120 rpm), and strains carrying the suicide or the Cre plasmids were cultivated by adding 5 μg/ml Km, 20 μg/ml Gm or 5 μg/ml Tet. For cultivation on solid LB medium and FSM, 1.5% (w/v) agar was added. Cultivation from single *M. gryphiswaldense* colonies was performed by transferring cell material into 150 μl FSM in 96-deep-well-plates (Eppendorf, Hamburg, Germany), prior to gradually increasing the culture volume. The optical density (OD) at 565 nm and magnetic response (C_{mag}, i.e., a proxy for the average magnetic orientation of bacterial cells in liquid media based on light-scattering) of cells in the exponential growth phase were measured photometrically as previously reported [37].

Growth experiments were performed by using precultures grown for two daily passages under microaerobic conditions at 28 °C. Cultures were adjusted to an initial OD of 0.01 and grown in an Infinite F200pro microplate reader (Tecan, Switzerland) under aerobic conditions at 28 °C or moderate heat stress at 33 °C. For induction of oxidative stress,

20 μM H_2O_2 were added prior to starting the growth experiments.

Molecular and genetic techniques

Oligonucleotides used as primers for amplification of DNA fragments were deduced from the working draft genome sequence of *M. gryphiswaldense* (GenBank accession number CP027526) [42] and purchased from Sigma-Aldrich (Steinheim, Germany). Plasmids were constructed by standard recombinant techniques as described below. Generated constructs were sequenced by Macrogen Europe (Amsterdam, Netherlands) and sequence data analyzed with Geneious 8.0.5 (Biomatters Ltd., New Zealand).

Construction of loxP site vectors and mutant strains

Upstream and downstream regions of about 1–2.5 kb of deletion targets were amplified and subcloned into *loxP* suicide plasmids pAL01 and pAL02/2 [29], respectively. Resulting vectors were sequence-verified by PCR and conjugated into *M. gryphiswaldense* using *E. coli* WM3064 as donor strains. Insertion mutants were distinguished from the WT by Km, and Km plus Gm selection. Addition of *Cre* recombinase plasmid pLYJ87 [43] by conjugational transfer resulted in the excision of target regions, and the plasmid was subsequently cured from each mutant by several transfers in FSM without any antibiotics. Deletions were verified by PCR and sequencing.

Construction of markerless gene deletion vectors and mutants

Generation of single and multiple deletion mutants was accomplished by a tailored *galK* counterselection system as described previously [34] (Fig. S1). The pORFM-GalK-vector was digested using EcoRV to insert fused upstream and downstream fragments each of about 1–2.5 kb. For larger fragments (> 20 kb), flanking regions between 1.5–2.5 kb were amplified while for deletion of smaller fragments, homologous regions < 1.5 kb were used. Proper construction of resulting plasmids was verified by PCR and sequencing. The latter were transferred into *M. gryphiswaldense* strains by conjugation using *E. coli* WM3064 as donor. Genomic insertion mutants were identified using a kanamycin resistance marker (Km^r, aminoglycoside 3′-phosphotransferase type IIa encoded by the *aph(3′)-IIa* gene) [44] which was present on the suicide vector. After ~ 5 d of incubation at 28 °C, Km^r clones were picked and re-grown in up to 1 ml FSM at 28 °C. For generation of double crossover mutants, selected clones were plated onto FSM agar containing 2.5% galactose to counterselect for vector integration by

the lethal activity of galactokinase (GalK). This enzyme catalyzes the phosphorylation of galactose. Since *M. gryphiswaldense* is unable to metabolize galactosephosphate, this product accumulates to toxic levels inside the cell. As a result, only cells that have undergone a second recombination event and thus, have removed the plasmid backbone, are able to survive. Deletions were verified by PCR and sequencing.

Analytical methods

Re-sequencing of genomic DNA

Genomic DNA (gDNA) was isolated following the manual instructions of Quick-DNA Midiprep Plus Kit (Zymo Research Europe GmbH). For each isolated gDNA, two sequencing libraries were prepared, one for sequencing on the MiSeq platform (Illumina Inc., NL), and one for sequencing on the GridION platform (Oxford Nanopore Technologies (ONT), UK). The former was constructed using the TruSeq DNA PCR-free Library Kit (Illumina Inc., The Netherlands) and was run in a 2×300 nt run using a 600 cycle MiSeq Reagent Kit v3 (Illumina Inc., The Netherlands). For ONT sequencing, the Ligation Sequencing Kit SQK-LSK109 was used to prepare the libraries, which were in turn run on a R9.4.1 flow cell. Basecalling of the raw ONT data was performed with GUPPY v3.2.8 [45]. For assembly, three assemblers were utilized: The CANU assembler v1.8 [46] was used to assemble the ONT data. The resulting assembled contigs were polished using first the ONT data with RACON v1.3.3 [47] and MEDAKA v0.11.5 (Oxford Nanopore Technologies), both relying on MINIMAP2 v2.17-r943 [48] for mapping, followed by switching to the Illumina data and the PILON polisher v1.22 [49] for a total of 10 rounds. For the first 5 rounds, BWA MEM [50] was used as a mapper, for the final 5 cycles, BOWTIE2 [51] was applied. In addition, the Illumina data was assembled using NEWBLER v2.8 [52] and both data sets were assembled using UNICYCLER [53]. All assemblies were compared with each other and checked for synteny using R2CAT [54]. All three assemblies were combined and manually curated using CONSED [55]. Annotation of the finished genomes was performed using PROKKA v1.11 [56] SNPs and small indels were identified using SNIPPY v4.0 [57] while larger rearrangements were identified manually using SNAP-GENE (GSL Biotech).

Preparation of samples for transmission electron microscopy (TEM)

For routine TEM of cell and magnetosome morphologies, cultures were grown under microoxic conditions in FSM. Overnight cultures were fixed in 1.5% formaldehyde and deposited onto carbon-coated copper-mesh grids (Science Services, Munich, Germany). TEM was performed on a JEOL 1400 (Japan) with an acceleration voltage of 80 kV. Micrographs were analyzed using the software ImageJ [58].

For analysis of unidentified electron dense particles (uEDP), bright field TEM, high-resolution (HR) TEM and energy-dispersive X-ray spectroscopy (XEDS) were performed on a spherical aberration corrected JEOL ARM 2100 at an acceleration voltage of 200 kV and an emission current of 10 μA.

Supplementary Information

The online version contains supplementary material available at https://doi.org/10.1186/s12866-021-02124-2.

> **Additional file 1.**

Availability of data and materials
The datasets used and analyzed during the current study are available from the corresponding author on reasonable request. Raw sequencing data are available under BioProject number PRJNA691753.

Ethics approval and consent to participate
Not applicable.

Consent for publication
Not applicable.

Competing interests
The authors declare that they have no competing interests.

Author details
[1]Department of Microbiology, University of Bayreuth, Bayreuth, Germany. [2]Institute of Bioengineering, Research Center of Biotechnology of the Russian Academy of Sciences, Moscow, Russia. [3]Center for Biotechnology, University of Bielefeld, Bielefeld, Germany. [4]Department of Biomaterials, Max Planck Institute of Colloids and Interfaces, Potsdam, Germany. [5]Aix-Marseille Université, CEA, CNRS, BIAM 13108, Saint Paul lez Durance, France.

References

1. McCausland HC, Komeili A. Magnetic genes: studying the genetics of biomineralization in magnetotactic bacteria. PLoS Genet. 2020;16(2): e1008499.
2. Lefèvre CT, Bazylinski DA. Ecology, diversity, and evolution of magnetotactic bacteria. Microbiol Mol Biol Rev. 2013;77(3):497–526.
3. Uebe R, Schüler D. Magnetosome biogenesis in magnetotactic bacteria. Nat Rev Microbiol. 2016;14:621–37.
4. Schleifer KH, Schüler D, Spring S, Weizenegger M, Amann R, Ludwig W, Köhler M. The genus Magnetospirillum gen. Nov. description of *Magnetospirillum gryphiswaldense* sp. nov. and transfer of *Aquaspirillum magnetotacticum* to *Magnetospirillum magnetotacticum* comb. nov. Syst Appl Microbiol. 1991;14:379–85.
5. Heyen U, Schüler D. Growth and magnetosome formation by microaerophilic Magnetospirillum strains in an oxygen-controlled fermentor. Appl Microbiol Biotechnol. 2003;61:536–44.
6. Mickoleit F, Schüler D. Generation of multifunctional magnetic nanoparticles with amplified catalytic activities by genetic expression of enzyme arrays on bacterial magnetosomes. Adv Biosys. 2018;2:1700109.
7. Mickoleit F, Lanzloth C, Schüler D. A versatile toolkit for controllable and highly selective multifunctionalization of bacterial magnetic nanoparticles. Small. 2020;16(16):e1906922.
8. Fernández-Castané A, Li H, Thomas ORT, Overton TW. Development of a simple intensified fermentation strategy for growth of *Magnetospirillum gryphiswaldense* MSR-1: physiological responses to changing environmental conditions. New Biotechnol. 2018;46:22–30.
9. Alphandéry E. Bio-synthesized iron oxide nanoparticles for cancer treatment. In J Pharm. 2020;586:119472.
10. Alphandéry E. Applications of magnetotactic bacteria and magnetosome for cancer treatment: a review emphasizing on practical and mechanistic aspects. Drug Discov Today. 2020;S1359–6446(20):30235–X.
11. Schüler D, Monteil CL, Lefèvre CT. Microbe of the Month: *Magnetospirillum gryphiswaldense*. Trends Microbiol. 2020;S0966-842X(20):30163.
12. Schüler D. Molecular analysis of a subcellular compartment: the magnetosome membrane in *Magnetospirillum gryphiswaldense*. Arch Microbiol. 2004;181(1):1–7.
13. Lang C, Schüler D. Biogenic nanoparticles: production, characterization, and application of bacterial magnetosomes. J Phys Condens Matter. 2006;18: 2815–28.
14. Lisy MR, Hartung A, Lang C, Schüler D, Richter W, Reichenbach JR, Kaiser WA, Hilger I. Fluorescent bacterial magnetic nanoparticles as bimodal contrast agents. Investig Radiol. 2007;42(4):235–41.
15. Schwarz S, Fernandes F, Sanroman L, Hodenius M, Lang C, Himmelreich U, Fama G, Schmitz-Rode T, Schüler D, Hoehn M, Zenke M, Hieronymus T. Synthetic and biogenic magnetite nanoparticles for tracking of stem cells and dendritic cells. J Magn Magn Mater. 2009;321(10):1533–8.
16. Heinke D, Kraupner A, Eberbeck D, Schmidt D, Radon P, Uebe R, Schüler D, Briel A. MPS and MRI efficacy of magnetosomes from wild-type and mutant bacterial strains. IJMPI. 2017;3(2):1706004.
17. Kraupner A, Eberbeck D, Heinke D, Uebe R, Schüler D, Biel A. Bacterial magnetosomes – Nature's powerful contribution to MPI tracer research. Nanoscale. 2017;9(18):5788–93.
18. Hergt R, Dutz S, Röder M. Effects of size distribution on hysteresis losses of magnetic nanoparticles for hyperthermia. J Phys Condens Matter. 2008;20: 385214.
19. Alphandéry E, Guyot F, Chebbi I. Preparation of chains of magnetosomes, isolated from *Magnetospirillum magneticum* strain AMB-1 magnetotactic bacteria, yielding efficient treatment of tumors using magnetic hyperthermia. Int J Pharm. 2012;434(1–2):444–52.
20. Pollithy A, Romer T, Lang C, Müller FD, Helma J, Leonhardt H, Rothbauer U, Schüler D. Magnetosome expression of functional camelid antibody fragments (nanobodies) in *Magnetospirillum gryphiswaldense*. Appl Environ Microbiol. 2011;77(17):6165–71.
21. Borg S, Rothenstein D, Bill J, Schüler D. Generation of multi-shell magnetic hybrid nanoparticles by encapsulation of genetically engineered and fluorescent bacterial magnetosomes with ZnO and SiO_2. Small. 2015;11(33): 4209–17.
22. Mickoleit F, Schüler D. Generation of nanomagnetic biocomposites by genetic engineering of bacterial magnetosomes. Bioinspired Biomim Nanobiomat. 2018;8(1):86–98.
23. Mickoleit F, Borkner CB, Toro-Nahuelpan M, Herold HM, Maier DS, Plitzko JM, Scheibel T, Schüler D. *In vivo* coating of bacterial magnetic nanoparticles by magnetosome expression of spider silk-inspired peptides. Biomacromolecules. 2018;19(3):962–72.
24. Mickoleit F, Jérôme V, Freitag R, Schüler D. Bacterial magnetosomes as novel platform for the presentation of immunostimulatory, membrane-bound ligands in cellular biotechnology. Adv Biosys. 2020;4(3):e1900231.
25. Faivre D, Schüler D. Magnetotactic bacteria and magnetosomes. Chem Rev. 2008;108(11):4875–98.
26. Schübbe S, Kube M, Scheffel A, Wawer C, Heyen U, Meyerdierks A, Madkour MH, Mayer F, Reinhardt R, Schüler D. Characterization of a spontaneous nonmagnetic mutant of *Magnetospirillum gryphiswaldense* reveals a large deletion comprising a putative magnetosome island. J Bacteriol. 2003;185: 5779–90.
27. Ullrich S, Kube M, Schübbe S, Reinhardt R, Schüler D. A hypervariable 130-kilobase genomic region of *Magnetospirillum gryphiswaldense* comprises a magnetosome island which undergoes frequent rearrangements during stationary growth. J Bacteriol. 2005;187:7176–84.
28. Ullrich S, Schüler D. Cre-*lox*-based method for generation of large deletions within the genomic magnetosome island of *Magnetospirillum gryphiswaldense*. Appl Environ Microbiol. 2010;76:2439–44.
29. Lohße A, Ullrich S, Katzmann E, Borg S, Wanner G, Richter M, Voigt B, Schweder T, Schüler D. Functional analysis of the magnetosome island in *Magnetospirillum gryphiswaldense*: the *mamAB* operon is sufficient for magnetite biomineralization. PLoS One. 2011;6:e25561.
30. Kolinko I, Jogler C, Katzmann E, Schüler D. Frequent mutations within the genomic magnetosome island of *Magnetospirillum gryphiswaldense* are mediated by RecA. J Bacteriol. 2011;193:5328–34.
31. Silva KT, Schüler M, Mickoleit F, Zwiener T, Müller FD, Awal RP, Weig A, Brachmann A, Uebe R, Schüler D. Genome-wide identification of essential and auxiliary gene sets for magnetosome biosynthesis in *Magnetospirillum gryphiswaldense*. mSystems. 2020;5(6):e00565–20.
32. Raschdorf O, Bonn F, Zeytuni N, Zarivach R, Becher D, Schüler D. A quantitative assessment of the membrane-integral sub-proteome of a bacterial magnetic organelle. J Proteome. 2018;172:89–99.
33. Schultheiss D, Kube M, Schüler D. Inactivation of the flagellin gene *flaA* in *Magnetospirillum gryphiswaldense* results in nonmagnetotactic mutants lacking flagellar filaments. Appl Environ Microbiol. 2004;70:3624–31.
34. Raschdorf O, Plitzko JM, Schüler D, Müller FD. A tailored *galK* counterselection system for efficient markerless gene deletion and chromosomal tagging in *Magnetospirillum gryphiswaldense*. Appl Environ Microbiol. 2014;80(14):4323–30.
35. Scheffel A, Gardes A, Grünberg K, Wanner G, Schüler D. The major magnetosome proteins MamGFDC are not essential for magnetite biomineralization in *Magnetospirillum gryphiswaldense* but regulate the size of magnetosome crystals. J Bacteriol. 2008;190:377–86.
36. Raschdorf O, Müller FD, Pósfai M, Plitzko JM, Schüler D. The magnetosome proteins MamX, MamZ and MamH are involved in redox control of magnetite biomineralization in *Magnetospirillum gryphiswaldense*. Mol Microbiol. 2013;89:872–86.
37. Schüler D, Uhl R, Bäuerlein E. A simple light-scattering method to assay magnetism in *Magnetospirillum gryphiswaldense*. FEMS Microbiol Lett. 1995; 132:139–45.
38. Dziuba MV, Zwiener T, Uebe R, Schüler D. Single-step transfer of biosynthetic operons endows a non-magnetotactic *Magnetospirillum* strain from wetland with magnetosome biosynthesis. Environ Microbiol. 2020; 22(4):1603–18.
39. Jiang X, Payne MA, Cao Z, Foster SB, Feix JB, Newton SM, Klebba PE. Ligand-specific opening of a gated-porin channel in the outer membrane of living bacteria. Science. 1997;276(5316):1261–4.
40. Zwiener T, Dziuba M, Mickoleit F, Rückert C, Busche T, Kalinowski J, Uebe R, Schüler D. Towards a 'chassis' for bacterial magnetosome biosynthesis: Genome streamlining of *Magnetospirillum gryphiswaldense* by multiple deletions. Microb Cell Fact. 2021;20:35.
41. Sambrook J, Russell DW. Molecular cloning: a laboratory manual. 3rd ed. Cold Spring Harbor: Cold Spring Harbor Laboratory Press; 2001.
42. Uebe R, Schüler D, Jogler C, Wiegand S. Reevaluation of the complete genome sequence of *Magnetospirillum gryphiswaldense* MSR-1 with single-

molecule real-time sequencing data. Genome Announc. 2018;6(17):e00309–18.

43. Li YJ, Bali S, Borg S, Katzmann E, Ferguson SJ, Schüler D. Cytochrome cd_1 nitrite reductase NirS is involved in anaerobic magnetite biomineralization in *Magnetospirillum gryphiswaldense* and requires NirN for proper d_1 heme assembly. J Bacteriol. 2013;195:4297–309.

44. Siregar JJ, Lerner SA, Mobashery S. Purification and characterization of aminoglycoside 3′-phosphotransferase type IIa and kinetic comparison with a new mutant enzyme. Animicrob Agents Chemother. 1994;38(4):641–7.

45. Wick RR, Judd LM, Holt KE. Performance of neural network basecalling tools for Oxford Nanopore sequencing. Genome Biol. 2019;20(1):129.

46. Koren S, Walenz BP, Berlin K, Miller JR, Bergman NH, Phillippy AM. Canu: scalable and accurate long-read assembly via adaptive k-mer weighting and repeat separation. Genome Res. 2017;27(5):722–36.

47. Vaser R, Sović I, Nagarajan N, Šikić M. Fast and accurate de novo genome assembly from long uncorrected reads. Genome Res. 2017;27(5):737–46.

48. Li H. Minimap2: pairwise alignment for nucleotide sequences. Bioinformatics. 2018;34(18):3094–100.

49. Walker BJ, Abeel T, Shea T, Priest M, Abouelliel A, Sakthikumar S, Cuomo CA, Zeng Q, Wortman J, Young SK, Earl AM. Pilon: an integrated tool for comprehensive microbial variant detection and genome assembly improvement. PLoS One. 2014;9(11):e112963.

50. Li H. Aligning sequence reads, clone sequences and assembly contigs with BWA-MEM. 2013;arXiv:1303.3997.

51. Langmead B, Salzberg SL. Fast gapped-read alignment with bowtie 2. Nat Methods. 2012;9(4):357–9.

52. Margulies M, Egholm M, Altman WE, Attiya S, Bader JS, Bemben L, Berka J, et al. Genome sequencing in microfabricated high-density picolitre reactors. Nature. 2005;437(7057):376–80.

53. Wick RR, Judd LM, Gorrie CL, Holt KE. Unicycler: resolving bacterial genome assemblies from short and long sequencing reads. PLoS Comput Biol. 2017; 13(6):e1005595.

54. Husemann P, Stoye J. r2cat: Synteny plots and comparative assembly. Bioinformatics. 2009;26(4):570–1.

55. Gordon D, Green P. Consed: a graphical editor for next-generation sequencing. Bioinformatics. 2013;29(22):2936–7.

56. Seemann T. Prokka: rapid prokaryotic genome annotation. Bioinformatics. 2014;30(14):2068–9.

57. Seemann T. snippy: fast bacterial variant calling from NGS reads; 2015.

58. Abràmoff MD, Magalhães PJ, Ram SJ. Image processing with imageJ. Biophoton Int. 2004;11:36–42.

Publisher's Note

Springer Nature remains neutral with regard to jurisdictional claims in published maps and institutional affiliations.

Supplementary Material

Identification and elimination of genomic regions irrelevant for magnetosome biosynthesis by large-scale deletion in *Magnetospirillum gryphiswaldense*

Theresa Zwiener[1], Frank Mickoleit[1], Marina Dziuba[1,2], Christian Rückert[3], Tobias Busche[3], Jörn Kalinowski[3], Damien Faivre[4,5], René Uebe[1], and Dirk Schüler[1#]

[1]Department of Microbiology, University of Bayreuth, Bayreuth, Germany

[2]Institute of Bioengineering, Research Center of Biotechnology of the Russian Academy of Sciences, Moscow, Russia

[3]Center for Biotechnology, University of Bielefeld, Bielefeld, Germany

[4]Max Planck Institute of Colloids and Interfaces, Department of Biomaterials, Potsdam, Germany

[5]Aix-Marseille Université, CEA, CNRS, BIAM 13108, Saint Paul lez Durance, France

#Address correspondence to Dirk Schüler, dirk.schueler@uni-bayreuth.de.

Table S1. Bacterial strains and plasmids used in this study.

Bacterial strain or plasmid	Relevant characteristics	Reference
Strains		
E. coli		
DH5α	F⁻*sup*E44 Δ*lac*U169 (Φ80*lac*ZDM15) *hsd*R17 *rec*A1 *end*A1 *gyr*A96 *thi*-1 *rel*A1	Invitrogen
WM3064	*thrB1004 pro thi rpsL hsdS lacZΔM15 RP4-1360 Δ(araBAD)567ΔdapA1341::[erm pir]*	W. Metcalf (unpublished)
M. gryphiswaldense	Archetype	(1)
M. gryphiswaldense ΔA13	R3/S1, Δ*mms6/mamGFDCop*, Δ*mamXY*	(2)
M. gryphiswaldense ΔA13Δ*mms5/mmxF*	R3/S1, Δ*mms6/mamGFDCop*, Δ*mamXY*, Δ*mms5/mmxF*	R. Uebe (unpublished)
Plasmids		
pTZ_028	pAL01 with *lox71*, insertion of homologous sequence *mamABop*	This study
pTZ_029	pAL02/2 with *lox66*, insertion of homologous sequence *mamABop*	This study
pTZ_030	pAL01 with *lox71*, insertion of homologous sequence M04	This study
pTZ_031	pAL02/2 with *lox66*, insertion of homologous sequence M04	This study
pTZ_052	pORFM-GalK derivate, insertion of homologous sequence MSR1_17870–17940	This study
pTZ_053	pORFM-GalK derivate, insertion of homologous sequence MSR1_19470	This study
pTZ_055	pORFM-GalK derivate, insertion of homologous sequence MSR1_13180	This study
pTZ_057	pORFM-GalK derivate, insertion of homologous sequence MSR1_30910–30940	This study
pTZ_058	pORFM-GalK derivate, insertion of homologous sequence MSR1_33570	This study

pTZ_057	pORFM-GalK derivate, insertion of homologous sequence MSR1_20490	This study
pTZ_061	pORFM-GalK derivate, insertion of homologous sequence *mamABop*	This study
pTZ_067	pORFM-GalK derivate, insertion of homologous sequence M04	This study
pTZ_070	pORFM-GalK derivate, insertion of homologous sequence MSR1_16710	This study
pTZ_071	pORFM-GalK derivate, insertion of homologous sequence MSR1_30840	This study
pTZ_083	pORFM-GalK derivate, insertion of homologous sequence MSR1_33770	This study
pTZ_088	pORFM-GalK derivate, insertion of homologous sequence M06	This study
pTZ_089	pORFM-GalK derivate, insertion of homologous sequence M10	This study
pTZ_092	pORFM-GalK derivate, insertion of homologous sequence *intA1*	This study
pTZ_093	pORFM-GalK derivate, insertion of homologous sequence *intA2*	This study
pTZ_094	pORFM-GalK derivate, insertion of homologous sequence P1.3	This study
pTZ_096	pORFM-GalK derivate, insertion of homologous sequence M15	This study
pTZ_097	pORFM-GalK derivate, insertion of homologous sequence M16	This study
pTZ_102	pORFM-GalK derivate, insertion of homologous sequence M07	This study
pTZ_103	pORFM-GalK derivate, insertion of homologous sequence M08	This study
pTZ_104	pORFM-GalK derivate, insertion of homologous sequence M11	This study
pTZ_105	pORFM-GalK derivate, insertion of homologous sequence M12	This study

pTZ_106	pORFM-GalK derivate, insertion of homologous sequence M14		This study
pTZ_107	pORFM-GalK derivate, insertion of homologous sequence M17		This study
pTZ_114	pORFM-GalK derivate, insertion of homologous sequence M13		This study
pLYJ87	Tet^r, *Cre* recombinase plasmid		(3)
pTpsMAG1	Km^r, Cm^r, p15A ori, mariner tps, *mamAB*, *mamGFDC*, *mms6*, *mamXY*, *feoAB1*		(4)

Table S2. Overview over single deletion mutants of MAI and its adjacent region.
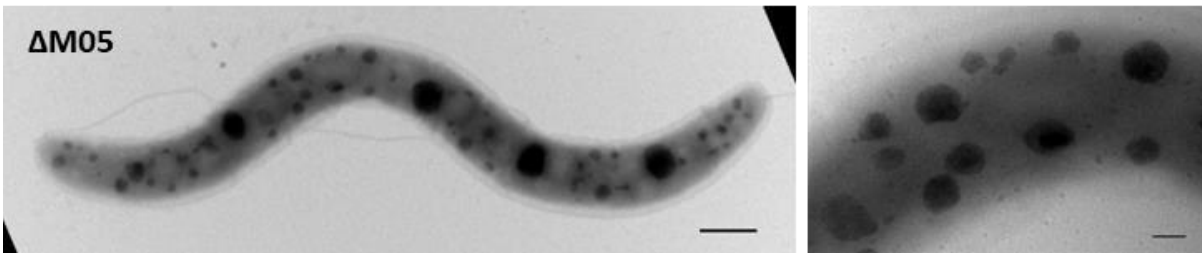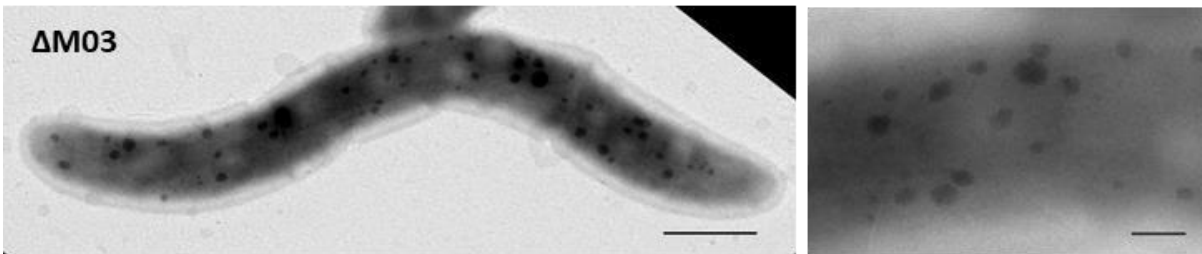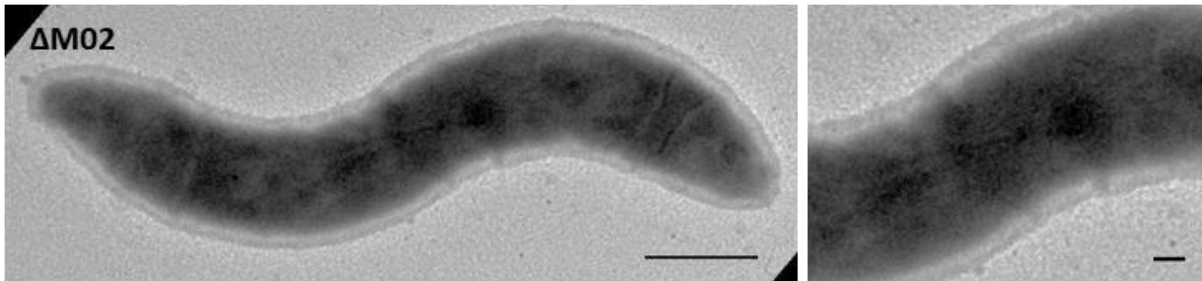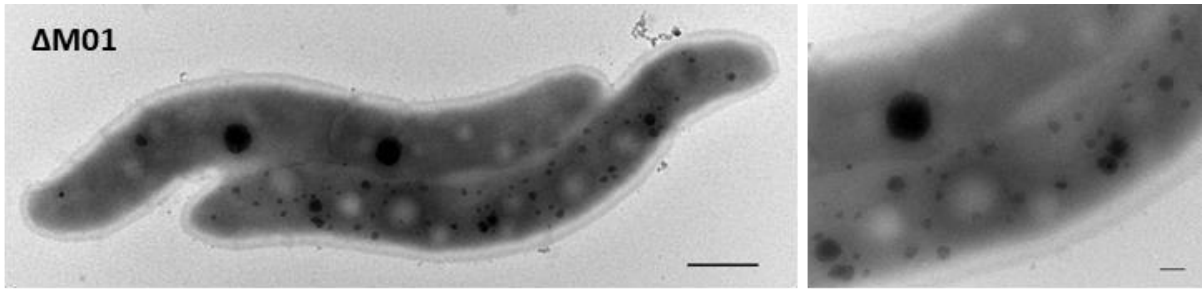
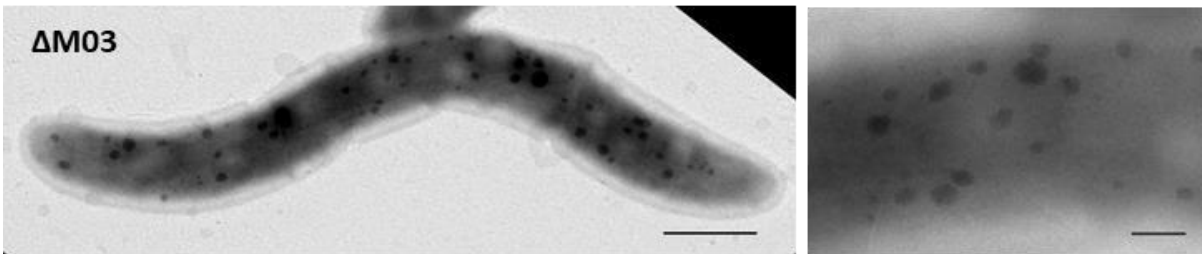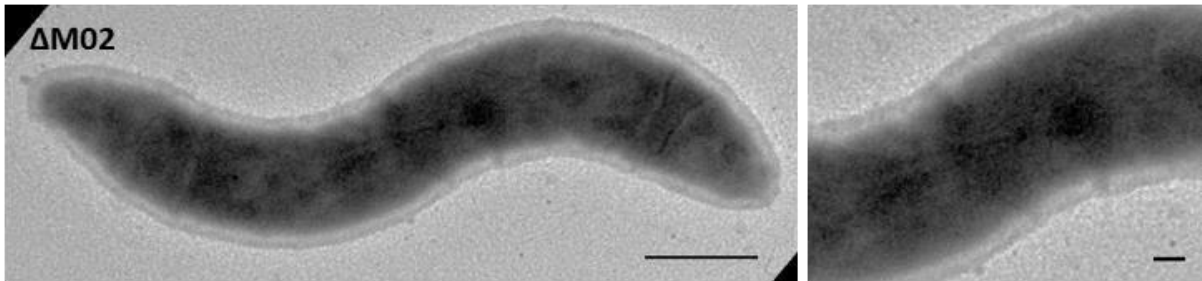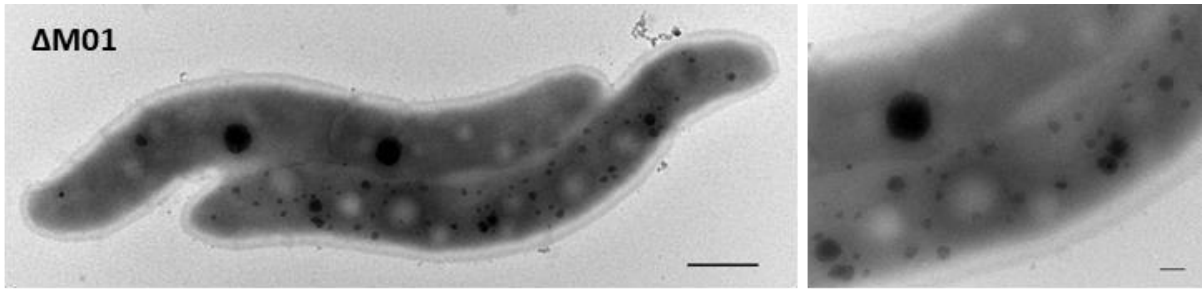| Name of single deletion mutant	Deleted genes	Total extent of deletion	Description
ΔM01	MSR1_03150 to MSR1_03220	27,424 bp	Non-magnetic, electron-dense particles
	MSR1_03340 to MSR1_03500		
	MSR1_03850 to MSR1_03880		
ΔM02	MSR1_02690 to MSR1_02700	28,419 bp	Non-magnetic, electron-dense particles
	MSR1_03150 to MSR1_03220		
	MSR1_03340 to MSR1_03500		
	MSR1_03850 to MSR1_03880		
ΔM03	MSR1_02660 to MSR1_02670	29,830 bp	Non-magnetic, electron-dense particles
	MSR1_03150 to MSR1_03220		
	MSR1_03340 to MSR1_03500		

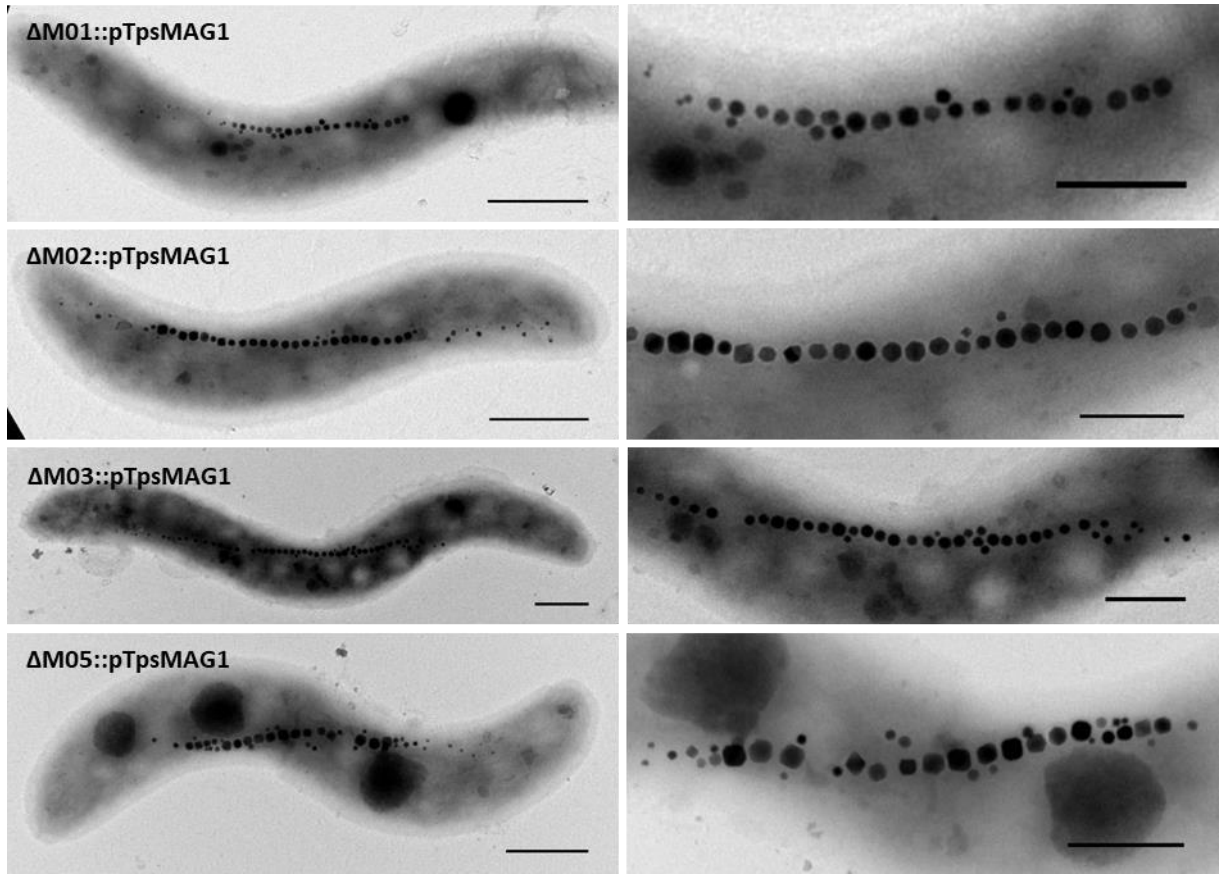|			
	MSR1_03850 to MSR1_03880		
ΔM04	MSR1_03150 to MSR1_03880	65,965 bp	Non-magnetic, electron-dense particles
ΔM05	MSR1_02690 to MSR1_02700	66,959 bp	Non-magnetic, electron-dense particles
	MSR1_03150 to MSR1_03880		
ΔM06	MSR1_02660 to MSR1_03140	35,049 bp	Not deletable in this study
ΔM07	MSR1_02660 to MSR1_03330	51,271 bp	Not deletable in this study
ΔM08	MSR1_02660 to MSR1_03500	67,533 bp	Not deletable in this study
ΔM09	MSR1_02660 to MSR1_03880	100,738 bp	Not deletable in this study
ΔM10	MSR1_03890 to MSR1_04210	32,801 bp	WT-like magnetic phenotype
ΔM11	MSR1_03510 to MSR1_04210	66,204 bp	WT-like magnetite crystals flanked by flake-like particles (5)
ΔM12	MSR1_03340 to MSR1_04210	82,756 bp	Non-magnetic, electron-dense particles
ΔM13	MSR1_03150 to MSR1_04210	98,984 bp	Non-magnetic, electron-dense particles
ΔM14	MSR1_03010 to MSR1_03140	11,238 bp	WT-like magnetic phenotype
ΔM15	MSR1_02680 to MSR1_02770	6,198 bp	WT-like magnetic phenotype
ΔM16	MSR1_03890 to MSR1_04010	10,849 bp	WT-like magnetic phenotype
ΔM17	MSR1_04020 to MSR1_04210	21,952 bp	WT-like magnetic phenotype
Δ*feoAB1op*	MSR1_02660 to MSR1_02670	2,406 bp	weakly magnetic

Table S3. Overview of all single deletion mutants outside the MAI.

Name of single deletion mutant	Extent of deletion (bp)	Phenotype	Species with orthologs present
Δ**MSR1_17870–MSR1_17940**	9,504	WT-like C_{mag} and magnetosomes	*Magnetospirillum* sp. 64-120, *M. aberrantis*
Δ**MSR1_20490**	31,026	reduced C_{mag}, WT-like magnetosomes, more spiralized cell shape, conserved in	*M. moscoviense*, *Magnetospirillum* sp. LM-5, *M. marisnigri*, *Magnetospirillum* sp. 15-1, *Magnetospirillum* sp. UT-4, *Magnetospirillum* sp. ME-1
Δ**MSR1_24180**	1,008	WT-like C_{mag} and magnetosomes, conserved in	*Magnetospirillum* sp. 64-120, *Magnetospirillum* sp. UT-4, *Magnetospirillum* sp. LM-5, *M. moscoviense*, *M. aberrantis*, *Magnetospirillum* sp. 15-1, *M. marisnigri*, *M. kuznetsovii*, *Magnetospirillum* sp. SS-4, *M. magneticum,* *M. magnetotacticum*, *Magnetospirillum* sp. XM-1
Δ**MSR1_30910–MSR1_30940**	3,493	reduced C_{mag}, WT-like magnetosomes	*M. caucaseum*, *M. magnetotacticum*, *M. magneticum*, *Magnetospirillum* sp. XM-1, *Magnetospirillum* sp. SS-4, *Magnetospirillum* sp. ME-1, *M. marisnigri*, *Magnetospirillum* sp. 15-1
Δ**MSR1_33570**	1,233	WT-like C_{mag} and magnetosomes	*Magnetospirillum* sp. 64-120, *M. moscoviense*, *M. magnetotacticum*, *M. marisnigri*, *Magnetospirillum* sp. XM-1
Δ**MSR1_33770**	306	WT-like C_{mag} and magnetosomes	*Magnetospirillum* sp. 64-120, *M. moscoviense*, *M. magnetotacticum*, *M. marisnigri*, *Magnetospirillum* ME-1, *Magnetospirillum* sp. XM-1, *M. caucaseum*

ΔMSR1_13180	270	WT-like C_{mag} and magnetosomes	*Magnetospirillum* sp. 64-120, *Magnetospirillum* sp. XM-1, *M. magnetotacticum*, *M. caucaseum*, *M. moscoviense*, *M. magneticum*
ΔMSR1_16710	249	WT-like C_{mag} and magnetosomes	*Magnetospirillum* sp. 64-120, *Magnetospirillum* sp. LM-5, *M. moscoviense*, *Magnetospirillum* sp. UT-4, *M. aberrantis*, *M. marisnigri*, *Magnetospirillum* sp. SS-4, *M. caucaseum*, *Magnetovibrio blakemorei*, *M. magnetotacticum*, *M. kuznetsovii*
ΔMSR1_19470	330	WT-like C_{mag} and magnetosomes	*Magnetospirillum* sp. SS-4, *M. aberrantis*, *M. magneticum*, *M. kuznetsovii. M. caucaseum*, *Magnetospirillum* sp. ME-1, *Magnetospirillum* sp. XM-1, *Magnetospirillum* sp. 15-1, *Magnetospirillum* sp. UT-4
ΔMSR1_30840	951	reduced C_{mag}, WT-like magnetosomes	*Magnetospirillum* sp. 64-120, *M. moscoviense*

ΔM01

ΔM02

ΔM03

ΔM05

ΔM01

ΔM02

ΔM03

ΔM05

ΔM01::pTpsMAG1

ΔM02::pTpsMAG1
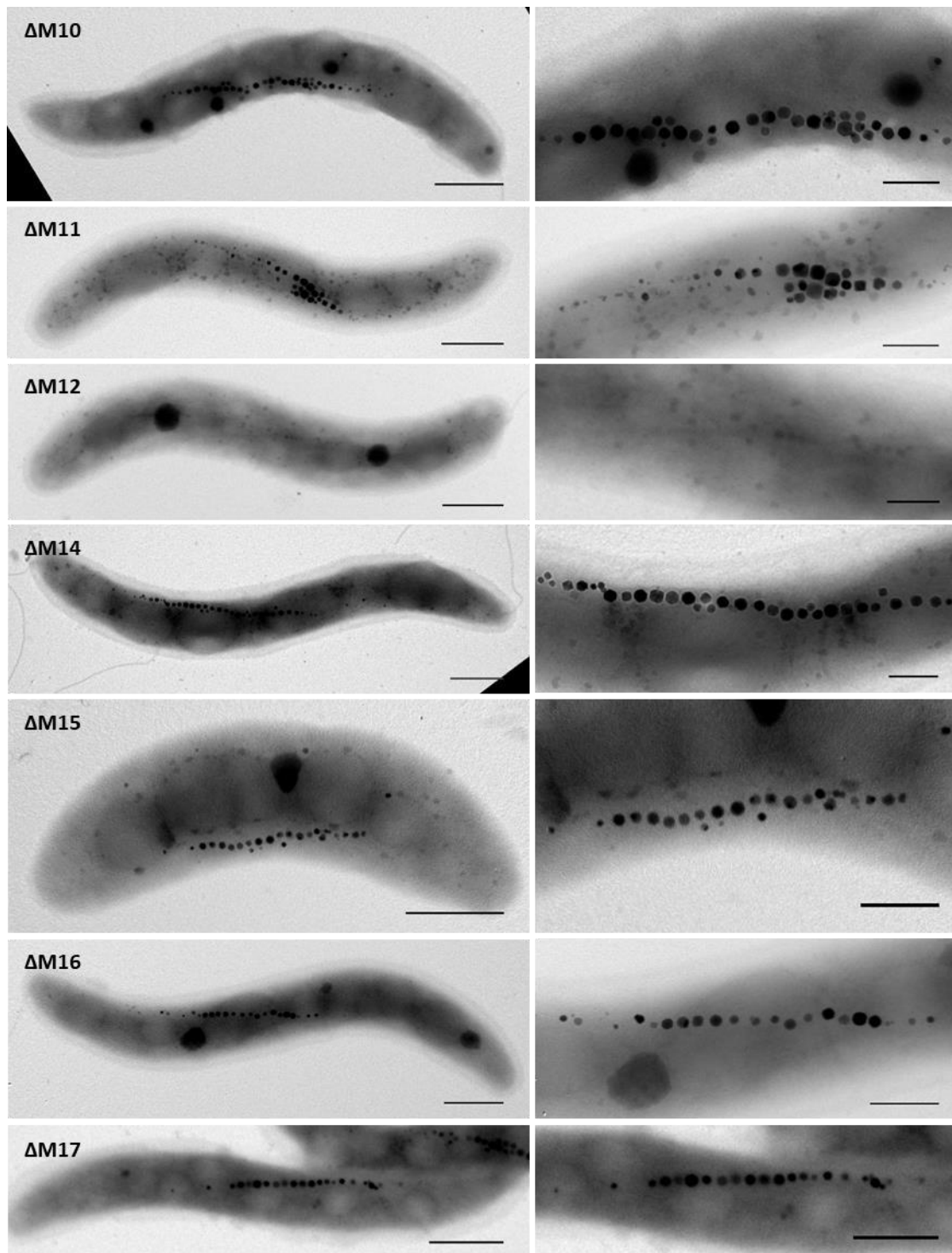
ΔM03::pTpsMAG1

ΔM05::pTpsMAG1
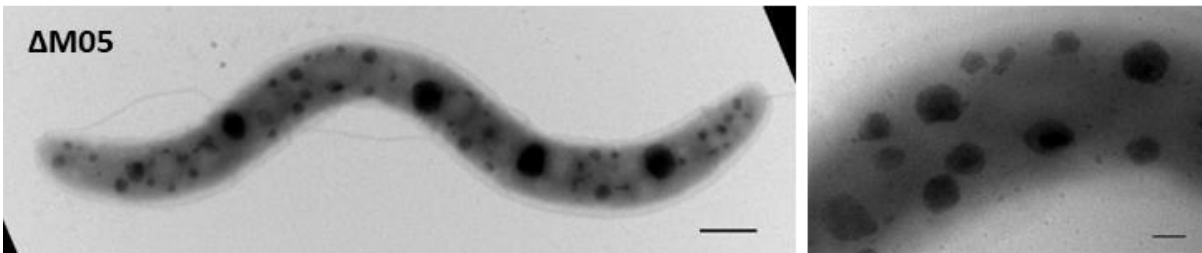
Figure S1. Morphology of all single deletion mutants of the MAI and adjacent regions and its complemented strains. Scale bars left side: 500 nm; right side: 100 nm.
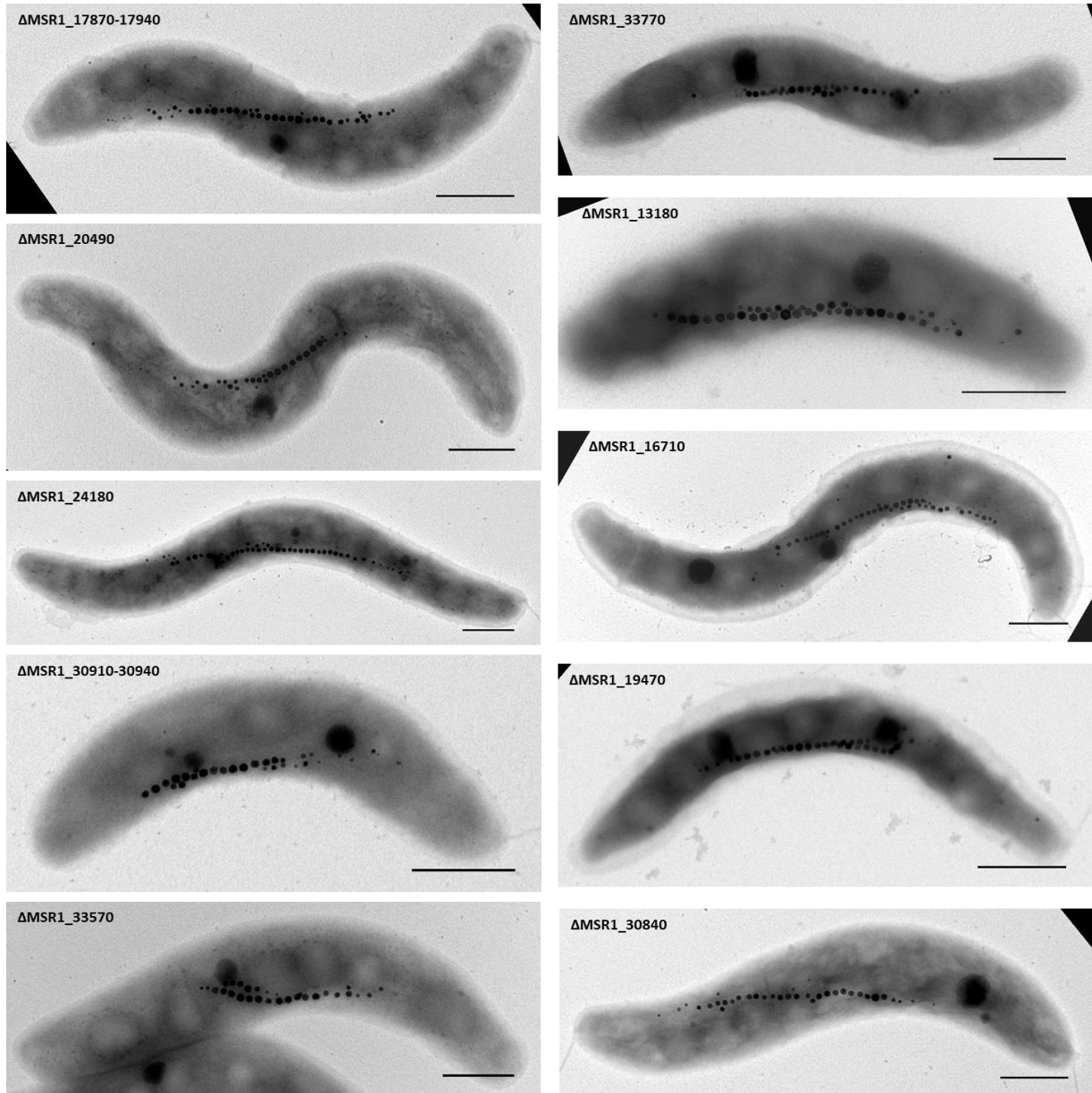
Figure S2. Single deletion mutants of Tn5-hits, candidates from proteome analysis and further gene clusters. Scale bars: 500 nm.

References Supplementary Material

1. Schüler D, Köhler M. The isolation of a new magnetic spirillum. Zentralblatt Mikrobiologie. 1992;147:150–51.

2. Lohße A, Ullrich S, Katzmann E, Borg S, Wanner G, Richter M, Voigt B, Schweder T, Schüler D. Functional analysis of the magnetosome island in *Magnetospirillum gryphiswaldense*: the *mamAB* operon is sufficient for magnetite biomineralization. PLoS One. 2011;6:e25561.

3. Li YJ, Bali S, Borg S, Katzmann E, Ferguson SJ, Schüler D. Cytochrome cd_1 nitrite reductase NirS is involved in anaerobic magnetite biomineralization in *Magnetospirillum gryphiswaldense* and requires NirN for proper d_1 heme assembly. J Bacteriol. 2013;195:4297–4309.

4. Dziuba MV, Zwiener T, Uebe R, Schüler D. Single-step transfer of biosynthetic operons endows a non-magnetotactic *Magnetospirillum* strain from wetland with magnetosome biosynthesis. Environ Microbiol. 2020;22(4):1603–18.

5. Raschdorf O, Müller FD, Pósfai M, Plitzko JM, Schüler D. The magnetosome proteins MamX, MamZ and MamH are involved in redox control of magnetite biomineralization in *Magnetospirillum gryphiswaldense*. Mol Microbiol. 2013;89:872–86.

CHAPTER VI:

Towards a 'chassis' for bacterial magnetosome biosynthesis: genome streamlining of *Magnetospirillum gryphiswaldense* by multiple deletions

Theresa Zwiener[1], Marina Dziuba[1,2], Frank Mickoleit[1], Christian Rückert[3], Tobias Busche[3], Jörn Kalinowski[3], René Uebe[1] and Dirk Schüler[1*]

[1] Department of Microbiology, University of Bayreut, Bayreuth, Germany

[2] Institute of Bioengineering, Research Center of Biotechnology of the Russian Academy of Sciences, Moscow, Russia

[3] Center for Biotechnology, University of Bielefeld, Bielefeld, Germany

RESEARCH

Towards a 'chassis' for bacterial magnetosome biosynthesis: genome streamlining of *Magnetospirillum gryphiswaldense* by multiple deletions

Theresa Zwiener[1] , Marina Dziuba[1,2], Frank Mickoleit[1], Christian Rückert[3], Tobias Busche[3], Jörn Kalinowski[3], René Uebe[1] and Dirk Schüler[1*]

Abstract

Background: Because of its tractability and straightforward cultivation, the magnetic bacterium *Magnetospirillum gryphiswaldense* has emerged as a model for the analysis of magnetosome biosynthesis and bioproduction. However, its future use as platform for synthetic biology and biotechnology will require methods for large-scale genome editing and streamlining.

Results: We established an approach for combinatory genome reduction and generated a library of strains in which up to 16 regions including large gene clusters, mobile genetic elements and phage-related genes were sequentially removed, equivalent to ~227.6 kb and nearly 5.5% of the genome. Finally, the fragmented genomic magnetosome island was replaced by a compact cassette comprising all key magnetosome biosynthetic gene clusters. The prospective 'chassis' revealed wild type-like cell growth and magnetosome biosynthesis under optimal conditions, as well as slightly improved resilience and increased genetic stability.

Conclusion: We provide first proof-of-principle for the feasibility of multiple genome reduction and large-scale engineering of magnetotactic bacteria. The library of deletions will be valuable for turning *M. gryphiswaldense* into a microbial cell factory for synthetic biology and production of magnetic nanoparticles.

Keywords: *Magnetospirillum gryphiswaldense*, Magnetotactic bacteria, Magnetosomes, Genome reduction, Chassis, IS elements

Background

Magnetosomes are membrane-enclosed organelles that are synthesized by various aquatic bacteria for their magnetotactic navigation in the Earth's geomagnetic field [1, 2]. Apart from their biological function as magnetic sensors, magnetosomes also represent microbially synthesized magnetic nanoparticles (MNP) consisting of monocrystalline magnetite (Fe_3O_4) or greigite (Fe_3S_4).

Because of their strictly controlled biomineralization, bacterial magnetosomes have exceptional properties, such as high chemical purity and crystallinity, strong magnetization, and uniform sizes and shapes, which are largely unknown from chemically synthesized MNP [3–5]. This makes them highly attractive for a number of biotechnological and biomedical applications [6–8]. For examples, magnetosomes isolated from the magnetic bacterium *Magnetospirillum gryphiswaldense* were successfully tested as multimodal reporters for magnetic imaging [9, 10], nanocarriers for magnetic drug targeting [11–13], and for magnetic hyperthermia applications [14,

*Correspondence: dirk.schueler@uni-bayreuth.de
[1] Department of Microbiology, University of Bayreuth, Bayreuth, Germany
Full list of author information is available at the end of the article

Zwiener *et al. Microb Cell Fact*   (2021) 20:35

Page 2 of 17

15]. In addition, the functionality of magnetosomes can be extended by genetically fusing foreign functional moieties and polypeptides, such as fluorophores, enzymes, antibodies, and organic shells [16–22] to magnetosome membrane anchors. Moreover, the bacteria were utilized as a model to study the molecular mechanisms of human diseases related to homologs of certain magnetosome proteins [23].

However, applications of bacteria and their magnetosomes so far have been hampered by the limited number of appropriate production strains and difficulties in their large-scale cultivation and genetic manipulation. One of the most extensively investigated model organisms for studying magnetosome biosynthesis is the freshwater alphaproteobacterium *M. gryphiswaldense* [24, 25]. It typically produces 15–25 cuboctahedral magnetite particles per cell that are about 40 nm in size [26], while genetic overexpression of gene clusters governing magnetosome biosynthesis generated an overproducing strain forming > 100 (up to 170) particles per cell with enlarged sizes [27]. Because of its genetic tractability and relatively straightforward cultivation, *M. gryphiswaldense* recently has also emerged as host strain for bioproduction and synthetic biology of magnetosomes [20, 21, 27–31].

Despite of this recent progress, since its isolation [24, 32, 33] the usability of the undomesticated *M. gryphiswaldense* as a biotechnological workhorse has been limited due to several unwanted features. For example, one obstacle is the rather fastidious and sometimes fluctuating growth, which makes cultivation difficult to reproduce at larger scale. In other bacteria, this erratic growth behavior has been attributed to the presence of prophage genes, which are often known to exhibit some latent activity, resulting in a negative impact on the robustness of growth and the performance of bioprocesses [34–36]. Another adverse feature is the inherent genetic instability of *M. gryphiswaldense*, and in particular of the magnetic phenotype, which makes genetic manipulation and magnetosome production cumbersome. For example, spontaneous loss or impairment of magnetosome biosynthesis has been observed frequently during subcultivation, which had been traced back to spontaneous deletions and rearrangements within the large genomic **ma**gnetosome **i**sland (MAI) [37–39]. This chromosomal region extends across about 100 kb and comprises discontiguous clusters of more than 30 genes responsible for magnetosome formation organized in the five polycistronic operons *feoAB1*, *mms6*, *mamGFDC*, *mamAB* and *mamXY* [1, 40]. In addition, the MAI harbors regions of irrelevant gene content and numerous mobile genetic elements, which might be responsible for the frequent rearrangements and loss of magnetic phenotype in *M. gryphiswaldense* [37, 38, 41].

For future synthetic biology applications as well as large-scale magnetosome bioproduction, a simplified and potentially more robust version of the *M. gryphiswaldense* genome would be highly beneficial. In other bacteria, moderate genome reduction, which comprises the targeted deletion of multiple dispensable genes, has been shown to optimize metabolic pathways, enhance the expression of recombinant protein productivity, and improve physiological performance and growth [42–46]. For instance, by removing non-essential, recombinogenic or mobile DNA and cryptic virulence genes, genome reduction of *Escherichia coli* resulted in several favorable properties, such as increased electroporation efficiency and improved propagation of recombinant genes [47]. Deletion of prophage genes improved growth and transformation efficiency in *Corynebacterium glutamicum* [34], enhanced genotypic stability in *Pseudomonas putida* [35, 48, 49], and increased robustness toward stress in *Vibrio natriegens* or *Shewanella oneidensis* MR-1 [36, 50]. Furthermore, deletion of active mobile genetic elements caused enhanced protein productivity in *C. glutamicum* [51], and increased transformability and reduced mutation rates in *Acinetobacter baylyi* [52].

In magnetotactic bacteria, comparable genome reduction approaches so far have been impeded because of the unavailability of efficient methods for large-scale engineering of these recalcitrant microorganisms. To overcome these current limitations, we recently started a systematic approach to engineer the model strain *M. gryphiswaldense* at the genome level. In a previous study, we established a method for large-scale deletion mutagenesis and utilized it for the generation of 24 single deletions covering about 167 kb of non-redundant genome content. We thereby identified large regions inside and outside the MAI irrelevant for magnetosome biosynthesis [53]. Here, we continued our work by constructing genome-reduced strains of *M. gryphiswaldense* with multiple combinatorial deletions of irrelevant and detrimental gene content. We provide a proof of concept for large-scale genome editing and improvement towards a future chassis [54], which may turn *M. gryphiswaldense* into a microbial cell factory for the synthetic biology and high-yield production of magnetic nanoparticles.

Results
Overview over the experimental strategy
The features of a genome reduced future 'chassis' should include first the elimination of problematic and harmful gene content such as prophage genes as well as active IS elements known to cause genetic instability [50–52]. Second, the genome should be freed of as much of gene content unnecessary for magnetosome biosynthesis, growth

and fitness under lab conditions as possible. Third, neutral and favorable scarless deletions should be combined into one or few single strains. Ultimately, the native biosynthetic gene clusters within the MAI plus multiple large portions of 'junk' between and adjacent to them should be substituted by a compact cassette comprising all key genes for magnetosome biosynthesis (plasmid pMDJM3). Final strains were tested for growth, fitness, and genetic stability (for an overview over the experimental workflow see Fig. 1a).

Identification and elimination of prophage genes

Since its isolation [24, 32, 33], our lab persistently experienced occasional problems with the cultivation of *M. gryphiswaldense*, such as poorly reproducible and fluctuating growth, which could not only be explained by unintended subtle variations in handling, media constituents and incubation alone. In other bacteria, similar observations could be traced back to the latent activity and induction of prophages, which are known to often have a negative impact on robustness of growth and the performance of bioprocesses [34]. In the genome of *M. gryphiswaldense*, we detected seven putative prophage regions (referred to as P1–P7) (Fig. 1b) by the phage search tool PHAST [55]. Two of them (P1, 26 kb, and P6, 34.1 kb) were predicted as intact (Figs. 1b and 2a, b), but upon closer inspection only P6 is contiguous and seems to have a full complement of typical phage genes (e.g. integrases, tail, and major capsid proteins), whereas P1 is interspersed with tRNA genes (Fig. 2a, b). Predicted prophage P2 seems to be incomplete as well, consistent with its small size (7.2 kb) and its accumulation of several transposon genes. Region P3 (20 kb) comprises some putative essential genes (e.g. encoding transcriptional regulators, chaperones) and a phage integrase *intA1.* Incomplete P4 (31.2 kb) and P5 (14.3 kb) are also interspersed with genes of unrelated, but important functions, e.g. chaperones of DnaJ-class, a transcriptional regulator and a ribonuclease, respectively. Incomplete P7 (11.3 kb) resides inside the part of the MAI (Fig. 1b) that was non-deletable in previous experiments [53]. From the identified putative phages, the following regions were selected as targets for deletion: P1 was divided into two parts excluding the essential tRNA genes (P1.2, 19.4 kb, and P1.3, 12.8 kb) that were both deleted separately (Fig. 2a). Since deletion of whole P6 failed, only genes encoding putative capsid proteins (7.65 kb) and a recombinase (*hin2*, 1.34 kb) were deleted separately (Fig. 2b). Furthermore, inside and adjacent to these predicted prophages, we identified several putative integrases and excisionases that might be involved in the reactivation of lysogenic prophages to the lytic cycle and decided to delete several

candidates as well (*intA1* 1.28 kb, *intA2* 1.22 kb and *alpA* 225 bp) (Fig. 1b).

Under aerobic and anaerobic conditions, growth of all prophage deletants was largely indistinguishable from the WT (data not shown). After incubation with 0.2 µg/ml MMC, which is known to trigger the cellular SOS response and to induce prophages to enter the lytic cycle [36, 56], growth was indistinguishable from the WT for most deletants. A notable exception was Δ*hin2* (*msr1_37790*), which proved to be less sensitive and could be re-grown after incubation with up to 0.3 µg/ml MMC (Fig. 2c).

Deletion of active mobile genetic elements

Previous observations had revealed a genetic instability of the *M. gryphiswaldense* WT strain: first, the ability to form magnetosomes often became spontaneously reduced or lost entirely, which had been hypothesized to be caused by the presence and activity of numerous mobile elements, resulting in insertions by transposition activity [53], plus deletions and rearrangements caused by homologous recombination between identical copies [37, 38, 41]. Second, during the course of routine genetic manipulation, we frequently also observed spontaneous inactivation of introduced foreign genes, such as chromogenic reporters (e.g. *gusA*, unpublished observations) or genetic markers for antibiotic or counterselection (e.g. *galK*) [53]. Our preliminary analysis revealed that inactivation was often due to insertion of mobile genetic elements belonging to two types, each with two variants: the first type is a bipartite insertion element (in the following referred to as *ISMgr2*; Fig. 3a), composed of genes encoding a putative IS2 repressor TnpA, and an IS2 transposase TnpB, respectively. *ISMgr2* belongs to the IS3 family that is common in many α-Proteobacteria [57]. Three copies of *ISMgr2* (*ISMgr2-1*, *ISMgr2-2* and *ISMgr2-3*) with 99.8% protein identity (99.9% nucleotide identity) are present in the genome of *M. gryphiswaldense* (Fig. 3a), with one of them residing within the MAI (Fig. 1b, *ISMgr2-3*). Two additional homologs of *tnpB*, termed *ISMgr2-tnpB-hyp-1* and *ISMgr2-tnpB-hyp-2,* with lower (20.8%) protein identity (52.6% nucleotide identity) compared to the first three copies *ISMgr2-1*, *ISMgr2-2* and *ISMgr2-3* (Fig. 3b) could be identified. Each of these latter two homologs are associated with two conserved hypothetical genes upstream of the IS2 transposon gene *tnpB* instead of *tnpA*. We first deleted each of the five homologs individually in the WT background (1–1.25 kb each). As expected, single deletion mutants of all five strains displayed WT-like growth and magnetosome biosynthesis under aerobic and anaerobic conditions, and under oxidative and moderate heat stress (data not

Zwiener *et al. Microb Cell Fact*   (2021) 20:35

Page 4 of 17
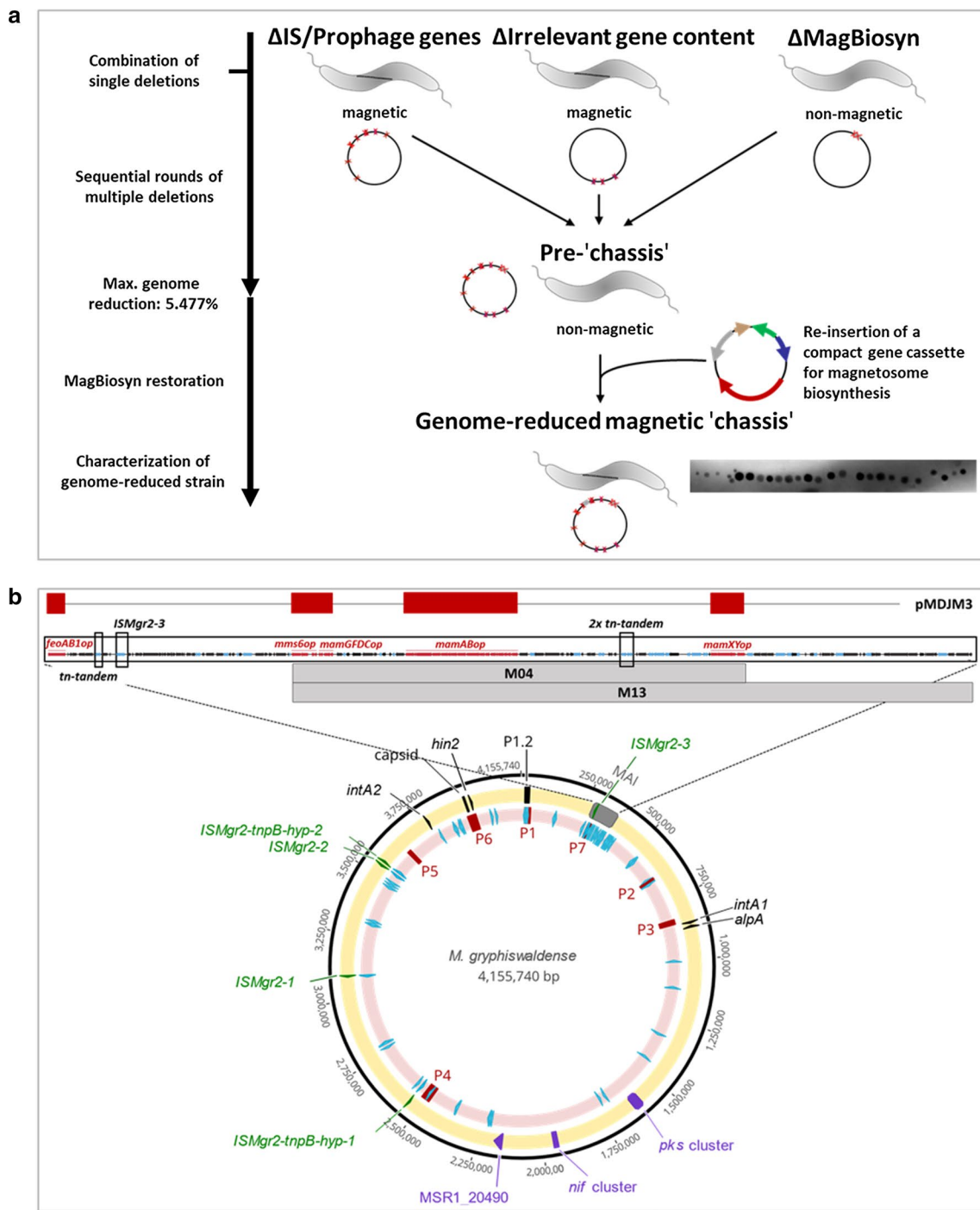
Fig. 1 Overview over the experimental workflow (**a**), and the genomic positions of deletion targets in *M. gryphiswaldense* (**b**). Yellow circle (**b**) shows genes or gene sets targeted for multiple deletions. Grey: magnetosome island (MAI); black arrows: parts of predicted prophage sets and phage-related integrase and excisionase genes; green arrows: insertion element genes identified as most active in this study; purple: irrelevant gene clusters. Pink circle (**b**) indicates predicted prophage sets (dark red) and mobile genetic elements (light blue). The enlarged area shows the genetic organization of the native MAI with all five known magnetosome biosynthesis operons (red), genes of known or unknown function irrelevant for magnetosome formation (black), mobile genetic elements (light blue). The grey bars indicate the extent of regions M04 (~65 kb) and M13 (~100 kb), which were shown to be deletable en bloc in our previous study [53]. The presence of key magnetosome biosynthesis genes within the compact expression cassette of the applied vector pMDJM3 is indicated by red bars while connecting lines designate eliminated gene content

Zwiener *et al. Microb Cell Fact* (2021) 20:35

Page 5 of 17

Fig. 2 Molecular organization and analysis of predicted prophages P1 (**a**), P6 (**b**), deleted genes and growth characteristics of selected cultures (**c**, **d**). **a**, **b** Black: hypothetical genes or genes with known function; red: putative prophage genes; green: mobile genetic elements; blue: deleted genes. **c** Growth characteristics of Δ*intA2* under aerobic and anaerobic conditions compared to WT. Growth of other prophage deletants (not shown) was virtually identical. **d** Growth profiles of mitomycin C-treated (MMC) cultures of a selected single prophage deletion mutant and the WT. Cultures were incubated for 8 h at MMC concentrations of 0.2 or 0.3 µg/ml, washed twice, and adjusted to the initial OD. Growth experiments were performed at 28 ℃ under aerobic conditions. Each strain was analyzed in triplicates, the curve represents the calculated average (standard deviations were < 5%)

shown). We therefore later decided to sequentially delete these five homologs altogether (see below strains ΔTZ-05, ΔTZ-06, ΔTZ-09, ΔTZ-10 and ΔTZ-11 in Fig. 4).

The second type of active mobile elements is represented by a transposon tandem (*tn-tandem*) of genes sharing 52.3% nucleotide identity (31.25% protein

identity) (Fig. 3c): its first gene (*tn1*) encodes a putative transposase of the IS4/5 family [57], and the second gene (*tn2*) a DDE domain transposase [57] (Fig. 3c). This tandem pair is present in the genome of *M. gryphiswaldense* in 19 identical (100% nt) copies, and in addition *tn2* alone in two more identical single copies. Four of the 19

Zwiener *et al. Microb Cell Fact*   (2021) 20:35

Page 6 of 17

Fig. 3 Overview over identified active mobile genetic elements in *M. gryphiswaldense*. **a** One group of active insertion elements (*ISMgr2tnpA* and *ISMgr2tnpB*, green) belongs to the IS3 family, all three copies were deleted in this study. **b** The second variant of this group contains two hypothetical genes (black) and an *ISMgr2tnpB* gene. Both copies were deleted. **c** A further group of active mobile elements is represented by a transposon tandem (*tn-tandem*). The first transposon (*tn1*) of the *tn-tandem* is a member of the putative transposase of IS4/5 family and contains a DUF4096 domain known to bind the end of a transposon and to catalyze the movement of the transposon to another part of the genome by cut and paste or replicative transposition mechanism. The second *tn-tandem* transposon (*tn2*) contains a DDE domain, named after a conserved amino acid triad Asp, Asp, Glu, the active site [57]. **d** *tn2* is present in two single copies in the WT genome. Two copies of *tn-tandem* were deleted in ΔTZ-16::MAG-*gusA* and ΔTZ-17::MAG-*gusA*

tn-tandem pairs reside within the MAI, with two of them comprised within the deletable regions M04 and M13 [53] (Fig. 1b). However, due to the unavailability of multiplex genetic tools for *M. gryphiswaldense*, the high copy number of the *tn-tandem* pairs proved prohibitive for sequential or simultaneous deletion of all copies.
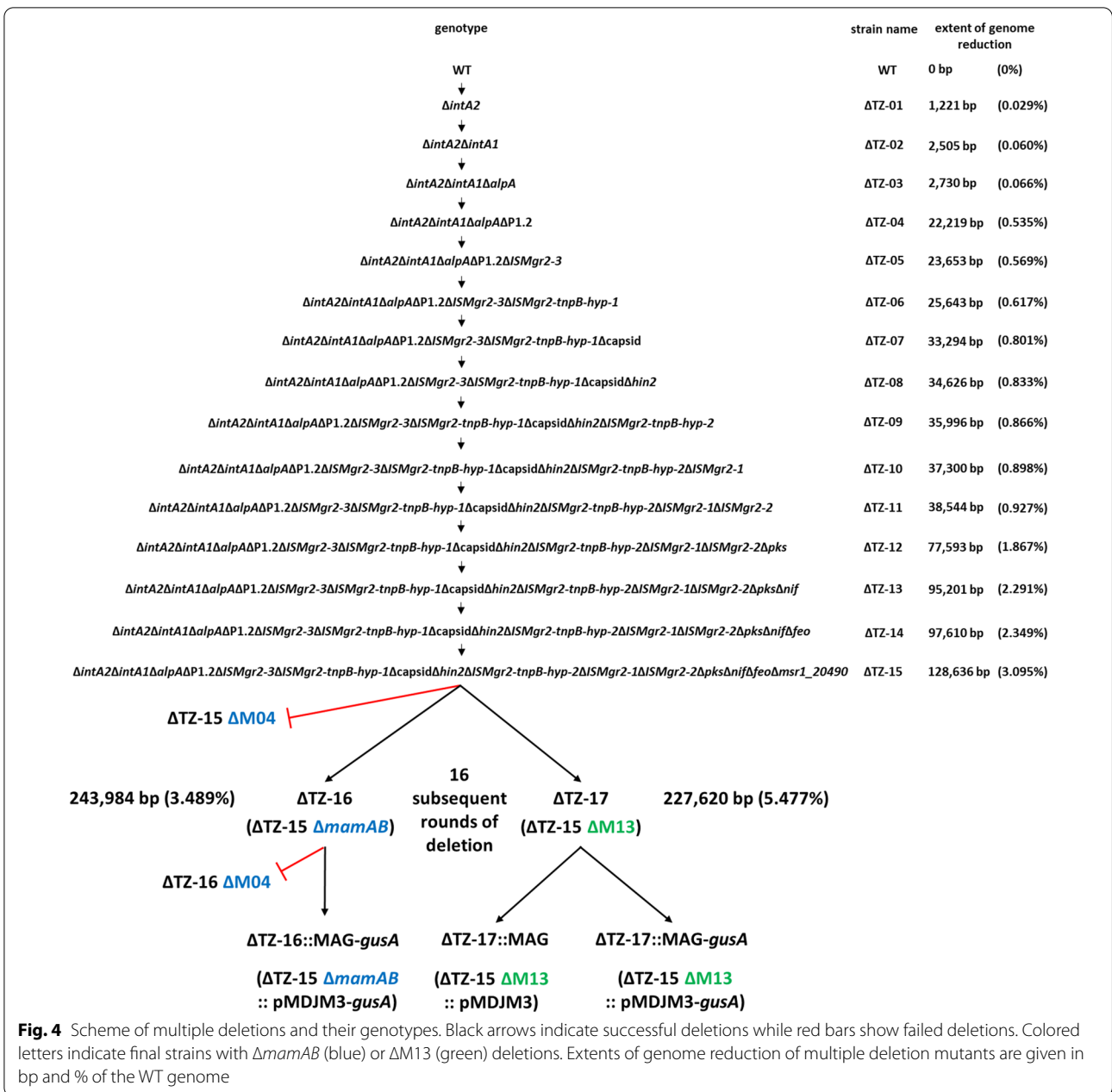
Identification and elimination of further gene clusters irrelevant for cell growth and magnetosome biosynthesis

Next, to eliminate further larger non-essential chromosomal stretches outside the MAI, we exemplary targeted two gene clusters that are likely irrelevant for magnetosome biosynthesis and fitness in lab conditions (Additional file 1: Table S1): (i) A *nif* operon comprising 16 genes, namely *nifWABZTHDK*, *fixABC*, *draGT* and three ferredoxin genes (*msr1_18560*; *msr1_18600*; *msr1_18640*). The *nif* operon is likely linked to nitrogen fixation in *M. gryphiswaldense* [58] (Additional file 1: Fig. S1) which is irrelevant under the denitrifying conditions optimal for magnetosome biosynthesis [28]. We generated a mutant in which ~20 kb of this *nif* cluster comprising 20 genes were deleted (Additional file 1: Fig. S1). (ii) Several uncharacterized clusters encoding a putative non-ribosomal peptide synthetase (NRPS) and

a polyketide synthase (PKS) were predicted [59]. Since it was unlikely to be necessary for magnetosome biosynthesis, we deleted three large ORFs encoding putative PKS proteins from one of the clusters (termed *pks*) extending over ~40 kb (Fig. 1b; Additional file 1: Table S1). As expected, strains harboring single deletions in *nif* or *pks* clusters were indistinguishable from the WT with regard to magnetosome formation, cell growth and motility, which confirmed their irrelevance for magnetosome biosynthesis and fitness under lab conditions (Additional file 1: Table S1, Fig. S4).

Combinatory mutagenesis

In order to combine all previously tested favorable or neutral deletions into one or two single strains, we employed the following strategy (Fig. 4): starting with the ΔintA2 strain as a parent, we first proceeded by deleting further selected prophage genes (ΔTZ-01−ΔTZ-04), then continued with the mobile genetic elements (ΔTZ-05 and ΔTZ-06) and further prophage genes and IS elements (ΔTZ-07−ΔTZ-11) and ended with deletion of irrelevant gene clusters and magnetosome biosynthesis genes (ΔTZ-12−ΔTZ-17). One round of deletion was completed as soon as the loss of kanamycin resistance marker

Fig. 4 Scheme of multiple deletions and their genotypes. Black arrows indicate successful deletions while red bars show failed deletions. Colored letters indicate final strains with Δ*mamAB* (blue) or ΔM13 (green) deletions. Extents of genome reduction of multiple deletion mutants are given in bp and % of the WT genome

(Km^r) was verified by replica plating. After each round, magnetic responses of mutant strains as well as their growth under aerobic and anaerobic conditions, oxidative and moderate heat stress were tested. This was found to be WT-like for all offspring strains including ΔTZ-15 (Additional file 1: Fig. S2).

After fifteen successful rounds of deletions, the resulting mutant ΔTZ-15 was used as a parent to delete large parts of the MAI including all magnetosome biosynthesis operons. In a previous study, a contiguous stretch of ~66 kb termed region M04 was found to be deletable

in the WT-background, including all *mam* and *mms6* operons (~27 kb) plus ~39 kb of irrelevant or problematic gene content, such as two copies of *tn-tandem* (Fig. 1b, enlargement, grey bar) [53]. This had no obvious effects on growth, and magnetosome biosynthesis could be restored to WT-level by complementation with a compact expression cassette comprising the *mam* and *mms6* operons only [53]. In addition, a ~100 kb region termed M13 (Fig. 1b) could be excised, again including all *mam* and *mms6* operons, plus an additional ~33 kb flanking region. Despite of its slightly impaired growth in

Zwiener *et al. Microb Cell Fact*   (2021) 20:35

Page 8 of 17

oxidative stress conditions [53], the M13 region was chosen as an additional target to generate a strain with the largest possible genome reduction.

However, we failed to delete M04 in strain ΔTZ-15 despite of several attempts (Fig. 4), although its deletion had been readily achieved before in the WT background [53]. Instead, upon repeated attempts of conjugation and counterselection, we obtained a number of conspicuous clones with either magnetic or non-magnetic phenotypes, which had supposedly excised the deletion target as suggested by PCR, but lost their insensitivity against kanamycin, indicating that parts of the suicide vector harboring the Km^r marker were likely still maintained in the genome. In our previous study, similar observations could be traced back to the inactivation of the *galK* gene encoding the lethal galactokinase, followed by spontaneous rearrangements in the absence of rigorous counterselection [53]. This explained our failure to enforce the proper deletion during counterselection in the presence of galactose, and in fact, the entire M04 region was still present in the genome (see Additional file 1: Fig. S3 for detail). To circumvent this problem, we separately deleted the essential *mamABop* first in strain ΔTZ-15, yielding strain ΔTZ-16, in which we attempted subsequent deletion of the residual M04 region. Several kanamycin sensitive (Km^s), non-magnetic clones were obtained in this regime, which however again yielded diverse PCR products only roughly similar to the expected size spanning over the targeted excision site. Nevertheless, one of the clones (still tentatively termed ΔTZ-16), was selected as parent for later re-insertion of pMDJM3 harboring a compact version of the magnetosome biosynthesis gene clusters (see below).

In contrast to the troublesome M04 deletion, one-step deletion of the even larger region M13 in the background of ΔTZ-15 was obtained readily and yielded plenty of expected non-magnetic clones, in which the proper deletion of M13 could be confirmed by PCR spanning over the targeted excision site. This yielded strain ΔTZ-17. Like the respective single deletion mutants ΔM04 and ΔM13 in the WT background [53], both intermediate strains ΔTZ-16 and ΔTZ-17 showed conspicuous irregularly shaped electron dense particles (EDPs) between 10 and 125 nm in size in electron micrographs (see Fig. 6a below, white arrows), which were previously shown to be rich in potassium, phosphorus and oxygen, and to be unrelated to magnetosome biosynthesis [53].
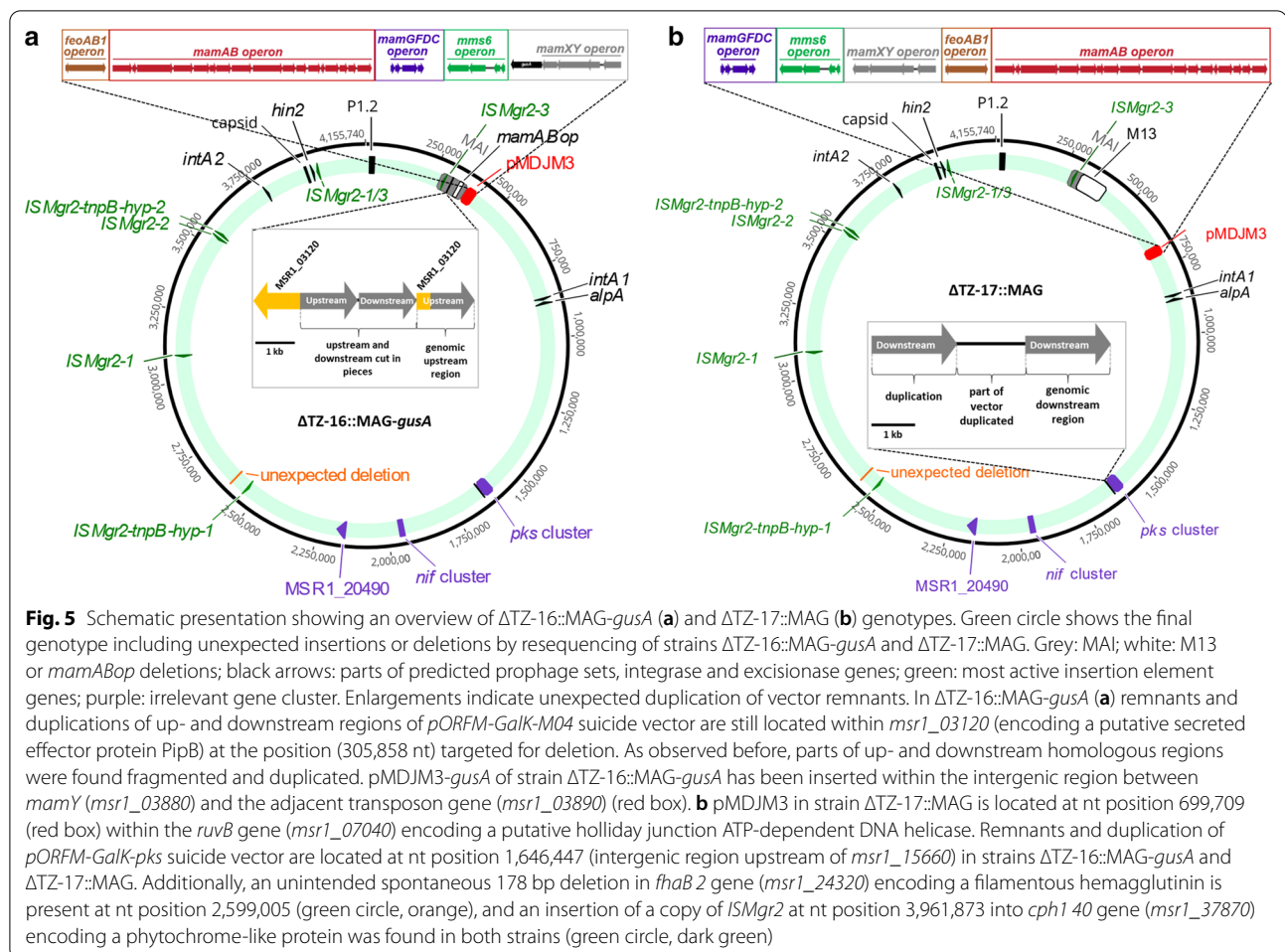
In the final step, restoration of magnetosome biosynthesis was attempted in the two multiple deletion strains. This was achieved by insertion of pMDJM3 or pMDJM3-*gusA*, variants of pTpsMAG1 [60] harboring the compact set of *mam/mms/feo* genes and *lox* sites for restoration of antibiotic resistance to generate a marker-less mutant,

and in case of pMDJM3-*gusA* in addition encoding the enzyme GusA (glucuronidase) as a chromogenic reporter. The *gusA* gene was added next to the *mamXYop* as entrapment for spontaneous mutations in a genetic stability assay to ΔTZ-16 and ΔTZ-17 (see below). As control, *gusA* was also inserted into the WT strain at the same genomic position next to the *mamXYop* as in pMDJM3. The region downstream of *mamXYop* was chosen as site for *gusA* insertion, since spontaneous deletions, insertions and rearrangements of this particular region were observed repeatedly as a virtual hotspot during routine genetic manipulation (unpublished observations). This is possibly caused by its close proximity (~ 11.4 kb) to the two *tn-tandem* copies described above, and often accompanied by impaired magnetosome phenotypes akin a *mamXYop* deletion [61]. Thus, the strains ΔTZ-16::MAG-*gusA*, ΔTZ-17::MAG, ΔTZ-17::MAG-*gusA* and WT-*gusA* (Fig. 4) were generated.

Genome analysis of final multiple mutant strains

To verify the multiple introduced deletions, as well as possible unintended mutations and rearrangements that might have occurred during the numerous rounds of manipulation, at this point the two final multiple mutant strains ΔTZ-16::MAG-*gusA* and ΔTZ-17::MAG were subjected to genome resequencing. In strain ΔTZ-16::MAG-gusA this revealed that the region M04, which we attempted to delete in the last step, was still present as already suspected, except for *mamABop*, which had been removed already in the previous step in ΔTZ-16. As a consequence, ΔTZ-16::MAG-*gusA* is merodiploid for all magnetosome operons but *mamABop* and *feoAB1op*. All introduced *mam/mms/feo* genes were found to be present next to endogenous *mamXYop* (Fig. 5a, red box), although some with silent or neutral point mutations. However, conspicuously, the order of the introduced operons (*feoAB1-mamAB-mamGFDC-mms6-gusA-mamXY*) was shuffled compared to their original order on pMDJM3-*gusA* (*mamAB-feoAB1-mamXY-gusA-mms6-mamGFDC*). Apart from the failed M04 deletion, all other deletions introduced into ΔTZ-16::MAG-*gusA* were exactly as intended. However, besides a number of point mutations, a few larger indel mutations were found in genome regions likely to be irrelevant for magnetosome biosynthesis. These include the *pORFM-GalK-M04* suicide vector within *msr1_03120* (nt position 305,858), a 178 bp spontaneous deletion at nt position 2,599,005 in *msr1_24320* (encoding a filamentous hemagglutinin) and an insertion of a copy of *ISMgr2* at nt position 3,961,873 (with *msr1_37870* encoding a phytochrome-like protein).

In ΔTZ-17::MAG the entire M13 region was confirmed to be deleted exactly as intended (Fig. 5b, green circle).

Zwiener *et al. Microb Cell Fact* (2021) 20:35

Page 9 of 17

Fig. 5 Schematic presentation showing an overview of ΔTZ-16::MAG-*gusA* (**a**) and ΔTZ-17::MAG (**b**) genotypes. Green circle shows the final genotype including unexpected insertions or deletions by resequencing of strains ΔTZ-16::MAG-*gusA* and ΔTZ-17::MAG. Grey: MAI; white: M13 or *mamABop* deletions; black arrows: parts of predicted prophage sets, integrase and excisionase genes; green: most active insertion element genes; purple: irrelevant gene cluster. Enlargements indicate unexpected duplication of vector remnants. In ΔTZ-16::MAG-*gusA* (**a**) remnants and duplications of up- and downstream regions of *pORFM-GalK-M04* suicide vector are still located within *msr1_03120* (encoding a putative secreted effector protein PipB) at the position (305,858 nt) targeted for deletion. As observed before, parts of up- and downstream homologous regions were found fragmented and duplicated. pMDJM3-*gusA* of strain ΔTZ-16::MAG-*gusA* has been inserted within the intergenic region between *mamY* (*msr1_03880*) and the adjacent transposon gene (*msr1_03890*) (red box). **b** pMDJM3 in strain ΔTZ-17::MAG is located at nt position 699,709 (red box) within the *ruvB* gene (*msr1_07040*) encoding a putative holliday junction ATP-dependent DNA helicase. Remnants and duplication of *pORFM-GalK-pks* suicide vector are located at nt position 1,646,447 (intergenic region upstream of *msr1_15660*) in strains ΔTZ-16::MAG-*gusA* and ΔTZ-17::MAG. Additionally, an unintended spontaneous 178 bp deletion in *fhaB 2* gene (*msr1_24320*) encoding a filamentous hemagglutinin is present at nt position 2,599,005 (green circle, orange), and an insertion of a copy of *ISMgr2* at nt position 3,961,873 into *cph1 40* gene (*msr1_37870*) encoding a phytochrome-like protein was found in both strains (green circle, dark green)

pMDJM3 was inserted at nt position 699,709 (Fig. 5b, green circle, red box). All introduced *mam/mms/feo* genes were found to be identical to pMDJM3 with respect to sequences and order. In addition to the successful M13 deletion, also all other introduced deletions were exactly as intended. A short remnant (3 558 bp) of suicide vector *pORFM-GalK-pks* was found inserted at nt position 1,646,447 (considered to be neutral), showing a duplication of the downstream homologous region like in ΔTZ-16::MAG-*gusA*. Again, the same spontaneous indel mutations in other chromosomal regions as in strain ΔTZ-16::MAG-*gusA* were also present in

ΔTZ-17::MAG, indicating that these mutations had occurred already at an earlier stage of mutagenesis.

Phenotypic characterization of ΔTZ-16::MAG-*gusA* and ΔTZ-17::MAG-*gusA*

Growth characteristics and magnetosome biomineralization
Complementation of non-magnetic ΔTZ-16 (lacking 3.489% of the WT genome) and ΔTZ-17 (lacking 5.477%) with pMDJM3 restored the formation of WT-like magnetosome numbers and sizes, and cells had electron dense particles (EDP) (Fig. 6a, white arrows), similar as observed before in the corresponding single deletion

(See figure on next page.)
Fig. 6 Phenotypic characterization of multiple deletion mutants. **a** Electron micrographs of the non-magnetic pre-'chassis' strains ΔTZ-16 and ΔTZ-17 and the final complemented prospective chassis ΔTZ-16::MAG-*gusA* and ΔTZ-17::MAG-*gusA* (scale bars 500 nm), white arrows indicate EDPs and **b** cell growth under aerobic and anaerobic conditions as well as oxidative stress (H_2O_2) and heat stress (33 °C). Each strain was analyzed in triplicates and the curves show the average while standard deviation was below 5%. **c** Growth curves and C_{mag} (i.e., a proxy for the average magnetic orientation of bacterial cells in liquid media based on light-scattering [63]) of WT strain and ΔTZ-16::MAG-*gusA* during anaerobic fermentation
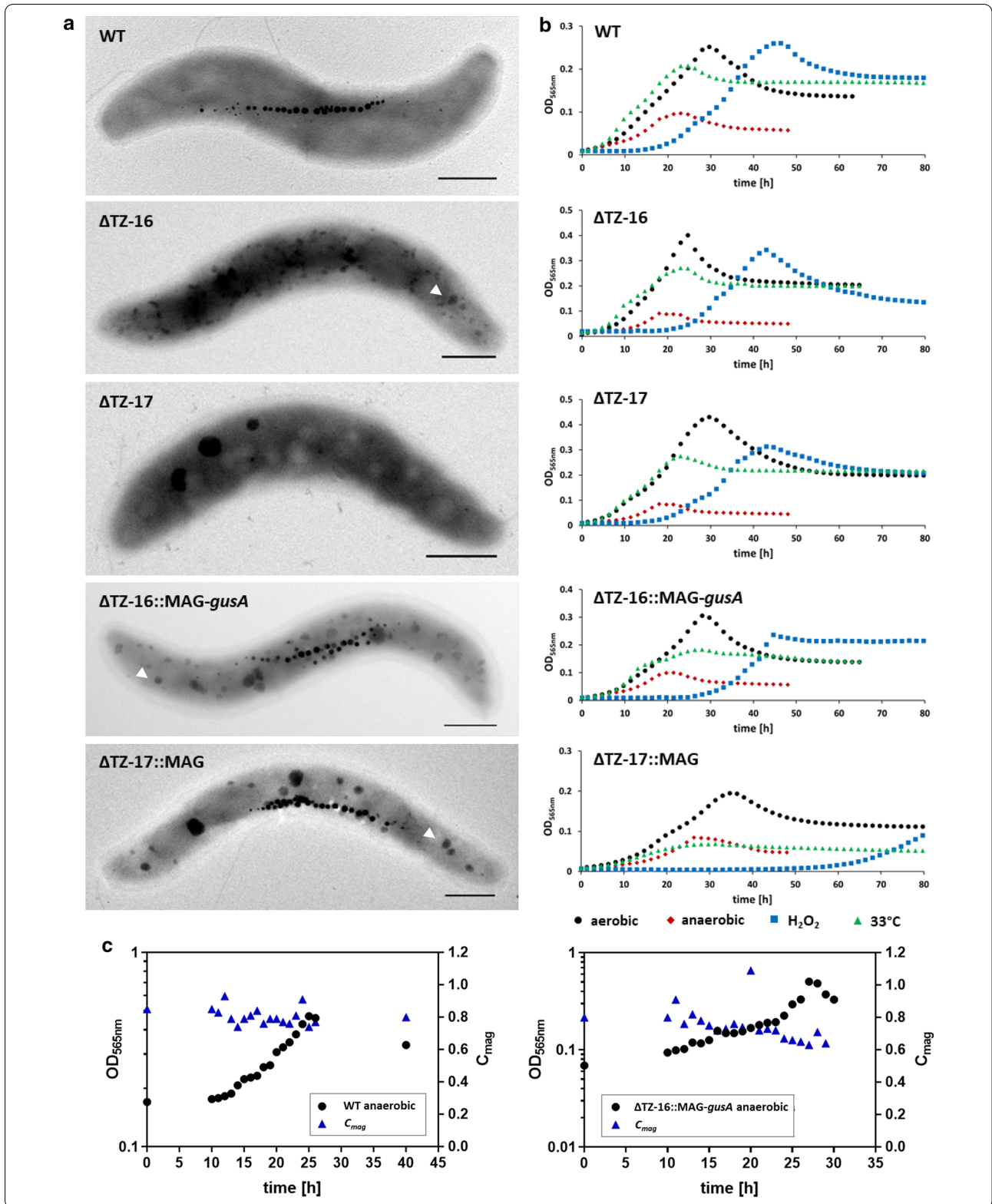
Zwiener *et al. Microb Cell Fact*   (2021) 20:35

Page 10 of 17

Zwiener *et al. Microb Cell Fact*   (2021) 20:35

Page 11 of 17

Table 1 Overview of identified mutations in the reporter gene *gusA*

	Point mutations	Insertions		Deletions
		Tn-tandem	*ISMgr2* (TnpA/B)	
t0				
WT-*gusA*	64	32	–	–
ΔTZ-16::MAG-*gusA*	90	6	–	–
ΔTZ-17::MAG-*gusA*	87	9	–	–
t10				
WT-*gusA*	56	30	8	2
ΔTZ-16::MAG-*gusA*	81	15	–	–
ΔTZ-17::MAG-*gusA*	86	10	–	–

strains of the eliminated parts of the MAI [53]. Microplate-scale experiments with strains ΔTZ-16::MAG-*gusA* and ΔTZ-17::MAG-*gusA* under aerobic and anaerobic nitrate-reducing conditions indicated WT-like or slightly delayed cell growth compared to WT (Fig. 6b). To analyze growth at higher cell densities, strains ΔTZ-16::MAG-*gusA* and ΔTZ-17::MAG-*gusA* were in addition cultivated in a larger volume (3 l) in a bioreactor under controlled anaerobic conditions, which are known to be optimal for magnetosome biomineralization [28, 62]. Figure 6c shows exemplary results for strain ΔTZ-16::MAG-*gusA* compared to the WT. Both strains reached a final OD of > 0.5, compared to only ca. 0.1 typically observed in microplate growth. Again, growth of strains ΔTZ-16::MAG-*gusA* and ΔTZ-17::MAG-*gusA* was WT-like, indicating that loss of the eliminated genes was neutral for growth under controlled conditions. Strains ΔTZ-16::MAG-*gusA* and ΔTZ-17::MAG were also tested regarding their growth performance after challenging them with the antibiotic MMC. Similar as the single deletion strain of the putative phage integrase gene *hin2*, both strains survived concentrations up to 0.3 μg/ml MMC, while WT was entirely inhibited at 0.3 μg/ml MMC (Additional file 1: Fig. S4).

Stability of the reporter gene gusA and the magnetic phenotype

To analyze whether the combined multiple deletion of IS elements in *M. gryphiswaldense* affects the incidence of spontaneous mutations, we employed an assay to estimate the genetic stability of expressed foreign genes as well as the stability of the magnetic phenotype using the reporter gene *gusA* as a 'trap' (Additional file 1: Fig. S5A), similar as reported for other marker genes in different bacteria [64]. Mutational inactivation of *gusA* causes the loss of the ability to cleave X-Gluc into blue dye, hence

resulting in white (magnetosome-free) or brownish (magnetosome forming) colonies (Additional file 1: Fig. S5). After ten sequential passages under aerobic conditions (alternating between 4 h at 4 °C and 44 h at 28 °C, conditions which were previously found to favor spontaneous mutations [41], 12 independent parallels (equivalent to ~ 4.2 * 10^3 cells for each strain and time point) were plated and visually screened. Out of ~ 2.5 * 10^4 cells in total, 2–3% of colonies had lost their blue color. Overall, among the about 7.1 * 10^2 white clones, we analyzed 192 white clones of each WT-*gusA*, ΔTZ-16::MAG-*gusA* and ΔTZ-17::MAG-*gusA* in which *gusA* was found to be inactivated by different types of mutations, including point mutations (80.6%), insertions (19.1%) and deletions (0.3%). The majority of the point mutations observed were base deletions (40%) and insertions (50%) causing frame shifts, while base substitutions represented the minority (10%). The types of point mutation were independent from time point or strain, and most mutations were found within a range of 500 bp of the *gusA* gene encoding the catalytic center of the GusA enzyme [65]. Furthermore, deletions of 62 bp of the *gusA* gene were found within the 25% N-terminal portion of the GusA protein.

All larger *gusA* insertions were found to belong exclusively to the two types of IS elements that we had already identified in our preliminary experiments described above [*ISMgr2* (7.3%) and *tn-tandem* (92.7%)], present both in cells before (t0) and after (t10) passaging. The high frequency observed for *tn-tandem* insertions might have been probably caused by its high abundance or close proximity (~ 11.4 kb) of a copy to the *gusA* reporter. While the total number of mutations between time points t0 and t10 did not significantly vary (Table 1), the number of all insertions was substantially reduced by ca. 60–75% in ΔTZ-16::MAG-*gusA* and ΔTZ-17::MAG-*gusA* compared to WT-*gusA*, likely due to the successful elimination of several active IS elements described above.

In addition to mutations in *gusA*, reduction or loss of the magnetic phenotype was found in a minority of clones from white or brown colonies which had lost their blue color. Reduced magnetic phenotypes displaying WT-like magnetite crystals flanked by flake-like particles could be observed in several of WT-*gusA* clones after ten passages (Additional file 1: Fig. S5B), which likely indicates a second mutation (i.e., in addition to the point mutations within *gusA*) in *mamXYop* [61]. Furthermore, the loss of the magnetic phenotype coincident with *gusA* inactivation could be observed in three clones of ΔTZ-16::MAG-*gusA* for time point t10. This could be the result of spontaneous homologous recombination between identical stretches of DNA in this partially merodiploidic strain.

Zwiener *et al. Microb Cell Fact*   (2021) 20:35

Page 12 of 17

Discussion

In this study, we established an approach for large-scale combinatory genome reduction of the magnetotactic bacterium *M. gryphiswaldense*. By repeated circles of deletion, we generated a library of strains in which different multiple genomic segments were erased. These strains might each serve as different starting points in future genome streamlining approaches by recombination with further favorable deletions and insertions.

In total, we completed the combination of 16 single deletions from this and our previous work [53] into each of the two strains ΔTZ-16 and ΔTZ-17, in which in addition large parts of the fragmented MAI were functionally replaced by a compact version of the magnetosome biosynthesis gene clusters.

On average, one round of deletion typically took about 3 weeks, and after some technical streamlining, the 16 subsequent rounds could have been completed in about 12 months of work. Independent of the target size, all rounds of successful deletions were largely completed with similar efficiencies as for respective single deletions. An exception was the unsuccessful deletion of the M04 region which might be especially problematic due to the abundance of transposon genes close to the regions targeted for homologous recombination. Several undesired mutations and spontaneous rearrangements were found to have occurred during recursive deletions. This emphasizes the need of genome resequencing of key intermediates and final strains. Again, most of these spontaneous rearrangements were caused by either homologous or illegitimate recombination and could be traced back to the spontaneous inactivation of the lethal *galK* marker harbored on the suicide vectors for homologous recombination, thereby preventing effective counterselection of proper double-crossovers.

However, despite of these caveats, we succeeded in the construction of one final strain (ΔTZ-17) with a genome reduction by non-overlapping ~227,600 bp, which is equivalent to about 5.5% of the entire genome. In this strain all targeted deletions and the reinsertion of the compacted magnetosome gene clusters were found to be exactly as intended, with only few minor spontaneous mutations in regions irrelevant for growth and magnetosome biosynthesis under laboratory conditions. This confirms that if used with caution, the method is sufficiently efficient and reliable for multiple genome editing.

In other bacteria, multiple genome reductions of different extents by similar approaches were previously reported. For example, one of the first studies in *E. coli* K12 resulted in a genome reduction up to 15% [47], and the genome of *E. coli* could be further shrunk by > 29%, changing cell size and nucleoid organization of engineered cells [66]. A "MiniBacillus" was constructed from *Bacillus subtilis*, in which a total of 42.3% was eliminated [67]. However, top-down genome reduction approaches in model organisms other than *E. coli* and *B. subtilis* have been more limited, and in some cases involved the combined, stepwise efforts of several labs [43]. For example, in *C. glutamicum* multiple approaches resulted first in the targeted deletion of 11 distinct regions with a total size of 250 kilobase pair (kbp) [68, 69], followed by an untargeted approach via insertion and excision [70]. In another random approach, 42 mutants in a range of 0.2–186 kb were generated, which revealed a total of 393.6 kb (11.9%) of the *C. glutamicum* R genome to be non-essential under standard laboratory conditions [70]. More recently, five of the 36 single large deletions identified by Unthan et al. [46] were later combined in a chassis strain of *C. glutamicum*, in which 13.4% of the genome were eliminated [45]. Similar approaches with *P. putida* resulted in genome reductions of 4.1% [71], 4.3% [48] and 4.12% [72], respectively, as well as in *Lactococcus lactis* (2.83% reduction) [73], *Streptomyces avermitilis* (1.4 Mb reduction) [74, 75], while in *S. chattanoogensis* 1.3 Mb and 0.7 Mb regions were eliminated [76]. With a comparable reduction by nearly 5.5% of the genome, our study represents the first proof-of-principle for the feasibility of similar targeted approaches in a magnetotactic bacterium.

While many of the genome streamlining approaches described above led to beneficial properties, such as improved growth and recombinant protein production, as well as robustness against several stresses [34, 45, 47, 50, 77], others resulted in negative effects, such as growth deficiencies, decreased resistance against antibiotics and under several stress conditions, and reduced transformation efficiencies [45, 78]. In our study, most deletions were neutral with respect to magnetosome biosynthesis and growth. For example, our preliminary analysis suggested that neither the conjugation efficiency with replicative and insertional plasmids, nor the weak latent propensity of spontaneous cell lysis was affected in strains ΔTZ-16::MAG-*gusA* and ΔTZ-17::MAG-*gusA* (data not shown). As observed in our previous study, deletion of *mamABop* in ΔTZ-16 and ΔTZ-17 resulted in a growth advantage which became lost after 're-magnetization' by complementation. Among the several putative prophage genes of *M. gryphiswaldense*, only deletion of the recombinase gene *hin2* from P6 had an effect and resulted in a slightly improved resilience to mitomycin c (MMC)-induced stress in the final strains. This provides an indirect hint that P6 may be an active prophage, whose excision might be induced by MMC in WT cells, but further work, such as the identification of phage particles, will be necessary to confirm this. However, the

Zwiener *et al. Microb Cell Fact*   (2021) 20:35

Page 13 of 17

combined deletion of other phage-related genes did neither further increase MMC resistance, nor generally enhance growth. On the contrary, deletion of the M13 region and prophage genes slightly impaired growth in the presence of oxidative stress, possibly for similar reasons as suggested by Wang et al. [78], who found that the presence of cryptic prophages may help bacteria to cope with adverse conditions and provide multiple benefits. For comparison, ΔTZ-16 lacks the ΔM13 deletion and therefore could be useful as an alternative parent strain with improved growth characteristics in follow-up genome streamlining studies.

From the ~ 120 transposable elements predicted in the 4.155 Mbp genome of *M. gryphiswaldense*, 30 are encoded within the ca. 100 kb MAI, and nine in addition in its ~ 33 kb adjacent region [1, 53]. However, our systematic approach revealed that only a minority of them, belonging to two families, seems to be responsible for the majority of spontaneous insertions. We detected an increased stability of the reporter *gusA* in both final multiple deletion strains, which was likely a result of the successful elimination of all *ISMgr2* elements described above, including one from the MAI. Future approaches should also aim for the removal of *ISMgr2-1*, *ISMgr2-2* and *ISMgr2-3* which might further decrease the rate of spontaneous mutations. However, deletion of multiple copies of the *tn-tandem*, the second group of identified troublemakers, or even the generation of a chassis stripped of all copies as accomplished in several other bacteria [51, 52] is currently not within realistic reach, due to the numerous abundance and extensive sequence similarity between multiple copies of IS elements, as well as their persistent tendency to spread during genetic manipulation.

Conclusion

Overall, in this study we succeeded in further domestication and large-scale engineering of magnetotactic bacteria and showed the potential of combining multiple scarless deletions with high precision. We also generated a library of deletions, which represent building blocks for recombination with favorable deletions and insertions that can be used for the construction of improved 'chassis' strains in the future. Ultimately, this may turn *M. gryphiswaldense* into a versatile platform and microbial cell factory for synthetic biology and magnetosome production.

Methods
Bacterial strains, vectors, and cultivation conditions
Bacterial strains and plasmids used in this work are listed in Additional file 1: Table S1. *E. coli* strains were grown

as previously reported [79]. *E. coli* WM3064 strains were grown in lysogeny broth (LB) medium supplemented with 25 μg/ml (final concentration) kanamycin (Km), and 1 mM DL-α,ε-diaminopimelic acid (DAP) at 37 °C. Liquid cultures of *M. gryphiswaldense* strains were grown microaerobically in flask standard medium (FSM) [28] at 28 °C under moderate shaking (120 rpm). Strains carrying the suicide or complementation plasmid were cultivated by adding 5 μg/ml Km. For cultivation on solid LB medium or FSM, 1.5% (w/v) agar was added. Cultivation from single *M. gryphiswaldense* colonies was conducted by transferring cell material into 150 μl FSM in 96-deep-well-plates (Eppendorf, Hamburg, Germany), prior to gradually increasing the culture volume. Optical density (OD) and magnetic response (C_{mag}, i.e., a proxy for the average magnetic orientation of bacterial cells in liquid media based on light-scattering) of cells in the exponential growth phase were measured photometrically at 565 nm as previously described [63].

Growth experiments of *M. gryphiswaldense* were performed by using pre-cultures grown for two daily passages under microaerobic conditions at 28 °C. Cultures were adjusted to an initial OD of 0.01 and grown in a microplate reader (Tecan) under aerobic conditions at 28 °C or moderate heat stress at 33 °C. For induction of oxidative stress, 20 μM H_2O_2 were added prior to starting the growth experiments.

For cell growth after mitomycin C (MMC) induction, pre-cultures were adjusted to an initial OD of 0.08 and treated with MMC concentrations of 0.1–0.3 μg/ml for 8 h. Non-induced strains (0 μg/ml) served as controls. Then cultures were washed twice in FSM, and an initial OD of 0.01 was used to start growth experiments in the microplate reader under aerobic conditions at 28 °C.

In preliminary experiments, conditions could be defined (i.e. incubation with 0.2 μg/ml MMC for 8 h) in which growth of the WT was already somewhat impaired, yet still reached substantial yields (final OD of ca. 0.3), while slightly increased MMC concentrations (0.3 μg/ml) entirely abolished growth. Therefore, we used 8 h and 0.2–0.3 μg/ml MMC as efficient incubation conditions to analyze survival of mutants compared to the WT strain.

For cultivation in the fermenter, modified FSM was used adding 10 mM $NaNO_3$ instead of 4 mM $NaNO_3$ as alternative electron acceptor under anaerobic conditions. Growth experiments of WT and final strains were performed in 3 l BioFlow® 320 reactors (Eppendorf Bioprocess) equipped for the automatic control of pH (with H_2SO_4 or KOH), temperature, agitation, and nitrogen concentration. Data were directly saved at unit or in Bio-Command software. Seed train was prepared 56 h before

Zwiener *et al. Microb Cell Fact*   (2021) 20:35

Page 14 of 17

inoculation in falcon tubes and scaled up to 1 l flasks under anaerobic conditions.

Molecular and genetic techniques

Oligonucleotides used as primers for amplification of DNA fragments were inferred from the working draft genome sequence of *M. gryphiswaldense* (GenBank accession number CP027526) [80] and purchased from Sigma-Aldrich (Steinheim, Germany). Construction of plasmids was performed by standard recombinant techniques as described in Zwiener et al. [53]. Generated constructs were sequenced by Macrogen Europe (Amsterdam, Netherlands) and sequence data analyzed with Geneious 8.0.5 (Biomatters Ltd).

Construction of markerless gene deletion vectors and mutants

Generation of single and multiple deletion mutants and WT-*gusA* insertion mutant was carried out by a tailored *galK* counterselection system as previously reported [53, 81].

We used chromosomal insertion and expression of magnetosome biosynthetic gene clusters, since previous work has shown that episomal expression in *M. gryphiswaldense* resulted in instability and inhomogenous expression of foreign and magnetosome genes [82, 83]. Multiple deletion mutants were complemented with the pMDJM3 cassette, a recyclable variant of pTpsMAG1 [60] containing *lox* sites next to the antibiotic marker and all operons necessary for magnetosome formation. For insertion of the chromogenic marker *gusA* into pMDJM3, RedET recombineering [84] was performed according to BAC Subcloning Kit (Gene Bridges) technical protocols.

Analytical methods
Analysis of putative prophages

Analysis of putative prophages was performed by the phage search tool PHAST [55]. In PHAST, a prophage-like element was considered incomplete if its completeness score was less than 60, questionable if the score was in the range between 60 and 90, and complete if the score was above 90.

Re-sequencing of genomic DNA

Genomic DNA was isolated following the manual instructions of Quick-DNA Midiprep Plus Kit (Zymo Research Europe GmbH). For each isolated gDNA, two sequencing libraries were arranged, one for sequencing on the MiSeq platform (Illumina Inc, NL), and the second for sequencing on the GridION platform [Oxford Nanopore Technologies (ONT), UK]. The former was established using the TruSeq DNA PCR-free Library Kit (Illumina Inc., The Netherlands) and was carried out in

a 2×300 nt run using a 600 cycle MiSeq Reagent Kit v3 (Illumina Inc, The Netherlands). For ONT sequencing, the Ligation Sequencing Kit SQK-LSK109 was used to arrange the libraries, which were in turn run on a R9.4.1 flow cell. Basecalling of the raw ONT data was carried out with GUPPY v3.2.8 [85]. For assembly, three assemblers were used: the CANU assembler v1.8 [86] was utilized to assemble the ONT data. The resulting assembled contigs were polished applying first the ONT data with RACON v1.3.3 [87] and MEDAKA v0.11.5 (Oxford Nanopore Technologies), both relying on MINIMAP2 v2.17-r943 [88] for mapping, followed by switching to the Illumina data and the PILON polisher v1.22 [89] for a total of 10 rounds. For the first 5 rounds, BWA MEM [90] was utilized as a mapper, for the final 5 cycles, BOWTIE2 [91] was applied. In addition, the Illumina data was assembled using NEWBLER v2.8 [92] and both data sets were gathered using UNICYCLER [93]. All assemblies were compared with each other and examined for synteny using R2CAT [94]. All three assemblies were combined and manually curated using CONSED [95]. Annotation of the finished genomes was carried out using PROKKA v1.11 [96] SNPs and small indels were identified using SNIPPY v4.0 [97] while larger rearrangements were recognized manually using SnapGene (GSL Biotech).

Preparation of samples for transmission electron microscopy (TEM)

For conventional transmission electron microscopy (TEM) of cell and magnetosome morphologies, cultures were grown under microoxic conditions in FSM at 28 °C. Overnight cultures were fixed in 1.5% formaldehyde and adsorbed onto carbon-coated copper-mesh grids (Science Services, Munich, Germany). TEM was performed on a JEOL 1400 (Japan) with an acceleration voltage of 80 kV and micrographs were analyzed using the software ImageJ [98].

Genetic stability assay

To test genetic stability of the reporter *gusA*, overnight cultures were transferred to 96-well-plates and incubated for ten passages under aerobic conditions alternating between 4 h at 4 °C and 44 h at 28 °C. 12 independent parallels of each strain were plated on FSM agar moistened with 250 μl of a 10 mg/ml X-Gluc stock solution on its surface. Clones producing active GusA could be visually screened by their blue color, while mutations inside *gusA* resulted in the loss of the ability to cleave X-Gluc, and thus in in white or brownish colonies after 7–10 days of incubation at 28 °C. Colonies were counted at time points 0 (t0) and after ten passages (t10) and mutations identified by PCR and sequencing.

Zwiener *et al. Microb Cell Fact*   (2021) 20:35

Page 15 of 17

Supplementary Information

The online version contains supplementary material available at https://doi.org/10.1186/s12934-021-01517-2.

Additional file 1 of "Towards a 'chassis' for bacterial magnetosome biosynthesis: genome streamlining of *Magnetospirillum gryphiswaldense* by multiple deletions": Table S1. Overview of all single deletion mutants which were also combined in strains ΔTZ-16 and ΔTZ-17. **Table S2.** Overview of primers used in this study. UF = upstream forward; UR = upstream reverse; DF = downstream forward; DR = downstream reverse. **Figure S1.** Molecular organization of *nif* operon in *M. gryphiswaldense*. The deleted nitrogen fixation cluster comprises 16 genes necessary for nitrogen fixation (shown in red): *nifWABZTHDK, fixABC, draGT* and three ferredoxins (MSR1_18560; MSR1_18600; MSR1_18640). Black arrows represent other genes encoding a putative rubrerythrin protein (MSR1_18580), a SIR2-like domain containing protein (MSR1_18630), a GAF domain-containing protein (MSR1_18650), a biliverdin-producing heme oxygenase (MSR1_18660) and a tRNA (MSR1_18670). **Figure S2.** Phenotypic characterization of multiple deletion mutants. Electron micrographs of combinatorial deletion mutants ΔTZ-01–ΔTZ-15. Scale bars: left columns 500 nm; right columns 100 nm. Cell growth of strains ΔTZ-01–ΔTZ-15 under aerobic and anaerobic conditions as well as oxidative stress (H_2O_2) and moderate heat stress (33 °C). Each strain was analyzed in triplicates and each curve shows the average. **Figure S3.** Genetic organization of the Km^r, false positive mutant ΔTZ-15ΔM04 K752 Km^r. The targeted M04 had not been deleted but was still maintained in the genome. A large part (~ 9.1 kb) of the 10.2 kb deletion vector *pORFM-GalK-M04* harboring the Km^r gene was found to be inserted at the intended site, but harboring a spontaneous duplication of both the upstream and downstream homologous regions intended for targeted insertion of the deletion construct by homologous recombination. In addition, the *galK* gene was inactivated by insertion of a copy of the IS element *ISMgr2* into the central region. **Figure S4.** Growth profiles of these strains induced with MMC with concentrations between 0.2 and 0.3 µg/ml MMC, induced 8 h. Cells were washed twice, adjusted to initial OD and growth experiments started at 28 °C under aerobic conditions and each strain was analyzed in triplicates while each curve shows its average (standard deviation < 5%). **Figure S5.** Experimental procedure of the genetic stability assay (**A**) and identified magnetosome phenotypes (**B**). Blue arrows indicate blue colonies while white/brown colonies are marked by black arrows (**A**). TEM micrographs (**B**) show WT-like magnetosome chains (upper micrograph) and flake-like particles (lower micrograph, white arrows) could be observed in several of WT-*gusA* clones after ten passages. Scale bars: 100 nm.

Abbreviations

MAI: Magnetosome Island; WT: Wild type; IS element: Insertion element; MNP: Magnetic nanoparticles; MMC: Mitomycin C; *tn-tandem*: Transposon-tandem; Km^r: Kanamycin resistant; Km^s: Kanamycin sensitive; EDP: Electron dense particles; X-Gluc: 5-Bromo-4-chloro-3-indolyl-β-D-glucuronide; DAP: DL-α,ε-Diaminopimelic acid.

Authors' contributions

TZ and DS conceived the study and designed the experiments. TZ carried out the genetic manipulations and the characterization of the strains. TZ, DS, FM and RU designed genetic stability assay. MD designed and generated plasmid pMDJM3. CR, TB and JK performed resequencing of strains. TZ and DS wrote the manuscript. All authors read and approved the final manuscript.

Author details

^{1} Department of Microbiology, University of Bayreuth, Bayreuth, Germany. ^{2} Institute of Bioengineering, Research Center of Biotechnology of the Russian Academy of Sciences, Moscow, Russia. ^{3} Center for Biotechnology, University of Bielefeld, Bielefeld, Germany.

References

1. Uebe R, Schüler D. Magnetosome biogenesis in magnetotactic bacteria. Nat Rev Microbiol. 2016;14:621–37.
2. Lefèvre CT, Bazylinski DA. Ecology, diversity, and evolution of magnetotactic bacteria. Microbiol Mol Biol Rev. 2013;77(3):497–526.
3. Faivre D, Schüler D. Magnetotactic bacteria and magnetosomes. Chem Rev. 2008;108(11):4875–98.
4. Sun C, Lee JSH, Zhang M. Magnetic nanoparticles in MR imaging and drug delivery. Adv Drug Deliv Rev. 2008;60(11):1252–65.
5. Taukulis R, Widdrat M, Kumari M, Heinke D, Rumpler M, Tompa É, Uebe R, Kraupner A, Cebers A, Schüler D, Pósfai M, Hirt AM, Faivre D. Magnetic iron oxide nanoparticles as MRI contrast agents—a comprehensive physical and theoretical study. Magnetohydrodynamics. 2015;51(4):721–47.
6. Alphandéry E. Applications of magnetosomes synthesized by magnetotactic bacteria in medicine. Front Bioeng Biotechnol. 2014;2:5.
7. Vargas G, Cypriano J, Correa T, Leão P, Bazylinski DA, Abreu F. Applications of magnetotactic bacteria, magnetosomes and magnetosome crystals in biotechnology and nanotechnology: mini-review. Molecules. 2018;23(10):2438.
8. Orlando T, Mannucci S, Fantechi E, Conti G, Tambalo S, Busato A, Innocenti C, Ghin L, Bassi R, Arosio P, Orsini F, Sangregorio C, Corti M, Casula MF, Marzola P, Lascialfari A, Sbarbati A. Characterization of magnetic nanoparticles from *Magnetospirillum gryphiswaldense* as potential theranostics tools. Contrast Media Mol Imaging. 2016;11(2):139–45.
9. Heinke D, Kraupner A, Eberbeck D, Schmidt D, Radon P, Uebe R, Schüler D, Briel A. MPS and MRI efficacy of magnetosomes from wild-type and mutant bacterial strains. IJMPI. 2017;3(2):1706004.
10. Kraupner A, Eberbeck D, Heinke D, Uebe R, Schüler D, Biel A. Bacterial magnetosomes—nature's powerful contribution to MPI tracer research. Nanoscale. 2017;9(18):5788–93.
11. Lang C, Schüler D. Biogenic nanoparticles: production, characterization, and application of bacterial magnetosomes. J Phys Condens Matter. 2006;18:2815–28.
12. Lisy MR, Hartung A, Lang C, Schüler D, Richter W, Reichenbach JR, Kaiser WA, Hilger I. Fluorescent bacterial magnetic nanoparticles as bimodal contrast agents. Invest Radiol. 2007;42(4):235–41.
13. Schwarz S, Fernandes F, Sanroman L, Hodenius M, Lang C, Himmelreich U, Fama G, Schmitz-Rode T, Schüler D, Hoehn M, Zenke M, Hieronymus T. Synthetic and biogenic magnetite nanoparticles for tracking of stem cells and dendritic cells. J Magn Magn Mater. 2009;321(10):1533–8.

Zwiener *et al. Microb Cell Fact*   (2021) 20:35

Page 16 of 17

14. Hergt R, Dutz S, Röder M. Effects of size distribution on hysteresis losses of magnetic nanoparticles for hyperthermia. J Phys Condens Matter. 2008;20:385214.

15. Alphandéry E, Guyot F, Chebbi I. Preparation of chains of magnetosomes, isolated from *Magnetospirillum magneticum* strain AMB-1 magnetotactic bacteria, yielding efficient treatment of tumors using magnetic hyperthermia. Int J Pharm. 2012;434(1–2):444–52.

16. Mickoleit F, Schüler D. Generation of multifunctional magnetic nanoparticles with amplified catalytic activities by genetic expression of enzyme arrays on bacterial magnetosomes. Adv Biosyst. 2018;2:1700109.

17. Mickoleit F, Lanzloth C, Schüler D. A versatile toolkit for controllable and highly selective multifunctionalization of bacterial magnetic nanoparticles. Small. 2020;16(16):e1906922.

18. Pollithy A, Romer T, Lang C, Müller FD, Helma J, Leonhardt H, Rothbauer U, Schüler D. Magnetosome expression of functional camelid antibody fragments (nanobodies) in *Magnetospirillum gryphiswaldense*. Appl Environ Microbiol. 2011;77(17):6165–71.

19. Borg S, Rothenstein D, Bill J, Schüler D. Generation of multi-shell magnetic hybrid nanoparticles by encapsulation of genetically engineered and fluorescent bacterial magnetosomes with ZnO and SiO$_2$. Small. 2015;11(33):4209–17.

20. Mickoleit F, Schüler D. Generation of nanomagnetic biocomposites by genetic engineering of bacterial magnetosomes. Bioinspired Biomim Nanobiomater. 2018;8(1):86–98.

21. Mickoleit F, Borkner CB, Toro-Nahuelpan M, Herold HM, Maier DS, Plitzko JM, Scheibel T, Schüler D. *In vivo* coating of bacterial magnetic nanoparticles by magnetosome expression of spider silk-inspired peptides. Biomacromolecules. 2018;19(3):962–72.

22. Mickoleit F, Jérôme V, Freitag R, Schüler D. Bacterial magnetosomes as novel platform for the presentation of immunostimulatory, membrane-bound ligands in cellular biotechnology. Adv Biosyst. 2020;4(3):e1900231.

23. Zeytuni N, Uebe R, Maes M, Davidov G, Baram M, Raschdorf O, Friedler A, Miller Y, Schüler D, Zarivach R. Bacterial magnetosome biomineralization-a novel platform to study molecular mechanisms of human CDF-related Type-II diabetes. PLoS ONE. 2014;9(5):e97154.

24. Schleifer KH, Schüler D, Spring S, Weizenegger M, Amann R, Ludwig W, Köhler M. The genus *Magnetospirillum* gen. nov. description of *Magnetospirillum gryphiswaldense* sp. nov. and transfer of *Aquaspirillum magnetotacticum* to *Magnetospirillum magnetotacticum* comb. nov. Syst Appl Microbiol. 1991;14:379–85.

25. Schüler D, Monteil CL, Lefèvre CT. Microbe of the month: *Magnetospirillum gryphiswaldense*. Trends in Microbiol. 2020. https://doi.org/10.1016/j.tim.2020.06.001.

26. Müller F, Schüler D, Pfeiffer D. A compass to boost navigation: cell biology of bacterial magnetotaxis. J Bacteriol. 2020. https://doi.org/10.1128/JB.00398-20.

27. Lohße A, Kolinko I, Raschdorf O, Uebe R, Borg S, Brachmann A, Plitzko JM, Müller R, Zhang Y, Schüler D. Overproduction of magnetosomes by genomic amplification of biosynthesis-related gene clusters in a magnetotactic bacterium. Appl Environ Microbiol. 2016;82(10):3032–41.

28. Heyen U, Schüler D. Growth and magnetosome formation by microaerophilic Magnetospirillum strains in an oxygen-controlled fermentor. Appl Microbiol Biotechnol. 2003;61:536–44.

29. Alphandéry E. Bio-synthesized iron oxide nanoparticles for cancer treatment. J Pharm. 2020;586:119472.

30. Alphandéry E. Applications of magnetotactic bacteria and magnetosome for cancer treatment: a review emphasizing on practical and mechanistic aspects. Drug Discov Today. 2020. https://doi.org/10.1016/j.drudis.2020.06.010.

31. Fernández-Castané A, Li H, Thomas ORT, Overton TW. Development of a simple intensified fermentation strategy for growth of *Magnetospirillum gryphiswaldense* MSR-1: physiological responses to changing environmental conditions. New Biotechnol. 2018;46:22–30.

32. Schüler D. Versuche zur Isolierung und Charakterisierung magnetotaktischer Bakterien. Diplomarbeit, Ernst-Moritz-Arndt Universität Greifswald. 1990.

33. Schüler D, Köhler M. The isolation of a new magnetic spirillum. Zentralblatt Mikrobiologie. 1992;147:150–1.

34. Baumgart M, Unthan S, Rückert C, Sivalingam J, Grünberger A, Kalinowski J, Bott M, Noack S, Frunzke J. Construction of a prophage-free variant of *Corynebacterium glutamicum* ATCC 13032 for use as a platform strain for basic research and industrial biotechnology. Appl Environ Microbiol. 2013;79(19):6006–15.

35. Martínez-García E, Nikel PI, Aparicio T, de Lorenzo V. Pseudomonas 2.0: genetic upgrading of *P. putida* KT2440 as an enhanced host for heterologous gene expression. Microb Cell Fact. 2014;13:159.

36. Gödeke J, Paul K, Lassak J, Thormann KM. Phage-induced lysis enhances biofilm formation in *Shewanella oneidensis* MR-1. ISME J. 2011;5(4):613–26.

37. Schübbe S, Kube M, Scheffel A, Wawer C, Heyen U, Meyerdierks A, Madkour MH, Mayer F, Reinhardt R, Schüler D. Characterization of a spontaneous nonmagnetic mutant of *Magnetospirillum gryphiswaldense* reveals a large deletion comprising a putative magnetosome island. J Bacteriol. 2003;185:5779–90.

38. Ullrich S, Kube M, Schübbe S, Reinhardt R, Schüler D. A hypervariable 130-kilobase genomic region of *Magnetospirillum gryphiswaldense* comprises a magnetosome island which undergoes frequent rearrangements during stationary growth. J Bacteriol. 2005;187:7176–84.

39. Ullrich S, Schüler D. Cre-*lox*-based method for generation of large deletions within the genomic magnetosome island of *Magnetospirillum gryphiswaldense*. Appl Environ Microbiol. 2010;76:2439–44.

40. McCausland HC, Komeili A. Magnetic genes: studying the genetics of biomineralization in magnetotactic bacteria. PLoS Genet. 2020;16(2):e1008499.

41. Kolinko I, Jogler C, Katzmann E, Schüler D. Frequent mutations within the genomic magnetosome island of *Magnetospirillum gryphiswaldense* are mediated by RecA. J Bacteriol. 2011;193:5328–34.

42. Martínez-García E, Fraile S, Espeso DR, Vecchietti D, Bertoni G, de Lorenzo V. Naked bacterium: emerging properties of a surfome-streamlined *Pseudomonas putida* strain. ACS Synth Biol. 2020;9(9):2477–92.

43. Martínez-García E, de Lorenzo V. The quest for the minimal bacterial genome. Curr Opin Biotechnol. 2016;42:216–24.

44. Fehér T, Birland V, Pósfai G. In the fast lane: large-scale bacterial genome engineering. J Biotechnol. 2012;169(1–2):72–9.

45. Baumgart M, Unthan S, Kloß R, Radek A, Polen T, Tenhaef N, Müller MF, Küberl A, Siebert D, Brühl N, Marin K, Hans S, Krämer R, Bott M, Kalinowski J, Wiechert W, Seibold G, Frunzke J, Rückert C, Wendisch V, Noack S. *Corynebacterium glutamicum* chassis C1*: building and testing a novel platform host for synthetic biology and industrial biotechnology. ACS Synth Biol. 2017;7(1):132–44.

46. Unthan S, Baumgart M, Radek A, Herbst M, Siebert D, Brühl N, Bartsch A, Bott M, Wiechert W, Marin K, Hans S, Krämer R, Seibold G, Frunzke J, Kalinowski J, Rückert C, Wendisch VF, Noack S. Chassis organism from *Corynebacterium glutamicum*—a top-down approach to identify and delete irrelevant gene clusters. Biotechnol J. 2015;10:290–301.

47. Pósfai G, Plunkett G 3rd, Fehér T, Frisch D, Keil GM, Umenhoffer K, Kolisnychenko V, Stahl B, Sharma SS, de Arruda M, Burland V, Harcum SW, Blattner FR. Emerging properties of reduced-genome *Escherichia coli*. Science. 2006;312(5776):1044–6.

48. Lieder S, Nikel PI, de Lorenzo V, Takors R. Genome reduction boosts heterologous gene expression in *Pseudomonas putida*. Microb Cell Fact. 2015;14:23.

49. Martínez-García E, Jatsenko T, Kivisaar M, de Lorenzo V. Freeing *Pseudomonas putida* KT2440 of its proviral load strengthens endurance to environmental stresses. Environ Microbiol. 2015;17(1):76–90.

50. Pfeifer E, Michniewski S, Gätgens C, Münch E, Müller F, Polen T, Millard A, Blombach B, Frunzke J. Generation of a prophage-free variant of the fast-growing bacterium *Vibrio natriegens*. Appl Environ Microbiol. 2019;85(17):e00853-e919.

51. Choi JW, Yim SS, Kim MJ, Jeong KJ. Enhanced production of recombinant proteins with *Corynebacterium glutamicum* by deletion of insertion sequences (IS elements). Microb Cell Fact. 2015;14:207.

52. Suárez GA, Renda BA, Dasgupta A, Barrick JE. Reduced mutation rate and increased transformability of transposon-free *Acinetobacter baylyi* ADP1-ISx. Appl Environ Microbiol. 2017;83(17):e01025-e1117.

53. Zwiener T, Mickoleit F, Dziuba M, Rückert C, Busche T, Kalinowski J, Faivre D, Uebe R, Schüler D. Identification and elimination of irrelevant genomic content for magnetosome biosynthesis by large-scale deletion in *Magnetospirillum gryphiswaldense*. BMC Microbiol. 2021 **(Accepted for publication, 2021)**.

54. de Lorenzo V, Krasnogor N, Schmidt M. For the sake of the bioeconomy: define what a synthetic biology chassis is! New Biotechnol. 2021;60:44–51.

55. Zhou Y, Liang Y, Lynch KH, Dennis JJ, Wishart DS. PHAST: a fast phage search tool. Nucl Acids Res. 2011;39:W347–52.

Zwiener *et al. Microb Cell Fact* (2021) 20:35

Page 17 of 17

56. Engelhardt T, Sahlberg M, Cypionka H, Engelen B. Induction of prophages from deep-subseafloor bacteria. Environ Microbiol Rep. 2011;3:459–65.

57. Siguier P, Gourbeyre E, Chandler M. Bacterial insertion sequences: their genomic impact and diversity. FEMS Microbiol Rev. 2014;38(5):865–91.

58. Bazylinski DA, Dean AJ, Schüler D, Phillips EJP, Levley DR. N$_2$-dependent growth and nitrogenase activity in the metal-metabolizing bacteria, *Geobacter* and *Magnetospirillum* species. Environ Microbiol. 2000;2(3):266–73.

59. Araujo ACV, Abreu F, Silva KT, Bazylinski DA, Lins U. Magnetotactic bacteria as potential sources of bioproducts. Mar Drugs. 2015;13(1):389–430.

60. Dziuba MV, Zwiener T, Uebe R, Schüler D. Single-step transfer of biosynthetic operons endows a non-magnetotactic *Magnetospirillum* strain from wetland with magnetosome biosynthesis. Environ Microbiol. 2020;22(4):1603–18.

61. Raschdorf O, Müller FD, Pósfai M, Plitzko JM, Schüler D. The magnetosome proteins MamX, MamZ and MamH are involved in redox control of magnetite biomineralization in *Magnetospirillum gryphiswaldense*. Mol Microbiol. 2013;89:872–86.

62. Riese C, Uebe R, Rosenfeldt S, Schenk AS, Jérôme V, Freitag R, Schüler D. An automated oxystat fermentation regime for microoxic cultivation and magnetosome production in *Magnetospirillum gryphiswaldense*. Microb Cell Fact. 2020;19:206.

63. Schüler D, Uhl R, Bäuerlein E. A simple light-scattering method to assay magnetism in *Magnetospirillum gryphiswaldense*. FEMS Microbiol Lett. 1995;132:139–45.

64. Bartosik D, Sochacka M, Baj J. Identification and characterization of transposable elements of *Paracoccus pantotrophus*. J Bacteriol. 2003;185(13):3753–63.

65. Little MS, Ervin SM, Walton WG, Tripathy A, Xu Y, Liu J, Redinbo MR. Active site flexibility revealed in crystal structure of *Parabacteroides merdae* β-glucuronidase from human gut microbiome. Protein Sci. 2018;27(12):2010–22.

66. Hashimoto M, Ichimura T, Mizoguchi H, Tanaka K, Fujimitsu K, Keyamura K, Ote T, Yamakawa T, Yamazaki Y, Mori H, Katayama T, Kato J. Cell size and nucleoid organization of engineered *Escherichia coli* cells with a reduced genome. Mol Microbiol. 2005;55(1):137–49.

67. Reuß DR, Commichau FM, Gundlach J, Zhu B, Stülke J. The blueprint of a minimal cell: *MiniBacillus*. Microbiol Mol Biol. 2016;80(4):955–87.

68. Ikeda M, Nakagawa S. The *Corynebacterium glutamicum* genome: features and impacts on biotechnological processes. Appl Microbiol Biotechnol. 2003;62:99–109.

69. Suzuki N, Nonaka H, Tsuge Y, Inui M, Yukawa H. New multiple-deletion method for the *Corynebacterium glutamicum* genome, using a mutant *lox* sequence. Appl Environ Microbiol. 2005;71(12):8472–80.

70. Tsuge Y, Suzuki N, Inui M, Yukawa H. Random segment deletion based on *IS31831* and *Cre/loxP* excision system in *Corynebacterium glutamicum*. Appl Microbiol Biotechnol. 2007;74:1333–41.

71. Leprince A, de Lorenzo V, Völler P, van Passel MWJ, Martins dos Santos VAP. Random and cyclical deletion of large DNA segments in the genome of *Pseudomonas putida*. Environ Microbiol. 2012;14(6):1444–53.

72. Liang P, Zhang Y, Xu B, Zhao Y, Liu X, Gao W, Ma T, Yang C, Wang S, Liu R. Deletion of genomic islands in the *Pseudomonas putida* KT2440 genome can create an optimal chassis for synthetic biology applications. Microb Cell Fact. 2020;19:70.

73. Zhu D, Fu Y, Liu F, Xu H, Saris PEJ, Qiao M. Enhanced heterologous protein productivity by genome reduction in *Lactococcus lactis* NZ9000. Microb Cell Fact. 2017;16:1.

74. Komatsu M, Uchiyama T, Omura S, Cane DE, Ikeda H. Genome-minimized *Streptomyces* host for the heterologous expression of secondary metabolism. PNAS. 2010;107(6):2646–51.

75. Ikeda H, Shin-ya K, Omura S. Genome mining of the *Streptomyces avermitilis* genome and development of genome-minimized hosts for heterologous expression of biosynthetic gene clusters. J Ind Microbiol Biotechnol. 2014;41(2):233–50.

76. Bu Q-T, Yu P, Wang J, Li Z-Y, Chen X-A, Mao X-M, Li Y-Q. Rational construction of genome-reduced and high-efficient industrial *Streptomyces chassis* based on multiple comparative genomic approaches. Microb Cell Fact. 2019;18:16.

77. Umenhoffer K, Draskovits G, Nyerges Á, Karcagi I, Bogos B, Tímár E, Csörgő B, Herczeg R, Nagy I, Pál C, Pósfai G. Genome-wide abolishment of mobile genetic elements using genome shuffling and CRISPR/Cas-assisted MAGE allows the efficient stabilization of bacterial chassis. ACS Synth Biol. 2017;6(8):1471–83.

78. Wang X, Kim Y, Ma Q, Hong SH, Pokusaeva K, Sturino JM, Wood TK. Cryptic prophages help bacteria cope with adverse environments. Nat Commun. 2010;1:147.

79. Sambrook J, Russell DW. Molecular cloning: a laboratory manual. 3rd ed. Cold Spring Harbor: Cold Spring Harbor Laboratory Press; 2001.

80. Uebe R, Schüler D, Jogler C, Wiegand S. Reevaluation of the complete genome sequence of *Magnetospirillum gryphiswaldense* MSR-1 with single-molecule real-time sequencing data. Genome Announc. 2018;6(17):e00309-e318.

81. Raschdorf O, Plitzko JM, Schüler D, Müller FD. A tailored *galK* counterselection system for efficient markerless gene deletion and chromosomal tagging in *Magnetospirillum gryphiswaldense*. Appl Environ Microbiol. 2014;80(14):4323–30.

82. Borg S, Hofmann J, Pollithy A, Lang C, Schüler D. New vectors for chromosomal integration enable high-level constitutive or inducible magnetosome expression of fusion proteins in *Magnetospirillum gryphiswaldense*. Appl Environ Microbiol. 2014;80(8):2609–16.

83. Kolinko I, Lohße A, Borg S, Raschdorf O, Jogler C, Tu Q, Pósfai M, Tompa É, Plitzko JM, Brachmann A, Wanner G, Müller R, Zhang Y, Schüler D. Biosynthesis of magnetic nanostructures in a foreign organism by transfer of bacterial magnetosome gene clusters. Nat Nanotechnol. 2014;9:193–7.

84. Muyrers JPP, Zhang Y, Stewart AF. Recombinogenic engineering: new options for cloning and manipulating DNA. Trends in Biochem Sci. 2001;23:325–31.

85. Wick RR, Judd LM, Holt KE. Performance of neural network basecalling tools for Oxford Nanopore sequencing. Genome Biol. 2019;20(1):129.

86. Koren S, Walenz BP, Berlin K, Miller JR, Bergman NH, Phillippy AM. Canu: scalable and accurate long-read assembly via adaptive *k*-mer weighting and repeat separation. Genome Res. 2017;27(5):722–36.

87. Vaser R, Sović I, Nagarajan N, Šikić M. Fast and accurate de novo genome assembly from long uncorrected reads. Genome Res. 2017;27(5):737–46.

88. Li H. Minimap2: pairwise alignment for nucleotide sequences. Bioinformatics. 2018;34(18):3094–100.

89. Walker BJ, Abeel T, Shea T, Priest M, Abouelliel A, Sakthikumar S, Cuomo CA, Zeng Q, Wortman J, Young SK, Earl AM. Pilon: an integrated tool for comprehensive microbial variant detection and genome assembly improvement. PLoS ONE. 2014;9(11):e112963.

90. Li H. Aligning sequence reads, clone sequences and assembly contigs with BWA-MEM. 2013. arXiv:1303.3997.

91. Langmead B, Salzberg SL. Fast gapped-read alignment with Bowtie 2. Nat Methods. 2012;9(4):357–9.

92. Margulies M, Egholm M, Altman WE, Attiya S, Bader JS, Bemben L, Berka J, et al. Genome sequencing in microfabricated high-density picolitre reactors. Nature. 2005;437(7057):376–80.

93. Wick RR, Judd LM, Gorrie CL, Holt KE. Unicycler: resolving bacterial genome assemblies from short and long sequencing reads. PLoS Comput Biol. 2017;13(6):e1005595.

94. Husemann P, Stoye J. r2cat: synteny plots and comparative assembly. Bioinformatics. 2009;26(4):570–1.

95. Gordon D, Green P. Consed: a graphical editor for next-generation sequencing. Bioinformatics. 2013;29(22):2936–7.

96. Seemann T. Prokka: rapid prokaryotic genome annotation. Bioinformatics. 2014;30(14):2068–9.

97. Seemann T. snippy: fast bacterial variant calling from NGS reads. 2015.

98. Abràmoff MD, Magalhães PJ, Ram SJ. Image processing with imageJ. Biophotonics Int. 2004;11:36–42.

Publisher's Note

Springer Nature remains neutral with regard to jurisdictional claims in published maps and institutional affiliations.

Additional file 1

Table S1. Overview of all single deletion mutants which were also combined in strains ΔTZ-16 and ΔTZ-17.

Name of single deletion mutant	Deleted genes	Total extent of deletion
ΔM04	MSR1_03150 to MSR1_03880	65,965 bp
ΔM13	MSR1_03150 to MSR1_04210	98,984 bp
Δ*feoAB1op*	MSR1_02660 to MSR1_02670	2,406 bp
Δ*mamABop*	MSR1_03340 to MSR1_03500	16,364 bp
ΔP7	MSR1_02780 to MSR1_02990 **not deletable in this study**	12,793 bp
Δ*intA1*	MSR1_08690	1,284 bp
Δ*intA2*	MSR1_36030	1,226 bp
Δ*hin2*	MSR1_37790	1,333 bp
Δ*alpA*	MSR1_08890	255 bp
ΔP1.2	MSR1_00080 to MSR1_00280	19,489 bp
ΔP1.3	MSR1_00140 to MSR1_00280	12,826 bp
Δcapsid	MSR1_37460 to MSR1_37540	7,651 bp
Δ*pks* cluster	MSR1_15630 to MSR1_15650	39,049 bp
Δ*nif* cluster	MSR1_18530 to MSR1_18720	17,608 bp
ΔMSR1_20490	MSR1_20490	31,026 bp
Δ*ISMgr2-1*	MSR1_29210 to MSR1_29220	1,244 bp
Δ*ISMgr2-2*	MSR1_33470 to MSR1_33480	1,304 bp
Δ*ISMgr2-3*	MSR1_02780 to MSR1_02790	1,434 bp
Δ*ISMgr2-tnpB-hyp-1*	MSR1_23730 to MSR1_23750	1,214 bp
Δ*ISMgr2-tnpB-hyp-2*	MSR1_33640 to MSR1_33660	1,990 bp

Table S2. Overview of primers used in this study. UF = upstream forward; UR = upstream reverse; DF = downstream forward; DR = downstream reverse.

Primer	Sequence (5' to 3')	Description
TZ199	AACTCTCCAGCGCTTCGGCAAAAG	ΔM04 UF
TZ200	CAGACGGATCGCTTCTCGCCGAACATAAGGGCTGCTCCCGTGG	ΔM04 UR
TZ201	CCACGGGAGCAGCCCTTATGTTCGGCGAGAAGCGATCCGTCTG	ΔM04 DF
TZ202	GCGCCCATCAGCTTGGCCC	ΔM04 DR
TZ515	CACAGCGCAGCGCATTG	ΔM13 UF
TZ516	TTGCGTGACTGTTAACTAAACAACGTTAAGGTGGACTTG	ΔM13 UR
TZ517	TAGTTAACAGTCACGCAACGGCGC	ΔM13 DF
TZ509	GGTGGTGGGCACGCC	ΔM13 DR
RU423	GGAGGAGTTCCAGGGTCTTGTTCTGGTGGCGGAGCG	Δ*feoAB1op* UF
RU424	CAGCAGCTGCGCCATGCTGTCCG	Δ*feoAB1op* UR
RU425	GCCTTGCCAGCTGCGCATGC	Δ*feoAB1op* DF
RU426	CACCAGAACAAGACCCTGGAACTCCTCCTTAT	Δ*feoAB1op* DR
TZ049	AGCTAACAAACAACGCGCTGCCTC	Δ*mamABop* UF
TZ196	GCGCTCCGGGCAGAATGTCGCTGGGACGCTGGCTCGGC	Δ*mamABop* UR
TZ197	GCCGAGCCAGCGTCCCAGCGACATTCTGCCCGGAGCGC	Δ*mamABop* DF
TZ198	ATCCGACCGGGCGGCCTC	Δ*mamABop* DR
TZ435	GATGGTACCTAGGATGAGGGTCATGGCC	ΔP7 UF
TZ436	ATGAAGCCTTTGCCCGTGAATCCTGCCGTT	ΔP7 UR
TZ437	CGGCAGGATTCACGGGCAAAGGCTTCATCG	ΔP7 DF
TZ438	AGCGGCCGCATCGATCGCGTTCTGCTCTCG	ΔP7 DR
TZ425	GGTTTTCGTGAATATAATTTTTCAGCC	Δ*intA1* UF
TZ426	TAGCCCCCCCGAGCGAGCCCCCGA	Δ*intA1* UR
TZ427	GGGCTCGCTCGGGGGGGCTATGCCC	Δ*intA1* DF
TZ428	GGATACGCCTCCAGGCTTC	Δ*intA1* DR
TZ430	CAGTCTGGAACGGCGC	Δ*intA2* UF
TZ431	TCCCCGGCGGGGCCGAATCTCCATGGG	Δ*intA2* UR
TZ432	AGATTCGGCCCCGCCGGGGAAAAATATT	Δ*intA2* DF
TZ433	GTCTTATTCCCGATCTTGACCG	Δ*intA2* DR
TZ666	CCGCCGCATCCACGATGAG	Δ*hin2* UF
TZ667	GGCGGTCATTCATCGGCTGGTCTCCAACTTGC	Δ*hin2* UR
TZ668	AGCCGATGAATGACCGCCGACATCCGG	Δ*hin2* DF

TZ669	CGATCCCGCAGCAGAAAGGTATG	Δ*hin2* DR
TZ448	TGGTACCTAGGATAAATAGCCTCCCCGACACG	Δ*alpA* UF
TZ449	AAAGGGAGAAATCCGGGCCATCCCCGTTT	Δ*alpA* UR
TZ450	AACGGGGATGGCCCGGATTTCTCCCTTTCG	Δ*alpA* DF
TZ451	CGGCCGCATCGATCCCTCTCTCCAGCATCTTGC	Δ*alpA* DR
TZ531	AACCGGCCAACACGCC	ΔP1.2 UF
TZ457	GGGCTGTTCAGCTTTTCAAGGGCTTAGCG	ΔP1.2 UR
TZ458	TGAAAAGCTGAACAGCCCTGATAGGTCAGG	ΔP1.2 DF
TZ532	CGCGTGGCCTTGAAACC	ΔP1.2 DR
TZ460	TGCAGTAGGTCGACGATGGCAGCTTGCGCATACCGT TC	ΔP1.3 UF
TZ461	GGGCTGTTCCCGTTAGCGTTGAACAGCC	ΔP1.3 UR
TZ462	CGCTAACGGGAACAGCCCTGATAGGTCAGG	ΔP1.3 DF
TZ463	GCTTGCGGCAGCGTGAAGCGCGTGGCCTTGAAACC	ΔP1.3 DR
TZ671	CGAGACGTGGGCGTCCG	Δcapsid UF
TZ672	ATGAACACGCGAGTGTGTCCATGATCGGGG	Δcapsid UR
TZ673	ACACACTCGCGTGTTCATCTGGCAGAACGTTCAC	Δcapsid DF
TZ674	TGTCAAATAACTCTTACCGTCAGGCC	Δcapsid DR
TZ628	ACGCCGCCTTGTTCG	Δ*pks* cluster UF
TZ629	CTGGATCGGGCTCATGCGCGCTCTC	Δ*pks* cluster UR
TZ630	CGCATGAGCCCGATCCAGCATAATATGCGC	Δ*pks* cluster DF
TZ631	GACCGCATAGGCCAAGACC	Δ*pks* cluster DR
TZ232	GCGACGAGGCGAAGAAACTGGC	Δ*msr1_20490* UF
TZ233	TTCCCCGAAGTCAGATTCTATGCCGCCCGCCGTGAAT TTA	Δ*msr1_20490* UR
TZ234	GCGGGCGGCATAGAATCTGACTTCGGGGAAAAGTAC ACTGAG	Δ*msr1_20490* DF
TZ235	CGCCGCCGCATCGAGGAATTG	Δ*msr1_20490* DR
TZ564	TTTGTGTTCATTCGTGTCGCC	Δ*ISMgr2-1* UF
TZ565	GCCCCCTAAAATTCATTGCCATGCGCCAA	Δ*ISMgr2-1* UR
TZ566	CAATGAATTTTAGGGGGCTGAAACAGAGC	Δ*ISMgr2-1* DF
TZ567	GCCGACAACAGGTTGCCA	Δ*ISMgr2-1* DR
TZ569	TTCTAAAATTTGCTGTGGTGCCC	Δ*ISMgr2-2* UF
TZ685	GCCCCCTAAATGAGGAACGTCCCGCTTC	Δ*ISMgr2-2* UR
TZ686	GTTCCTCATTTAGGGGGCTGAAACACTCATTG	Δ*ISMgr2-2* DF
TZ687	TCATCCGGTCTTATGGAACGAAAG	Δ*ISMgr2-2* DR
TZ618	AAATAGCTTCGAGACATACCCCC	Δ*ISMgr2-3* UF
TZ619	CCCCTAAAATGCCCAATGGGCGAGA	Δ*ISMgr2-3* UR
TZ620	CATTGGGCATTTTAGGGGGCTACAACACAAAG	Δ*ISMgr2-3* DF
TZ621	TCAGACATGGCCCTCGG	Δ*ISMgr2-3* DR
TZ662	GTGGAAAAACGGGCCCCCG	Δ*ISMgr2-tnpB-hyp-1* UF
TZ663	CCGCATGGGTCAGATCGGCGCATCCTTACCG	Δ*ISMgr2-tnpB-hyp-1* UR

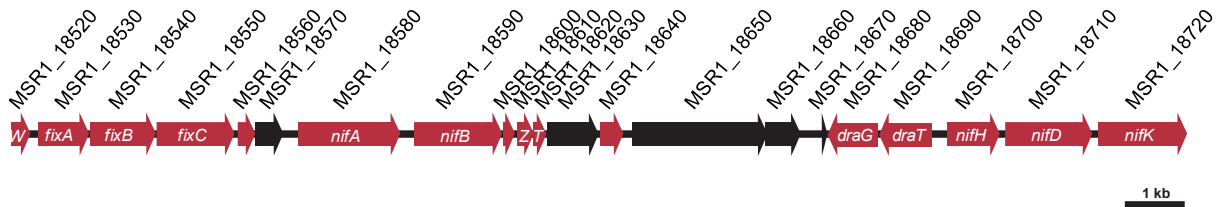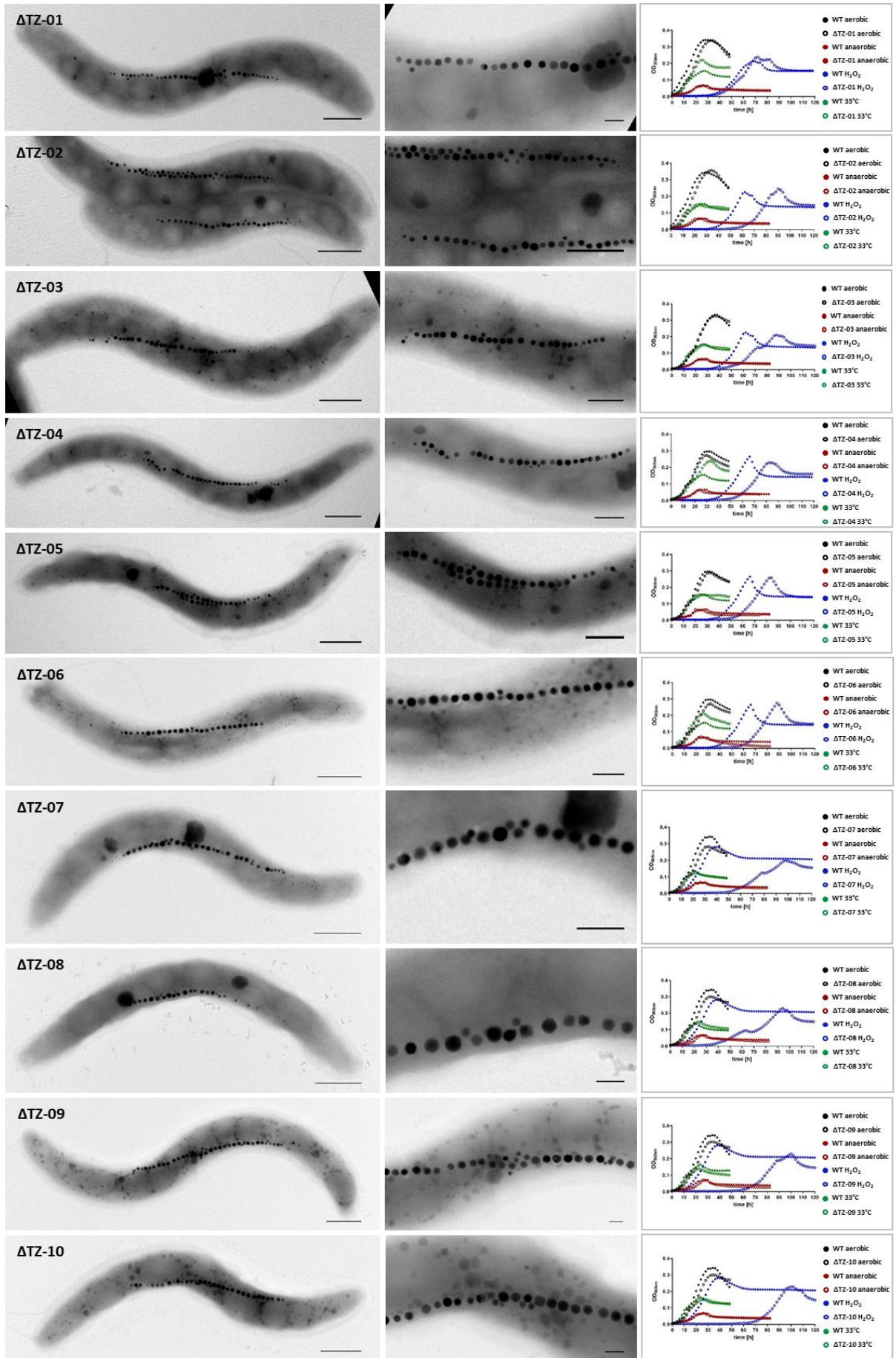| TZ664 | CCGATCTGACCCATGCGGAACACTGCGC | Δ*ISMgr2-tnpB-hyp-1* DF |
TZ665	GCGATTTCAGCCAGCGTTGATTG	Δ*ISMgr2-tnpB-hyp-1* DR
TZ608	CATCCCGGAAATCAGCCAG	Δ*ISMgr2-tnpB-hyp-2* UF
TZ609	CTTAGCCTCATCCACCCCACACATCTAATACACC	Δ*ISMgr2-tnpB-hyp-2* UR
TZ610	GGGGTGGATGAGGCTAAGATCTCCGCACG	Δ*ISMgr2-tnpB-hyp-2* DF
TZ611	ATGTAATCGCAATAGGCCGC	Δ*ISMgr2-tnpB-hyp-2* DR

Figure S1. Molecular organization of *nif* operon in *M. gryphiswaldense*. The deleted nitrogen fixation cluster comprises 16 genes necessary for nitrogen fixation (shown in red): *nifWABZTHDK*, *fixABC*, *draGT* and three ferredoxins (MSR1_18560; MSR1_18600; MSR1_18640). Black arrows represent other genes encoding a putative rubrerythrin protein (MSR1_18580), a SIR2-like domain containing protein (MSR1_18630), a GAF domain-containing protein (MSR1_18650), a biliverdin-producing heme oxygenase (MSR1_18660) and a tRNA (MSR1_18670).
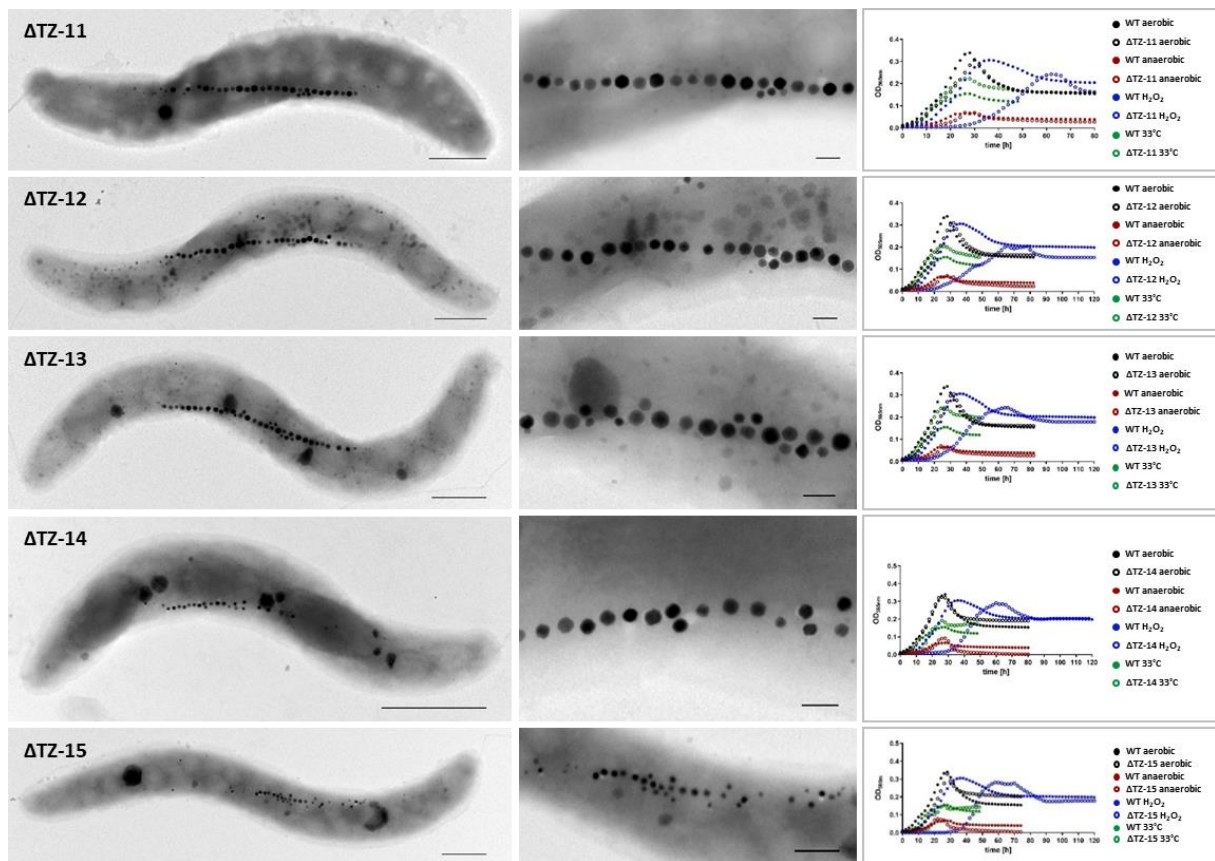
Figure S2. Phenotypic characterization of multiple deletion mutants. Electron micrographs of combinatorial deletion mutants ΔTZ-01–ΔTZ-15. Scale bars: left columns 500 nm; right columns 100 nm. Cell growth of strains ΔTZ-01–ΔTZ-15 under aerobic and anaerobic conditions as well as oxidative stress (H_2O_2) and moderate heat stress (33°C). Each strain was analyzed in triplicates and each curve shows the average.
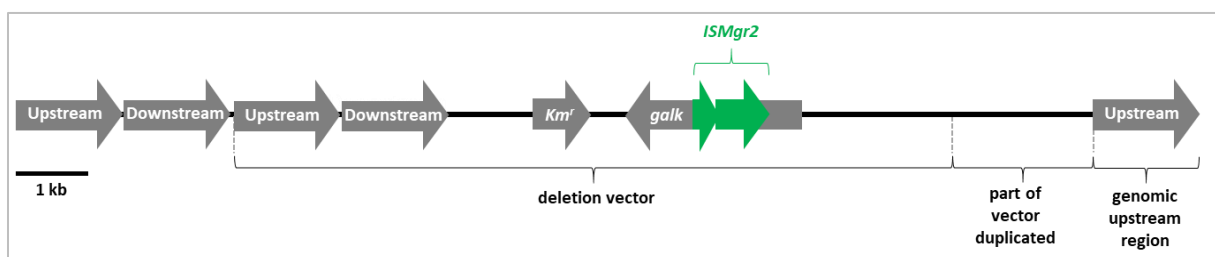

Figure S3. Genetic organization of the Km^r, false positive mutant ΔTZ-15ΔM04 K752 Km^r. The targeted M04 had not been deleted but was still maintained in the genome. A large part (~9.1 kb) of the 10.2 kb deletion vector *pORFM-GalK-M04* harboring the *Km^r* gene was found to be inserted at the intended site, but harboring a spontaneous duplication of both the upstream and downstream homologous regions intended for targeted

insertion of the deletion construct by homologous recombination. In addition, the *galK* gene was inactivated by insertion of a copy of the IS element *ISMgr2* into the central region.
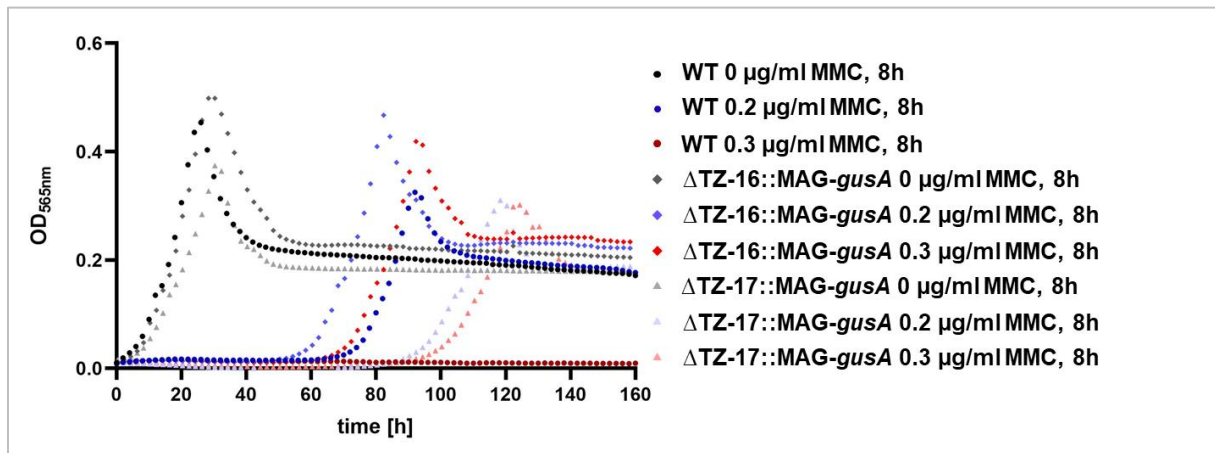

Figure S4. Growth profiles of these strains induced with MMC with concentrations between 0.2–0.3 µg/ml MMC, induced 8 h. Cells were washed twice, adjusted to initial OD and growth experiments started at 28°C under aerobic conditions and each strain was analyzed in triplicates while each curve shows its average (standard deviation <5%).
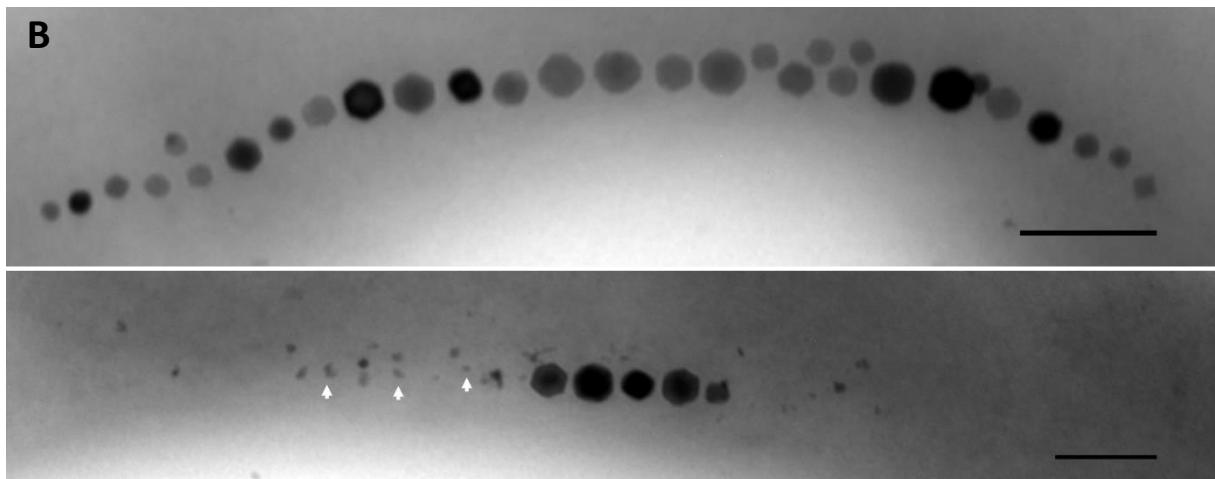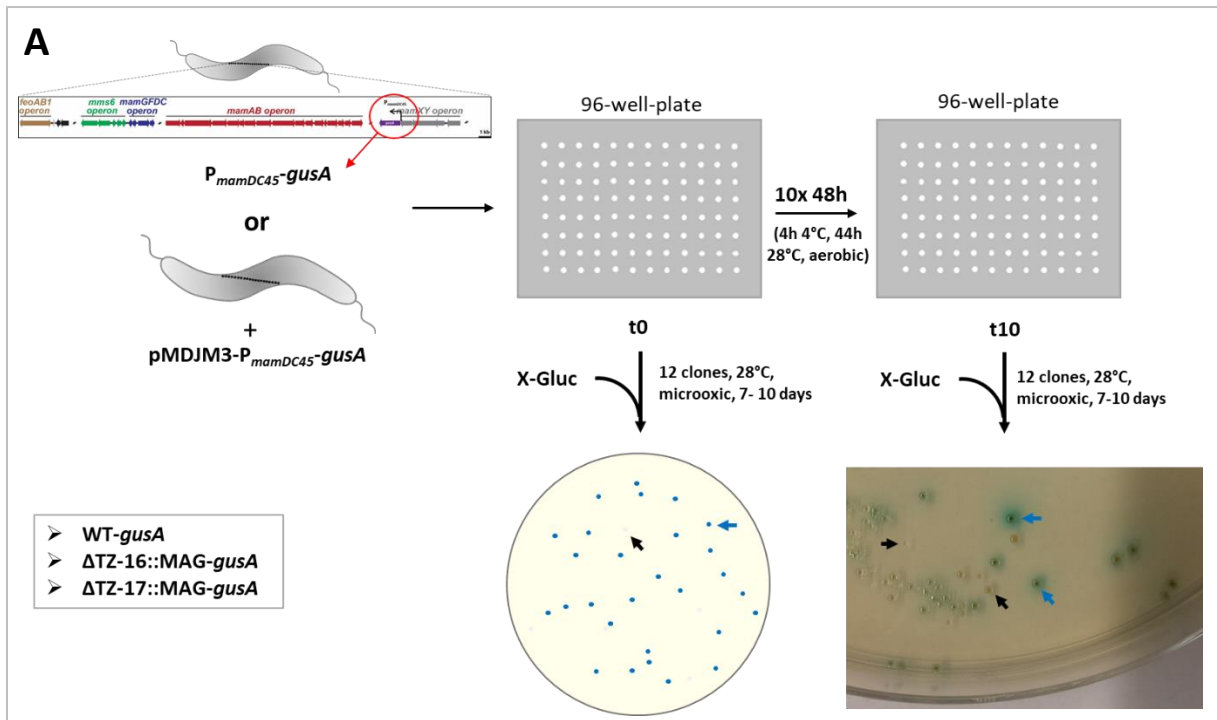
Figure S5. Experimental procedure of the genetic stability assay (A) and identified magnetosome phenotypes (B). Blue arrows indicate blue colonies while white/brown colonies are marked by black arrows **(A)**. TEM micrographs **(B)** show WT-like magnetosome chains (upper micrograph) and flake-like particles (lower micrograph, white arrows) could be observed in several of WT-*gusA* clones after ten passages. Scale bars: 100 nm.

ACKNOWLEDGEMENTS

First, I would like to thank my supervisor Professor Dr. Dirk Schüler for giving me the opportunity to work in his lab on these exciting and forward-looking projects. I am deeply grateful for his continuous support, trust, and encouragement during the whole thesis. Microbiology itself is an own, fascinating world and I am most thankful for the opportunity working with one of the most special and interesting bacteria – *Magnetospirillum gryphiswaldense*.

I would like to express my sincere gratitude to Dr. Frank Mickoleit, Dr. Marina Dziuba, Dr. Margarete Schüler, Dr. Daniel Pfeiffer, Dr. René Uebe, Dr. Frank Müller and Cornelius Riese for many helpful scientific discussions and support.

Furthermore, I thank all the past and present members of the 'Magnetolab', especially Matthias Schlotter, Lydia Stauber, Katharina Silbermann, Emriye Tekin, Ulrike Brandauer, Agatha Kässbohrer, Gabriele Zaus, and Brigitte Melzer for providing me assistance and making the lab a wonderful place to work.

Many thanks go to my undergraduate student Sabrina Stäbler for her commitment.

My deepest gratitude goes to my partner Stephan, who supports me unconditionally and enthusiastically in every phase of my life and encourages me in whatever I want to do.

Finally, I am very grateful to my mother for her support.

EIDESSTATTLICHE VERSICHERUNGEN UND ERKLÄRUNGEN

(§ 9 Satz 2 Nr. 3 PromO BayNAT)

Hiermit versichere ich eidesstattlich, dass ich die Arbeit selbstständig verfasst und keine anderen als die von mir angegebenen Quellen und Hilfsmittel benutzt habe (vgl. Art. 64 Abs. 1 Satz 6 BayHSchG).

(§ 9 Satz 2 Nr. 3 PromO BayNAT)

Hiermit erkläre ich, dass ich die Dissertation nicht bereits zur Erlangung eines akademischen Grades eingereicht habe und dass ich nicht bereits diese oder eine gleichartige Doktorprüfung endgültig nicht bestanden habe.

(§ 9 Satz 2 Nr. 4 PromO BayNAT)

Hiermit erkläre ich, dass ich Hilfe von gewerblichen Promotionsberatern bzw. -vermittlern oder ähnlichen Dienstleistern weder bisher in Anspruch genommen habe noch künftig in Anspruch nehmen werde.

(§ 9 Satz 2 Nr. 7 PromO BayNAT)

Hiermit erkläre ich mein Einverständnis, dass die elektronische Fassung meiner Dissertation unter Wahrung meiner Urheberrechte und des Datenschutzes einer gesonderten Überprüfung unterzogen werden kann.

(§ 9 Satz 2 Nr. 8 PromO BayNAT)

Hiermit erkläre ich mein Einverständnis, dass bei Verdacht wissenschaftlichen Fehlverhaltens Ermittlungen durch universitätsinterne Organe der wissenschaftlichen Selbstkontrolle stattfinden können.

……………………………………………………………………………………….

Ort, Datum, Unterschrift